DANMARKS OG GRØNLANDS GEOLOGISKE UNDERSØGELSE **RAPPORT 2020/53**

General geology of southern Kattegat, the Hesselø wind farm area

Desk Study

Jørn Bo Jensen

GEOLOGICAL SURVEY OF DENMARK AND GREENLAND
DANISH MINISTRY OF CLIMATE, ENERGY AND UTILITIES

G E U S

DANMARKS OG GRØNLANDS GEOLOGISKE UNDERSØGELSE **RAPPORT 2020/53**

General geology of southern Kattegat, the Hesselø wind farm area

Desk Study

Report for Energinet Eltransmission A/S

Jørn Bo Jensen

GEOLOGICAL SURVEY OF DENMARK AND GREENLAND
DANISH MINISTRY OF CLIMATE, ENERGY AND UTILITIES

G E U S

Table of contents

1. Summary

Energinet A/S has requested that GEUS undertakes a geological desk study of the Hesselø Offshore Wind Farm (OWF) region. The study has resulted in a general geological description and establishment of a geological model. The study is based on existing data and is to be used as a background for future interpretations of new seismic data, geotechnical investigations and an archaeological screening.

In this study we have used a combination of published work, archive seismic data and sediment core data to assess the general geological development of the southern Kattegat area, including the planned Hesselø OWF and the cable corridor.

A geological description is provided, and a geological model has been developed.

As a result of the geological desk study it has been possible to establish a relative late glacial and Holocene sea-level curve for the area and to describe the palaeo development relevant for an archaeological screening.

The general geological description includes the complete geological succession from the general pre-Quaternary framework, the pre-Quaternary surface, glacial deposits, the deglaciation and late glacial and Holocene deposits.

The geological model of the southern Kattegat is based on sequence stratigraphical studies by Jensen et al. (2002) customized to the Hesselø OWF and cable corridor case.

On the basis of the presented geological model the Integrated Ocean Drilling Program (IODP) Expedition 347 in September 2013 carried out a more than 200 m deep drilling at site M0060. The obtained sediment succession was divided into seven different lithostratigraphical units and description of lithology and downhole core logging were performed including physical parameters.

A parallel scientific multichannel survey was carried out the same year and a detailed correlation has been carried out between the seismic data and core M0060.

In the southernmost part of the Hesselø OWF area and the cable corridor, detailed studies of late glacial and early Holocene sea-level changes as well as the development of a Holocene barrier spit/estuary complex formed the basis for the evaluation of the geological model as well as input for construction of palaeo stratigraphical maps.

The maps reveal late glacial and early Holocene archaeological interesting coastal complexes in the time period for the Ahrensburg and Maglemose cultures. while the area was transgressed by the sea during younger cultures.

In relation to geotechnical challenges a number of focal points has been raised such as neotectonics, recent earthquakes, gas in sediments, glaciotectonic deformations, great thickness of weakly consolidated glaciomarine clay, Holocene sand and clay with high organic contents.

2. Introduction

GEUS has been asked by Energinet to provide an assessment of the Hesselø Offshore Wind Farm (OWF) and the proposed cable transects, consisting of establishment of a geological model on basis of existing data as background for future interpretation of seismic data and a marine archaeological screening. (Figure 2.1).

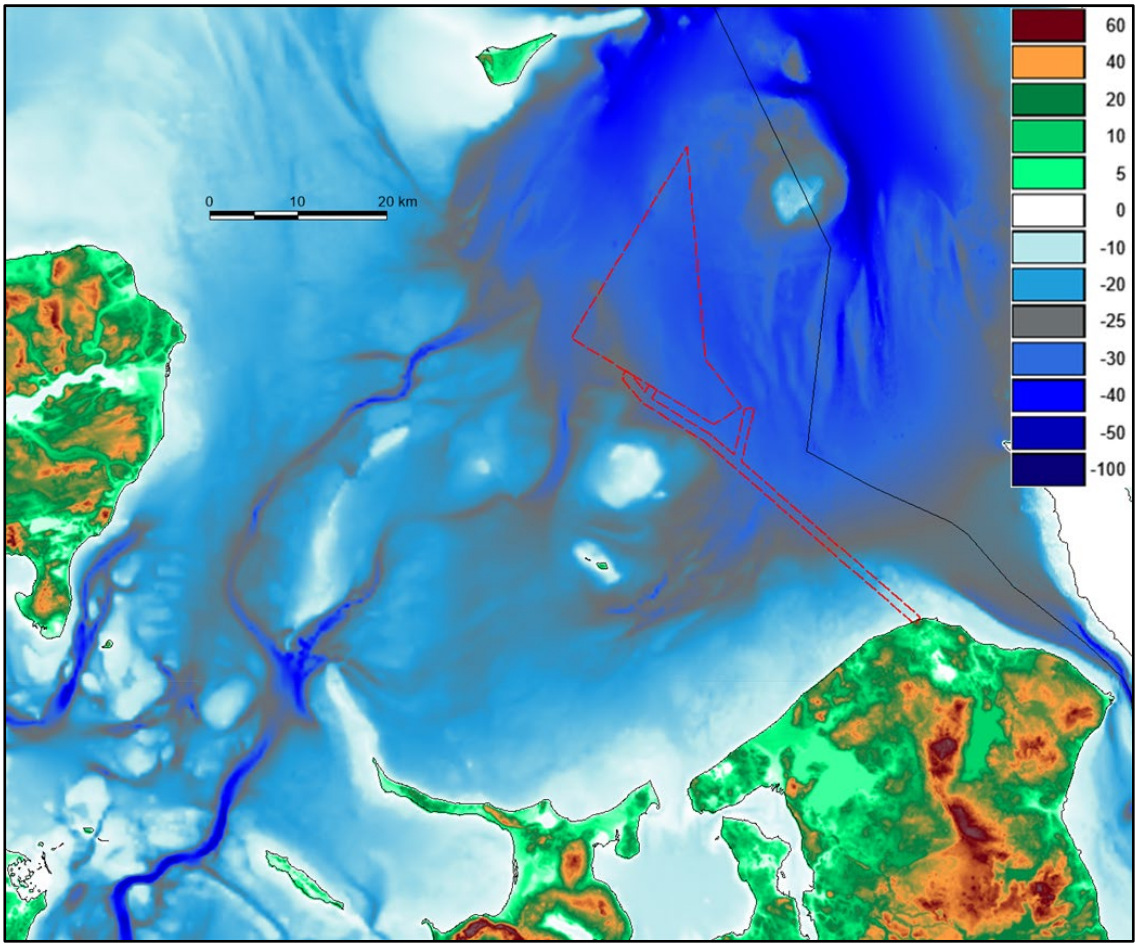

Figure 2.1. The location of the proposed Hesselø Offshore Wind Farm (polygon) and cable transects in the southern part of the Kattegat region. Bathymetry from Emodnet.

3. Data background

As a background for the desk study, deep seismic information has been compiled from scientific papers, but the seismic data are available from the GEUS Oil and Gas database (http://data.geus.dk/geusmap/?mapname=oil_and_gas&lang=en#baslay=baseMapDa&optlay=&extent=-741060,5683270,1783060,6766730), while the GEUS Marta database (https://www.geus.dk/produkter-ydelser-og-faciliteter/data-og-kort/marin-raastofdatabase-marta/) is the main supply of shallow seismic data and vibro-core data (Figure 3.1). In addition, scientific multichannel data not included in Marta have been used as well as data from IOPD core M0060.

3.1 GEUS archive shallow seismic data and sediment cores

The Marta database includes available offshore shallow seismic data and core data in digital and analog format. An increasing part of the seismic lines can be downloaded as SGY files from the web portal.

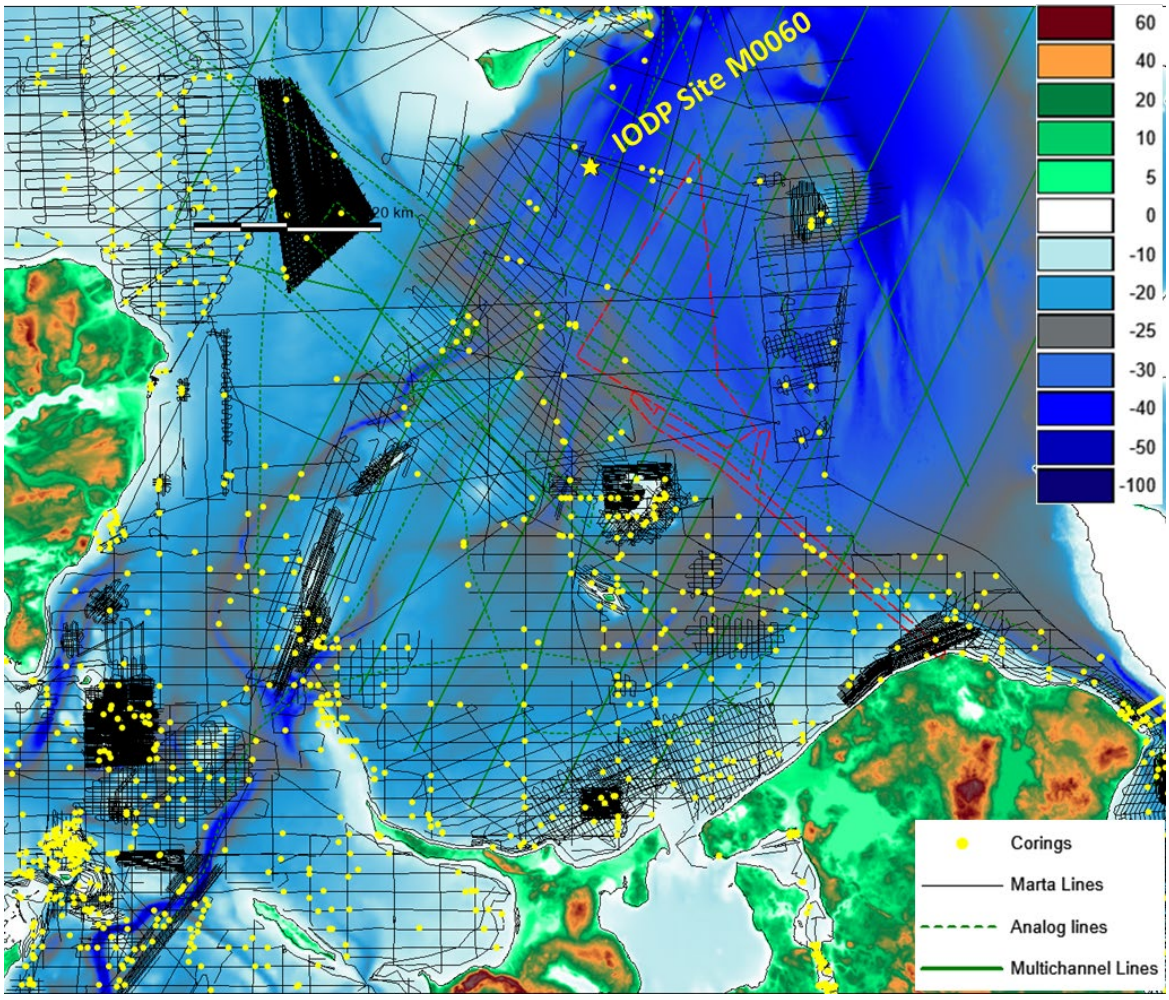

Figure 3.1. Distribution of Marta database seismic grid and core data in the southern and central Kattegat region. IODP Site M0060 is located by a yellow star. The location of the proposed Hesselø Offshore Wind Farm (OWF) and cable transects is indicated by read lines. The bathymetry is from Emodnet.

3.2 IODP Site M0060 data types

Important information about the sediment types in the Hesselø Windfarm area can be obtained from the nearby IODP core M0060 descriptions that can be downloaded from the IODP homepage (http://publications.iodp.org/proceedings/347/104/104_3.htm). Data results can be downloaded from (https://doi.org/10.1594/PANGAEA.838349).

An overview paper of the drilling results is presented in Appendix A. (Andrén et al. 2015b)

Descriptions of the drilling results include:

- Lithostratigraphy
- Biostratigraphy
- Geochemistry
- Physical properties
- Microbiology
- Stratigraphic correlation
- Downhole measurements

4. Existing knowledge of the region's geology

4.1 General pre-Quaternary framework

The Kattegat area of Denmark is crossed by the Sorgenfrei–Tornquist Zone, a fundamental tectonic lineament that runs north-west from Poland into the Scandinavian area. It crosses north-eastern Denmark in a NW–SE direction and extends as far as the Viking Graben in the North Sea (Pegrum 1984). The lineament has its origin in Precambrian times, and it is characterised by complex extensional and strike-slip faulting and structural inversion (Liboriussen et al. 1987; Mogensen & Korstgård 2003; Erlström and Sivhed 2001). The old crustal weakness zone was repeatedly reactivated during Triassic, Jurassic and Early Cretaceous times with dextral transtensional movements along the major boundary faults.

Jurassic – Early Cretaceous subsidence was restricted primarily to the area between the two main faults in the Sorgenfrei–Tornquist Zone, the Grenå–Helsingborg Fault and the Børglum Fault (Figure 4.1 and Figure 4.2). This restriction of basin development indicates a change in the regional stress field at the Triassic–Jurassic transition

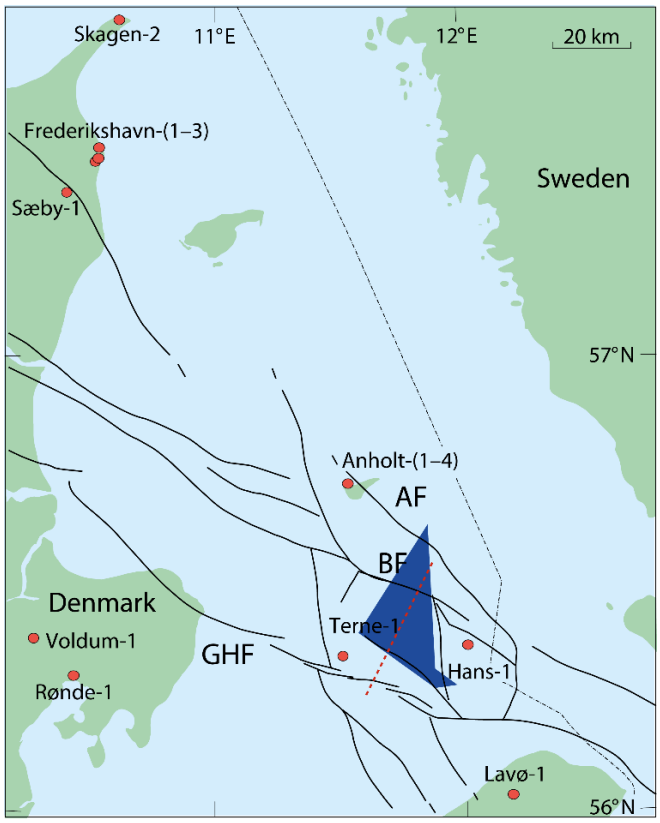

Figure 4.1. Major faults in the Kattegat area. The faults form part of the Sorgenfrei–Tornquist Zone. BF: Børglum Fault, GHF: Grenå–Helsingborg Fault, AF: Anholt Fault. The location of the Hesselø OWF is indicated. The red dashed line shows the location of the section in Figure 4.2.

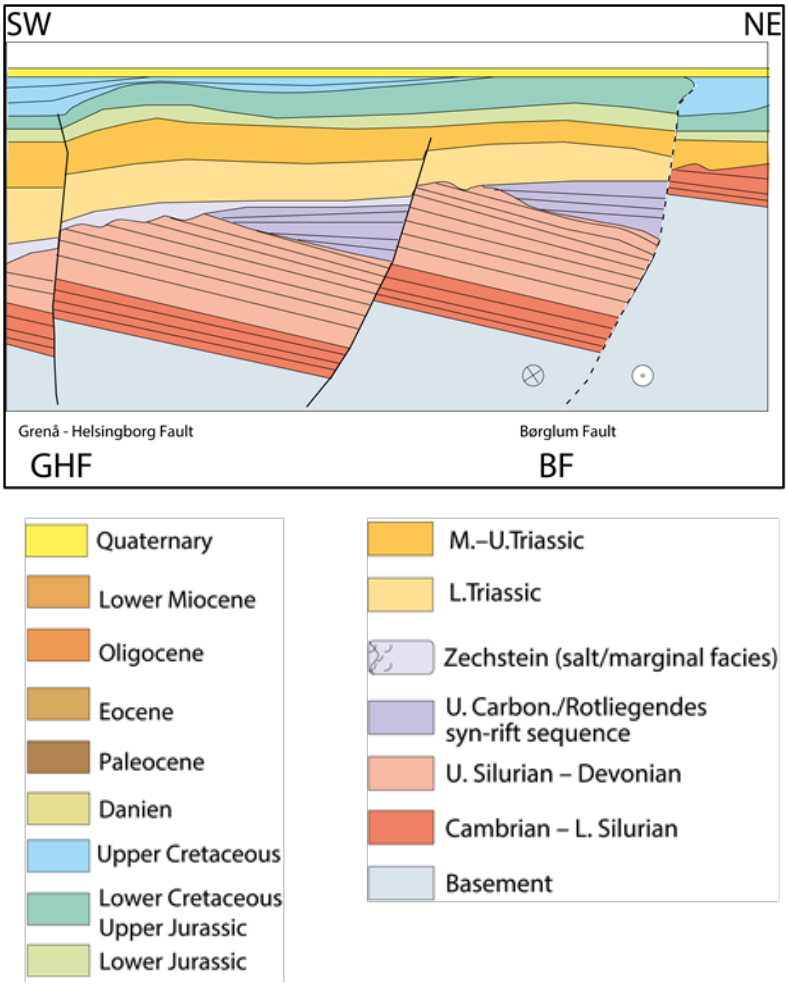

Figure 4.2. Cross section of the Sorgenfrei–Tornquist zone in the middle of the Hesselø OWF (Mogensen & Korstgård 2003). The location of the section is indicated on Figure 4.1.

In the Late Cretaceous, the fault-controlled subsidence within the Sorgenfrei-Tornquist Zone came to an end and the Jurassic–Lower Cretaceous depocenter became inverted during the Late Cretaceous and Early Palaeogene. This resulted from a change in the regional stress orientations to a predominantly compressive regime, associated with Alpine deformation in northern Europe and the opening of the North Atlantic.

Compression and crustal shortening were accommodated by reactivation of the main faults incorporated in the Sorgenfrei–Tornquist Zone. The inversion was caused by right lateral transpression along the zone. Compression from the south resulted in a dextral strike-slip motion along the main faults in the Kattegat area (Figure 4.3). This resulted in an oblique reverse activation of the Børglum Fault. The absence of major inversion features along the Anholt Fault implies that compression was accommodated along this fault by dextral strike-slip displacement. The inverted uplifted area was bordered to the north and south by subsiding basins, where sedimentation continued throughout the Late Cretaceous–Early Palaeogene.

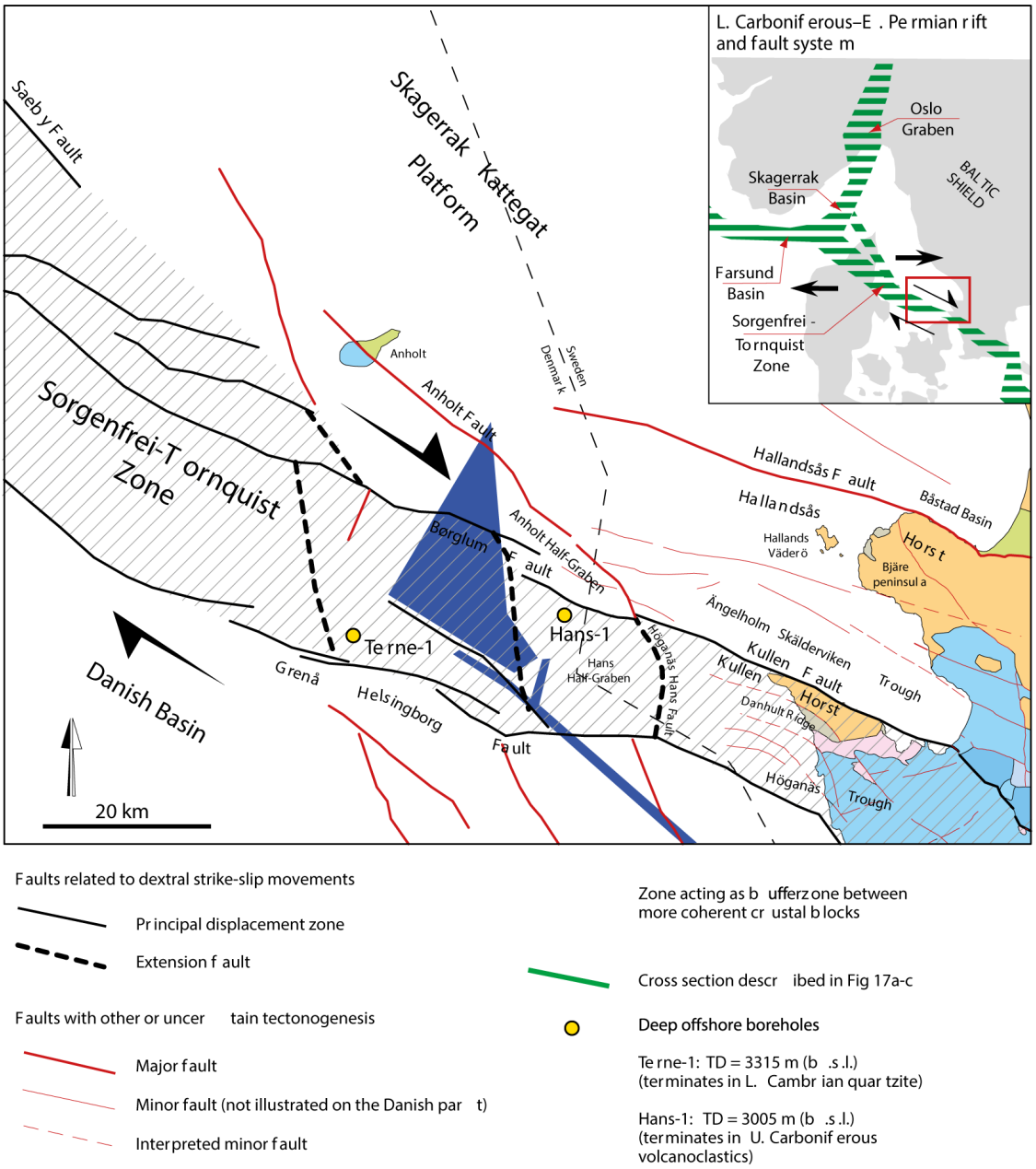

Figure 4.3. Regional structures in the southern part of the Kattegat (Erlström and Sivhed 2001). The location of the Hesselø OWF is indicated.

The pre-Quaternary stratigraphy and surface morphology have been studied by Gyldenholm et al. (1993), Lykke-Andersen et al. (1993) and Binzer & Stockmarr (1994). These studies show that the NW-dipping crystalline anticlinorium is bounded by Jurassic, Cretaceous and Tertiary sediment strata in a mainly fault-dominated structural setting (Figure 4.4).

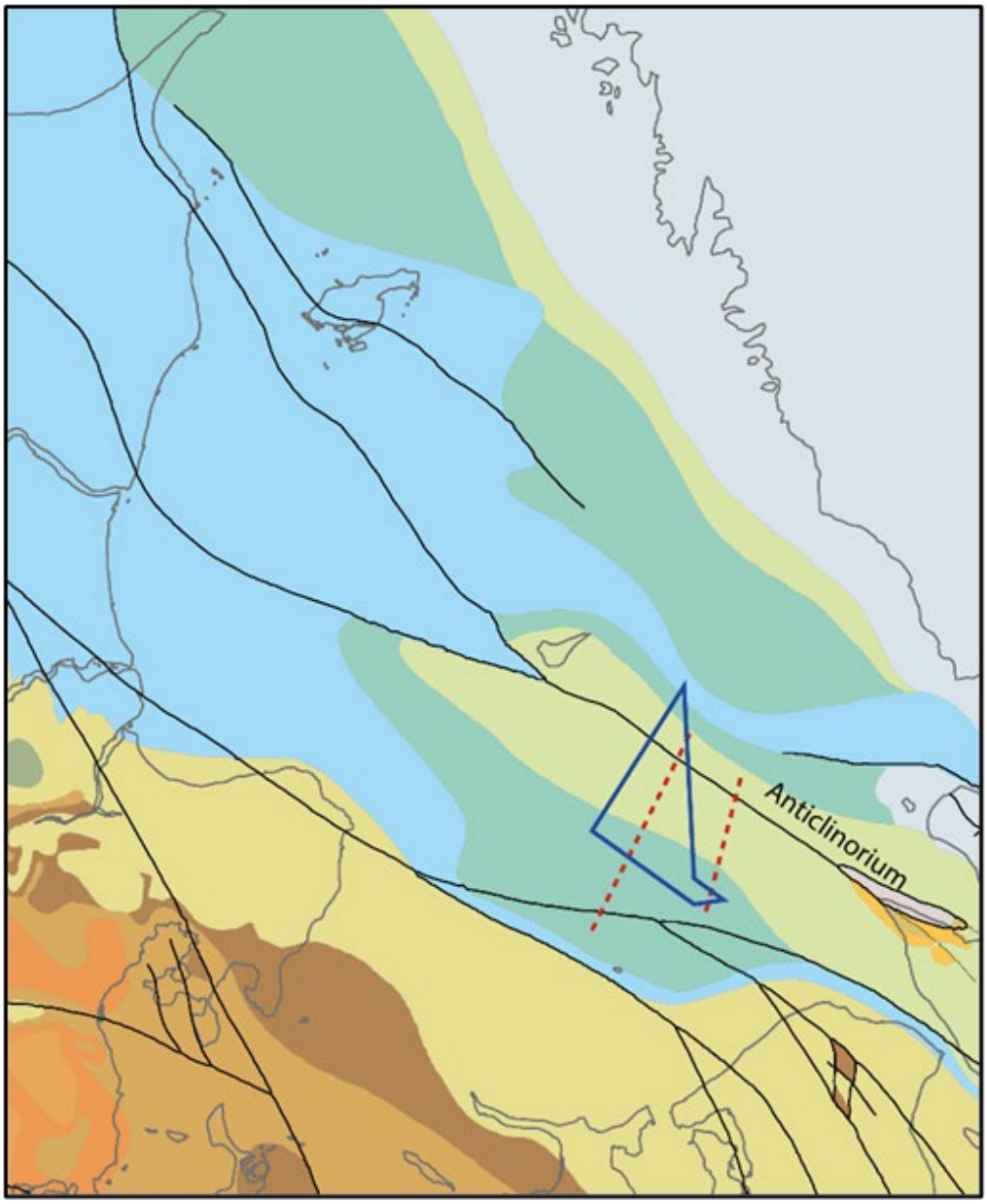

Figure 4.4. Pre-Quaternary surface geology and major faults in the Kattegat. For legend see Figure 4.2. The location of the Hesselø OWF is indicated.

Records of recent earthquake activity along the Fennoscandian Border Zone and the relationship to recent geological motion shows that the border zone is still an active zone (Gregersen et al. 1996).

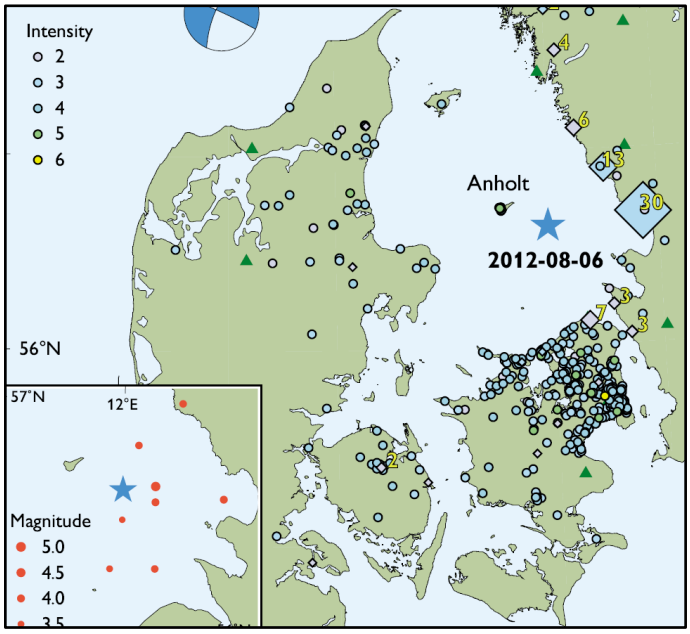

Figure 4.5. On 6 August 2012 there was a magnitude 4.1 earthquake in the Kattegat (blue star). The dots show reports on this earthquake from the public. The inset map shows all known, instrumentally recorded events over magnitude 3.5 (Dahl-Jensen et al. 2013).

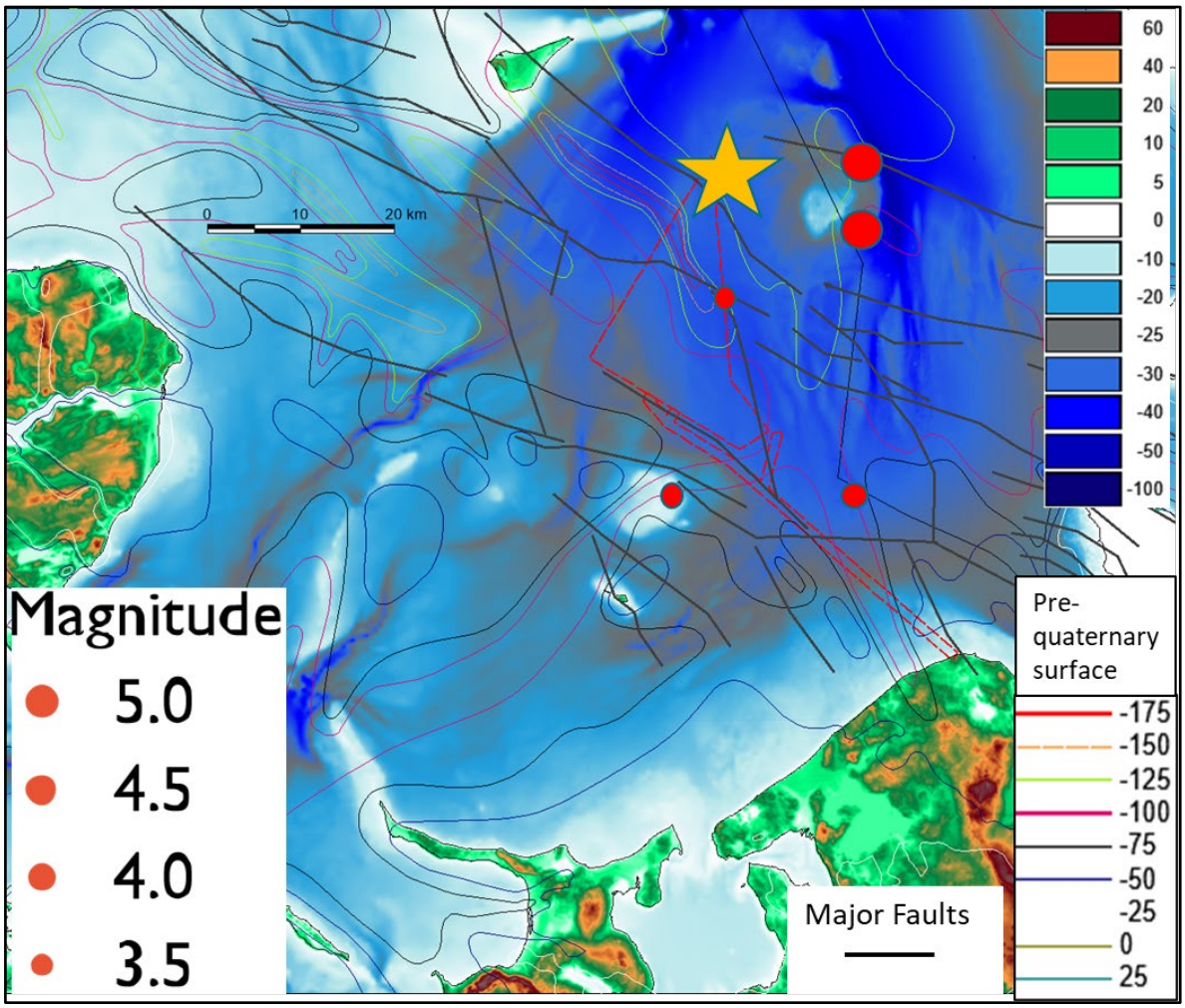

Figure 4.6. Most recent earthquakes in the Kattegat. The yellow star shows the location of a magnitude 4.1 earthquake that occurred on 6 August 2012 (Gregersen et al. 1996; Jensen et al. 2013))

4.2 Pre-Quaternary surface

The general geological development of the study area has resulted in a characteristic pre-Quaternary morphology (Binzer & Stockmarr (1994; Figure 4.7). The major faults reflect the trans tensional motions within the fault blocks.

Model based sandbox studies by Wu et al. (2009) of dextral wrench systems show that trans tension strike-slip produces elongated, sigmoidal to rhomboidal pull-apart systems, with uniquely basin margin en echelon oblique-extensional faults and development of depocenters in distinct narrow grabens. In cross-section the pull-apart basins are initiated as asymmetric grabens (Figure 4.8).

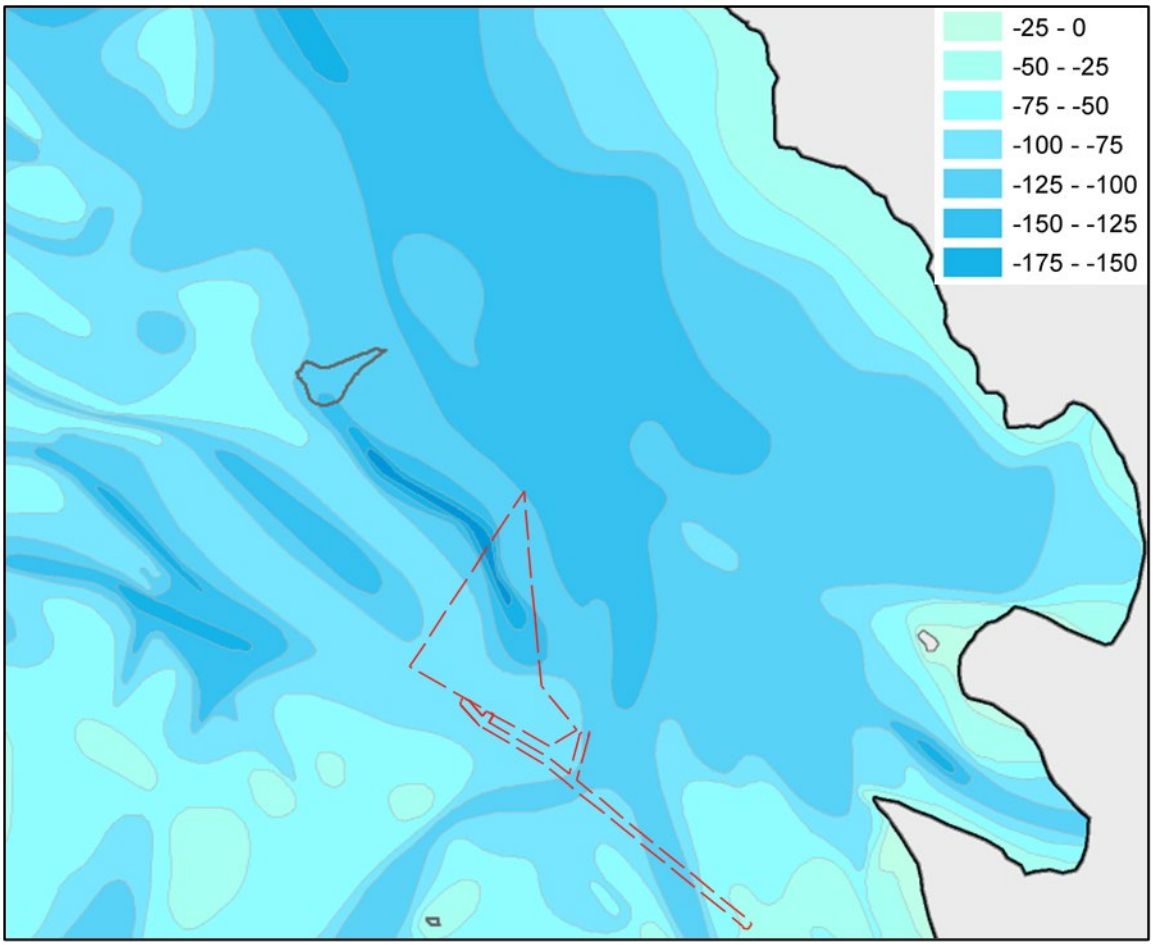

Figure 4.7. Pre-Qaternary morphology (Binzer & Stockmarr 1994). The location of the Hesselø OWF is indicated.

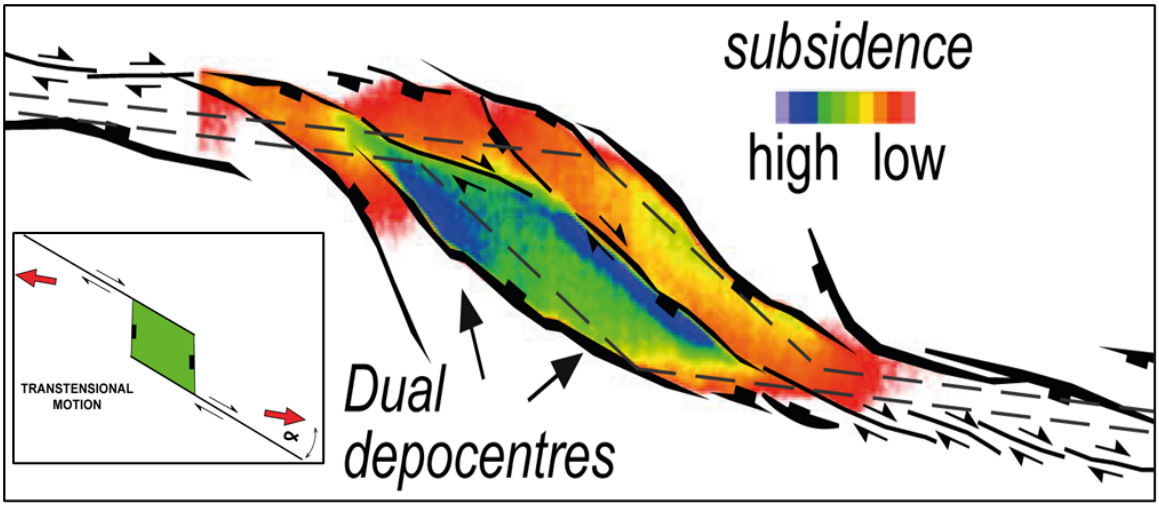

Figure 4.8. Model based sandbox study of a dextral wrench system (Wu et al. 2009).

In a combined presentation of present bathymetry, major faults and pre-Quaternary morphology (Figure 4.9) the close relationship between the wrench system faults and the depocenters is obvious. It is seen that the Hesselø OWF crosses deep faults and a pull-apart basin depocenter in the northern part of the windfarm.

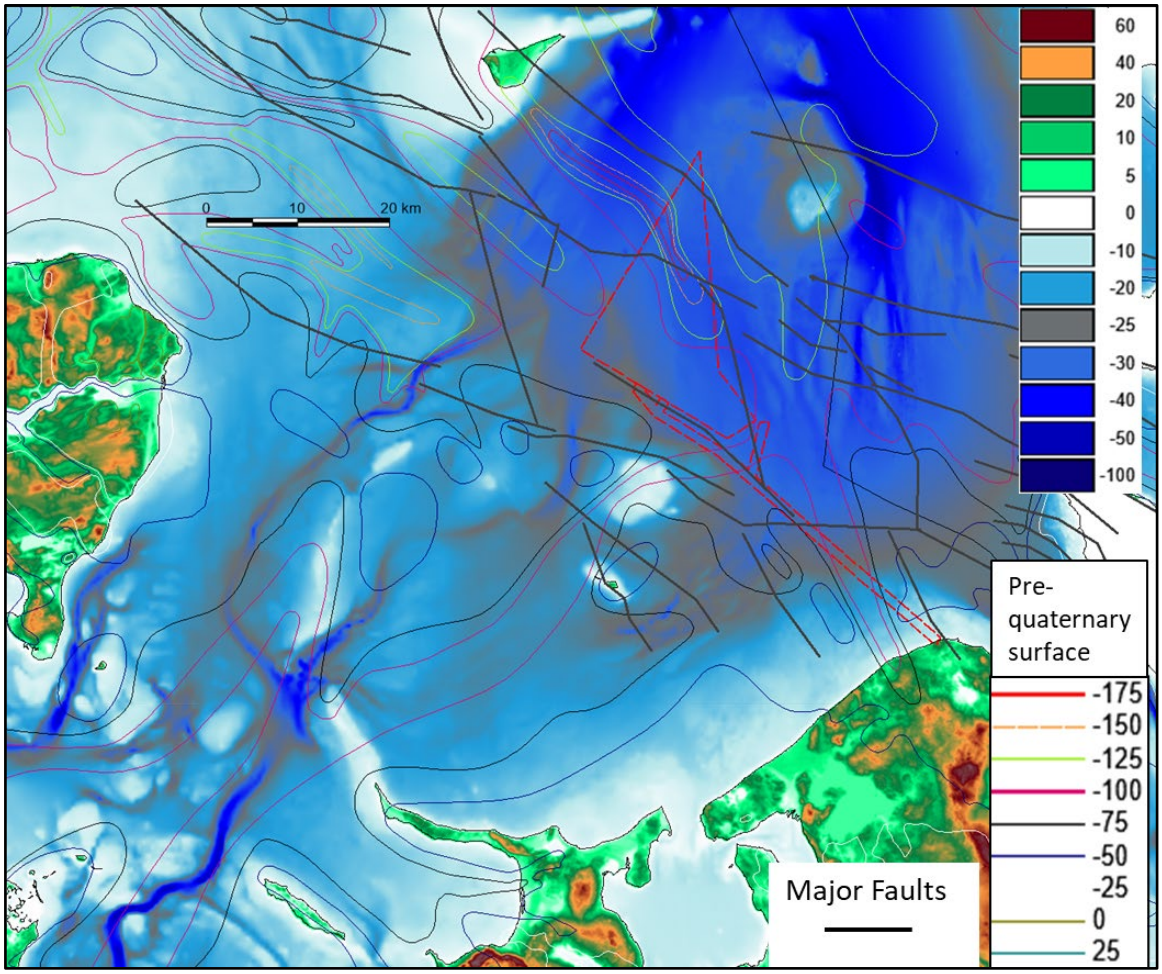

Figure 4.9. Present bathymetry, major faults and Pre-Quaternary surface morphology. The location of the Hesselø OWF is indicated.

4.3 Glacial deposits and deglaciation

Five significant Late Saalian to Late Weichselian glacial events, each separated by periods of interglacial or interstadial marine or glaciolacustrine conditions, have been identified in northern Denmark. The thickness of Quaternary sediments in central and northern Vendsyssel as well as in northern Kattegat exceeds more than 250 m and decreases towards the south, where it wedges out (Larsen et al. 2009). South of Anholt till from Last Weichselian glaciation as well as late glacial and Holocene deposits are found. The Scandinavian Ice Sheet reached its maximum extent in Denmark about 22 ka BP followed by stepwise retreat. The oldest deglaciation dates give 19 ka BP, but most deglaciation dates lie around 17 ka BP.

Around 18 ka BP the sea began to inundate northern Denmark. It led to the development of an archipelago in Vendsyssel (Richardt 1996) and to rapid deglaciation (Houmark-Nielsen and Kjær 2003; Figure 4.10).

In central Denmark ice from Sweden steadily retreated, which caused the opening of the Kattegat depression and transgression of the area. A glaciomarine environment was established with ice bergs, arctic seals, arctic whales and polar bears (Figure 4.10, Figure 4.11).

Shortly after 18 ka BP a forced regression caused by glacio-isostatic rebound is registered in Vendsyssel, the Kattegat and northern Øresund. During the general deglaciation, an ice stream readvance from the Baltic moved westward and reached the East Jylland ice marginal line at about the same time as the first marine invasion in Vendsyssel. This Young Baltic Ice advance created strong glaciotetonic deformations along the margin.

At ca. 17 ka BP the ice margin had retreated to the Halland coastal moraines along the Swedish west coast (Figure 4.10).

At ca. 15 ka BP, at the beginning of the Bølling Interstadial (Figure 4.10), calving in Skagerrak, near the present-day mouth of Oslo Fjord, sent ice bergs into the Norwegian Channel, with glaciers having abandoned the south Norwegian coast some thousand years earlier. In Sweden, ice had retreated to the central and southern uplands giving way to an ice-dammed lake in the southern part of the Baltic depression. As the ice stream in the Baltic was wasting, a glacio-eustatic transgression characterised the Skagerrak and Kattegat southwards along the Swedish west coast into the northern Øresund region. From ca. 17 to 15 ka BP marine environments changed from arctic to boreo-arctic, and the mud dominated Yoldia clay in Vendsyssel was generally succeeded by the littoral Saxicava Sand and Zirfaea Beds.

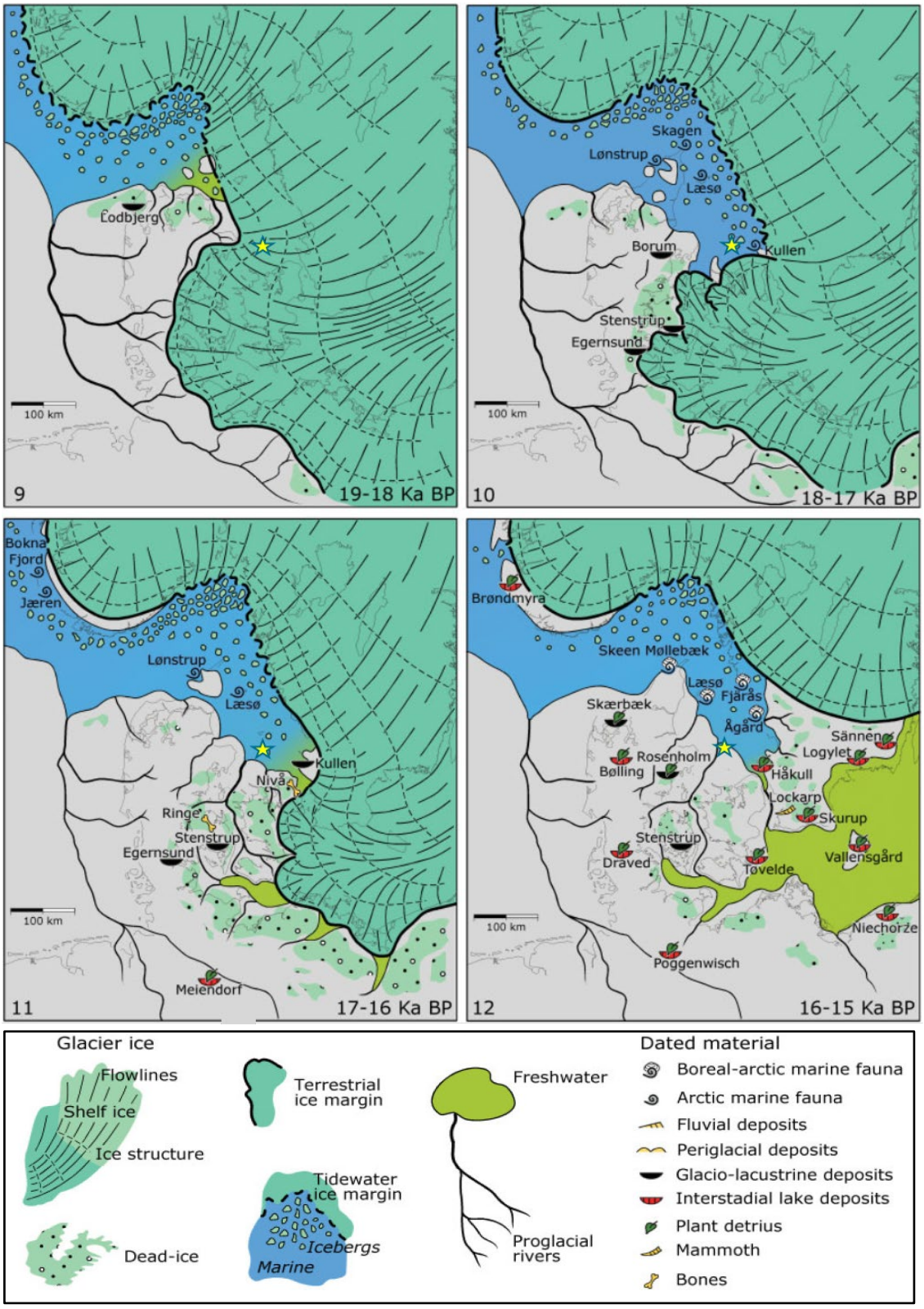

Figure 4.10. Palaeogeographical reconstructions of the last deglaciation of southern Scandinavia (19–15 ka BP; Houmark-Nielsen and Kjær 2003).

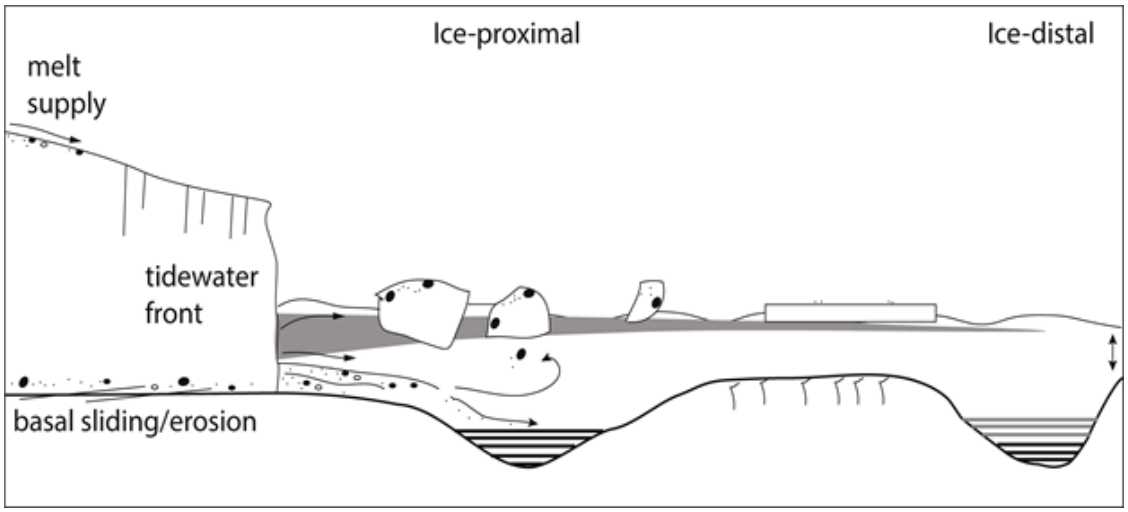

Figure 4.11. Illustration of a glaciomarine depositional environment.

On the basis of the GEUS archive data combined with the Emodnet bathymetry as well as the GEUS updated surface sediment map it is possible to revise earlier models of ice marginal ridges in the Hesselø Offshore Wind Farm study area.

The morphological pronounced Sjællands Odde ice marginal ridge continues offshore in a big curve and cuts the southernmost corner of the Hesselø Offshore Wind Farm area and the connected cable corridor and continues northward to the Store Middelgrund area (Figure 4.12) where evidence of glaciotectonic deformations is seen on sparker line 5003 north of Store Middelgrund.

The interpretation of retreating ice marginal ridges is supported by the seabed surface sediment map (Figure 4.13) where the ridges in general consist of till, often superimposed by Holocene transgressive sand and gravel, coastal sediments eroded and redeposited on the margins of the till core.

The Hesselø OWF area is situated between two major ice marginal ridges in a basin with up to 100 m thick late glacial glaciomarine basin deposits (Figure 4.11) documented in IODP core M0060.

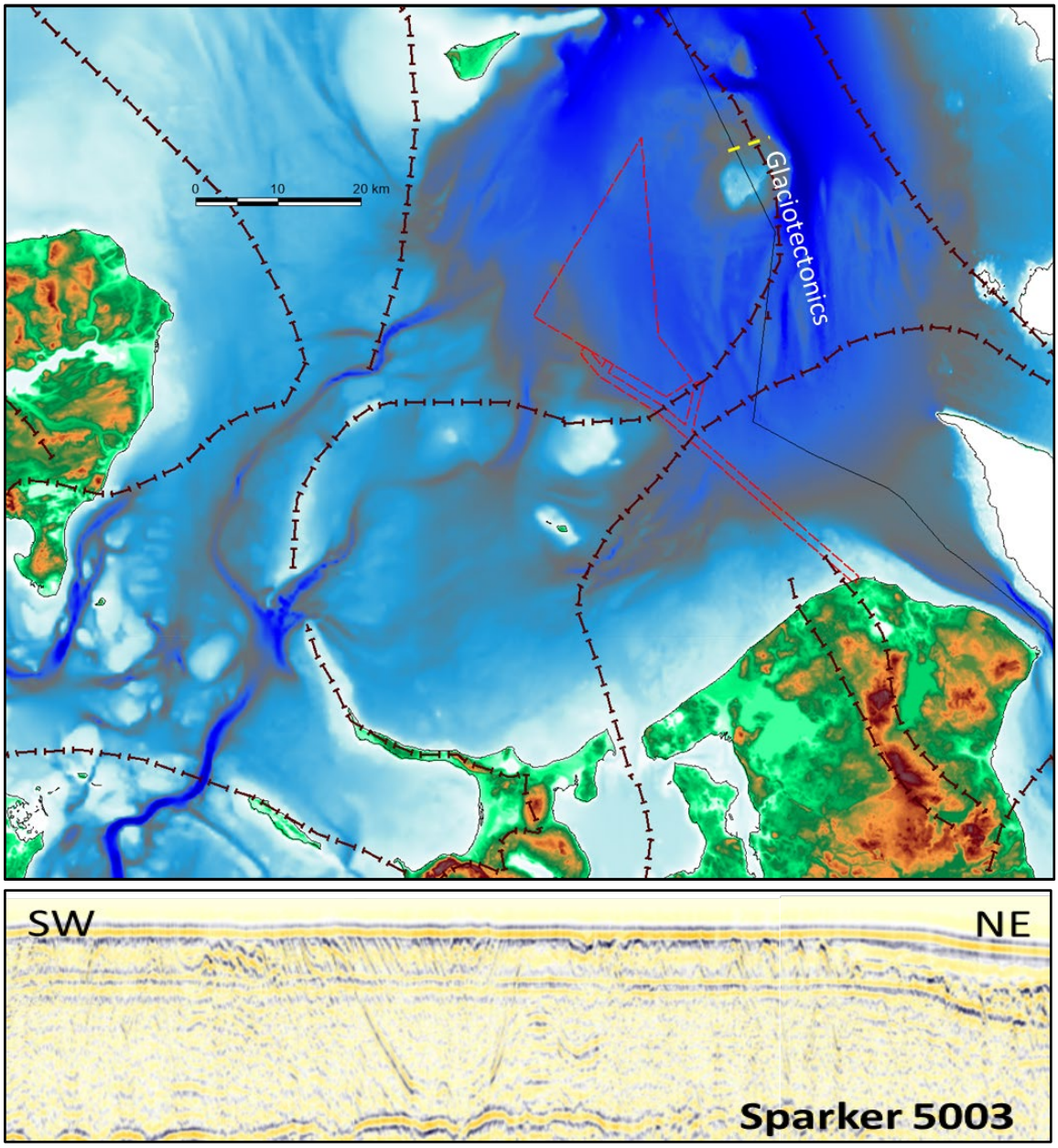

Figure 4.12. Upper figure: Interpreted ice marginal ridges in the southern part of the Kattegat. Lower figure: Sparker profiler showing evidence of glaciotectonic deformation north of Store Middelgrund (yellow dashed line on upper figure). Bathymetry from Emodnet. The location of the Hesselø OWF is indicated.

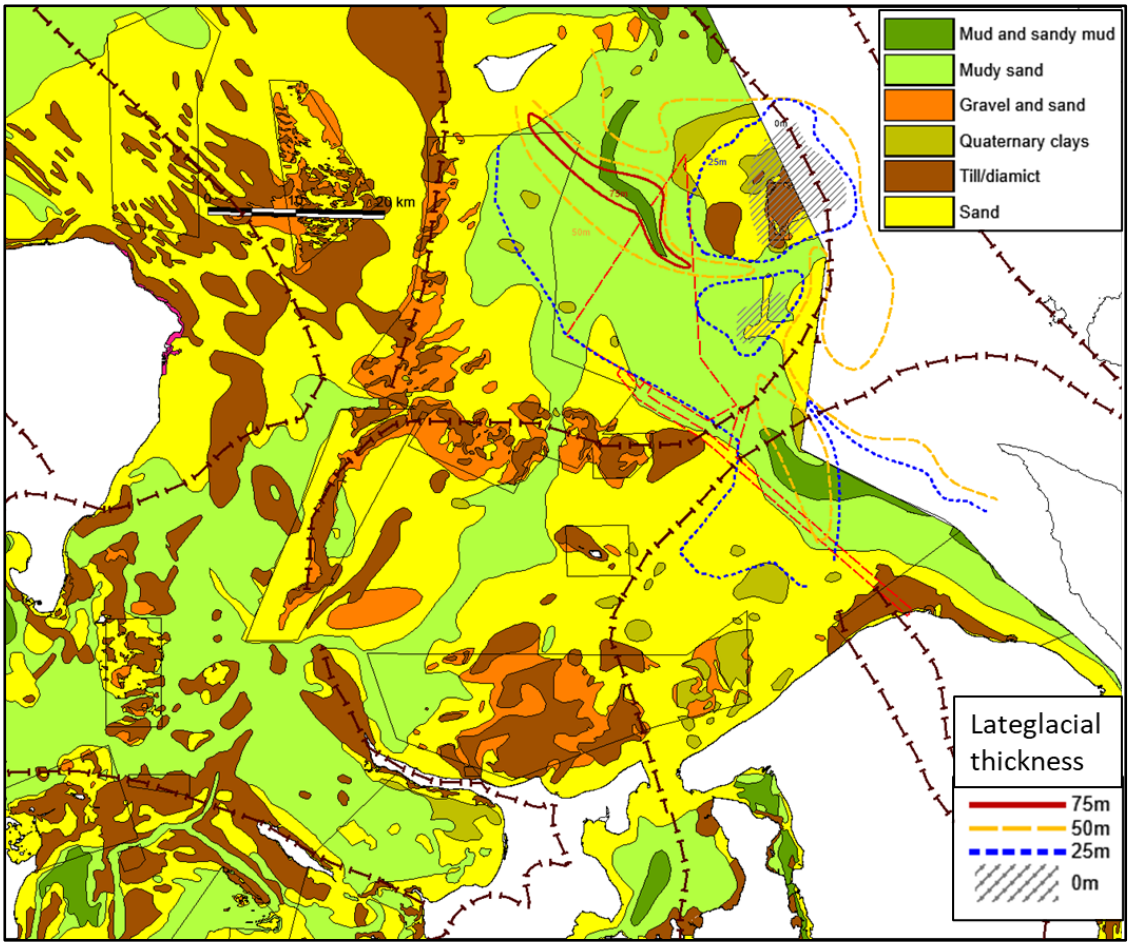

Figure 4.13. Seabed surface sediment map, interpreted ice marginal ridges and thickness of late glacial glaciomarine basin deposits. The location of IODP core M0060 (yellow star) and Hesselø OWF is indicated.

4.4 Late glacial and Holocene

In the period after the deglaciation the southern Kattegat area was characterised by high-stand sea-level conditions, followed by a continuous moderate regression until the eustatic sea-level rise surpassed the glacio-isostatic rebound in the early Holocene (Figure 4.14).

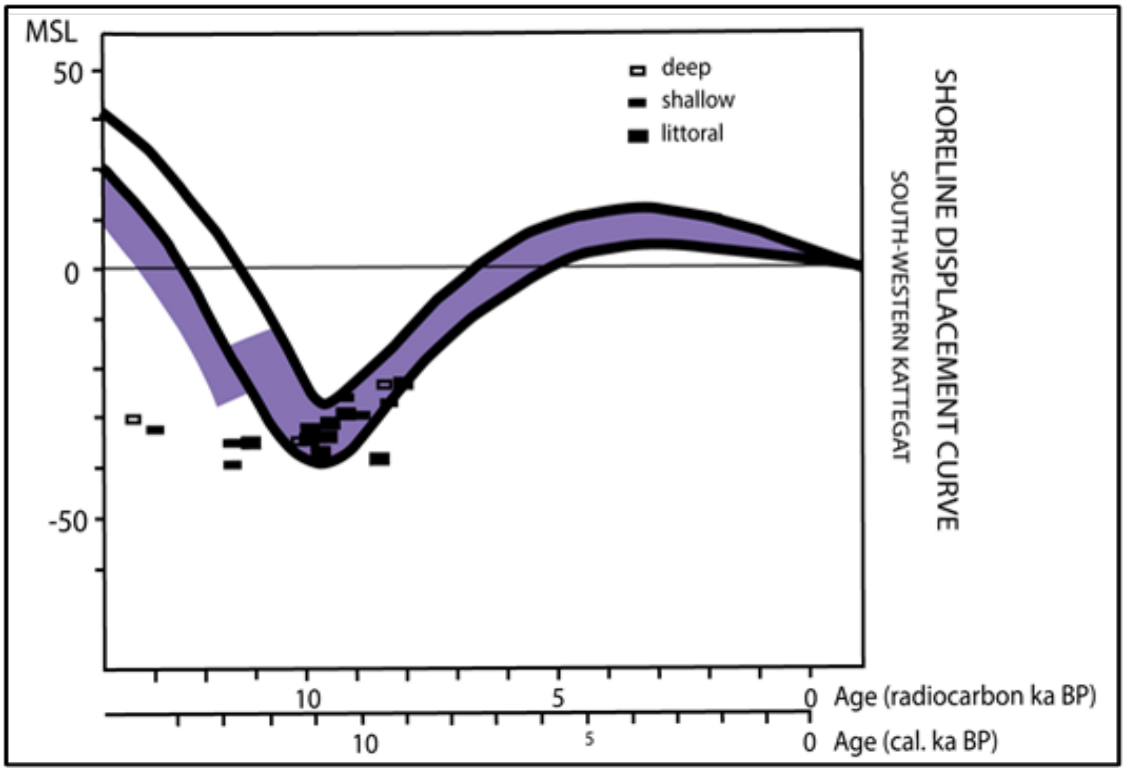

Figure 4.14. Shoreline displacement curves for the southern Kattegat. The two solid black lines indicate the range of shoreline displacements in non-faulted regions of the study area (modied from Mörner 1983). The purple area indicates the relative sea level changes interpreted from the sequence stratigraphy in the down-faulted NW–SE striking depression. Radiocarbon dated samples are indicated as deep >10 m, shallow 2–10 m or littoral 0–2 m.

Late Weichselian subaqueous sediments occur typically as basin infill in the area north of the anticlinorium, or in local depressions elsewhere.

In the early Holocene the relative sea level began to rise, as the eustatic sea-level rise surpassed the isostatic uplift of the crust. Mörner (1969, 1983) made comprehensive pioneer studies of the relative sea-level changes in the Younger Dryas–Holocene Kattegat, while later studies have resulted in more detailed palaeogeographic reconstructions based on sequence stratigraphical studies (Bennike et al. 2000; Jensen et al. 2002; Bendixen et al. 2015, 2017).

The Hesselø OWF area has been submerged most of the time after the last deglaciation, but in the lowstand period around 10.5 ka BP only partly, and lowstand sediments must be expected (Figure 4.15). Already in the initial phase of the Holocene transgression the Hesselø OWF area was fully submerged, while the cable corridor area has a longer transgression history.

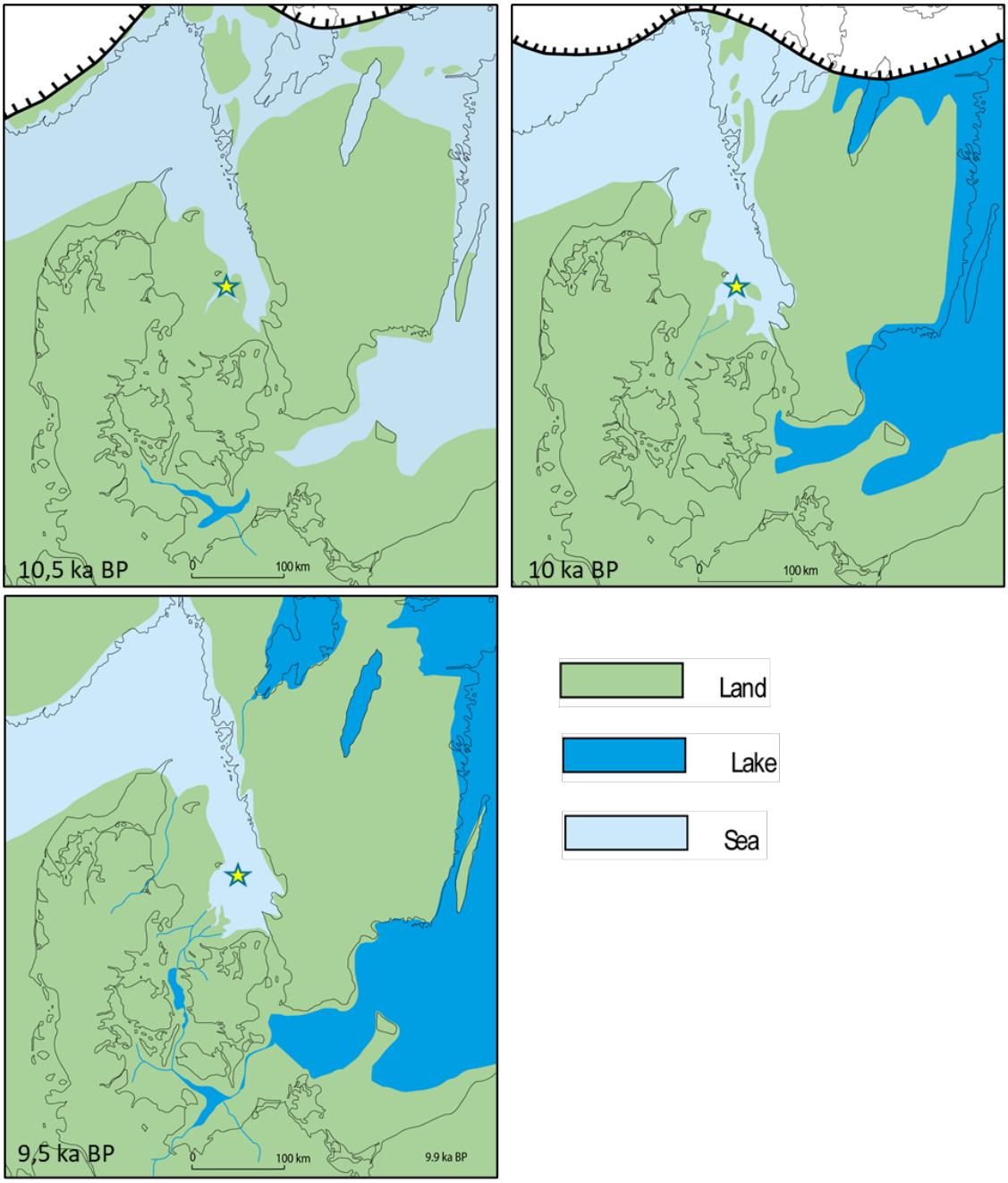

Figure 4.15. Palaeogeographical scenarios focusing on the southern Kattegat lowstand 10.5 ka BP, and the initial transgression period 10 ka BP and 9.5 ka BP. (Jensen et al 2002). The yellow star shows the location of IODP core M0060.

5. Sequence stratigraphical model for southern Kattegat

A sequence stratigraphical model of the southern Kattegat region was developed by Jensen et al. (2002). It will be presented shortly in this chapter illustrated by key seismic examples from the Hesselø OWF area.

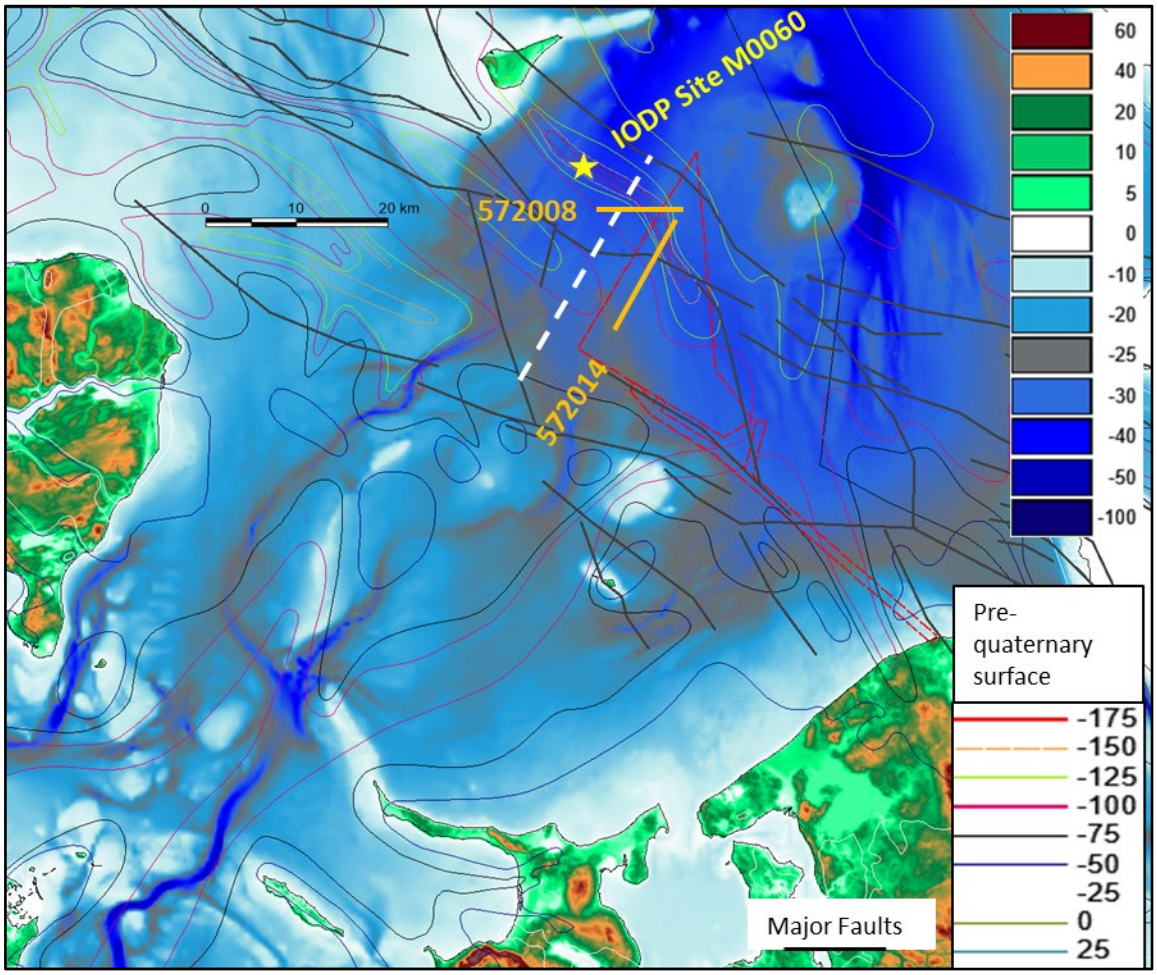

Figure 5.1. Key seismic lines 572008 and 572014 as well as location of general model line (white dashed line) and IODP site M0060 (yellow star) on a map showing present bathymetry, major faults and pre-Quaternary surface morphology. The location of the Hesselø OWF is indicated by red dashed lines.

5.1 Methods

For shallow seismic data acquisition, an EG & G Uni-boom system (0.8–16 kHz) and a high frequency Sparker system (about 0.4–14 kHz) were used. The Boomer data were acquired with a shooting interval of 250 ms, a sampling frequency of 10 kHz and a high–low pass filter setting of 800–2400 Hz, while the Sparker data were shot with a shooting interval of 1000 ms, a sampling frequency of 10 kHz, and a high–low pass filter setting of 300–2000 Hz. The Boomer set-up for the study area allows a vertical resolution of about 0.3 m and a maximum penetration of 100 m, while the Sparker resolution is 0.5–1 m and the maximum penetration

about 200 m. The seismic data were interpreted following depositional sequence stratigraphical principles introduced by Vail et al. (1977). This interpretation method was later adjusted to high-resolution settings by Posamentier et al. (1992).

A characterization of the depositional environment was inferred from the seismic information and used for the selection of core sites.

Sediment samples were collected with a 6 m long vibrocorer. After detailed lithological description, the cores were subsampled for studies of molluscs and foraminifers. Selected shells of marine bivalves were radiocarbon dated by accelerator mass spectrometry (AMS) at the Institute of Physics, Aarhus University.

5.2 Seismic facies units

The following description of the seismic facies units presents a subdivision into bedrock (BR) and glacial (GL) deposits, underlying two different Late Weichselian (LG I and LG II) sequences, which form basin infills with a maximum thickness of about 100 m. The existence of two LG sequences points to an unexpected, early relative sea-level highstand in the area before the Early Holocene transgression and associated deposition of the Holocene (H) sequence.

5.2.1 BR – Bedrock

The bedrock forms the acoustic basement. Earlier studies of the pre-Quaternary surface topography (Gyldenholm et al. 1993; Binzer & Stockmarr 1994) show that elongated NW–SE-trending depressions (Figure 4.7 and Figure 4.3) follow the general dextral wrench fault pattern in the Fennoscandian Border Zone (Liboriussen et al. 1987). These studies also report that the central NW-dipping crystalline anticlinorium is bounded by Jurassic, Cretaceous and Tertiary sedimentary strata, which are generally associated with major faulting (Figure 4.4). The top of the bedrock has a high intensity return, and for the Jurassic strata strongly dipping internal reflectors are seen, while the crystalline bedrock shows no true internal reflections (Figure 5.2).

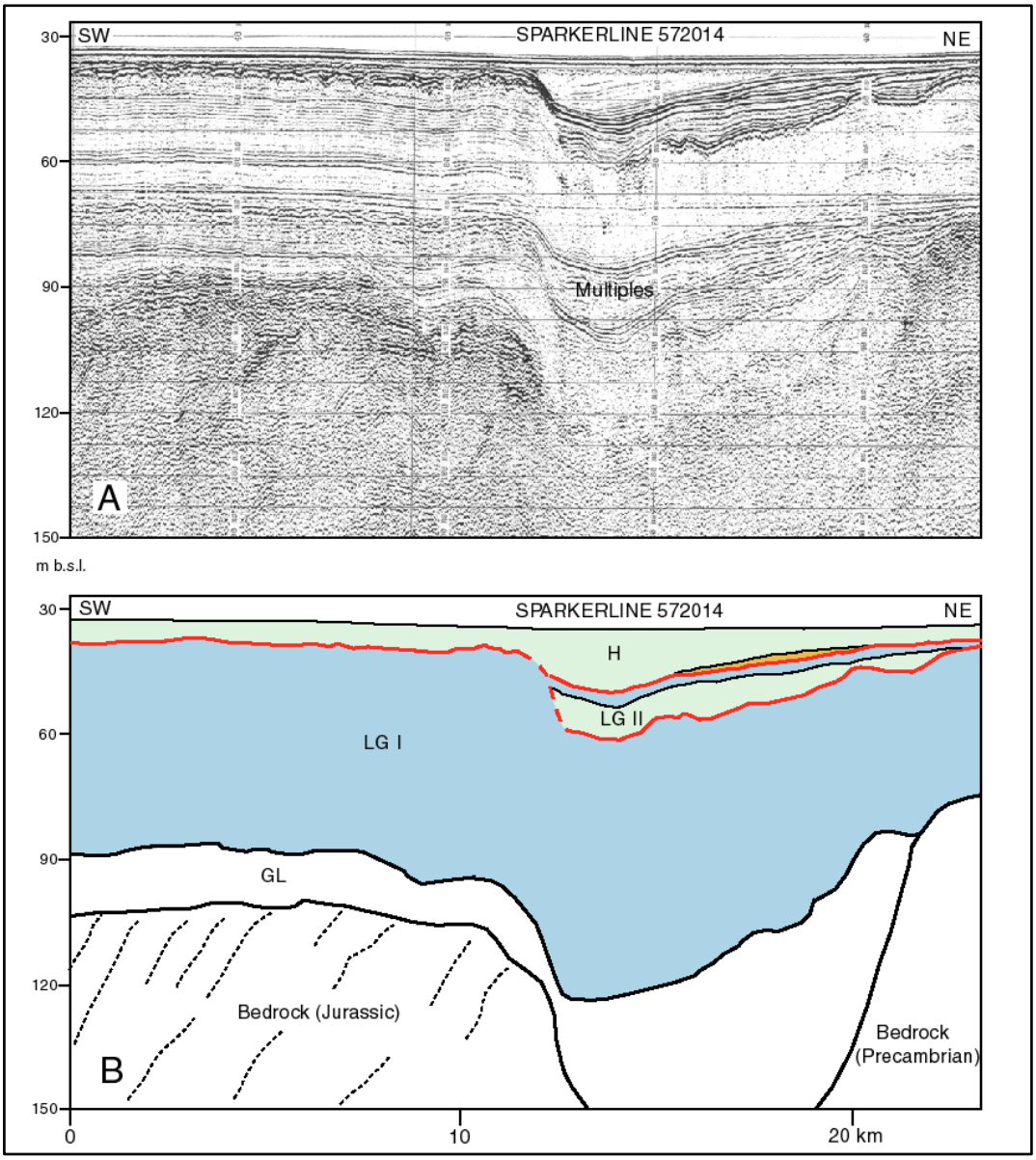

Figure 5.2. Sparker section 572014 (A) and interpretation (B). Legend is seen in figure 5.4. The location of the seismic section is indicated in Figure 5.1.

5.2.2 GL – Glacial deposits

This unit is characterized by rugged lower and upper boundaries with few distinct reflectors in a dominating pattern of chaotic internal reflectors (Figure 5.2). The unit shows a strongly varying thickness ranging from a few metres in the central survey area to 50 m in the Store Middelgrund area (SGU 1989). Earlier studies in the region (Gyldenholm et al. 1993; Nielsen & Konradi 1990; SGU 1989) indicate that the unit represents Weichselian and older glacial deposits.

5.2.3 LG I – Older late glacial deposits

The LG I sediments have a maximum thickness of about 60 m in the study area (Figure 5.2). The lower boundary of the unit is sharp, and the internal reflection pattern is semi-transparent with parallel reflectors conformably draping the underlying GL surface. In the shallow areas, the upper boundary appears as a rugged erosional unconformity, which gradually changes to a conformity seen all over the deeper basins, where depths exceed 40 to 45 m. The sedimentological characteristics in the central part of the study area are illustrated by core 572007 (Figure 5.4 and Figure 5.5), which contains 5 m of weakly laminated to structureless clay with dropstones, without macroscopic evidence of marine influence.

In the southernmost part of the area, where an interlayering of fine sand and clay suggests a more proximal setting, a few shells of the marine bivalve species *Hiatella arctica* were found. AMS radiocarbon dating of a shell yielded an age of about 16 cal. ka BP (Jensen et al 2002), demonstrating that the basal part of the unit was deposited shortly after the deglaciation of the area. This is supported by previous indications of a glaciomarine fauna in the same unit, as described by Nielsen & Konradi (1990) and by Bergsten & Nordberg (1992). The latter authors described similar lithological facies types (facies IV and III) and characterized these as ice-proximal to shelf sediments with a high arctic fauna referred to the same period.

The general sea-level history of the area shows an early late glacial highstand with a marine limit about 60 m a.s.l. in the northern part of Denmark (Petersen1984; Richardt 1996) and a level close to the present sea level in the coastal areas south of Kattegat (Lagerlund & Houmark-Nielsen 1993). Mörner (1983) studied areas along the Swedish west coast and presented a model which suggests that the highstand was followed by a more or less continuous and moderate regression due to glacio-isostatic rebound until the eustatic sea-level rise surpassed the isostatic rise in the early Holocene. Unit LG I represent the highstand period, as illustrated by the draping of the lower boundary. The fact that the sequence is bounded by an upper erosional unconformity to a level of 40–45 m b.s.l. (Figure 5.2) indicates a lowstand level, below which conformity prevails with continuous sedimentation also during the regression. However, the fact that LG I is followed by another, Late Weichselian sequence (LG II) indicate the existence of an extra local highstand before the Holocene transgression, which is in contradiction to the regional sea-level rise model.

5.2.4 LG II – Younger late glacial deposits

The northern basin (Figure 4.7) and the depressions in the anticlinorium (Figure 5.1) contain a second late glacial seismic sequence LG II with a thickness of up to 50 m. The lower boundary is a sharp erosional unconformity in shallow areas down to about 40 m b.s.l. (Figure 5.2 and Figure 5.4) and below this level a conformity can be identified throughout the area. The internal reflection pattern points to a lower transgressive systems tract with reflectors onlapping in the shallow part and downlapping towards the basin. Furthermore, an upper highstand systems tract is indicated, bounded below by the maximum transgression surface (maximum flooding surface) and above by a type I sequence boundary (Posamentier et al. 1992).

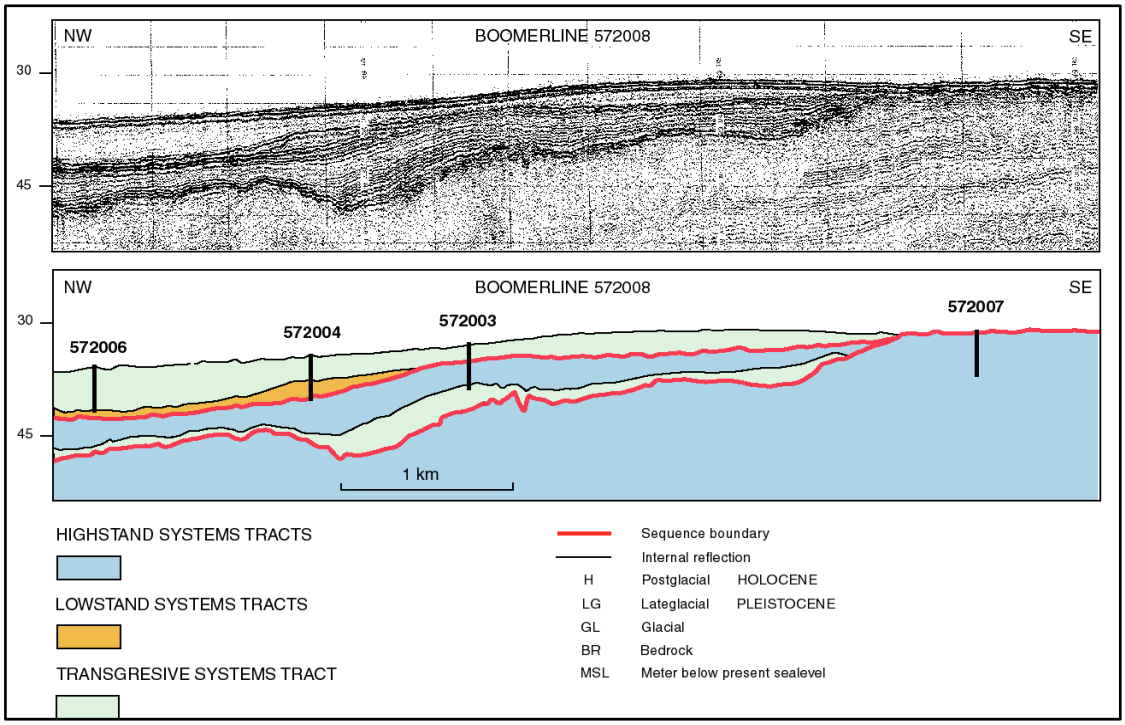

Figure 5.3. Boomer seismic section 572008. For location of the seismic example see Figure 5.1

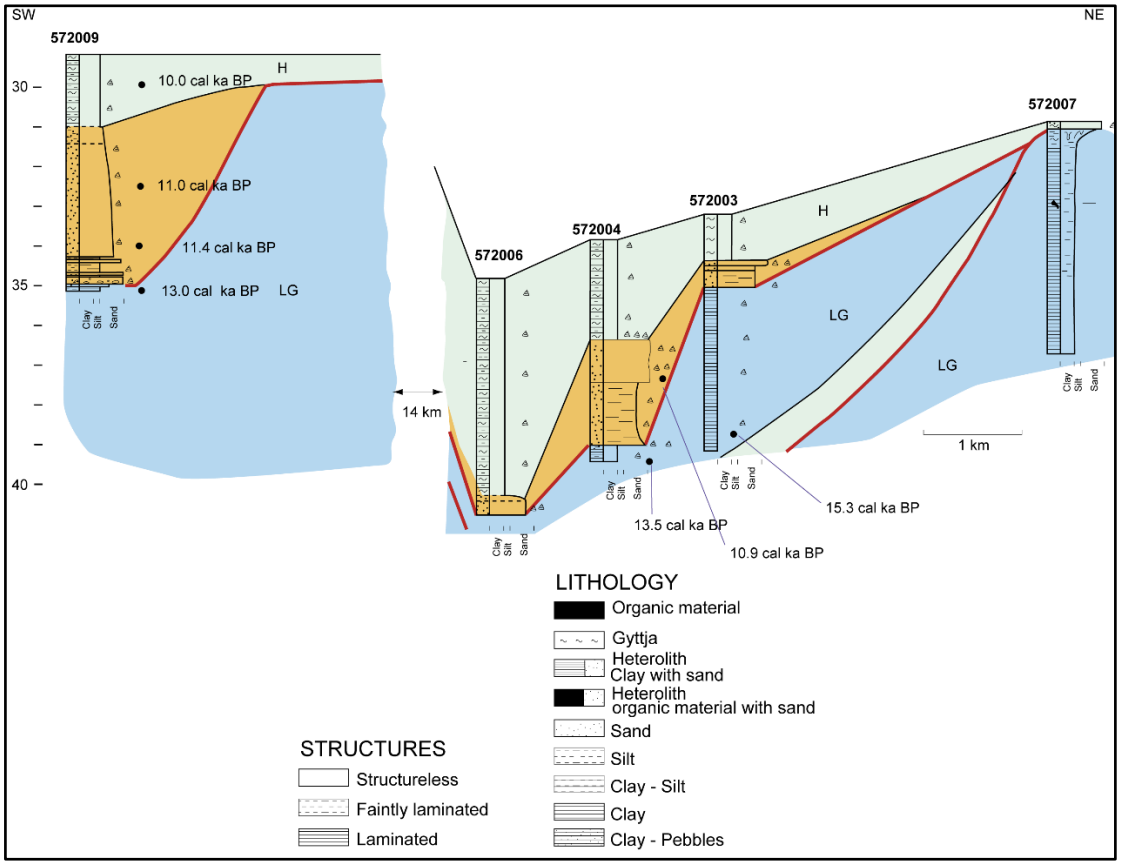

Figure 5.4. Sedimentological logs and log correlations. Sedimentological signatures are indicated; for description of stratigraphical signatures see Figure 5.4. Detailed information on C-14 dating results are given in Jensen et al. (2002).

The internal reflectors are distinct and show onlap in the shallow, landward direction and downlap in the basin-ward direction.

The vibrocores 572003 and 572004 (Figure 5.3 and Figure 5.4) penetrated into the highstand sediments, which consist of structureless clay with marine shells and a mixture of silt and fine sand. Distinct bioturbation is also observed.

Age determinations of a shell of *Portlandia arctica* (572003) from the unit's lower part and of a shell of *Astarte borealis* from the upper part gave dates for the highstand sedimentation period to 15.0–13.5 cal. ka BP.

The LG II sequence thus indicates a relative sea-level fluctuation in the area, but a close look at the sparker line 572014 (Figure 5.2) reveals that below the local depression the parallel reflectors of sequence LG I are heavily contorted, and in the bedrock a depression is observed.

Comparisons with interpretations of deep seismic data (Lykke-Andersen et al. 1993) and the morphology of the pre-Quaternary surface (Figure 5.1) show that the NW–SE-elongated depression south-east of Anholt may originate from normal fault activity along one of the major fault zones in the Kattegat region (Liboriussen et al. 1987), as also suggested by Gregersen et al. (1996).

Further support for such a normal fault activity is the presence of a sharp erosional LGII lower boundary down to a level of about 60 m b.s.l. in the area of the local depression (Figure 5.2). This form a marked contrast to the conformity elsewhere identified at basin depths greater than about 40 m b.s.l. A plausible explanation for this phenomenon is that the initial fast isostatic rebound resulted in a regression producing a general erosional unconformity down to a level of about 40 m b.s.l. At about 15 cal. ka BP the isostatic adjustment was accompanied by reactivation of the blocks in the old wrench zone (piano-key tectonics (Eyles & McCabe 1989)), which caused downfaulting in elongated depressions and led to a local relative water level rise and the development of an extra depositional unit. The upper boundary of this extra unit developed after downfaulting had ceased at about 13.5 cal. ka BP. Thereafter, the general regression continued until the eustatic sea-level rise surpassed the isostatic rise in the early Holocene.

5.2.5 Distribution of late glacial deposits

The distribution of the combined thickness of the late glacial deposits LG I and LG II has previously been estimated in a general mapping project by (Lykke-Andersen 1987) the distribution in the Hesselø OWF and cable corridor is presented in Figure 5.5 and shows a maximum thickness of more than 75m in the northern Hesselø OWF and in general more than 25m.

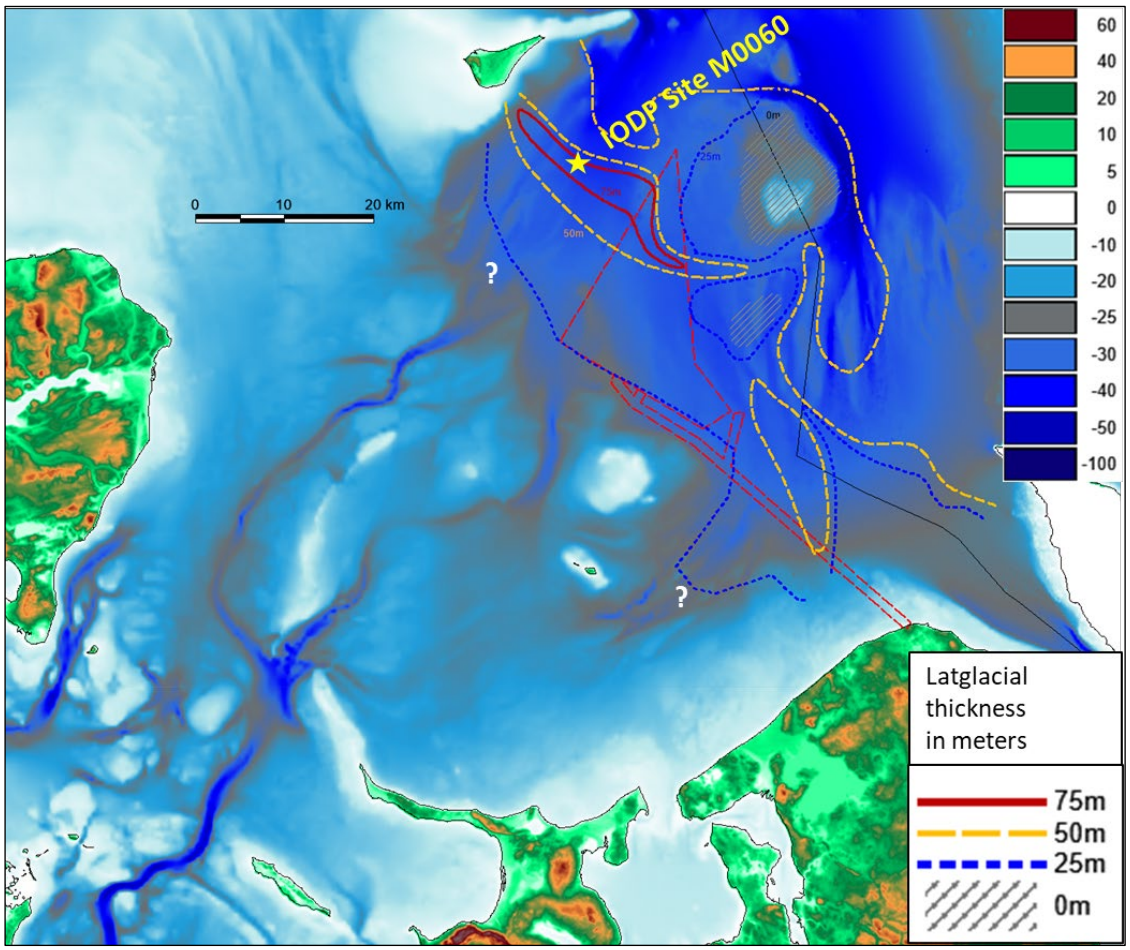

Figure 5.5 Distribution of the combined thicknes of Unit LG I and LG II late glacial deposits. Modified from Lykke-Andersen, 1987.

5.2.6 H – Holocene deposits

Unit H is the youngest seismic sequence in the region. Its thickness varies from about 20 m in the basins to less than a few metres in the shallow areas (Figure 5.2 and Figure 5.4). The lower boundary, i.e. a type I sequence boundary, is an erosional unconformity seen down to a level of about 35 m below sea level, below which conformity prevails. On the basis of the internal reflection pattern, the sequence is divided into a lower lowstand systems tract and an upper transgressive systems tract. The lowstand systems tract is developed as wedge-shaped structures in the basin areas (Figure 5.4) and as a beginning infill of incised palaeo-Storebælt valleys (Figure 5.5; vibrocore 572009). In both cases the systems tract is characterized by rather chaotic internal reflection patterns. The transgressive systems tract consists of basin deposits with reflectors that onlap in the landward direction, and downlap in the basin-ward direction (Figure 5.2 and Figure 5.4). A more complex transgressive palaeo-barrier lagoon/estuary system existed in the more shallow southern part of the survey area (Bennike et al. 2000, Bendixen et al. 2015, 2017).This lagoon system was characterized by an initial transgression unit, backstepping barrier-lagoon sediments and younger, deeper-water sediments. The lowstand wedge structures are lithological documented by vibrocores 572003, 572004 and 572006 (Figure 5.5). The sediments consist mainly of weakly laminated,

medium- to coarse grained sand with abundant shallow-water marine molluscs and foraminifers. Radiocarbon dating of *Mytilus edulis* from core 572004 shows that the lowstand sedimentation took place in the early Holocene (Jensen et al. 2002). The infill of the incised palaeo-Storebælt valley found in vibrocore 572009 (Figure 5.5) consists of a basal, 1 m thick unit of interlayered medium and coarse grained sand layers and laminated silt containing littoral and shallow-water marine molluscs and foraminifers. The sediment succession as well as the dating of *Betula nana* bark fragments point to an initial lowstand littoral deposition at about 13 cal. ka BP. The sedimentary conditions ranged from a normal low-energy environment upstream to a high-energy environment exposed to storm surges in the estuary. This initial phase is followed by an interval represented by about 3.5 m of structureless, fining upwards, medium to fine grained sand also with abundant littoral and shallow-water marine molluscs and foraminifers. Dating results (Jensen et al. 2002) demonstrate that the incised valley infill corresponds to the basin lowstand wedge sedimentation from the early Holocene. The uppermost 1.5 m of vibrocore 572009 consists of structureless clay to fine sand, which contains marine molluscs and foraminifers indicative of shallow to deeper-water marine environments. These sediments are dated to about 10 cal. ka BP.

5.2.7 Stratigraphy of southern Kattegat depositional sequences

The stratigraphic relationship and geometry of the described depositional sequences are illustrated by a schematic stratigraphical cross section (Figure 5.6), while the chronological evolution is shown by a chronostratigraphic chart (Figure 5.7). In addition, the regional relative sea-level changes are presented as shoreline displacement curves in comparison with the local relative sea level changes indicated by the sequence stratigraphy in the downfaulted depressions (Figure 5.8). In the non-faulted depositional areas, the seismic data and vibrocores 572009 and 572017 support the existing Late Weichselian model for the region (Mörner 1969,1983). This model shows that the last deglaciation progressed under highstand sea-level conditions, followed by a continuous moderate regression until the eustatic sea-level rise surpassed the glacio-isostatic rebound in the early Holocene (Figure 5.8). Our detailed sequence-stratigraphical studies show, however, that the Late Weichselian isostatic adjustment must have resulted in reactivation of major faults in the Fennoscandian Border Zone. Heavily contorted parallel reflectors in the late glacial sequence LG I associated with a local NW–SE-elongated depression in the underlying bedrock and the existence of an extra sequence LG II with a sharp erosional lower boundary supports the normal fault reactivation of Late Cretaceous and Tertiary inversion reverse faults. Thus, we provide further evidence for late glacial faulting in Fennoscandia, which can be related to isostatic rebound as previously reported by Arvidsson (1996). AMS C-14 dating of molluscs from the transgressive and highstand systemstracts of sequence LGII in vibrocores 572003 and 572004 reveal that the downfaulting took place in the time interval 15–13 cal. ka BP. The littoral samples from the lowstand systemstract around 11 cal. ka BP, however, do not yield evidence of a difference in water level (Figure 5.8). This implies that the reactivation started shortly before 15 cal. ka BP.

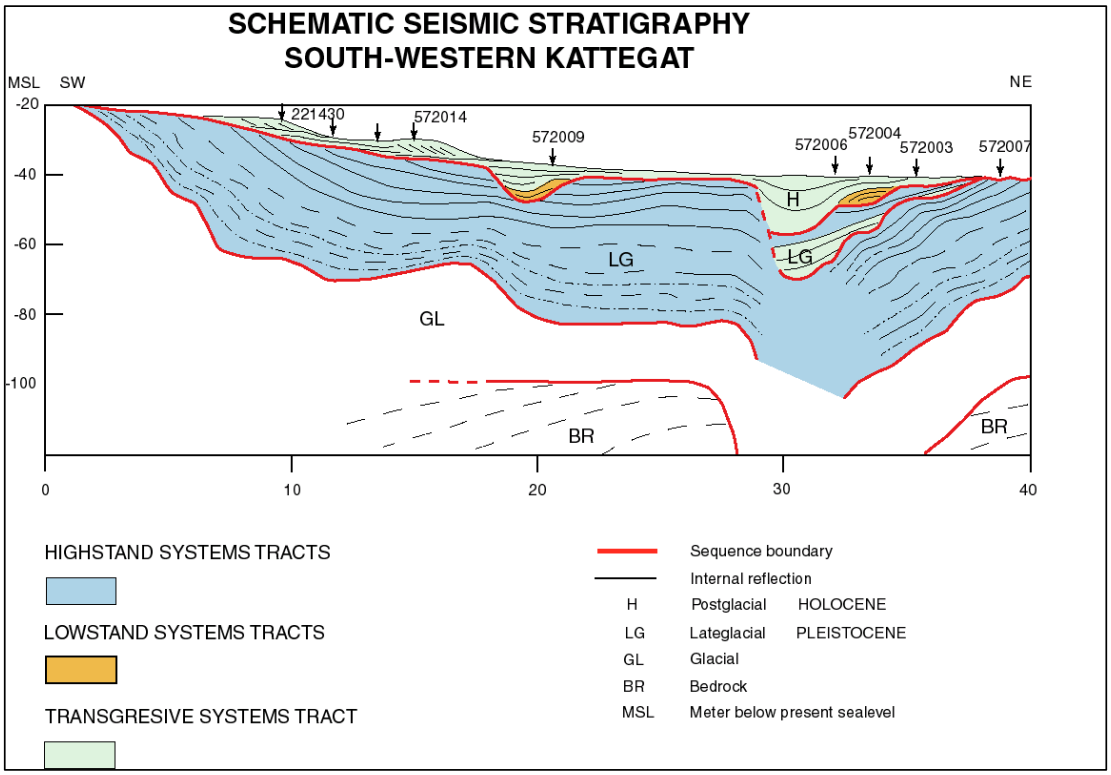

Figure 5.6. A schematic SW–NE-orientated stratigraphic cross-section for southern Kattegat. For location see Figure 5.1

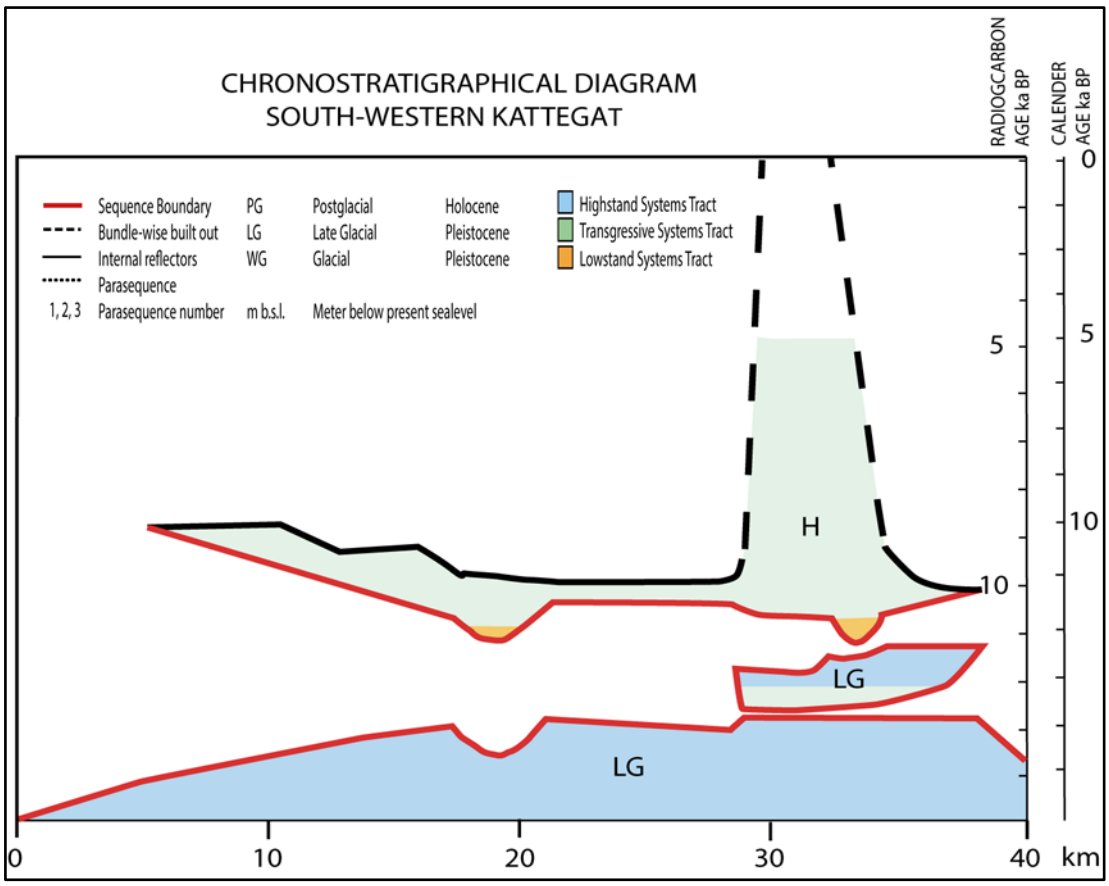

Figure 5.7. A chronostratigraphical chart for southern Kattegat.

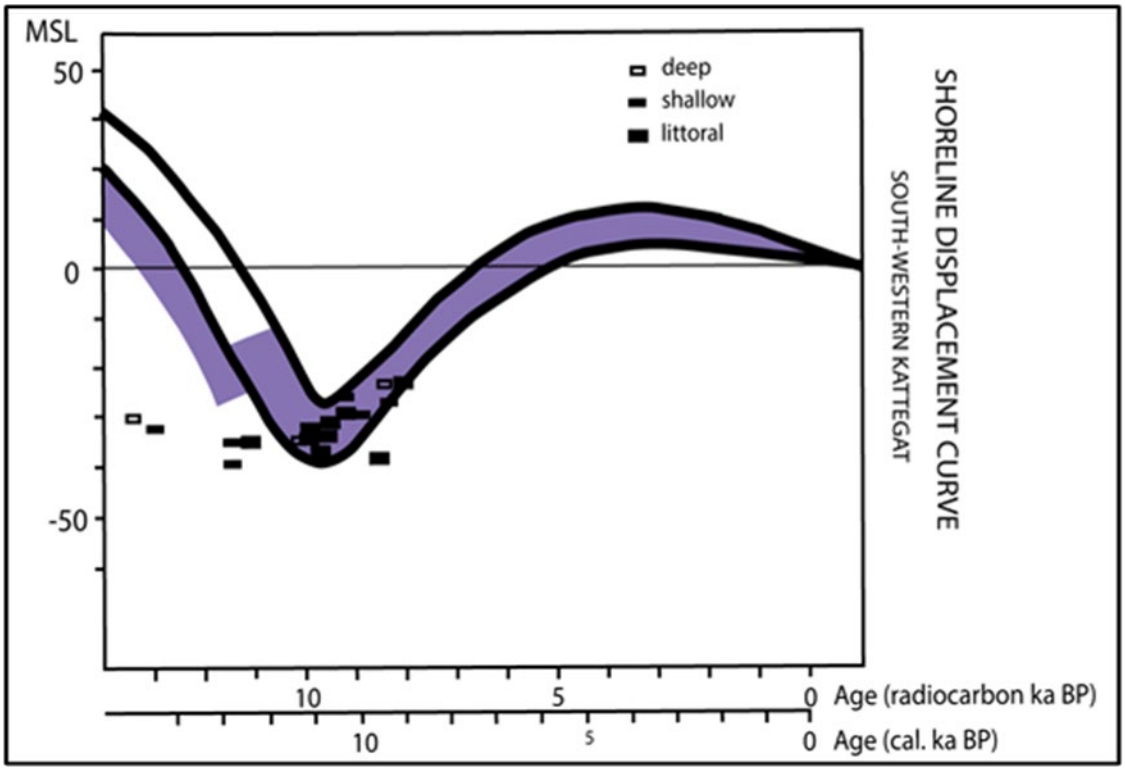

Figure 5.8. Shoreline displacement curves for the southern Kattegat. The two solid black curves indicate the range of shoreline displacements in non-faulted regions of the study area (modied after Mörner 1983), while the purple area indicates the relative sea level changes interpreted from the sequence stratigraphy in the down-faulted NW–SE-striking depression. Radiocarbon-dated samples are indicated as deep >10 m, shallow 2–10 m or littoral 0–2 m.

Large-scale surging and a general recession of the continental ice sheet margins around the North Atlantic may have result in fast isostatic adjustment and subsequent faulting in the ice marginal zones. At that time the regression had already reached a level of about 30 m b.s.l. in southern Kattegat, producing an erosional (wave-induced) unconformity down to a level of about 40 m b.s.l., which was subsequently downfaulted to about 60 m b.s.l. in the reactivated area (Figure 5.2). The local relative water level rise (Figure 5.8) in the fault depression resulted in the development of an extra sequence (Figure 5.6 and Figure 5.7). The reactivation had ceased before 11 cal. ka BP when the regression stopped in the early Holocene. Early Holocene lowstand basinal onlapping and littoral sand deposition occurred before the ongoing transgression of the shallower parts of the southern Kattegat produced basal transgression deposits followed by backstepping barrier lagoon sediments and younger deeper water sediments (Bennike et al. 2000).

Initiation of the NW–SE-elongated downfaulting shortly before 15 cal. ka BP and the formation of an extra sequence LGII may support previous conclusions by Bergsten & Nordberg (1992) that the Baltic Ice Lake suddenly was drained through the Øresund about 15 cal. ka BP. Our findings suggest that fault reactivation may have triggered the Baltic Ice Lake drainage, and simultaneously favoured the inflow of marine water from the Skagerrak.

6. IODP M0060 contribution to geological model

During Integrated Ocean Drilling Program (IODP) Expedition 347 in September 2013, cores were recovered from two holes at Site M0060 (near Anholt island), with an average site recovery of 90.69%. The water depth was 31.2 m, with a tidal range of <30 cm. A total depth of 232.50 m b.s.f. was reached. Piston coring was used for the uppermost ~83 m b.s.f., where recovery was >90%. Between 83 and 200 m b.s.f., a combination of piston coring, nonrotating core barrel, and extended nose coring was used to optimize recovery (IODP link http://publications.iodp.org/proceedings/347/104/104_3.htm). The obtained sediment sequence was divided into seven different lithostratigraphic units (Andrén et al. 2015).

Description of lithology and downhole core logging was performed with physical parametres illustrated in Figure 6.1.

Later scientific studies of biostratigraphy and radiocarbon dating has resulted in a age-depth model for the three upper units in the interval 0–81.60 m b.s.f. (Friberg 2015; Hyttinen 2020).

6.1 Unit I 0–6.00 m b.s.f.

Unit I is composed of grey, massive, fine to medium thickly bedded sand with common marine bivalve and gastropod shell fragments, including *Cerastoderma* sp., *Macoma balthica*, and *Turritella communis*. Two distinct fining-upward shell-rich beds were found in this unit as well. The sand is generally well sorted, and quartz sand grains are subrounded to rounded. The sand was deposited in a near-shore marine depositional environment. Fining-upward shell-rich beds signal deposition near the wave base; therefore, the approximate bathymetry would be similar to the modern situation.

Unit I corresponds to Holocene deposits (H) described in chapter 5.2.6.

6.2 Unit II 6.10–24.70 m b.s.f.

Unit II consists of dark greenish grey interlaminated sandy clayey silt and fine- medium grained sand with dispersed clasts. Sand laminae are 0.5–3 cm thick and occur in packages unequally spaced within the silt. The laminae are inclined, and they are deformed as a primary sedimentary structure. Quartz sand grains dispersed within the silt are angular to subrounded, and the sediment is moderately well sorted. Reworked mollusc shell fragments are found throughout, and reworked diatom fragments are common in smear slides from this unit. Sparse bioturbation is observed near the bottom of this unit between black, presumably iron sulphide laminae. Gypsum was observed macroscopically and in smear slides. The bottom of the unit is sparsely bioturbated between iron sulphide laminated intervals, possibly due to changing stratification of the water column coupled to salinity changes. The deformation in the upper part of the unit is likely due to slumping and possibly the result of increased sedimentation rate. With the presence of dispersed outsized gravel clasts, the lithologic changes can be interpreted as a prograding, ice-influenced deltaic environment.

Unit II corresponds to Younger late glacial deposits (LG II) described in chapter 5.2.4.

6.3 Unit III 24.70-81.60 m b.s.f.

Unit III is characterized by dark greyish brown to grey parallel laminated clay and silt with dispersed clasts. In Subunit IIIa, discrete millimetre-scale silt and fine sand laminae occur as packages of 2–4 laminae and are either well preserved or disrupted, possibly due to loading or bioturbation. Laminae are irregularly spaced and generally 3–6 mm thick, and their abundance increases upward through the unit. Subunit IIIa locally has a reddish hue. Numerous black, possibly iron sulphide, bands are present throughout the unit and become especially prominent in Subunit IIIb. Subunit IIIc has a minor interlaminated sand component. This unit can be interpreted as an ice-influenced lake or marginal marine environment. Silt laminae in Subunit IIIa may represent bottom current activity. The outsized gravel clasts may have originated from ice rafting from a calving glacier at a distance from the drilled location. The presence of iron sulphide bands within the sediment, especially in Subunit IIIb, may be due to periodic oxygen-poor conditions and a stratified water column, where organic matter may have accumulated to form the precursor to the diagenetic sulphides.

Unit III corresponds to Older late glacial deposits (LG I) described in chapter 5.2.3.

6.4 Unit IV 81.60–85.70 m b.s.f.

Grey interbedded sand, silt, and clay with dispersed clasts and clast-poor diamicton were identified in Unit IV. Both rock clasts and intraclasts are common in this unit, and the strata are intensely folded or contorted. Clast assemblages are polymict. The moderately to poorly sorted character of sediments, the polymict clast assemblage, and the abrupt shifts in lithologies may indicate deposition in an ice-proximal depositional environment. The deformation of the sediments may be due to slumping into an aquatic depositional environment.

6.5 Unit V 95.04–116.7 m b.s.f.

This unit is characterized by black and grey sandy silty clay with dispersed clasts. Mollusc shell fragments are common, especially *Turritella* sp. Multiple horizons with shell fragments are present. Cores in this interval are poorly recovered and highly disturbed as a result of drilling. This unit probably represents a shallow-marine depositional environment.

6.6 Unit VI 116.70–146.10 m b.s.f.

Unit VI consists of grey, fine to medium, massive well-sorted sand. Rare shell fragments occur near the top and the bottom of this unit. The sand is quartz-rich, and quartz grains are well rounded. Some decimetre-scale clay and silt-rich interbeds are recorded. At the bottom of the unit, pebbles and intraclasts are found. Based on the well-sorted nature of the sand, this unit may represent a high-energy fluvial or deltaic depositional environment. The mud interbeds may represent over-bank deposits or channel fills. The rare shell fragments are likely locally reworked.

6.7 Unit VII 146.10–229.60 m b.s.f.

Unit VII is dominated by a dark grey clast-poor sandy diamicton with dispersed (<1%) to uncommon (1%–5%) charcoal clasts up to 3 cm in diameter. The structure is mostly homogeneous with localized very rare silty to clayey laminae a few centimetres in thickness. Isolated intervals of dispersed (<1%) white carbonate rock fragments, fine mollusc shell fragments and silt intraclasts are present. The uppermost part consists of grey well-sorted clay/silt with locally clast-poor muddy to sandy diamicton. The clay appears mostly homogeneous with some weak lamination by colour, especially in the upper part. Higher organic contents and strong odor were common. Fining upward of Unit VII between 158 and 146.1 m b.s.f. was recorded. The base of this moderately sorted unit extends deeper than 229.6 m b.s.f., as it was not penetrated. However, on open holing to 232.50 m b.s.f., the string became stuck and it was not possible to recover a sample to verify the lithology. Because of the general lack of visible grading and moderate sorting of Unit VII, deposition by mass transport processes like massive debris flows is possible. The contacts between and thickness of individual debris flow beds are uncertain and potentially macroscopically not visible. The high charcoal content could be related to the outcropping of Jurassic sediments east of Site M0060. During the time of deposition, it is possible that large amounts of reworked Jurassic sediments including fossil soil horizons with coal seams were delivered to this location.

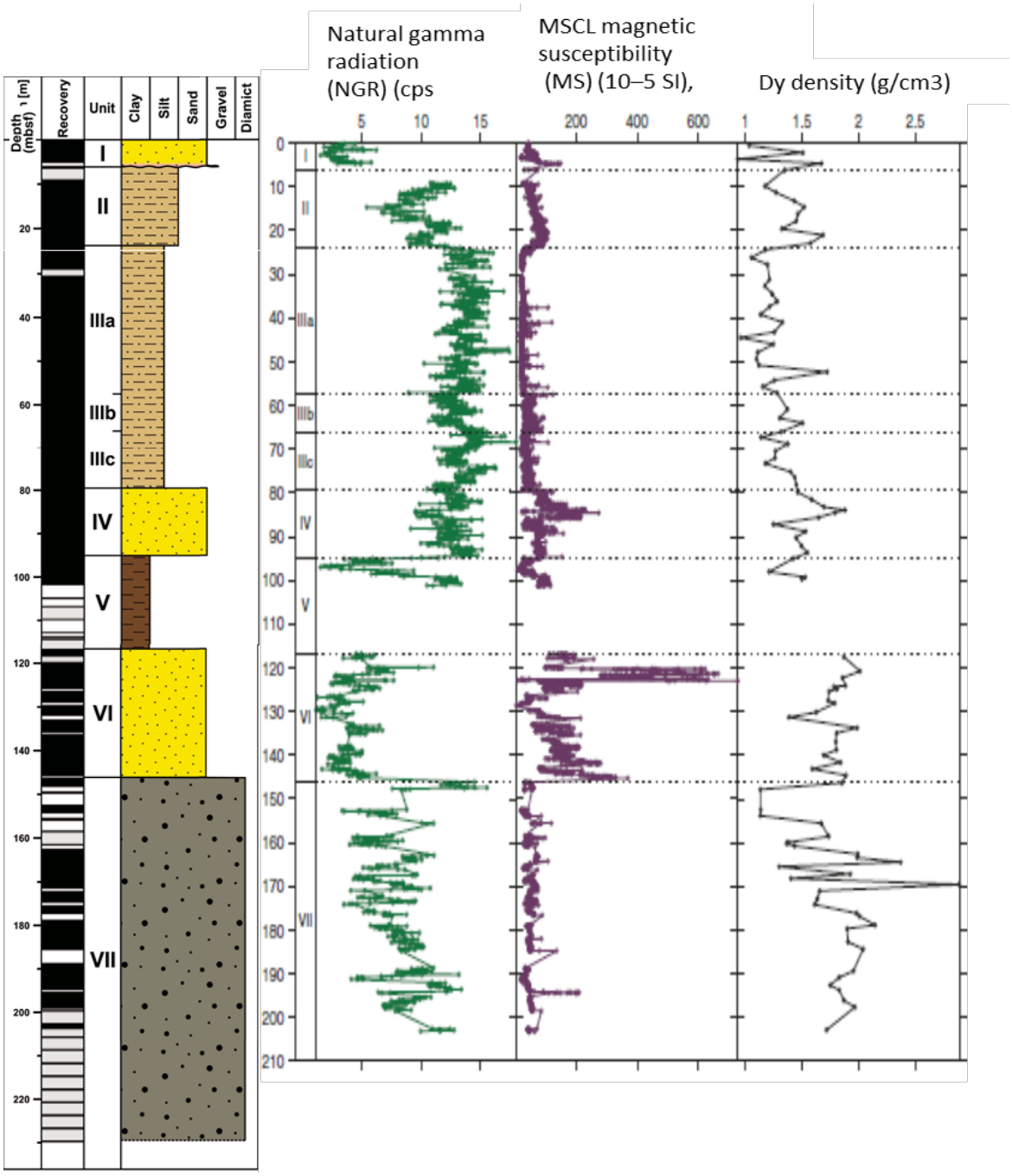

Figure 6.1. IODP Site M0060 core lithology and downhole logging results.

6.8 Age–depth model

An age–depth model for the uppermost 80 m of IODP Site M0060 has been established. The studied sequence shows evidence for the onset of deglaciation at c. 18 ka BP. Sedimentation at the site of core M0060 was relative continuous until 13 ka BP, when there is a large hiatus in the record until c. 8.3 ka BP. The uppermost sediment unit contains redeposited material, but it is estimated to represent only the last c. 8.3 ka BP. The age–depth model is based on

17 radiocarbon dated samples. This gives us an idea about major changes in the environment, such as transition from glaciomarine proximal to glaciomarine distal to marine conditions, and their connections to known events and processes in the region.

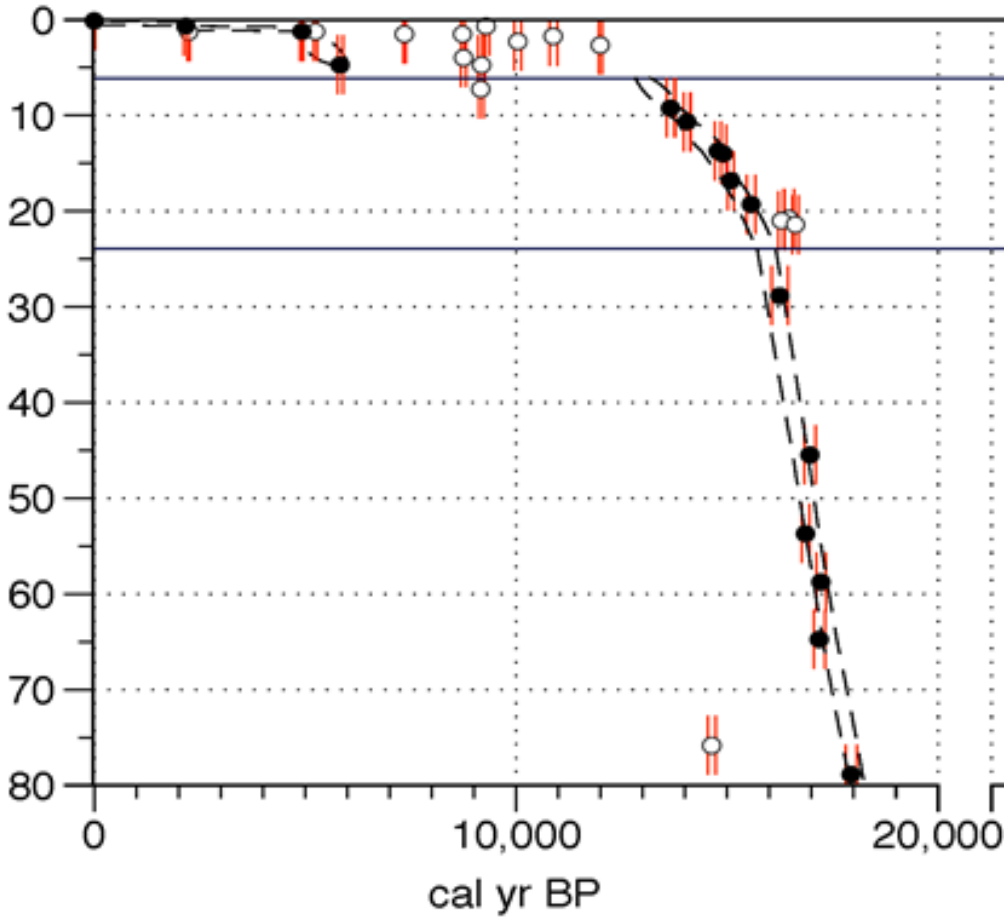

Figure 6.2. Age–depth model for the IODP site M0060. Dating results are plotted against depth (mcd), ages used in the model are indicated by black dots. Samples with a white dot are omitted from the age–depth model. The age scale is in calibrated years before present (cal yr BP; BP=1950 AD). The dashed lines indicate a 95.4-% likelihood age range and the solid horizontal lines show the boundaries between Unit I, Unit II and Unit III (Hyttinen et al. 2020).

According to the age–depth model, the top of Unit III at 23.84 mcd has an age of 15.9 ka. This age is an upward extrapolation from the uppermost sample in the unit at 28.8 mcd, based on the average sedimentation rate within Unit III.

In a similar way, the top of Unit II at 6.0 mcd is dated to 13.0 ka (± 100 yr) based on the uppermost accepted sample at 9.22 mcd. This estimate gives a minimum mean sedimentation rate for Unit I of 0.05 cm/yr. However, using the lowermost accepted sample in Unit I at 4.17 mcd (5.8 ka), the average sedimentation rate in the upper part of Unit I is 0.072 cm/yr.

The lower boundary of Unit I is dated is to 8.3 ka.

7. Seismic correlation to IODP site M0060

The seismic data from 2002 and the later 2013 data show a clear correlation to the M0060 lithological units and a detailed age-depth model covering the late glacial and Holocene time periods.

7.1 Stratigraphic correlation of 2002 seismic data and site M0060

The correlation shows that only a thin top unit of a few metres represent the Holocene time period while more than 70 m represent the late glacial time period.

The late glacial period is divided into two units due to neotectonic adjustment (downfaulting).

The glacial deposits are in general thin except in the down faulted narrow basins represented by site M0060.

2002 seismic units	Site M0060 Units	Age intervals
H – Holocene deposits	Unit I 0–6.00 m b.s.f.	5.8 - 8.3 ka BP
LG II – Younger late glacial deposits	Unit II 6.10–24.70 m b.s.f.	13.0 - 15.9 ka BP
LG I – Older late glacial deposits	Unit III 24,70-81,60 m b.s.f.	18.0 - 15.9 ka BP
GL Glacial depoists	Unit IV 81.60–85.70 m b.s.f.	
GL Glacial depoists	Unit V 95.04–116.7 m b.s.f.	
GL Glacial depoists	Unit VI 116.70–146.10 m b.s.f.	
GL Glacial depoists	Unit VII 146.10–229.60 m b.s.f.	

Figure 7.1 Correlation of 2002 seismic data and IODP site M0060

7.2 The DAN-IODP-SEIS survey

In 2013 the DAN-IODP-SEIS KAT 2013 High Resolution 2D seismic survey was carried out in a cooperation between GEUS, the Swedish Geological Survey (SGU) and Aarhus University.

The cruise was carried out from 12 June to 14 July on board the SGU survey ship *Ocean Surveyor*. The expenses of the ship time were covered by funding from the Danish Centre for Marine Research (DCH) and by the SGU mapping program.

The Ocean Surveyor standard equipment includes a 10-inch sleeve gun and a SIG 6-channel streamer, Edo Western sediment echosounder, Benthos 1624 and Klein 3000 side scan so-

nars and Kongsberg EM2040 multibeam echosounder. In addition, GEUS, Copenhagen University and Aarhus University provided high resolution 2D airgun and sparker energy sources and a multichannel streamer. The purpose of the cruise was to acquire airgun seismic data down to a maximum of 1.5 sec., sparker seismic data down to 0.5 sec. and Innomar medium parametric sediment echo sounder data down to maximum 100 ms.

7.2.1 DAN-IODP-SEIS line 8008

The NW–SE orientated Line 8008 follows the centre of an elongated depression with a perfect fit to the M0060 lithology and the seismic units.

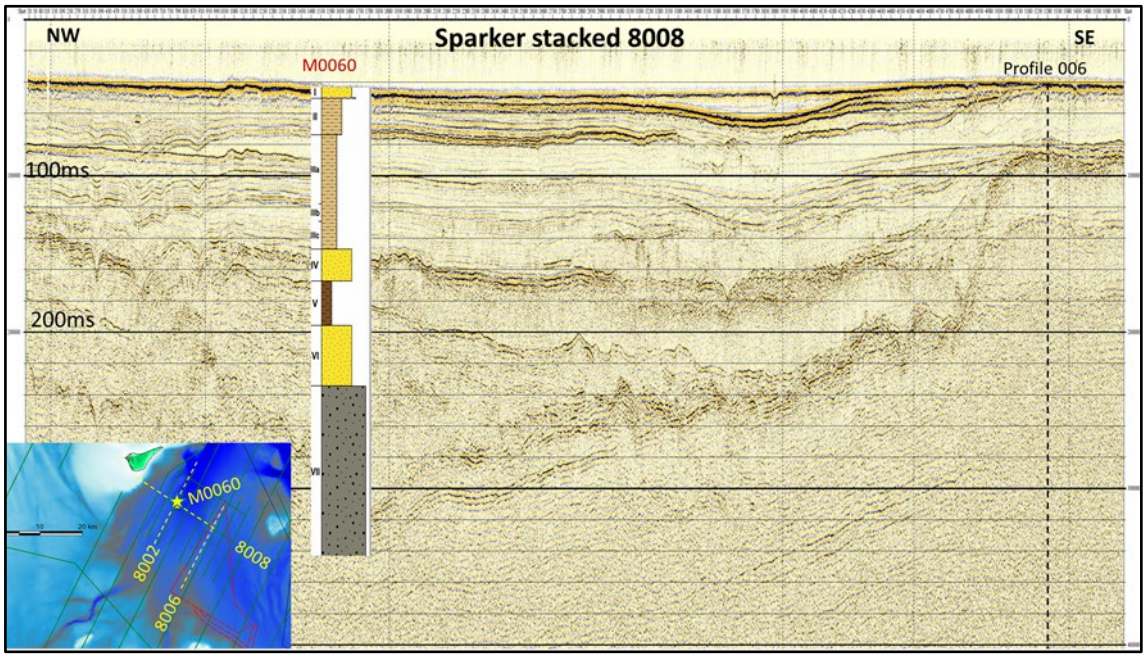

Figure 7.2. Seismic multichannel sparker profile 8008. Core IODP M0060 is indicated, for details se Figure 6.1.

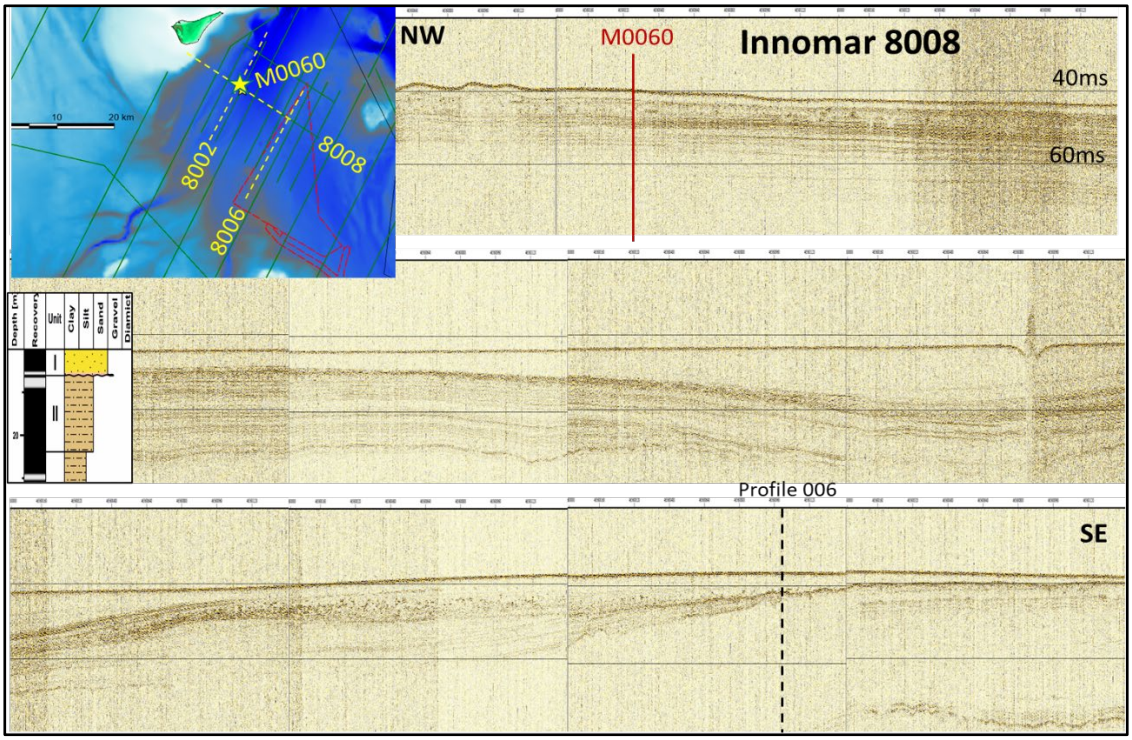

Figure 7.3. Seismic Innomar profile 8008 shows seismic details.

The thick late glacial basin meets a steep boundary close to seismic section 8006 within the Hesselø OWF area.

The overall architecture is presented in Figure 7.2 and details of the internal reflectors of the Holocene basin, the lowstand coastal deposits and the younger late glacial deposits are shown in Figure 7.3.

7.2.2 DAN-IODP-SEIS line 8002

The SW–NE orientated Line 8002 crosses perpendicular to the depression with a perfect fit to the M0060 lithology and the seismic units.

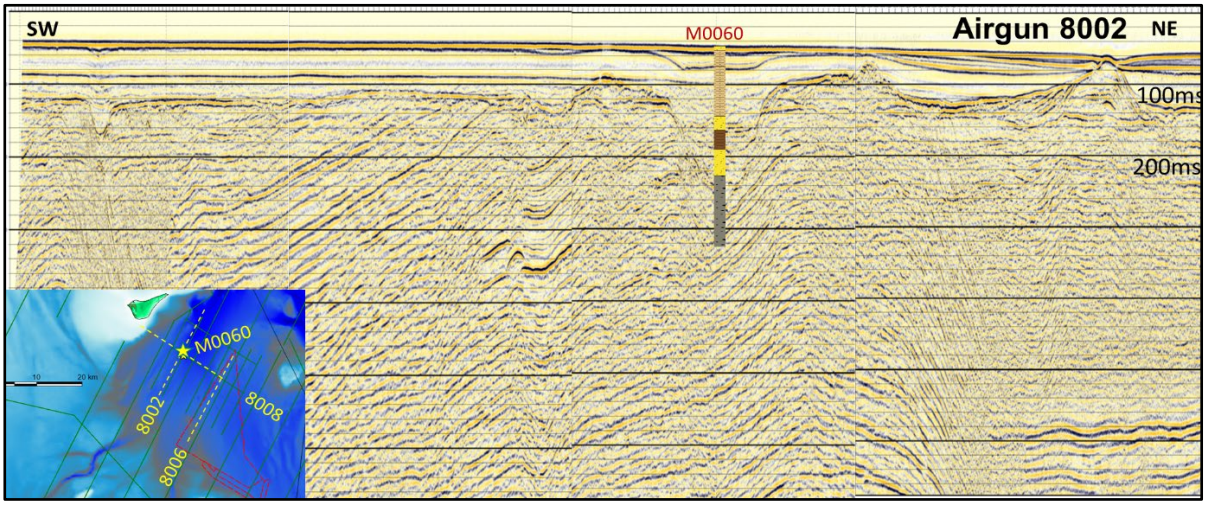

Figure 7.4. Seismic multichannel airgun profile 8002. IODP M0060 indicated, for details se Figure 6.1

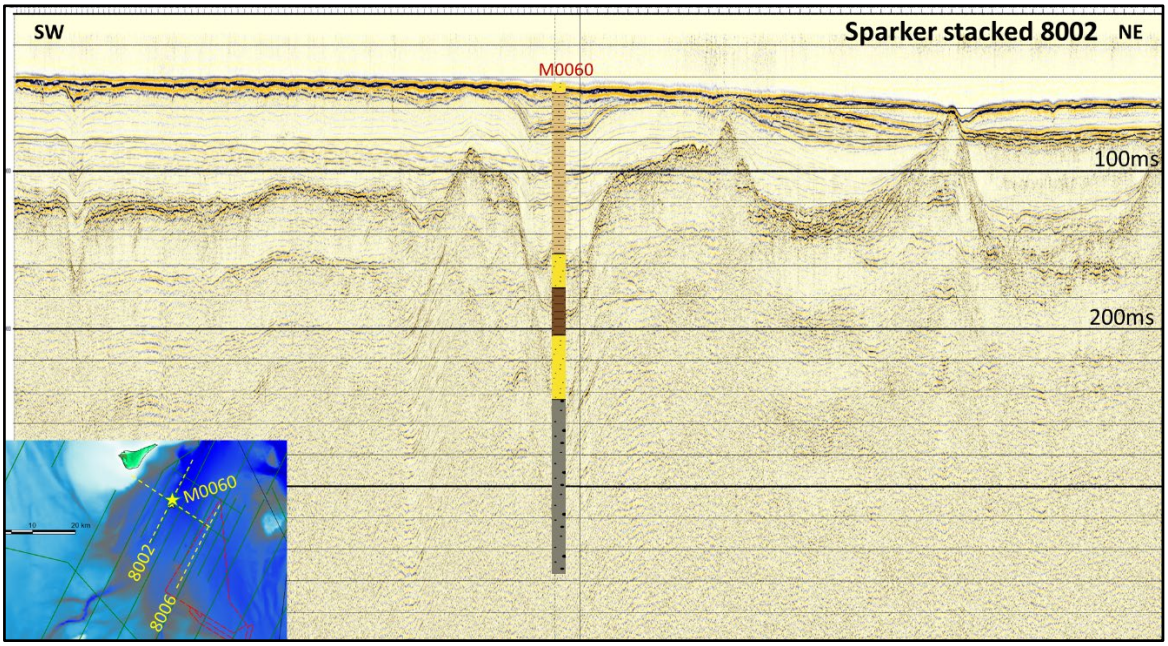

Figure 7.5. Seismic multichannel sparker profile 8002. IODP core M0060 is indicated, for details se Figure 6.1.

The airgun section 8002 (Figure 7.4) shows the deeper bedrock structures, with a clear indication of faulting as the primary reason for the elongated deep basin. In addition, it is obvious that outside the elongated basin the glacial deposits are very thin and covered by nearly 100 ms of late glacial sediments.

Sparker line 8002 (Figure 7.5) cannot resolve the deeper bedrock structures, but it gives a clear impression of the extra sequence developed in unit II Younger late glacial deposits, due to downfaulting.

7.2.3 DAN-IODP-SEIS line 8006

The SW–NE orientated Line 8006 crosses perpendicular to the depression and is located within the Hesselø OWF area.

Line 8006 shows infill of Holocene sediments above the depression and a major thickening of the late glacial deposits. The late glacial deposits thins and fades out in the south-western part where a wedge of Holocene sediments are introduced on top of glacial deposits.

Areas with acoustic disturbance possibly caused by gas in the sediments are indicated (discussed more in chapter 7.2.4.

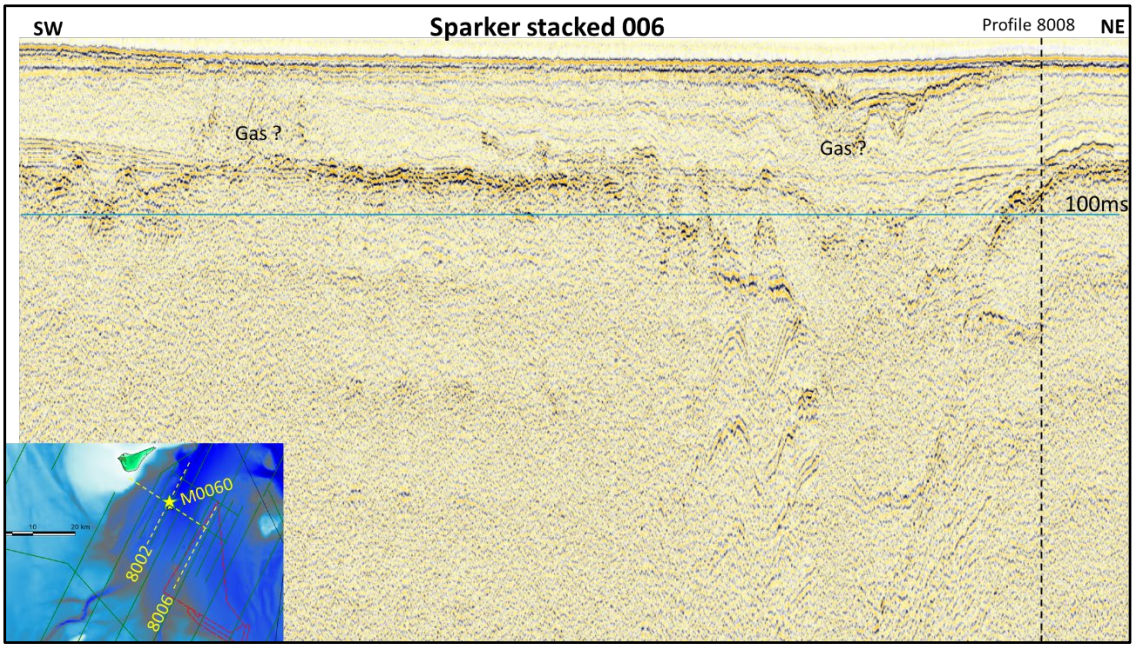

Figure 7.6. Seismic multichannel sparker section 8006.

7.2.4 Acoustic indications of gas in sediments

The DAN-IODP-SEIS survey data have identified a number of areas with acoustic disturbance that could indicate gas in the sediments (Figure 7.7).

This is mentioned as an observation point with reference to earlier gas escape in sediment cores observed both in an Anholt Windfarm core and in IODP core M0060.

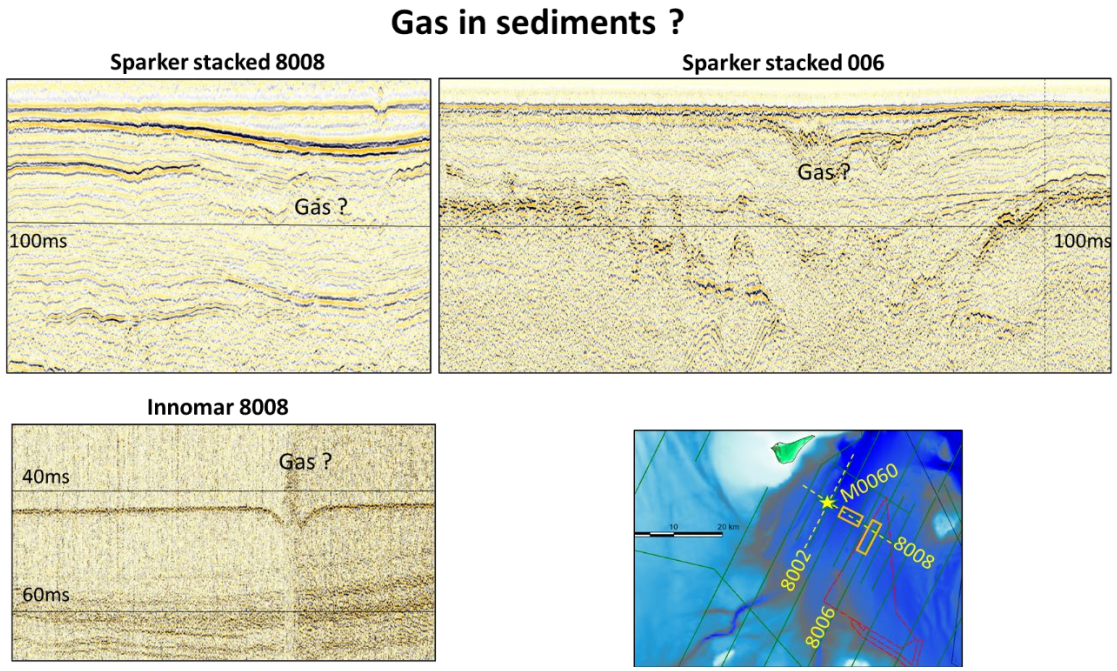

Figure 7.7. Examples of possible gas in the sediments.

The acoustic disturbance is often seen in connection with the elongated depressions but may be interpreted differently. Gas in the Holocene sediments may be related to degassing from organic-rich Holocene layers, that might even escape from the seabed and create pockmarks. Deeper disturbance in the late glacial deposits may be due to thermogenic gas coming from Jurassic sediments that are found close to the sea floor. No conclusive evidence has been found but it should be taken into consideration when planning coring.

8. Geological model Hesselø OWF South and cable corridor

In the previous chapters we have described the general Kattegat south model with focus on the late glacial and older sediments. In the following chapter we will concentrate on the late glacial and Holocene deposits, in the southernmost Hesselø OWF area and the cable corridor.

In the southernmost part of the Hesselø OWF area (Figure 8.1) and the cable corridor glacial deposits are covered by late glacial marine clay and silt with some drop stones. The late glacial deposits were deposited during the highstand period and the upper boundary is an erosional unconformity developed during the regression as already reached close to its maximum lowstand level in the Younger Dryas. The highstand systems tract deposits consist of fine-grained sediments (Jensen et al. 2002a). The unconformity is most significant where erosional channels are found reaching a maximum lowstand erosion depth at 30–40 m b.s.l. during the earliest Holocene, as documented by previous studies (e.g. Bennike et al. 2000; Jensen et al. 2002b). The lowstand period was followed by the initial phase of the Holocene transgression.

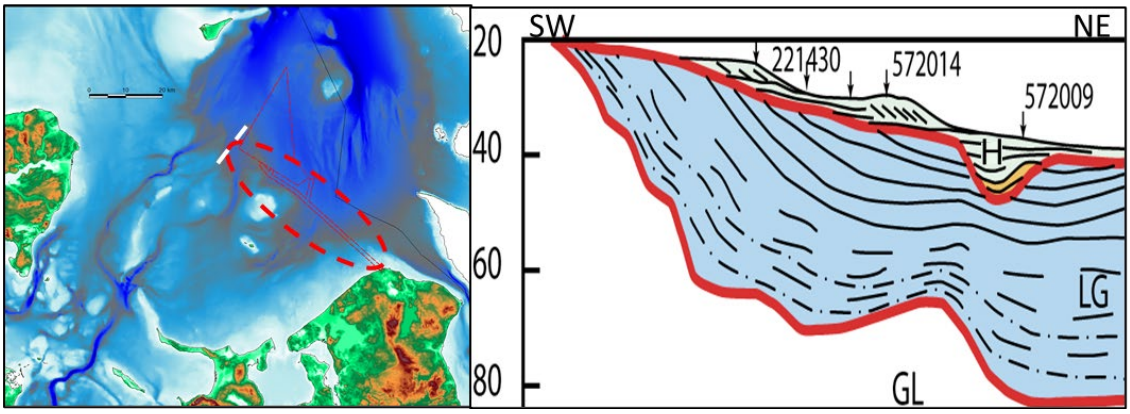

Figure 8.1. Southern focus area (red dashed line) on left figure and schematic section (white dashed line) presented in right figure (H=Holocene, LG=late glacial, GL=glacial).

8.1 Late glacial marine sediments Hesselø OWF South and cable corridor

In the southernmost part of the Hesselø OWF area and the associated cable corridor we are in the marginal part of the southern Kattegat late glacial glaciomarine basin deposition area. On Figure 8.2 the general thickness of the late glacial deposits are shown, based on mapping by Lykke-Andersen (1987). His mapping extended south-west to Lysegrund just south of the Hesselø OWF area. South-east of the windfarm in the area of the cable corridor the late glacial basin deposition continues with a maximum thickness of 50 m, as demonstrated by the raw material mapping program (Figure 8.3; Boomer section 21; Skov og Naturstyrelsen 1987).

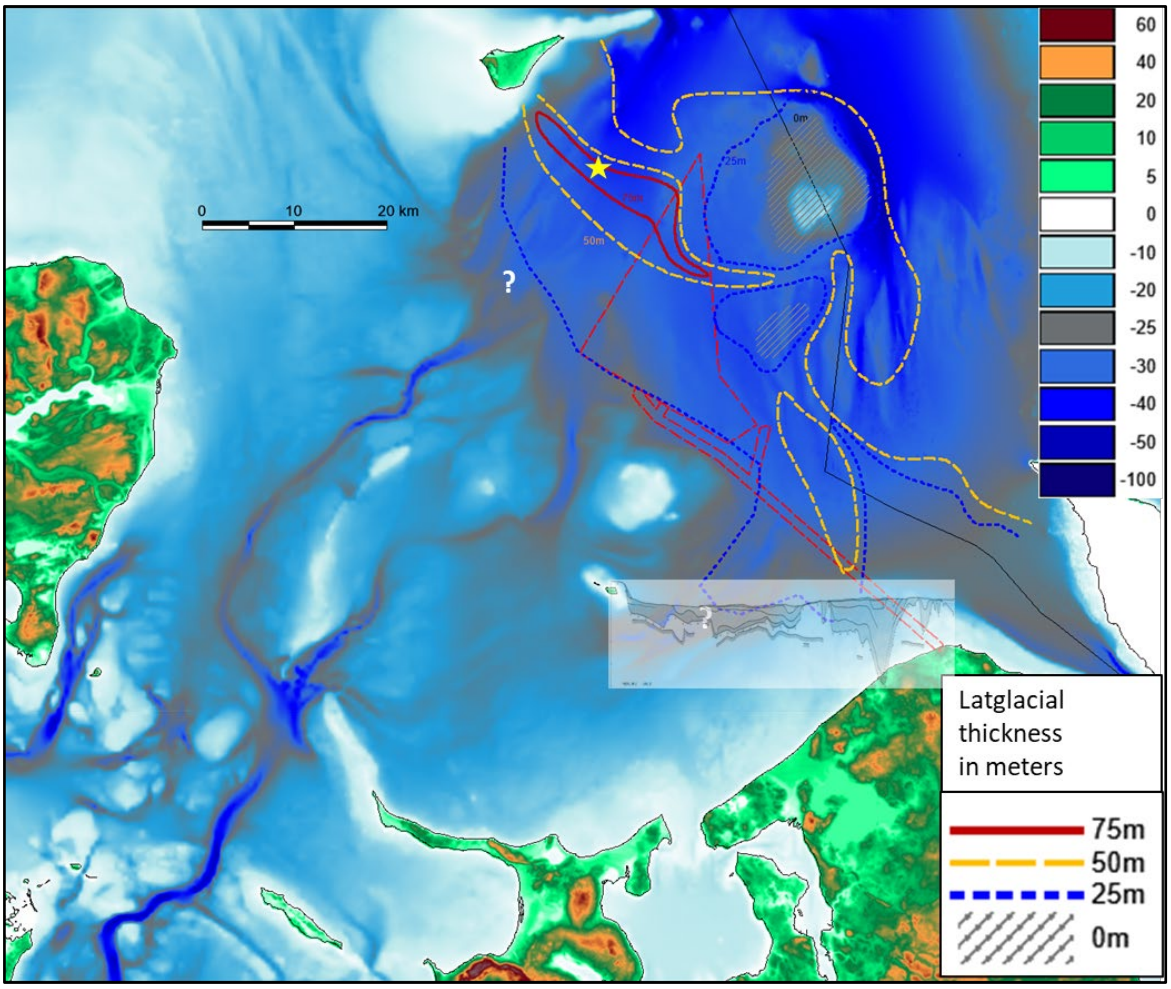

Figure 8.2. Distribution of the combined thicknes of Unit LG I and LG II late glacial deposits, modified from Lykke-Andersen (1987). Location of Boomer section 21 – for details see Figure 8.3.

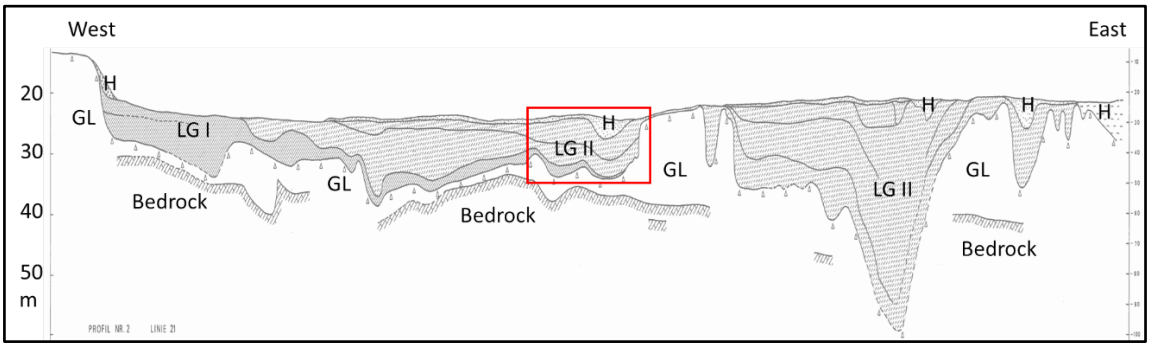

Figure 8.3. Interpreted boomer section 21 (Skov og Naturstyrelsen 1987) (Stratigraphy see Figure 7.1). The red rectangle shows the location of profile 2 in Figure 8.5

8.2 Holocene transgression sediments Hesselø OWF South west and cable corridor

A lowstand erosional unconformity characterizes the shallow areas and lowstand sandy deposits mark the lowstand relative sea-level around 35-40 m b.s.l. (Figure 8.4 and Figure 8.5). The lowstand was followed by a Holocene initial transgression resulting in the formation of a barrier/estuary system in the southwestern Hesselø OWF and a tidally dominated estuary in the southern part of the cable corridor, dominated by fine grained infill and large tidal mouth bars and banks.

8.2.1 Hesselø OWF South west spit barrier and estuary

During the early transgression, sand above the LG silt and clay is interpreted as lowstand Postglacial (PG I) sediment, deposited within erosional channels during coastal marine conditions. Shells of marine mollusks were dated to 10.8–11.7 cal. ka BP in cores 572011 and 572009 (Figure 8.4). The sediments consist primarily of sand with a few cobbles and pebbles, interpreted to be coastal deposits. The distinct difference in the internal reflection pattern of PG I suggests the presence of a primary western channel with more pronounced flow and a secondary eastern channel during the initial transgression. Gradually, the eustatic sea-level rise surpassed the diminishing isostatic rebound and a relative sea-level rise in Kattegat resulted in the deposition of PG II estuarine and coastal deposits. South of the estuary, freshwater channels formed a sandy spit, developed inside the estuary to the southwest, while sand bars and a silty spit formed at the mouth of the estuary, towards the north (Figure 8.4). Elongated ridges developed parallel to the flow of the palaeo-channels creating sand bars and spits located parallel to the channel inlets and with northwards internal progradation. The initial formation base of the spits was dated to 10.9 cal. ka BP on shell material from vibrocore 572016 while the fully developed spit system was dated to 9.9 cal. ka BP. The eastern spit shows a stacked internal pattern within PG II.2 (Figure 8.4), which may indicate an environment with tidal influence. This is also supported by the morphology of the estuary, which is mouth-shaped, as well as by the bar and spit distribution.

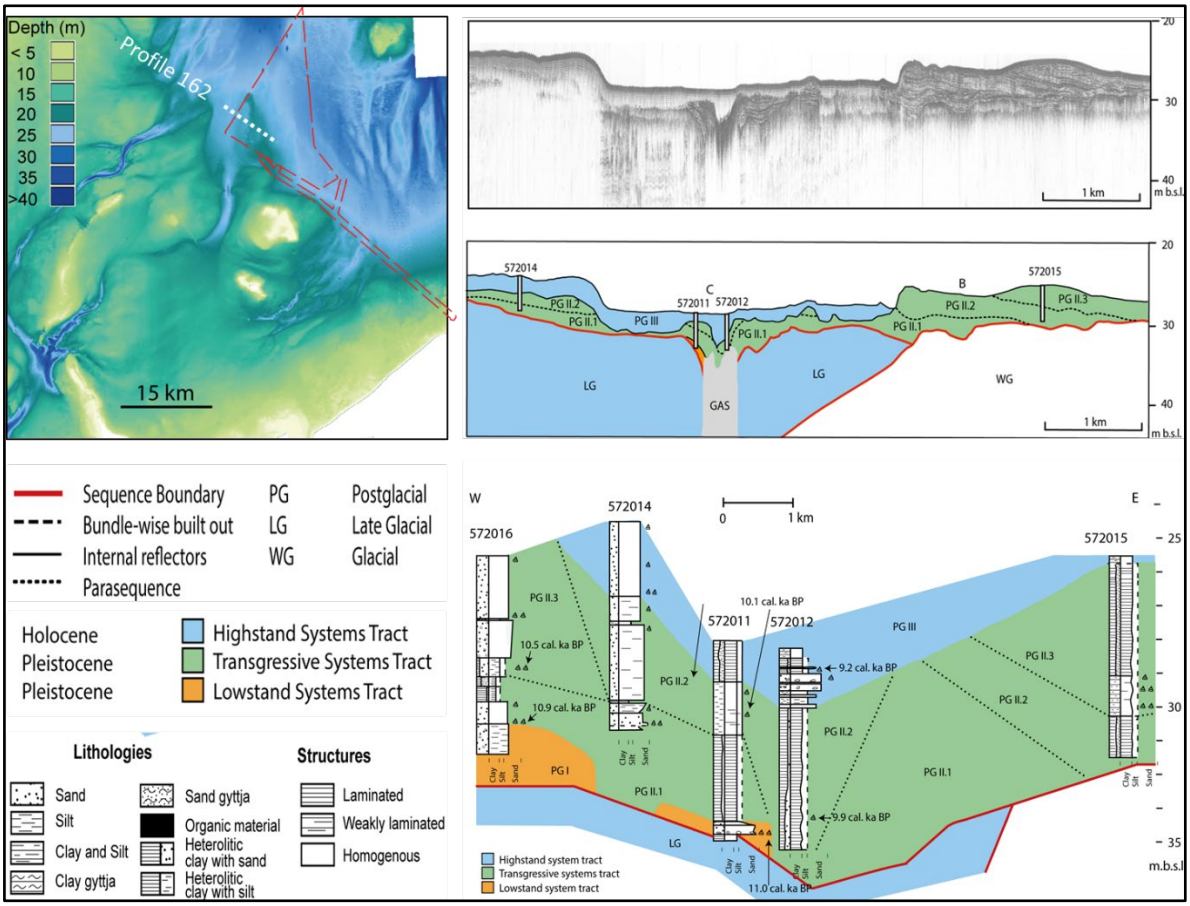

Figure 8.4. Pinger profile 162. The upper profile shows a seismic section from NW to SE and the lower section illustrates the sequence stratigraphical interpretation. The location of the profile is shown in the upper left map. Selected cores (572014, 572011, 572012 and 572015) are illustrated at lower right. Legend lower left.(from Bendixen et al. 2015).

8.2.2 Cable corridor, tidally dominated estuary

The bathymetry data in the cable corridor area (Figure 8.5) show that the water depth increases from the northern coast of Zealand towards the north-east to ca. 40 m, and elongated ridges and channels with a dominant SW–NE orientation occur within the area. The orientation of the ridges does not reflect the present-day hydrographical conditions in Hesselø Bay, southern Kattegat (Myrberg and Lehmann 2013), but represents a coastal setting of a palaeo-river mouth terminating in a funnel-shaped estuary.

The unconformity between late glacial (LG) and Postglacial (PG I), is most significant where erosional channels are found (Figure 8.5). The lowstand PG I sediments interpreted from the cores in this study consist of sand, underlain by peat. A shell of a marine mollusc just above the sand in core PSh-2542 was dated to 11.0 cal. ka BP (Figure 8.5; Christiansen et al.1993). The presence of peat inclusions indicates that, when the sea level was at its lowest, parts of the study area were dry land with coastal wetlands. Lowstand deposits within the Kattegat region have earlier been dated to 11.7–10.8 cal. ka BP (Bennike et al. 2000; Bendixen et al. 2013), which corresponds well with this area.

As the eustatic sea-level rise surpassed the isostatic rebound, the relative sea level in the Kattegat rose, resulting in deposition of PG II coastal and estuarine deposits. Freshwater channels originating from the west formed elongated ridges and bars inside the funnel shaped estuary parallel with the south–southwest to northeast water flow (Figure 8.5). PG II is represented by the elongated ridges and bars that are parallel to the flow of the palaeo-channel. PG II.1 forms the initial bars and deposits in the channels (Figure 8.5). Thereafter, PG II.2 was deposited during progradation towards the north-east. Palaeoenvironmental changes in cores from the southern Kattegat are seen at about 9.6 cal. ka BP (e.g. Christiansen et al. 1993). The foraminiferal assemblages in core PSh-2542 changed from initial shallow water lagoonal brackish water at ca. 11.0 cal. ka BP to conditions more and more influenced by marine conditions and higher sea level (Christiansen et al. 1993). The estuary existed in the period 10.3–9.2 cal. ka BP, during and after the Ancylus Lake maximum high-stand at about 10.3 cal. ka BP. It could be concluded that the drainage of the Ancylus Lake into the southern Kattegat occurred as a non-catastrophic drainage during estuary environment conditions (Bendixen et al. 2017).

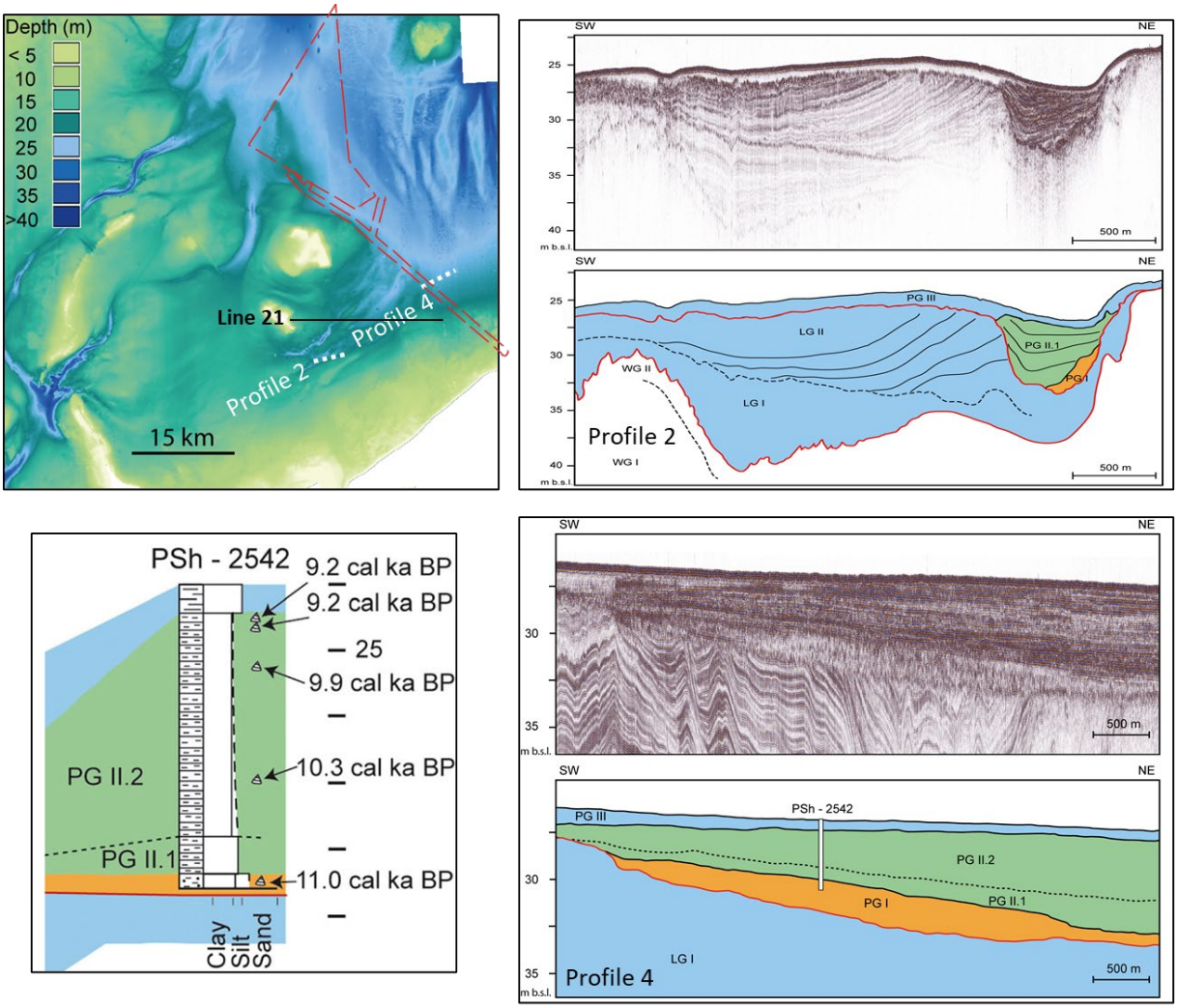

Figure 8.5. Pinger profiles 2 and 4. The upper profiles shows seismic sections from SW to NE and lower sections illustrates the sequence stratigraphical interpretation. The locations of the profiles are shown in upper left map. Location of line 21 from Figure 8.3 is shown. Selected core PSh-2542 is illustrated at lower left. (Reference profiles from Bendixen et al. 2017 and core PSh-2542 data from Christiansen et al. 1993). For legend see Figure 8.4.

8.2.3 Palaeogeographical development of Hesselø OWF South west and cable corridor

Based on the interpretations of the described data, palaeogeographical maps of the 11 cal. ka BP lowstand and the 9.9 cal. ka BP Holocene early transgression has been constructed (Figure 8.6). The palaeogeographic reconstruction is combined with the reconstruction by Bendixen et al. (2017) and it shows the coastal environment during the early Holocene in the southern Kattegat windfarm and cable corridor area. It illustrates lowstand 11cal. ka BP restricted sound through the area and the flow patterns of the multi-branches 9.9 cal. ka BP northern continuation of the palaeo-Great Belt freshwater channel into the Kattegat, with several estuaries and spits as well as numerous bars.

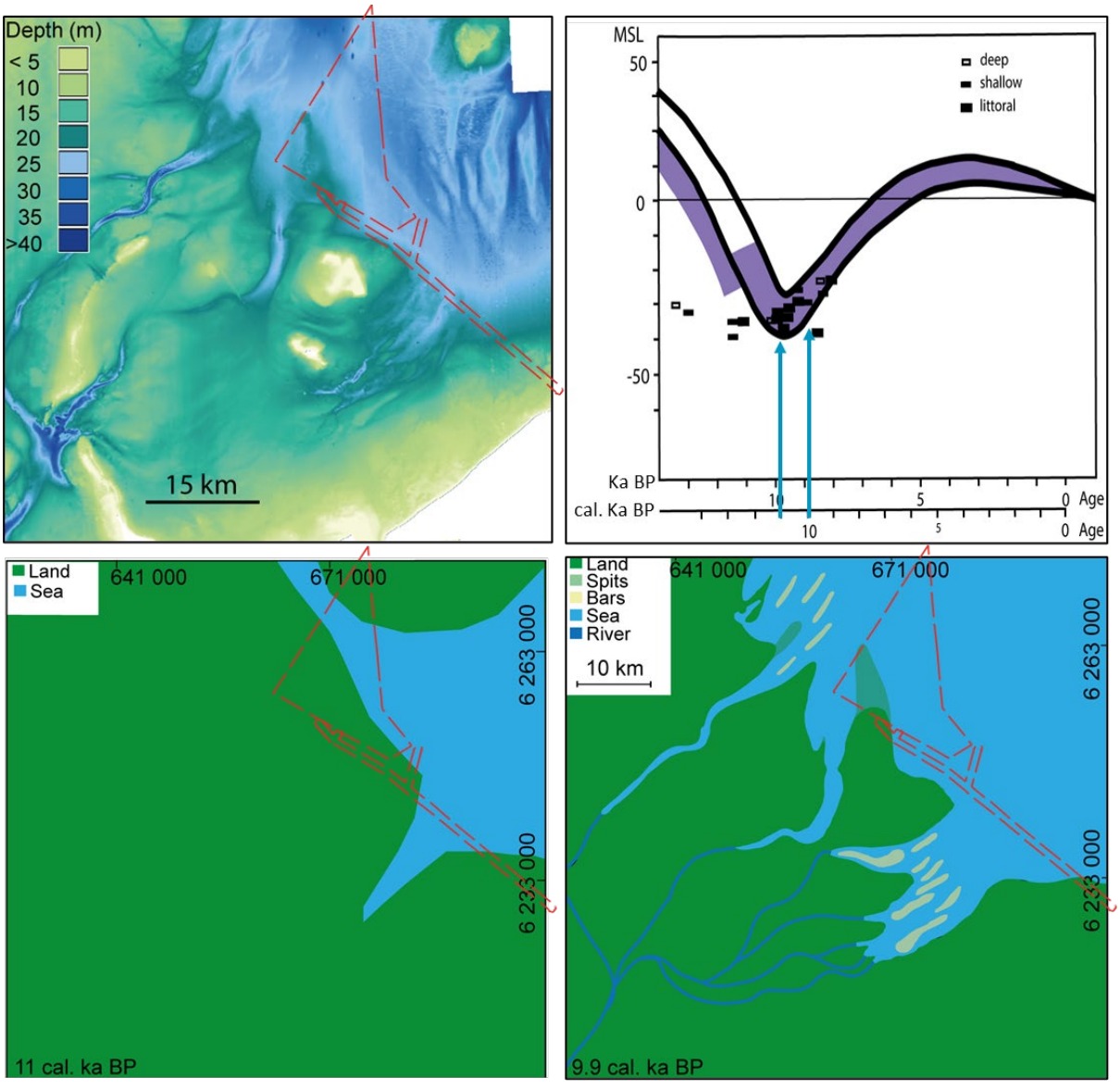

Figure 8.6. The present-day bathymetry shows a close resemblance to palaeogeographical maps of the 11 cal. ka BP lowstand and the 9.9 cal. ka BP Holocene early transgression as well as to the shore-level displacement map with arrows indicating the relative sea level.

9. Archaeological interests

In addition to geotechnical interests in a detailed geological model for the Hesselø OWF area and the cable corridor in order to be able to plan the detailed geotechnical investigations, it is also of great interest for an archaeological screening, to understand the development and distribution of land and sea after the last deglaciation.

As described in Chapter 4.4, highstand sea-level characterised the initial period after the deglaciation of central and southern Kattegat. Around 15 cal. ka BP Kattegat was deglaciated and all of the planned Hesselø OWF area and the cable corridor were covered by the glaci-omarine Younger Yoldia Sea (Figure 9.1). This corresponds to the archaeological Hamburg culture or Hamburgian (15.5–13.1 ka BP) – a Late Upper Palaeolithic culture of reindeer hunters.

The highstand period was followed by a regression and development of an erosional uncon-formity. Around 12 cal. ka BP, the Baltic Ice Lake reached its maximum shore level in the Baltic and the Kattegat regression continued. Possibly, a minor part of Store Middelgrund emerged from the sea in the north-easternmost part of the Hesselø OWF area (Figure 9.1) in the time period of the Ahrensburg culture or Ahrensburgian (12.9 to 11.7 ka BP) – a late Upper Palaeolithic nomadic hunter culture.

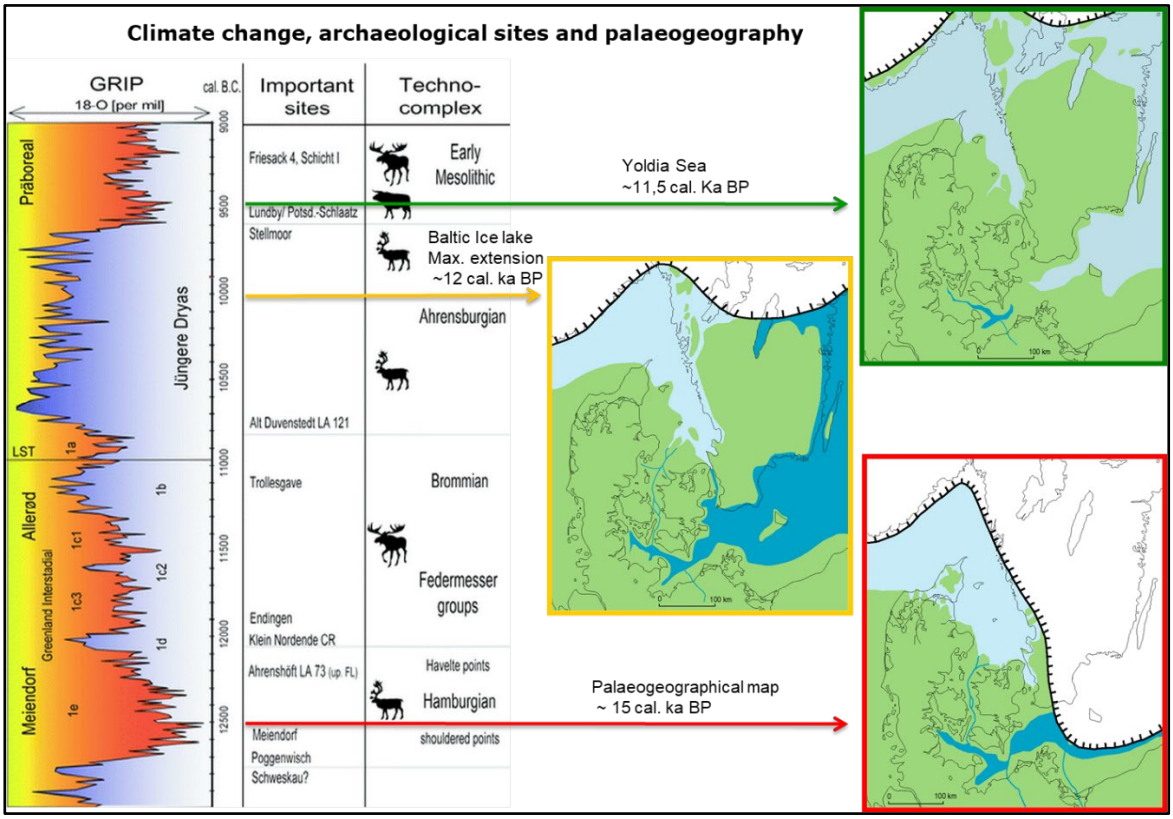

Figure 9.1. Late glacial and Holocene general palaeogeography in Kattegat and related archaeological cul-tures. (the maps are from Jensen et al. 2003).

The regression reached its maximum lowstand about 11.5 cal. ka BP, during a period when the Baltic was connected to the Kattegat via south-central Sweden (Figure 9.1). Large parts

of the Hesselø OWF area was land but divided by a NW–SE-oriented strait in the central part of the wind farm area. The cable corridor crosses the mouth of a possible fjord system (Figure 8.6). The lowstand coincides with the Early Maglemosian culture from 11.0 to 8.8 ka BP, a hunting and fishing culture with tools made from wood, bone and flint.

The regression was followed by the initial Holocene transgression and a major spit barrier/estuary system developed in large areas in the southernmost part of the Kattegat. About 9.9 cal. ka BP, the system was fully developed with a large tidally dominated river mouth system with a southward fluvial connection to the Baltic Ancylus Lake (Figure 8.6). A major fine-grained sand spit and back barrier estuary clay dominates the southwestern most part of the Hesselø OWF area and the outer part of a large tidally dominated mouth system characterised the cable corridor. The large spit barrier/estuary phase developed in the transition period between the Early Maglemosian culture 11.0–9.0 ka BP and the Middle Maglemosian culture 9.8–9.0 ka BP.

The present bathymetry (Figure 8.6) shows that the spit/ barrier/estuary has to a large degree been preserved, with only minor modification by the continued Holocene transgression. This leads to the conclusion that the following steep transgression (Figure 8.6) resulted in a coastal back-stepping over a relatively flat platform with a fast retreat of the coastline and only minor erosion of the spit barrier/estuary system.

Coastal deposits of the younger phases of the Holocene transgression is not represented in the Hesselø OWF area and is only of relevance in the southernmost part of the cable corridor close to the present coastline (Figure 8.6).

10. Conclusions

In this study we have used a combination of published work and archive seismic and sediment core data to assess the general geological development of the southern Kattegat area including the planned Hesselø OWF and the cable corridor.

A geological description has been provided and a geological model presented.

As a result of the geological desk study it has been possible to present a relative late glacial and Holocene sea-level curve for the area and to describe the development relevant for an archaeological screening.

A number of focal points are relevant for the future geotechnical and archaeological evaluation of the area:

- The study area is located in the Fennoscandian border zone characterised by pre-Quaternary dextral wrench faulting. Studies of late glacial clay show that neotectonic activities has created elongated restricted basins with syn-sedimentary infill that has continued in the Holocene. Recent earthquake activity in the area points to recent seismological activity.

- Acoustic disturbance on seismic profiles has been observed in the Quaternary sediments above fault zones and may be related to thermogenic degassing from deeper structures. Acoustic gas indications in Holocene sediments may be related to Neogene degassing.

- Glaciotectonic deformations has been recorded at store Middelgrund east of the Hesselø OWF area and similar features may be found in the south-eastern part of the windfarm area, close to Lysegrund.

- Weakly consolidated glaciomarine clay with a thickness of up to 100 m covers a majority of the Hesselø OWF area and must be taken into consideration.

- In connection with the Holocene transgression of the area, large parts became covered by a spit/estuary system consisting of fine-grained sand and clay, with high contents of organic material and geotechnical challenges must be expected.

- The late glacial and early Holocene coastal zone development of the Hesselø OWF area and cable corridor opens for an archaeological interest window in the time period for the Ahrensburg and Maglemosian cultures whereas the area was transgressed by the sea under the time windows of younger cultures.

11. References

Andrén, T, Jørgensen, B. B., Cotterill, C., Green, S. & Expedition 347 Scientists 2015a: Baltic Sea paleoenvironment. Proceedings of the IODP, Integrated Ocean Drilling Program 347. Integrated Ocean Drilling Program. Available at : http://publications.iodp.org/proceedings/347/347title.htm

Andrén, T., Jørgensen, B.B., Cotterill, C., Green, S., and the Expedition 347 Scientists 2015b: Site M0060. Proceedings of the Integrated Ocean Drilling Program, Volume 347.

Arvidsson, R. 1996: Fennoscandian earthquakes : whole crustal rupturing related to postglacia l rebound. Science 274, 744–745. Belknap, D. F. & Shipp, R. C. 1991: Seismic stratigraphy of glacial marine units, Maine inner shelf. In Anderson, J. B. & Ashley, G. M. (eds.): Glacial Marine Sedimentation , Palaeoclimatic Significance, 137–157. Geological Society of America Special Paper 261.

Bendixen. C., Jensen. J.B., Boldrell, L.O., Clausen, O.R., Bennike, O., Seidenkrantz, M-S, Nyberg J. and Hüb-scher, C. 2015: The Early Holocene Great Belt connection to the southern Kattegat, Scandina-via: Ancylus Lake drainage and Early Littorina Sea transgression. Boreas. Online

Bendixen. C., Boldrell, L.O, Jensen. J.B., Bennike, O., Clausen, O.R., Hübscher, C. 2017: Early Holocene estu-ary development of the Hesselø Bay area, southern Kattegat, Denmark and its implication for Ancylus Lake drainage. Geo-Mar Lett. 37, 579-591 June 2017

Bennike, O., Jensen, J. B., Konradi, P. B., Lemke, W. & Heinemeier, J. 2000: Early Holocene drowned lagoonal deposits from Kattegat, southern Scandinavia. Boreas 29, 272–286.

Bergsten, H. & Nordberg, K. 1992: Late Weichselian marine stratigraphy of the southern Kattegat, Scandinavia: evidence for drainage of the Baltic Ice Lake between 12,700 and 10,300 years BP. Boreas 21, 223–252.

Binzer, K. & Stockmarr, J. 1994: Pre-Quatrenary surface topography of Denmark. Geological Survey of Denmark, Map Series No. 44

Christiansen, C., Conradsen, K., Emelyanov, E., Trimonis, E., Heinemeier, J. & Rud, N. 1993: Hydrographi c changes in the southern Kattegat (Scandinavia) during the early Holocene transgression. Boreas 22, 349–356.

Dahl-Jensen, T., Voss, P.H., Larsen, T.B. and Gregersen, S. 2013: Seismic activity in Denmark: detection level and recent felt earthquakes. Geological Survey of Denmark and Greenland Bulletin 28, 41–44.

Eyles, N. & McCabe, A. M. 1989: The Late Devensian (<22,000 BP) Irish Sea Basin: the sedimentary record of a collapsed ice sheet margin. Quaternary Science Reviews 8, 307–351.

Erlström, M., Kornfält, K.-A. & Sivhed, U., 2001: Berggrundskartan 2D Tomelilla NO/2E Simrishamn NV. Sveriges geologiska undersökning Af 213.

Gregersen, S., Leth, J., Lind, G. & Lykke-Andersen , H. 1996: Earthquake activity and its relationship with geologically recent motion in Denmark. Tectonophysic s 257, 265–273.

Gyldenholm, K. G., Lykke-Andersen , H. & Lind, G. 1993: Seismic stratigraphy of the Quaternary and its substratum in southeastern Kattegat, Scandinava. Boreas 22, 319–327.

Houmark-Nielsen, M. and Kjær, K. H. 2003. Southwest Scandinavia, 40–15 ka BP: palaeogeography and environmental change. J. Quaternary Sci., Vol 18 pp. 769–786.

Hyttinen, O., Quintana Krupinski, N., Bennike, O., Wacker, L., Filipsson, H., Obrochta, S., Jensen, J.B., Lougheed, B., Ryabchuk, D., Passchier, S., Snowball, I., Herrero-Bervera, E., Andrén, T. & Kotilainen, A.T. 2020: Deglaciation dynamics of the Fennoscandian Ice Sheet in the Kattegat, the gateway between the North Sea and the Baltic Sea Basin. Boreas. https://doi.org/10.1111/bor.12494. ISSN 0300-9483.

Jensen, J. B., Bennike, O., Witkowski, A., Lemke, W. & Kuijpers, A. 1997: The Baltic Ice Lake in the southwestern Baltic: sequence- , chrono- and biostratigraphy . Boreas 26, 217–236.

Jensen, J. B., Bennike, O., Witkowski, A., Lemke, W. & Kuijpers, A. 1999: Early Holocene history of the southwestern Baltic Sea: the Ancylus Late stage. Boreas 28, 437–453.

Jensen, J. B., Petersen, K. S., Konradi, P., Kuijpers, A., Bennike, O., Lemke, W. & Endler, R. 2002: Neotectonics, sea-level changes and biological evolution in the Fennoscandian Border Zone of the southern Kattegat Sea. Boreas, Vol. 31, pp. 133–150.

Jensen, J.B. Kuijpers, A, Bennike, O. and Lemke, W. 2003: Thematic volume "BALKAT" The Baltic Sea without frontiers. Geologi Nyt fra GEUS. 2003, 19pp.

Larsen, N. K., Knudsen, K. L., Krohn, C. F., Kronborg, C., Murray, A. S. & Nielsen, O. B. 2009: Late Quaternary ice sheet, lake and sea history of southwest Scandinavia – a synthesis. Boreas, Vol. 38, pp. 732–761.

Liboriussen, J., Ashton, P. & Tygesen, T. 1987: The tectonic evolution of the Fennoscandian Border Zone in Denmark. Tectonophysics 137, 21–29.

Lykke-Andersen , H. 1987: Thickness of Quaternary deposits and their relation to the pre-Quaternar y in the Fennoscandian borderzone Kattegat and Vendsyssel . Boreas 16, 369–371.

Lykke-Andersen , H., Seidenkrantz , M.-S. & Knudsen, K. L. 1993: Quaternary sequences and their relations to the pre-Quaternary in the vicinity of Anholt, Kattegat, Scandinavia . Boreas 22, 291–298.

Mogensen, T.E., and Korstgård, J.A. 2003:Triassic and Jurassic transtension along part of the Sorgenfrei–Tornquist Zone in the Danish Kattegat. Geological Survey of Denmark and Greenland Bulletin 1, 439–458.

Myrberg K, Lehmann A (2013) Topography, hydrography, circulation and modelling of the Baltic Sea. In: Soomere T, Quak E (eds) Preventive methods for coastal protection. Springer, Cham, pp 31–64

Mörner, N.-A. 1969: The Late Quaternary history of the Kattegat Sea and the Swedish west coast. Sveriges Geologiska Undersökning C 640. 487 pp.

Mörner, N.-A. 1983: The Fennoscandia n Uplift: Geological Data and their Geodynamical Implication. In Mörner, N.-A. (ed.): Earth Rheology, Isostacy and Eustacy, 251–284. John Wiley & Sons. New York.

Nielsen, P. E. & Konradi, P. B. 1990: Seismic stratigraph y and foraminifera in Late Quaternary deposits, southern Kattegat, Denmark. In Kauranne, L. K. & Königsson, L.-K. (eds.): Quaternary Economic Geology in the Nordic Countries. Striae 29, 105–110.

Pegrum, R.M., 1984: The Evolution of the Tornquist Zone in the Norwegian North Sea. Norsk Geologisk Tidsskrift 64, 39–68.

Posamentier, H. W., Allen, G. P. & James, D. P. 1992: High resolution sequence stratigraphy – the East Coulee Delta. Journal of Sedimentary Petrology 62, 310–317.

Richardt, N. 1996: Sedimentologica l examination of the Late Weichselian sea-level history following deglaciation of northern Denmark. In Andrews, J. T., Austin, W. E. N., Bergsten, H. & BOREAS 31 (2002) Environmental changes, southern Kattegat Sea 149.

SGU (Sveriges Geologiska Underso¨kning) 1989: Maringeologiska Kartan Stora Middelgrund – Halmstad. Sveriges Geologiska Undersökning Am 4, mapsheet S.

Skov og Naturstyrelsen 1987: Nordsjælland Oversigt. Havbundsundersøgelser Råstoffer og fredningsinteresser. Skov og Naturstyrelsen.

Vail, P. R., Mitchum, R. M., Jr., Todd, R. G., Widmier, J. M., Thompson, S., III, Sangree, J. B., Bubb, J. N. & Hatlelid, W. G. 1977: Seismic stratigraphy and global changes of sea level. In Clayton, C. E. (ed.): Seismic Stratigraph y – Applications to Hydrocarbon Exploration. American Association of Petroleum Geologists Memoir 26, 49–212.

Wu, J.E., McClay, K., Whitehouse, P. and Dooley, T. 2009: 4D analogue modelling of transtensional pull-apart basins. Marine and Petroleum Geology 26. 1608–1623

12. Appendix A Site M0060

Site M0060[1]

T. Andrén, B.B. Jørgensen, C. Cotterill, S. Green, E. Andrén, J. Ash, T. Bauersachs, B. Cragg, A.-S. Fanget, A. Fehr, W. Granoszewski, J. Groeneveld, D. Hardisty, E. Herrero-Bervera, O. Hyttinen, J.B. Jensen, S. Johnson, M. Kenzler, A. Kotilainen, U. Kotthoff, I.P.G. Marshall, E. Martin, S. Obrochta, S. Passchier, N. Quintana Krupinski, N. Riedinger, C. Slomp, I. Snowball, A. Stepanova, S. Strano, A. Torti, J. Warnock, N. Xiao, and R. Zhang[2]

Chapter contents

[1] Andrén, T., Jørgensen, B.B., Cotterill, C., Green, S., Andrén, E., Ash, J., Bauersachs, T., Cragg, B., Fanget, A.-S., Fehr, A., Granoszewski, W., Groeneveld, J., Hardisty, D., Herrero-Bervera, E., Hyttinen, O., Jensen, J.B., Johnson, S., Kenzler, M., Kotilainen, A., Kotthoff, U., Marshall, I.P.G., Martin, E., Obrochta, S., Passchier, S., Quintana Krupinski, N., Riedinger, N., Slomp, C., Snowball, I., Stepanova, A., Strano, S., Torti, A., Warnock, J., Xiao, N., and Zhang, R., 2015. Site M0060. *In* Andrén, T., Jørgensen, B.B., Cotterill, C., Green, S., and the Expedition 347 Scientists, *Proc. IODP,* 347: College Station, TX (Integrated Ocean Drilling Program). doi:10.2204/iodp.proc.347.104.2015

[2] **Expedition 347 Scientists' addresses.**

Introduction

During Integrated Ocean Drilling Program (IODP) Expedition 347, cores were recovered from two holes at Site M0060 (near Anholt Island), with an average site recovery of 90.69%. The water depth was 31.2 m, with a tidal range of <30 cm. Existing data sets, including seismic reflection profiles, were evaluated prior to each site to attempt to guide the initial drilling with an anticipated lithologic breakdown. The total time spent on station was 8.35 days.

Operations

Transit to Hole M0060A

At 0835 h on 22 September 2013, the *Greatship Manisha* sailed from Site M0059 to the second coring site (M0060; proposed Site BSB-1) southeast of Anholt, Kattegat. The vessel arrived at 0100 h on 23 September.

Hole M0060A

Operations in Hole M0060A commenced at 0145 h on 23 September 2013 with a downpipe camera survey of the three proposed holes at this site (M0060A–M0060C) to assess the seabed, in accordance with the permissions required at this site.

Coring operations were then established (Table **T1**), with a longer setup period than expected due to installation of a new sample wire sealer for the piston corer system (PCS). However, on the second run, the sealer failed, and operations returned to the previous system of using an overshot release. Other technical issues slowed operations throughout 23 September, including breakage of the hydraulic hose to the seabed template, failure of the sample wire requiring the drill string to be retrieved, and cracking of the slips bowl.

Thirteen cores were recovered during the morning of 24 September, with operations running smoothly. Following this, a series of technical issues arose. The sample winch rope snapped, which led to tripping of the pipe following an unsuccessful fishing attempt. Once the overshot was recovered, the rope was tested to assess the cause of the breakage. Coring operations were reestablished but halted again because of damage to the manual roughneck. By 2240 h, the hole had been cleaned and washed down to 75.8 me-

doi:10.2204/iodp.proc.347.104.2015

ters below seafloor (mbsf), and coring operations continued throughout the night.

At 0600 h on 25 September, a decision to switch to the hammer sampler (HS) was made because of difficulties recovering harder lithologies, and a sample of compacted clay was recovered. At 97 mbsf, a lithologic change was noticed, and this change coincided with an overpressurized mudline. Coring continued, with the sampling methodology determined by the lithology encountered. PCS, HS, push coring assembly, and extended coring system coring were all undertaken in an attempt to optimize recovery in unpredictable lithologies. At 1545 h, the overshot was unable to pick up the piston corer because of sand infill, and it was necessary to repeatedly flush the hole before recovery could be achieved. PCS coring continued until 0220 h on 26 September, when the seabed template was recovered to deck because of failure of the clamps. Repairs were then carried out, and coring recommenced.

As drilling progressed, recovery rates varied, primarily because of the presence of sand lithologies. At 1335 h on 26 September, following use of the rotating core barrel, the barrel was recovered with no sample. However, the catchers were inverted and disturbed material was brought up. In order to avoid damage to the core, the coring strategy was changed and a flapper catcher with one basket was used. From 1725 h on 26 September until 0315 h on 27 September, coring continued with good recovery rates. During this period, deformation of the liner due to suction pressure was noted.

At 0315 h on 27 September, the overshot rope snapped, and it was necessary to trip pipe to recover the barrel (despite fishing attempts). Issues arose as a result of overtight joints and stuck drill collars. By 1400 h, it was possible to recommence running pipe back into the hole. The hole was then washed down with the noncoring assembly (NCA) in place to the level of the last sample taken before piston coring restarted (188.60 mbsf).

Coring continued throughout 28 September using a combination of open-hole and push core sampling. At 1715 h, it was noted that the string had become difficult to rotate. One further core was recovered before a sand blockage caused the string to become stuck.

This sand blockage resulted in the termination of Hole M0060A, and efforts were made throughout the evening of 28 September and the early morning of 29 September to free the string. Various options were investigated, which included use of the HS and running high pressure through the mudline. At 1020 h, it was decided that the best option was to back off the string and recover the remaining pipe. This plan was executed, but unfortunately a stick up of 14 m remained above the seabed (assessed with the remotely operated vehicle [ROV]). This was hammered in as far as possible and then flattened using the seabed template so that ~9 m of pipe was left lying horizontally on the seabed. ROV footage showed 4 m of visible pipe, with the remainder buried in sand at a shallow angle.

A total of 101 coring attempts were made in Hole M0060A to a maximum depth of 232.50 mbsf. Eighteen of these involved use of the NCA, covering 42.49 mbsf. Hole recovery was 83.06% when the open-hole sections were discounted.

Hole M0060B

Operations in Hole M0060B commenced at 1600 h on 29 September 2013. Because of the drilling issues associated with sand in Hole M0060A, it was agreed that the target depth of the hole would be 100 mbsf, with termination determined by the first presence of the sand lithology.

This hole was a designated microbiology hole, and intensive sampling was conducted in accordance with the developed scheme. PCS coring ran smoothly at this hole, with GS550 mud used for stabilization of the loose sand encountered at the seabed. The concentration was reduced as the hole progressed into clayey material to 30 mbsf; seawater was used as the drilling fluid for Cores 10H through 27H. There was excellent recovery throughout the hole until an aquifer was encountered at 82 mbsf (Core 28H). After difficulties in core recovery and a tight drill string, it was decided to terminate the hole slightly shallower than anticipated at 85.70 mbsf. By midnight, coring operations were complete and the drill floor was being prepared for downhole logging.

Downhole logging was completed in Hole M0060B by 0735 h on 1 October, with three successful tool runs to a maximum depth of 67 mbsf. The imaging tool did not appear to be operating correctly, but later investigation showed that despite a black screen data had been recorded by this instrument. The remaining drill string was tripped and the bottom-hole assembly bit cleaned and checked. Once the seabed template was on deck, the drill floor and all containers were prepared for transit.

A total of 28 coring attempts were made in Hole M0060B to a maximum depth of 85.7 mbsf. Hole recovery was 98.32%.

Lithostratigraphy

Two holes were drilled at Site M0060. Hole M0060A reached a total depth of 232.50 mbsf, and Hole M0060B was 85.70 mbsf deep. Hole M0060B was designated for microbiology sampling and was subject to whole-round sampling on board the ship prior to core description at the IODP Bremen Core Repository (Germany). In Hole M0060A, piston coring was used for the uppermost ~83 mbsf, where recovery was >90%. Between 83 and 200 mbsf, a combination of piston coring, nonrotating core barrel, and extended nose coring was used to optimize recovery. At ~100–120 and ~147–162 mbsf, a combination of open holing and extended nose drilling was used to advance through hard lithologies, which affected recovery and core quality. Between ~101 and 117 mbsf, all core material recovered (17 cm) was consumed by shipboard sampling. For this interval, no core descriptions exist and shipboard lithologic descriptions are limited to observations on one ~5 cm portion of a core catcher and some washed paleontology samples. Deeper than 200 mbsf, open holing, hammer sampling, and push coring were used to aid penetration through difficult lithologies; however, this produced limited core recovery (see **"Operations"**).

Lithostratigraphic divisions (Units I–VII) (Fig. **F1**) are based on descriptions of the cut face of the split core of Hole M0060A, augmented by available sections from Hole M0060B and observations from smear slides (see **"Core descriptions"**). Two of the unit boundaries in Hole M0060B were within core sections sampled for microbiology. For these sections, the boundaries were placed at the bottom of the interval that was sampled for microbiology.

Unit I

Intervals: 347-M0060A-3H-1, 0 cm, to 6H-1, 0 cm; 347-M0060B-1H-1, 0 cm, to 4H-1, 0 cm

Depths: Hole M0060A = 0–6.00 mbsf; Hole M0060B = 0–6.10 mbsf

Unit I is composed of gray, massive, fine to medium thickly bedded sand with common marine bivalve and gastropod shell fragments, including *Cerastoderma* sp., *Macoma baltica*, and *Turritella* sp. Two distinct fining-upward shell-rich beds were found in this unit as well. The sand is generally well sorted, and quartz sand grains are subrounded to rounded.

The sand was deposited in a near-shore marine depositional environment. Fining-upward shell-rich beds signal deposition near the wave base; therefore, the approximate bathymetry would be similar to the modern situation.

Unit II

Intervals: 347-M0060A-6H-1, 0 cm, to 12H-2, 14 cm; 347-M0060B-4H-1, 0 cm, to 9H-2, 60 cm

Depths: Hole M0060A = 6.00–23.84 mbsf; Hole M0060B = 6.10–24.70 mbsf below microbiology sample

Unit II consists of dark greenish gray interlaminated sandy clayey silt and fine–medium sand with dispersed clasts. Sand laminae are 0.5–3 cm thick and occur in packages unequally spaced within the silt. The orientation of the laminae is inclined, and they are deformed as a primary sedimentary structure. Quartz sand grains dispersed within the silt are angular to subrounded, and the sediment is moderately well sorted. Reworked mollusk fragments are found throughout, and reworked diatom fragments are common in smear slides from this unit. Sparse bioturbation is observed near the bottom of this unit between black, presumably iron sulfide, laminae. Gypsum was observed macroscopically and in smear slides.

The bottom of the unit is sparsely bioturbated between iron sulfide laminated intervals, possibly due to changing stratification of the water column coupled to salinity changes. The deformation in the upper part of the unit is likely due to slumping and possibly the result of increased sedimentation rate. With the presence of dispersed outsized gravel clasts, the lithologic changes can be interpreted as a prograding, ice-influenced deltaic environment.

Unit III

Subunit IIIa

Intervals: 347-M0060A-12H-2, 14 cm, to 23H-1, 56 cm; 347-M0060B-9H-2, 60 cm, to 19H-2, 125 cm

Depths: Hole M0060A = 23.84–57.46 mbsf; Hole M0060B = 24.7–58.35 mbsf

Subunit IIIb

Intervals: 347-M0060A-23H-1, 56 cm, to 25H-2, 146 cm; 347-M0060B-19H-2, 125 cm, to 22H-2, 59 cm

Depths: Hole M0060A = 57.46–66.46 mbsf; Hole M0060B = 58.35–67.59 mbsf

Subunit IIIc

Intervals: 347-M0060A-25H-2, 146 cm, to 30H-1, 42 cm; 347-M0060B-22H-2, 59 cm, to 27H-2, 50 cm

Depths: Hole M0060A = 66.46–79.52 mbsf; Hole M0060B = 67.59–81.60 mbsf

Unit III is characterized by dark grayish brown to gray parallel laminated clay and silt with dispersed clasts. In Subunit IIIa, discrete millimeter-scale silt and fine sand laminae occur as packages of 2–4 laminae and are either well preserved or disrupted, possibly due to loading or bioturbation. Laminae are irregularly spaced and generally 3–6 mm thick, and their abundance increases upward through the unit. Subunit IIIa locally has a reddish hue. Numerous black, possibly iron sulfide, bands are present throughout the unit and become especially prominent in Subunit IIIb (Fig. F2). Subunit IIIc has a minor interlaminated sand component.

This unit can be interpreted as an ice-influenced lake or marginal marine environment. Silt laminae in Subunit IIIa may represent bottom current activity. The outsized gravel clasts may have originated from ice rafting from a calving glacier at a distance from the drilled location. The presence of iron sulfide bands within the sediment, especially in Subunit IIIb, may be due to periodic oxygen-poor conditions and a stratified water column, where organic matter may have accumulated to form the precursor to the diagenetic sulfides.

Unit IV

Interval: 347-M0060A-30H-1, 42 cm, to 35H-1, 34 cm; 347-M0060B-27H-2, 50 cm, to end of hole

Depths: Hole M0060A = 79.52–95.04 mbsf; Hole M0060B = 81.60–85.70 mbsf

Gray interbedded sand, silt, and clay with dispersed clasts and clast-poor diamicton were identified in Unit IV. Both rock clasts and intraclasts are common in this unit, and the strata are intensely folded or contorted. Clast assemblages are polymict.

The moderately to poorly sorted character of sediments, the polymict clast assemblage, and the abrupt shifts in lithologies may indicate deposition in an ice-proximal depositional environment. The deformation of the sediments may be due to slumping into an aquatic depositional environment.

Unit V

Interval: 347-M0060A-35H-1, 34 cm, to 48H-1, 0 cm

Depth: 95.04–116.7 mbsf

This unit is characterized by black and gray sandy silty clay with dispersed clasts. Mollusk fragments are common, especially *Turritella* sp. Multiple horizons with shell fragments are present. Cores in this interval are poorly recovered and highly disturbed as a result of drilling.

This unit probably represents a shallow-marine depositional environment.

Unit VI

Interval: 347-M0060A-48H-1, 0 cm, to 58H-1, 0 cm

Depth: 116.70–146.10 mbsf

Unit VI consists of gray, fine to medium, massive well-sorted sand. Rare shell fragments occur near the top and the bottom of this unit. The sand is quartz rich, and quartz grains are well rounded. Some decimeter-scale clay and silt-rich interbeds are recorded. At the bottom of the unit, pebbles and intraclasts are found.

Based on the well-sorted nature of the sand, this unit may represent a high-energy fluvial or deltaic depositional environment. The mud interbeds may represent overbank deposits or channel fills. The rare shell fragments are likely locally reworked.

Unit VII

Interval: 347-M0060A-58H-1, 0 cm, to end of hole

Depth: 146.10–229.60 mbsf

Unit VII is dominated by a dark gray clast-poor sandy diamicton (Fig. F3) with dispersed (<1%) to uncommon (1%–5%) charcoal clasts up to 3 cm in diameter. The structure is mostly homogeneous with localized very rare silty to clayey laminae a few centimeters in thickness. Isolated intervals of dispersed (<1%) white carbonate rock fragments, fine mollusk shell hash, and silt intraclasts are present. The uppermost part consists of gray well-sorted clay/silt with locally clast-poor muddy to sandy diamicton. The clay appears mostly homogeneous with some weak lamination by color, especially in the upper part. Higher organic contents and strong odor were common. Fining upward of Unit VII between 158 and 146.1 mbsf was recorded. The base of this moderately sorted unit extends deeper than 229.6 mbsf, as it was not penetrated at the base of the hole. However, on open holing to 232.50 mbsf, the string became stuck and it was not possible to recover a sample to verify the lithology.

Because of the general lack of visible grading and moderate sorting of Unit VII, deposition by mass-transport processes like massive debris flows is possible. The contacts between and thickness of individual debris flow beds are uncertain and potentially macroscopically not visible. The high charcoal content could be related to the outcropping of Jurassic sediments east of Site M0060. During the time of deposition, it is possible that large amounts of reworked Jurassic sediments including fossil soil horizons with coal seams were delivered to this location.

The influence of mass-transport processes decreases to the top of this unit, indicated by increased sorting of clay/silt as a result of a change in the mode of sedimentation.

Biostratigraphy

Diatoms

With the exception of one sample containing chrysophycean cysts, only diatoms were found at Site M0060 (Hole M0060A only), and they were identified to species level. The sampling resolution consisted of one sample at every core top for all recovered intervals. However, some intervals were also sampled at every section top. In order to provide an initial paleoecological framework for Site M0060, diatoms were classified with respect to salinity tolerance. Salinity tolerance classification follows the Baltic Sea intercalibration guides of Snoeijs et al. (1993–1998), which divide taxa into five groups: marine, brackish-marine, brackish, brackish-freshwater, and freshwater.

Overall, diatoms occur in very low abundances. For this reason, only two transects of each slide were viewed for samples that did not contain numerous whole valves. The presence of diatom fragments and whole valves is shown in Figure **F4.** All analyzed samples were barren to 7.5 mbsf. Diatoms were present at low abundances from 7.5 to 10.5 mbsf. A low-diversity freshwater assemblage comprising diatoms of the genera *Aulacoseira*, *Cocconeis*, and *Martyana* is present at 7.5 mbsf. Only a single valve of the brackish water taxa *Martyana schulzii* was recorded. At 9 and 10.5 mbsf, the assemblage is mainly composed of freshwater taxa from the genera *Amphora*, *Aulacoseira*, and *Stephanodiscus*. Brackish and marine taxa are also present but are fragmentary. This assemblage could be interpreted as freshwater with allochthonous brackish and marine diatom fragments. Alternatively, the assemblage may be brackish with robust freshwater diatoms washed in.

Between 10.5 and 132.9 mbsf, most of the samples are barren of whole and fragmentary diatom fossils. The total number of whole valves found in two slide transects for any sample from this interval did not exceed four. In the interval from 132.9 to 202.5 mbsf, all slides contain rare diatom fragments. Table **T2** contains the diatom species, authorities, and habitat information for Site M0060, as well as presence/absence data for the interval between 7.5 and 10.5 mbsf. All Quaternary diatoms found in samples deeper than 10.5 mbsf co-occurred with Cretaceous coccolithophorids and rare fragments of Cretaceous diatoms from the genus *Stephanopyxis* (Table **T3**). These diatoms are therefore interpreted as redeposited.

Foraminifers

Results presented here include primarily those from samples taken from split-core sections during the Onshore Science Party (OSP) and supplementary information from core catcher samples studied offshore. A total of 152 samples (90 obtained offshore from core catchers and 62 onshore from split-core sections) were studied for foraminiferal biostratigraphy. Redeposited pre-Quaternary foraminifers occur intermittently throughout the site, indicated by a white, polished, or frosty surface and carbonate infilling (Rasmussen et al., 2005). Intervals with poor core recovery are not discussed in detail.

The shallowest sample (347-M0060A-3H-1, 11–13 cm; 0.13 mbsf) is dominated by *Ammonia beccarii*, *Bulimina marginata*, and *Cibicides lobatulus* (Table **T4**), which suggests a Holocene boreal marine assemblage (Seidenkrantz and Knudsen, 1993). The remaining upper part (upper 21 mbsf) of Site M0060 contains generally few benthic foraminifers (Fig. **F5A**), although taxonomic diversity is relatively high (4–13 species; Fig. **F5C;** Table **T4**). In this upper interval, the genus *Elphidium* is the most common benthic foraminifer with *Elphidium excavatum clavatum* generally composing the largest fraction of the assemblage (Fig. **F5B**) and *B. marginata*, *Cassidulina reniforme* (formerly *crassa*), and *Elphidium williamsoni* often present as accessories. Redeposited pre-Quaternary foraminifers occur occasionally. Taxonomic composition of this assemblage in combination with the presence of dropstones in this interval (see **"Lithostratigraphy"**) suggest cool-water marine conditions (Seidenkrantz, 1993b; Seidenkrantz and Knudsen, 1993). The presence of *E. williamsoni* may suggest shallow or intertidal waters (Knudsen et al., 2012) or transport of foraminifers from a nearby environment of this type.

Between 21 and 76 mbsf, the assemblage is of low diversity, and abundance varies from abundant to barren (Fig. **F5A**). *E. excavatum clavatum* and *C. reniforme* are often the only species present, with *E. excavatum clavatum* nearly always dominant. Redeposited foraminifers are rarely present. The dominance of *E. excavatum clavatum* and very low diversity suggest brackish and cold conditions (Seidenkrantz, 1993a; Seidenkrantz and Knudsen, 1993).

Between 76 and 99 mbsf, foraminiferal diversity increases (4–13 species; Fig. **F5C**) and foraminiferal abundance ranges from few to common. *E. excavatum clavatum* still typically composes the largest fraction of the assemblage (Fig. **F5B**), with *Elphidium ex-*

cavatum selseyensis, *Elphidium* spp., *Haynesina* spp., *B. marginata*, *Islandiella helenae*, *C. reniforme*, and *Hyalinea balthica* occurring frequently in low to moderate abundances. Redeposited pre-Quaternary foraminifers occur in more than half of the samples in this interval. The combination of subarctic (e.g., *I. helenae*) and boreal (e.g., *H. balthica*) species in this interval is an unrealistic combination, suggesting that some foraminifers are redeposited (Seidenkrantz and Knudsen, 1993). The characterization of this unit as slumped sands (see **"Lithostratigraphy"**) supports the interpretation that the sediments in this interval are indeed likely redeposited, although it is possible that occasional short periods of deposition in a marginal marine environment did occur.

Between 99 and 117 mbsf, sediment recovery was poor, preventing reliable environmental characterization.

Between 117 and 146 mbsf, foraminifers are very rare or absent, though a small number of *Elphidium* spp. and *I. helenae* specimens are present, as well as some pre-Quaternary redeposited specimens. Redeposition is additionally supported by the generally sandy grain size of the sediments and the occurrence of macroscopic shell fragments, which have been interpreted as derived from a deltaic environment (see **"Lithostratigraphy"**), although infrequent periods of sediment deposition in a cold and brackish environment could have occurred.

At 153.7–155.4 mbsf (Cores 347-M0060A-60H through 61H), foraminifers are abundant and the assemblage is among the most diverse found at Site M0060 (Fig. **F5C**). This interval contains few or no pre-Quaternary redeposited foraminifers and is dominated by *H. balthica* and *B. marginata*, with *Uvigerina mediterranea*, *I. helenae* (this taxon may possibly include *Cassidulina laevigata*), and *Melonis barleeanus* also occurring frequently. The fauna of this brief interval represents a typical marine boreal to lusitanian (i.e., warmer) assemblage (Seidenkrantz, 1993a; Seidenkrantz and Knudsen, 1993) and occurs in a thin, fine-grained, organic-rich, and weakly laminated subunit surrounded by diamicton; the surrounding diamicton may represent a delta slope environment in which periodic marine clay deposition occurred (see **"Lithostratigraphy"**). The thickness of this fine-grained unit is uncertain because of poor recovery and disturbed sediments above and below it. This interval may represent a short interstadial period or a longer warm period that has been partially eroded or poorly recovered at this site.

Between 160 and 190 mbsf, foraminifers are rare to nearly absent, but the assemblage is taxonomically diverse, with *Elphidium tumidum* (formerly *Elphidium groenlandicum*), *Elphidium* spp., and *I. helenae* dominant and pre-Quaternary redeposited foraminifers intermittently present. The foraminifers in this interval, which has been characterized as debris flow material in a deltaic environment including charcoal potentially of Jurassic age (see **"Lithostratigraphy"**), are likely redeposited.

Between 194 and 205 mbsf (Cores 347-M0060A-76H through 82P), foraminiferal abundance increases to generally common (ranging from very rare to abundant; Table **T4**) and the assemblage is among the most diverse at this site (Fig. **F5C**), although redeposited pre-Quaternary foraminifers occur. This interval is dominated by *E. excavatum clavatum* and *B. marginata*, but *H. balthica*, *Nonionella labradorica*, *I. helenae* (*C. laevigata*?), and *Elphidium* spp. also occur frequently. These species represent a marine boreal to lusitanian (i.e., warmer) assemblage and potentially greater water depths (Seidenkrantz, 1993a). Recovery in this interval is limited, and sediments are disturbed in some intervals. Core 347-M0060A-76H is a diamicton section and thus likely contains recently redeposited foraminifers, but the core below (347-M0060A-82P) is laminated silty sand and appears to contain in situ foraminifers.

Between 212 and 230 mbsf, foraminifers are rare to nearly absent and taxonomic diversity is low, with *E. tumidum* and other *Elphidium* spp. primarily occurring, as well as some redeposited pre-Quaternary specimens.

Ostracods

Ostracods were examined from 147 samples (including 90 core catchers) from Holes M0060A and M0060B during the OSP for Expedition 347. Samples were studied in the >125 µm fraction. Ostracods were present in 40 samples (Table **T5**).

Ostracod abundance per sediment volume from both holes is plotted in Figure **F6.** Ostracods mainly occur in the upper 20 mbsf (Holes M0060A and M0060B). Scattered occurrences of single valves are also observed over the entire record (Table **T5**). Ostracod abundance is the highest in the interval of 6–20 mbsf, ranging from 70 to 130 valves/20 cm^3 sample. A high juvenile to adult ratio and good preservation in this interval allows us to assume in situ burial (Fig. **F6**). The interval of highest ostracod abundance corresponds to the lithostratigraphic unit of sandy clayey silt and fine–medium sand (see **"Lithostratigraphy"** and **"Geochemistry"**).

Ostracods of three different ecological groups occur at this site, and their abundance variations suggest that salinity and water depth decreased uphole in the studied interval. The ecological groups distin-

guished are freshwater, shallow-water marine, and North Atlantic taxa.

The samples from 6.08 mbsf (Hole M0060A) and 6.66 mbsf (Hole M0060B) contain a shallow-water brackish-marine assemblage. The most abundant are *Sarsicytheridea punctillata*, *Acanthocythereis dunelmensis*, *Leptocythere* spp., *Elofsonella concinna*, and *Heterocyprideis sorbyana*. These are typical shallow-water species found on Arctic and North Atlantic shelves (Cronin, 1981; Cronin et al., 2010; Stepanova et al., 2007). These samples also include the freshwater taxon *Ilyocypris* sp. The valves are well preserved and include juveniles. This assemblage may indicate that the studied site was located close to the coastline and the freshwater specimens were transported from the continent.

In the interval 10.66–17.27 mbsf (Hole M0060A), a similar shallow-water assemblage comprising the shallow-water marine and brackish water taxa is distinguished.

In the samples containing in situ ostracods at 20.56 mbsf (Hole M0060A) and 15.92 mbsf (Hole M0060B), the assemblage is dominated by marine taxa typical of North Atlantic waters and high salinity ≥26–30 (Cronin et al., 1995; Frenzel et al., 2010), such as *Cytheropteron pseudomontrosiense*, *Cytheropteron arcuatum*, *Cytheropteron biconvexa*, and *Polycope* spp.

Palynological results

For Site M0060, palynological analyses focused on Hole M0060A. One sample per 1–2 cores was examined for palynomorphs. In most samples, concentrations of palynomorphs are extremely low and show indications of severe degradation/oxidation. Additionally, most samples from Hole M0060A contain reworked tertiary palynomorphs, sometimes in higher concentrations than the presumably autochthonous/in situ palynomorphs encountered. Only a few samples contained enough palynomorphs in situ to yield statistically relevant results. We therefore do not show a detailed pollen diagram for this site but give a general overview on palynological findings (main pollen types, marine/terrestrial ratio, and pollen concentration; Fig. **F7;** Table **T6;** see PalyM0060.xls in PALYNOLOGY in **"Supplementary material"**). Bisaccate pollen was included in the reference sum used for calculations, but for some samples, this pollen type may be overrepresented because of transportation bias and its particular resistibility to oxidation (Cheddadi and Rossignol-Strick, 1995). Dinocyst content varied depending on the type of sediment. Sediments with marine components (e.g., foraminifers) contained significant numbers of dinoflagellate cysts.

From Hole M0060A, 25 sediment samples were analyzed. With the exception of the uppermost sample (0.75 mbsf), all analyzed samples indicate a relatively high degree of oxidation due to the rarity/absence of taxa particularly susceptible to oxidation-based degradation and the higher percentages of robust pollen types and spores.

0.75 mbsf

This sample is characterized by high pollen concentration (resulting in a relatively high counting sum), whereas freshwater algae and reworked pollen occur in low amounts or are absent (Fig. **F7**). Pollen types that are generally more susceptible to oxidation are present (e.g., *Quercus*; Cheddadi and Rossignol-Strick, 1995). Thus, this sample may better reflect the original ecosystems than samples from greater depths. *Quercus* is the dominating nonsaccate pollen type in this sample; *Betula* and *Alnus* are also frequent. These findings, in combination with the presence of herbal pollen (e.g., Asteraceae), the absence of *Fagus* and *Tilia* pollen, and low *Corylus* and *Ulmus* pollen percentages, indicate an earlier Holocene age for this sample. It is also the only sample containing enough organic-walled dinoflagellate cysts (dinocysts) to make statistically relevant inferences about the dinocyst assemblages. *Operculodinium centrocarpum*/*Protoceratium reticulatum* is the dominating cyst type (61%). *Spiniferites* sp. cysts are also frequent (26%). *Lingulodinium machaerophorum* is present but only in low percentages (4%). Relatively long spines of the *Lingulodinium* specimens encountered, compared to samples from Site M0059, may indicate either cold or relatively saline conditions (Mertens et al., 2009); however, the number of *Lingulodinium* specimens measured is too low to yield robust results. The sample at 0.75 mbsf is the only one in which the genus *Ataxiodinium* was encountered.

15.69–40.60 mbsf

This interval is characterized by relatively lower percentages of bisaccate (particularly *Pinus*) pollen grains (Fig. **F7**). High percentages of freshwater algae and a high reworked/in situ pollen ratio may indicate that during the time interval reflected by these samples, tertiary material was transported to the site by freshwater inflow from land. The lower bisaccate pollen percentages compared to the interval immediately deeper may thus be a transport signal indicating that fluvial transport played a more important role for this interval than eolian transport.

48.68–202.67 mbsf

This interval is characterized by high percentages of bisaccate (particularly *Pinus*) pollen grains (Fig. **F7**),

lower percentages of freshwater algae, and a lower reworked/in situ pollen ratio compared to the interval between 15.69 and 40.60 mbsf. The amount of reworked pollen is still almost as high as, and in some cases even higher than, the amount of in situ pollen. Airborne pollen transport may have been of more importance for the sediments in this interval than for the overlying sediments because bisaccate pollen (particularly well suited for airborne transport) is very common.

Geochemistry

Interstitial water

Pore water data at Site M0060 largely reflect organic matter degradation that varies with lithology, related mineral reactions, and the presence of fresher water in two deeper sand layers at 80–95 mbsf (Unit IV) and 117–146 mbsf (Unit VI) and the return of more saline water in the deepest diamicton (Unit VII) (see "Lithostratigraphy").

Salinity variations: salinity, chloride, and alkalinity

The shipboard pore water salinity profiles (Fig. F8A; Table T7) indicate differences between Holes M0060A and M0060B. Salinities in the shallowest sections in both holes are ~30, which is consistent with chloride (Cl^-) measurements and calculations of Cl^- based salinity (Fig. F8B–F8C; Table T8). Largely similar salinity values are found to 70 mbsf in Hole M0060B, followed by a slight decrease to 25 between 70 and 85 mbsf. In contrast, shipboard salinity measurements in Hole M0060A evidence a drop from ~30 to 20 in the uppermost 45 mbsf, followed by a general but less steep decrease in salinity from 20 to 10 to ~120 mbsf. Shore-based Cl^- measurements for this interval are too discontinuous to verify the presence of distinct salinities in the two holes. Sediments deeper than 80 mbsf were only recovered from Hole M0060A. The profile indicates a low-salinity interval that corresponds to the sand layers of Units IV and VI. Deeper than 145 mbsf, salinity increases to ~20 in the underlying diamicton, indicating influence of deep and more saline waters.

Alkalinity measurements again indicate some differences between Holes M0060A and M0060B. In general there is a series of peaks in alkalinity. The most pronounced maximum of ~25 meq/L occurs at 15 mbsf, with smaller peaks of 10–15 meq/L at ~65, 85, 140, and 185 mbsf.

Organic matter degradation: methane, sulfate, hydrogen sulfide, ammonium, phosphate, iron, manganese, and pH

Several of the chemical profiles from Site M0060 preserve a record of microbial oxidation of organic matter. No methane is detected shallower than 90 mbsf, but the presence of methane (up to 2.2 mM) at ~100 mbsf and in the diamicton of Unit VII (Fig. F9A; Table T9) points to a deep subsurface zone of methanogenesis. Minima in sulfate (SO_4^{2-}) in the overlying sediment at 15 mbsf (1.7 mM SO_4^{2-}) and 60 mbsf (1.2 mM SO_4^{2-}) suggest two intervals of SO_4^{2-} reduction (Fig. F9B), although no hydrogen sulfide (H_2S) was detected in either hole (Fig. F9C). As expected, the minima in SO_4^{2-} correlate to peaks in the products of SO_4^{2-} reduction, such as alkalinity (Fig. F8D), ammonium (NH_4^+), and phosphate (PO_4^{3-}) (Fig. F9D–F9E). The amplitude of peaks in NH_4^+ and PO_4^{3-} concentration at 15 mbsf are more pronounced than those at 60 mbsf. Low concentrations of SO_4^{2-}, alkalinity, NH_4^+, and PO_4^{3-} occur from 120 to 140 mbsf in the sand layers of Unit VI, again suggesting a different water composition in this interval. Scattered and relatively low SO_4^{2-} concentrations ranging from 4 to 13 mM were observed below 150 mbsf (Table T7). Higher concentrations of alkalinity, NH_4^+, and PO_4^{3-} in the diamicton are consistent with evidence of methanogenesis in this layer.

Pore water concentrations of dissolved iron (Fe^{2+}) peak at 50 mbsf (300 µM), decrease to 45–110 µM in the sands of Unit VI, and are quite scattered (e.g., 0–150 µM) in the diamicton of Unit VII (Fig. F9F). Pore water dissolved manganese (Mn^{2+}) concentrations vary generally from 2 to 5 µM with a surface maximum of 10 µM and one high value of 30 µM in the diamicton (Fig. F9G). Variations in pH can be useful for determining the diagenetic reactions leading to the observed variations in pore water concentrations. Shipboard pore water pH is 8 ± 0.25 throughout the cored intervals with a broad minimum of ~7.3 from 20 to 70 mbsf, yet this minimum is only observed in Hole M0060B (Fig. F9H).

Mineral reactions: bromide, boron, sodium, potassium, magnesium, calcium, strontium, lithium, silica, and barium

The most obvious feature in the pore water concentrations of major and minor elements of seawater is the presence of water with a chemical composition distinctly different from seawater in the sand of Unit

VI at ~115–145 mbsf. Within this unit, low salinities are associated with lower concentrations of bromide (Br^-), boron (B), sodium (Na^+), potassium (K^+), magnesium (Mg^{2+}), and lithium (Li^+) and higher concentrations of calcium (Ca^{2+}) and strontium (Sr^{2+}) than seawater or the overlying and underlying pore waters (Figs. **F10, F11, F12**). These differences can also be seen to varying degrees in the element/Cl profiles (Fig. **F11E–F11H**). With the exception of the pore waters from the sand layers of Unit VI, most of the element/Cl ratios (Table **T8**) plot close to the seawater ratio. There appears to be evidence for a contribution of diagenetic reactions and/or ion exchange to an increase in pore water Na^+ and decreases in pore water Mg^{2+} and Ca^{2+} in Unit II (6–24 mbsf). The pore water profile of the upper 30 mbsf is also characterized by a decrease in K^+ (Fig. **F11B**) and Rb concentrations (Table **T7**), which might be related to uptake by clay minerals (Gieskes, 1983).

Concentrations of dissolved silica in pore water are generally determined by the amount and the solubility of sedimentary biogenic silica and silicate minerals. The maxima of dissolved silica at 10 and 60 mbsf (Fig. **F12D**) are likely associated with dissolution of biogenic silica (see **"Biostratigraphy"**). Dissolved silica values ranged from 200 to 700 µM in the diamicton. Peaks in the Ba^{2+} profile at 15 and 65 mbsf correlate well with minima in SO_4^{2-} (Figs. **F9B, F12B**), suggesting dissolution of barite. As noted for Site M0059, analyses of solid phases will be required to identify the reactions occurring.

Sediment

Carbon content

The total carbon (TC) content at Site M0060 ranges from 0.23 to 3.95 wt% (Table **T10;** Fig. **F13A**). Variation in total organic carbon (TOC) content is primarily related to changes in lithology and varies from 0.17 to 0.79 wt% in the greenish gray clays of Units II and III and from 0.01 to 0.21 wt% in the sandy intervals of Units V and VI. Comparatively high TOC values (up to 1.85 wt%) occur in the diamicton of Unit VII and may be caused by the presence of charcoal clasts interbedded in the sandy mineral matrix (see **"Lithostratigraphy"**).

The total inorganic carbon (TIC) ranges from 0.31 to 3.5 wt% in the uppermost 80 m of the profile, with values reaching a maximum between 63 and 78 mbsf (roughly corresponding to lithostratigraphic Subunit IIIc). Deeper than 120 mbsf, coinciding with the deposition of well-sorted sand (Unit VI) and the sandy diamicton (Unit VII), TIC values are generally low (0.5–1.2 wt%) and show only little variation compared to the overlying sections.

Sulfur content

Total sulfur (TS) values could only be determined for a limited number of samples from Site M0060, and the low resolution does not allow any apparent trends with depth to be recognized. In general, TS contents are low throughout the investigated profile, ranging from 0.14 to 0.25 wt% (Fig. **F13D**).

Physical properties

This section summarizes the preliminary physical property results from Site M0060. Two holes were drilled at this site. Hole M0060A was drilled to 232.50 mbsf, and Hole M0060B was drilled to 85.7 mbsf. A more complete data set of physical properties was produced for Hole M0060A during the OSP (Fig. **F14**) because Hole M0060B was designated as a microbiology hole (see **"Microbiology"**) and was extensively subsampled onboard. Core recovery was generally good in Hole M0060A, except for a gap between ~101.5 and 117 mbsf and from ~198 mbsf to the base of the hole, where coring alternated between hammer sampling and open-hole intervals. Although all physical property measurements described in **"Physical properties"** in the Methods chapter (Andrén et al., 2015) were conducted for Site M0060, whole-round core shipboard *P*-wave velocity data appear to be highly affected by artifacts, similar to those seen at Site M0059 (Little Belt). Discrete *P*-wave and thermal conductivity data are too sparsely distributed to exhibit any discernable downcore trends, and noncontact electrical resistivity data show little variability. Color reflectance variations do not correspond to other physical properties and lithostratigraphic units.

Natural gamma ray

High-resolution natural gamma ray (NGR) values are <5 cps near the core top in lithostratigraphic Unit I (Fig. **F14**). These low values reflect high coarse-grained content within lithostratigraphic Unit I (see **"Lithostratigraphy"**). NGR exhibits generally higher (>6 cps) and variable values in lithostratigraphic Unit II. Negative excursions potentially reflect an increase in silt or sand content, whereas positive excursions may result from an increase in clay content (see **"Lithostratigraphy"**). NGR values increase to ~15 cps at ~25 mbsf, near the lithostratigraphic Unit II/Subunit IIIa boundary, continuing at approximately this level downcore to the lithostratigraphic Unit IV/V boundary. High NGR values are interpreted as increased clay-sized sediment in lithostratigraphic Units III and IV (see **"Lithostratigraphy"**). NGR values drop to near zero at ~95 mbsf at the boundary of lithostratigraphic Units IV and V.

NGR values are low (<5 cps) in lithostratigraphic Unit VI from ~115 to ~145 mbsf, which is interpreted to result from increased silt and sand contents in this unit (see "Lithostratigraphy"). At ~145 mbsf, near the boundary of lithostratigraphic Units VI and VII, NGR values increase to ~15 cps. NGR is highly variable deeper than this throughout lithostratigraphic Unit VII.

Shipboard magnetic susceptibility

Magnetic susceptibility exhibits slightly increased values in lithostratigraphic Units I and II but near-zero values within all of lithostratigraphic Unit III (Fig. F14). lithostratigraphic Unit IV is characterized by higher and more variable values; this is also evident in the discrete values measured on cubes during the OSP (see "Paleomagnetism"). The synchronous increase in dry density suggests a lithologic change is reflected in the physical property measurements (see "Lithostratigraphy"). Below the break in recovery, from ~117 mbsf in lithostratigraphic Unit VI, excursions in magnetic susceptibility exhibit the highest magnitude in Hole M0060A. In lithostratigraphic Unit VII, values return to near zero.

Density

Discrete dry density values generally increase with depth and do not exhibit changes that correspond to lithologic boundaries (Fig. F14).

Gamma density was measured at 2 cm intervals during the offshore phase of Expedition 347. Values are not well correlated with the discrete bulk density measurements performed during the OSP (Fig. F15), either above the break in recovery (0–100 mbsf; r^2 = 0.28) or below (~117–200 mbsf; r^2 = 0.19), but exhibit an overall similar trend.

Paleomagnetism

To achieve the main objectives of the OSP paleomagnetic work, magnetic susceptibility measurements and rudimentary analyses of the natural remanent magnetization (NRM) were made on discrete specimens of known volume and mass (see "Paleomagnetism" in the "Methods" chapter [Andrén et al., 2015]). The discrete samples were taken from Hole M0060A, with a gap in sampling between 116 and 101 mbsf in the mid–lower sections of Unit V because of poor core recovery. Magnetic susceptibility (χ) ranged between 0.1 × 10^{-6} and 7 × 10^{-6} m^3/kg through the sequence, with values >2 × 10^{-6} m^3/kg confined to Unit VI, an interval of fine to medium massive well-sorted sand. Elevated χ values were also observed in an interval between 87 and 83 mbsf in Unit IV, most of Subunit IIIb, and the upper 22.23 mbsf of the hole (Units II and I). The stability of paleomagnetic pilot samples recovered from silt- and sand-rich intervals between the bottom of the hole (232.5 mbsf) and the top of Unit VI (116.7 mbsf) was poor, and this group of samples has very scattered inclinations with an average close to 0°. The majority of samples in Units III, II, and I carried normal polarity NRMs, with inclinations up to 30° shallower than a geocentric axial dipole (GAD) prediction. Samples with relatively high χ taken from Unit III and in particular Subunit IIIa acquired gyroremanent magnetization (GRM) during alternating field (AF) demagnetization above 60 mT, and these samples are associated with initial inclinations that approach the GAD prediction of 71°.

Discrete sample measurements

A total of 297 discrete samples were obtained from Hole M0060A. Samples were recovered at intervals of ~50 cm from within the site splice.

Magnetic susceptibility

The results of the magnetic analyses are shown in Figure F16. Magnetic susceptibility (χ), which was normalized to sample mass, ranges between 0.1 × 10^{-6} and 7 × 10^{-6} m^3/kg. Samples taken from Unit VII have χ values <0.5 × 10^{-6} m^3/kg. Overlying Unit VI has high χ values that exceed 2 × 10^{-6} m^3/kg in distinct intervals close to the bottom and top. The χ of Units IV and III is variable and includes one interval in Unit IV (87–83 mbsf) and one in Subunit IIIb (66–57.5 meters composite depth [mcd]) in which the values exceed 1 × 10^{-6} m^3/kg. One sample (347-M0060A-18H-1, 61–63 cm) in Subunit IIIa has an anomalously high χ value; otherwise the values are <0.2 × 10^{-6} m^3/kg and constant in the interval between 57.6 and 22.3 mcd. Unit II displays χ values that reach 0.7 × 10^{-6} m^3/kg, which trends upcore toward lower values that are characteristic of Unit I.

Sediment wet density and χ are not related to each other, although χ ranges over half an order of magnitude, which suggests that changes of the magnetic mineralogy and/or grain size are determining χ. Two trends are apparent in the biplot of χ versus NRM intensity, one that indicates high χ/NRM ratios and one that indicates low χ/NRM ratios (Fig. F16). The samples from Subunit IIIb have high χ/NRM ratios.

Natural remanent magnetization and its stability

Results of the pilot sample demagnetization (Fig. F17) indicate that an AF of 5 mT is sufficient to remove a weak viscous remanent magnetization. Three different responses to the sequential AF demagneti-

zation are displayed by samples from Site M0060. Category 1 includes the samples from the relatively coarse grained Units VII and VI, and they lose 50% of their NRM intensity at alternating fields <20 mT, with a small residual component left at 30 mT that is unaffected by more intense demagnetization levels. Category 2, which includes all other samples except those in Subunit IIIb and the interval 87–83 mbsf, is typified by a paleomagnetic vector that is smoothly demagnetized up to the maximum AF demagnetization level of 80 mT, with a vector that trends toward the origin of the orthogonal projection. Category 3 has a more complex behavior, which is characterized by the removal of a significant viscous remanence at the 5 mT demagnetization level. These samples subsequently acquired a GRM at field levels above 60 mT, with the vector moving into a plane perpendicular to the last demagnetization axis.

After removal of the viscous overprint, the NRM intensity of the samples recovered from Site M0060 lies in the range between 0.07×10^{-3} and ~250×10^{-3} A/m, with one outlier showing >500×10^{-3} A/m, and displays a general positive relationship with χ (Fig. **F16**). The relationship between NRM intensity and χ is, however, less obvious in Subunit IIIb, in which large peaks in NRM intensity are not reflected in the χ data.

Paleomagnetic directions

The directions of the paleomagnetic vectors are illustrated by the inclination data in Figure **F16.** The inclination data from Units VII, VI, and I are scattered, with an approximately equal number of positive and negative values. Only a few samples from these three units approach the GAD prediction for this site location. In contrast, the inclination data from Units IV and III group closer to the GAD prediction, but there is a bias toward lower values and some data points are negative or close to zero. It is notable that the samples taken from Unit IV and Subunit IIIb, which have high χ values and high NRM/χ, plot within a few degrees of the GAD prediction. The variable magnetic properties downhole and different categories of response to AF demagnetization, which includes samples that acquire GRM, probably preclude using the paleomagnetic data for relative dating purposes. In particular, pilot samples that have high NRM/χ and acquire GRM are restricted to intervals with inclinations that are close to the GAD prediction. These samples probably contain a secondary chemical remanent magnetization (CRM) carried by authigenic greigite (Fe_3S_4), which is known to acquire GRM (Snowball, 1997). The timing between sediment deposition and greigite precipitation is unknown and, therefore, the ability to use the paleomagnetic data at Site M0060 for relative dating purposes is very restricted.

Microbiology

Hole M0060B was drilled specifically for microbiology, interstitial water chemistry, and unstable geochemical parameters at Site M0060. Counts of microbial cells were made on board the ship by fluorescence microscopy using the acridine orange direct count (AODC) method and flow cytometry (FCM) using SYBR green DNA stain. Additional AODC counts were made during the OSP. Further counts by fluorescence microscopy will be done after the OSP using both acridine orange and SYBR green staining.

Microbial cells were enumerated at 28 sediment depths from independently taken samples for FCM (27 samples) and AODC (13 samples), both on the ship and during the OSP (Table **T11**). Microbial cell abundance is relatively low in the upper few meters (Fig. **F18**) with ~10^7 cells/cm^3 at 2.58 mbsf. The upper 6 mbsf at this site is well-sorted sand with high porosities and a very low TOC content (see **"Geochemistry"**), which is usually associated with smaller microbial cell densities. At 7.63 mbsf, microbial cell abundance increases to 3.61×10^8 cells/cm^3, and this community size is maintained for all the remaining samples in this hole to 84.43 mbsf with no significant difference between the counts ($t = 0.198$; degree of freedom [df] = 35 [not significant]).

Apart from the upper 6 m of sand, there are no major lithologic changes in the upper 80 m of this hole, which comprises silt-grade material (Fig. **F18**). It is interesting to note that there appears to be a higher TOC content in the upper parts of Unit II (see **"Geochemistry"**) where cell numbers concomitantly increase. The alkalinity profile shows a broad maximum between 7 and 30 mbsf reaching 24 meq/L compared to a background level of 10–12 meq/L for the rest of the hole. This suggests that microbial mineralization of buried organic matter is enhanced in the upper 6–30 m. However, there is no indication of a corresponding enhancement of the microbial community size over this depth range (Fig. **F18**).

Apart from the upper 6 m of this hole, all cell concentrations measured in Hole M0060B were extremely high, with values far above the upper prediction limit of the global regression of prokaryotic cells with depth (Fig. **F18**). The maximum deviation from the global regression occurred at 53.83 mbsf, where cell numbers were ~110 times greater than the global regression.

Cell counts were made by both AODC and FCM at the same sediment depths in 12 samples from Hole M0060B. A paired sample t-test on these data showed no significant difference between the two techniques (t = 0.044; df = 11 [not significant]). In Figure F19, FCM counts are plotted against AODC from the same depths. A calculated regression of this data set (data not shown), however, shows poor agreement between the two techniques, and a slope test showed a highly significant deviation from a slope of 1 (t = 5.735; df = 10; P < 0.001). This is not a surprise with this data set. The unvarying nature of the counts with depth means the data are clustered around one area on this graph and the result of the paired sample t-test should be regarded as indicative for the successful methods comparison.

Perfluorocarbon (PFC) contamination tracer was well above detection in the liner fluid and exteriors of all cores, indicating continuous PFC delivery into the borehole (Table T12). Liner fluid PFC concentrations fluctuated over 2–3 orders of magnitude (Fig. F20A), indicating variations in the rates of PFC delivery or mixing into the drilling fluid stream. Generally, the measured PFC concentrations were much below the target concentration of 1 mg PFC/L. Despite the fluctuations, PFC was above detection in the vast majority of core halfway and interior sections (Fig. F20B). Based on the fraction of liner fluid in cores, contamination was highest in the surface core, which consisted of sand, and it remained relatively high in Core 347-M0060B-3H, which consisted of organic-poor clay (Fig. F20C). Below that depth, drilling fluid intrusion (as estimated from liner fluid PFC values) fluctuated greatly with no clear relation to depth or lithology, except that PFC was below detection in the halfway and interior parts of the two lowermost cores (347-M0060B-25H and 27H). In addition to the surface cores, several deeper cores were highly contaminated (347-M0060B-6H, 10H, 17H, and 19H) and were estimated to potentially have 10^3–10^5 contaminant cells/cm^3 in the interiors (Fig. F20D).

Based on PFC data in core interiors, cores that are suitable for microbiological analyses include, in addition to Cores 347-M0060B-25H and 27H, Cores 5H, 9H, and 11H, in all of which PFC was below detection in the core interiors. Moreover, Cores 21H and 23H show a only moderate level of contamination, estimated to be <100 cells/cm^3 of sediment in the interiors (Table T12; Fig. F20D).

Stratigraphic correlation

At Site M0060, two holes were drilled, Holes M0060A (232.5 mbsf) and M0060B (85.7 mbsf). Hole M0060B was heavily subsampled offshore for microbiological studies, and the remaining core material after whole-round subsampling (see "Microbiology") was limited. Thus, it was not possible to produce a continuous splice record for this site. However, sediment cores from Hole M0060B were logged before subsampling using the Fast-track multisensor core logger (MSCL) (see "Physical properties"). Magnetic susceptibility data (4 cm resolution) from the Fast-track MSCL together with standard MSCL magnetic susceptibility measurements from Hole M0060A (2 cm resolution) enable correlation between holes and construction of a composite section for Site M0060 (Fig. F21).

The meters composite depth scale for Site M0060 is based primarily on correlation of magnetic susceptibility between holes (Fig. F21). Before analysis/correlation, all magnetic susceptibility data were cleaned for the top (0–5/20 cm) of each section, removing any outliers from the measurements. The depth offsets that define the composite section for Site M0060 are given in Table T13. Correlation between the susceptibility anomalies/data in Holes M0060A and M0060B is mainly good downhole to the end of Hole M0060B. Because of limited core material from Hole M0060B and the single hole recovery below 85.7 mbsf, there are several gaps in the composite record, and it was not possible to make a single spliced record for this site.

Similar to Site M0059, a compression or expansion correction was not applied to the data, so the offset within each core was equal for all points. Therefore, it might be that some features are not similarly aligned between holes. Thus, the meters composite depth values will approximately, but not precisely, correspond to the same stratigraphic horizons in adjacent holes.

Seismic units

Seismic sequence boundary-sediment core-MSCL log (magnetic susceptibility) correlations are shown in Figure F22. Correlation is based on the integration of seismic data and lithostratigraphy (see "Lithostratigraphy"). Two-way traveltime (time elapsed between when the acoustic pulses are sent to seabed and when they are received back at the surface) values were calculated for each lithostratigraphic unit boundary using sound velocity values measured during the OSP and offshore (see "Physical properties"; Table T14). Lithostratigraphic units and unit boundaries were examined at these calculated two-way traveltime values to define the extent of agreement between seismic boundaries and actual lithologic transitions and/or where the physical properties data indicate disconformable surfaces. Uncertainties in the time-depth function could have

resulted in minor inconsistencies between seismic features, sedimentological observations from cores, and MSCL logs.

Seismic Unit I

Two-way traveltime: 0.0541 ms
Lithology: fine to medium thickly bedded sand (lithostratigraphic Unit I)
Depth: 0–6.0 mbsf

This unit is characterized by strong reflectors in the seismic profile, as well as in physical properties like high magnetic susceptibility values measured in sediment cores.

Seismic Unit II

Two-way traveltime: 0.0768 ms
Lithology: interlaminated sandy clayey silt and fine–medium sand with dispersed clasts (lithostratigraphic Unit II)
Depth: 6.0–23.84 mbsf

Unit II shows increasing magnetic susceptibility values downcore. In the seismic profile, the lower limit of Unit II is visible, but it is not very clear at Site M0060 because of a strong seabed multiple in the seismic profile. At the lower limit of this unit, magnetic susceptibility values decrease rapidly.

Seismic Unit III

Two-way traveltime: 0.1495 ms
Lithology: laminated clay and silt with dispersed clasts (lithostratigraphic Unit III)
Depth: 23.84–79.52 mbsf

This seismic unit shows faint parallel layering in the seismic profile. Magnetic susceptibility values of this unit show high variability. The lower boundary of this unit corresponds relatively well to a change into a more seismically chaotic unit.

Seismic Unit IV

Two-way traveltime: 0.1683 ms
Lithology: interbedded sand, silt, and clay with dispersed clasts and clast-poor diamicton (lithostratigraphic Unit IV)
Depth: 79.52–95.04 mbsf

At this unit boundary, magnetic susceptibility values increase rapidly downcore.

Seismic Unit V

Two-way traveltime: 0.1947 ms
Lithology: sandy silty clay with dispersed clasts (lithostratigraphic Unit V)
Depth: 95.04–116.7 mbsf

Unit V coincides with a locally (partly) stratified seismic unit.

Seismic Unit VI

Two-way traveltime: 0.2282 ms
Lithology: fine to medium massive well-sorted sand (lithostratigraphic Unit VI)
Depth: 116.7–146.1 mbsf

Unit VI is characterized by a more chaotic seismic structure and relatively high magnetic susceptibility values. At the lower boundary of Unit VI, magnetic susceptibility values decrease rapidly downcore.

Seismic Unit VII

Two-way traveltime: 0.3215 ms
Lithology: sandy diamicton (lithostratigraphic Unit VII)
Depth: 146.1–229.6 mbsf

This unit shows some inclining seismic structures/reflectors. Some strong seismic reflectors occur in the lowermost part of this unit, but they are not seen in the lithology. However, some high magnetic susceptibility values might correspond to these seismic reflectors.

Downhole measurements

Logging operations

Downhole logging measurements in Hole M0060B were made after completion of coring to a total depth of 85.7 m DSF. In preparation for logging, the hole was circulated with seawater and the pipe was pulled back to ~17.5 m WSF.

For downhole logging in Hole M0060B three tool strings were deployed:

- The gamma ray tool (MCG)/array induction tool (MAI) tool string, measuring total gamma ray and electrical resistivity,
- The MCG/spectral gamma ray tool (SGS)/sonic sonde (MSS) tool string, measuring total gamma ray, spectral gamma ray, and sonic velocity, and
- The MCG/microimager (CMI) tool string, with total gamma ray and microimager tools.

The MCG/MAI tool string was lowered and downlogged to 67 m WSF. The hole was then uplogged to the seafloor. The wireline depth to the seafloor was determined from the step increase in gamma ray values.

The MCG/SGS/MSS tool string was lowered to 61 m wireline log depth below seafloor (WSF) and an uplog was started.

The MCG/CMI tool string was lowered to 56 m WSF with the calipers closed. The hole was then uplogged with open calipers at high resolution.

The tools provided continuous and good quality log data.

Logging units

Hole M0060B is divided into two logging units on the basis of the logs (Fig. F23). The uplog was used as the reference to establish the wireline log depth below seafloor depth scale.

Logging Unit 1: base of drill pipe to 23.5 m WSF

This logging unit is characterized by a fluctuation in gamma ray between 40 and 60 gAPI. Gamma ray values are driven by thorium and uranium; no potassium is measured in logging Unit 1. Resistivity values also show fluctuations and infiltration of borehole fluid into the formation (deep, medium, and shallow resistivity show different values). Sonic values are increasing. The fluctuations observed might be due to poor borehole conditions, but in this interval, no caliper data are available. The generally lower NGR values are explained by the sandy clayey silt as described in lithostratigraphic Unit II (see **"Lithostratigraphy"**).

Logging Unit 2: 23.5–67 m WSF

NGR values vary between 80 and 100 gAPI and are higher than in logging Unit 1. This can be explained by the increase in clay content from lithostratigraphic Units II and III (see **"Lithostratigraphy"**). Resistivity is constant throughout this unit, and the sonic log slightly decreases with depth. The caliper data in logging Unit 2 shows good borehole conditions with the hole slightly closing in the top part of the unit.

References

Andrén, T., Jørgensen, B.B., Cotterill, C., Green, S., Andrén, E., Ash, J., Bauersachs, T., Cragg, B., Fanget, A.-S., Fehr, A., Granoszewski, W., Groeneveld, J., Hardisty, D., Herrero-Bervera, E., Hyttinen, O., Jensen, J.B., Johnson, S., Kenzler, M., Kotilainen, A., Kotthoff, U., Marshall, I.P.G., Martin, E., Obrochta, S., Passchier, S., Quintana Krupinski, N., Riedinger, N., Slomp, C., Snowball, I., Stepanova, A., Strano, S., Torti, A., Warnock, J., Xiao, N., and Zhang, R., 2015. Methods. *In* Andrén, T., Jørgensen, B.B., Cotterill, C., Green, S., and the Expedition 347 Scientists, *Proc. IODP,* 347: College Station, TX (Integrated Ocean Drilling Program). **doi:10.2204/iodp.proc.347.102.2015**

Cheddadi, R., and Rossignol-Strick, M., 1995. Improved preservation of organic matter and pollen in Eastern Mediterranean sapropels. *Paleoceanography,* 10(2):301–309. **doi:10.1029/94PA02673**

Cronin, T.M. 1981. Paleoclimatic implications of late Pleistocene marine ostracodes from the St. Lawrence Lowlands. *Micropaleontology,* 27(4): 384–418. **doi:10.2307/1485193**

Cronin, T.M., Gemery, L.J., Briggs. W.M., Jr., Jakobsson, M., Polyak, L., and Brouwers, E.M., 2010. Quaternary sea-ice history in the Arctic Ocean based on a new Ostracode sea-ice proxy. *Quat. Sci. Rev.,* 29(25–26):3415–3429. **doi:10.1016/j.quascirev.2010.05.024**

Frenzel, P., Keyser, D., and Viehberg, F.A., 2010. An illustrated key and (palaeo)ecological primer for postglacial to Recent Ostracoda (Crustacea) of the Baltic Sea. *Boreas,* 39(3):567–575. **doi:10.1111/j.1502-3885.2009.00135.x**

Gieskes, J.M., 1983. The chemistry of interstitial waters of deep sea sediments: interpretation of deep sea drilling data. *In* Riley, J.P., and Chester, R. (Eds.), *Chemical Oceanography* (Vol. 8): London (Academic), 221–269. **doi:10.1016/B978-0-12-588608-6.50010-9**

Knudsen, K.L., Jiang, H., Gibbard, P.L., Kristensen, P., Seidenkrantz, M.-S., Janczyk-Kopikowa, Z., and Marks, L., 2012. Environmental reconstructions of Eemian Stage interglacial marine records in the Lower Vistula area, southern Baltic Sea. *Boreas,* 41(2):209–234. **doi:10.1111/j.1502-3885.2011.00232.x**

Mertens, K.N., Ribeiro, S., Bouimetarhan, I., Caner, H., Nebout, N.C., Dale, B., De Vernal, A., Ellegaard, M., Filipova, M., Godhe, A., Goubert, E., Grøsfjeld, K., Holzwarth, U., Kotthoff, U., Leroy, S.A.G., Londeix, L., Marret, F., Matsuoka, K., Mudie, P.J., Naudts, L., Peña-Manjarrez, J.L., Persson, A., Popescu, S.-M., Pospelova, V., Sangiorgi, F., van der Meer, M.T.J., Vink, A., Zonneveld, K.A.F., Vercauteren, D., Vlassenbroeck, J., and Louwye, S., 2009. Process length variation in cysts of a dinoflagellate, *Lingulodinium machaerophorum,* in surface sediments: investigating its potential as salinity proxy. *Mar. Micropaleontol.,* 70(1–2):54–69. **doi:10.1016/j.marmicro.2008.10.004**

Rasmussen, J.A., Heinberg, C., and Håkansson, E., 2005. Planktonic foraminifers, biostratigraphy and the diachronous nature of the lowermost Danian Cerithium Limestone at Stevns Klint, Denmark. *Bull. Geol. Soc. Den.,* 52(2):113–131. **http://2dgf.dk/xpdf/bull52-2-113-131.pdf**

Roussel, E.G., Bonavita, M.-A.C., Querellou, J., Cragg, B.A., Webster, G., Prieur, D., and Parkes, R.J., 2008. Extending the subseafloor biosphere. *Science,* 320(5879):1046. **doi:10.1126/science.1154545**

Seidenkrantz, M.-S., 1993a. Benthic foraminiferal and stable isotope evidence for a "Younger Dryas-style" cold spell at the Saalian-Eemian transition, Denmark. *Palaeogeogr., Palaeoclimatol., Palaeoecol.,* 102(1–2):103–120. **doi:10.1016/0031-0182(93)90008-7**

Seidenkrantz, M.-S., 1993b. Foraminifera from the Quaternary sequence in the Anholt boring, Denmark. *Boreas,* 22(4):283–290. **doi:10.1111/j.1502-3885.1993.tb00188.x**

Seidenkrantz, M.-S., and Knudsen, K.L., 1993. Middle Weichselian to Holocene palaeoecology in the eastern Kattegat, Scandinavia: foraminifera, ostracods and ^{14}C measurements. *Boreas,* 22(4):299–310. **doi:10.1111/j.1502-3885.1993.tb00190.x**

Snoeijs, P., Vilbaste, S., Potapova, M., Kasperoviciene, J., and Balashova, J. (Eds.), 1993–1998. *Intercalibration and Distribution of Diatom Species in the Baltic Sea* (Vol. 1–5): Uppsala, Sweden (Opulus Press).

Snowball, I.F., 1997. Gyroremanent magnetization and the magnetic properties of greigite-bearing clays in southern Sweden. *Geophys. J. Int.,* 129(3):624–636. **doi:10.1111/j.1365-246X.1997.tb04498.x**

Stepanova, A., Taldenkova, E., Simstich, J., and Bauch, H.A., 2007. Comparison study of the modern ostracod associations in the Kara and Laptev Seas: ecological aspects. *Mar. Micropaleontol.,* 63(3–4):111–142. **doi:10.1016/j.marmicro.2006.10.003**

Publication: 20 February 2015
MS 347-104

Figure F1. Graphic lithology log summary, Hole M0060A.

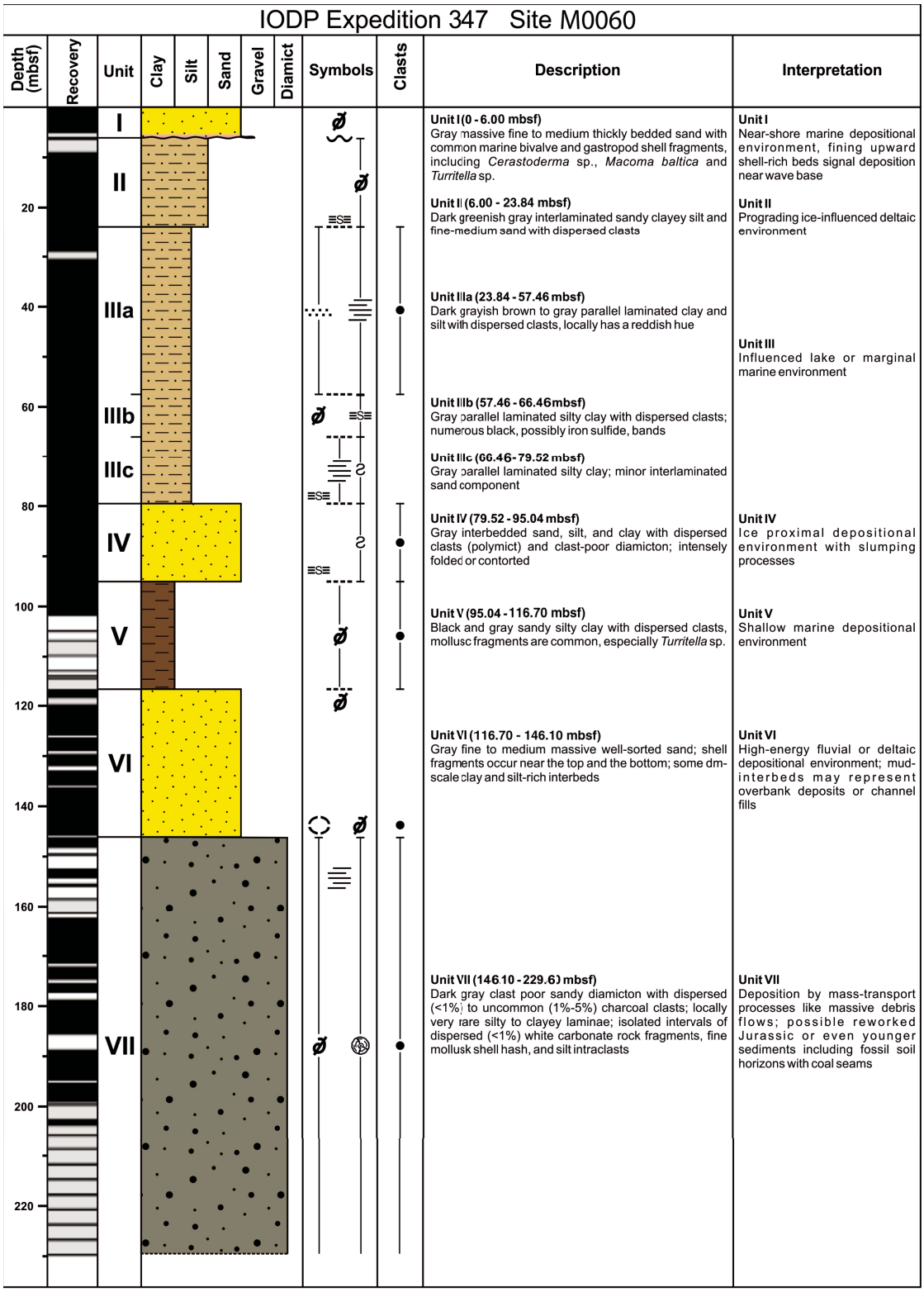

Figure F2. Contact between Subunits IIIa and IIIb (interval 347-M0060A-23H-1, 56–90 cm).

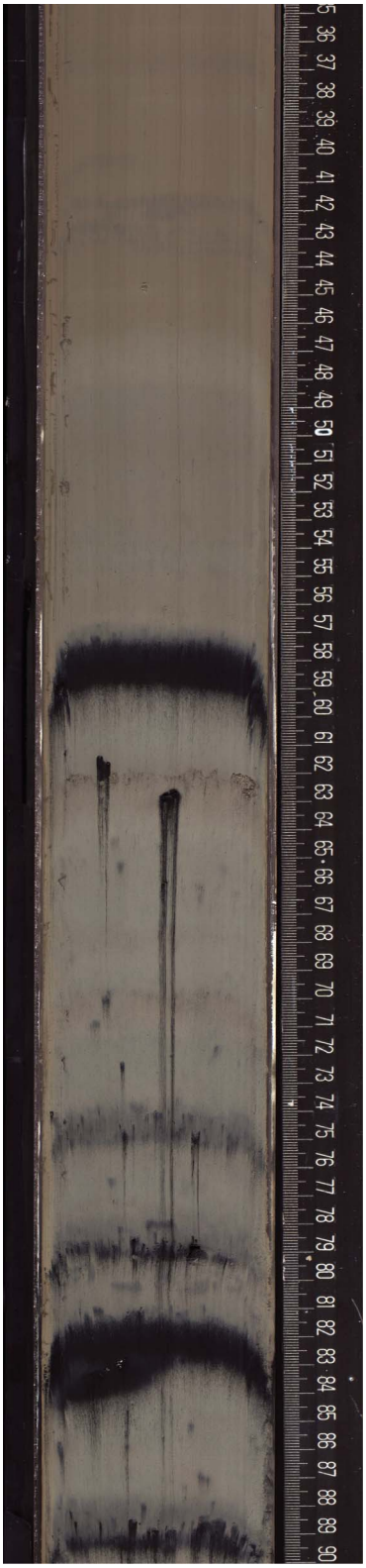

Figure F3. Clast-poor sandy diamicton (interval 347-M0060A-66H-1, 13–40 cm).

Figure F4. Analyzed levels and diatom occurrence, Hole M0060A. Only the upper parts of the core contain in situ diatom deposition. The majority of the core contains rare, reworked diatom fragments and individual valves.

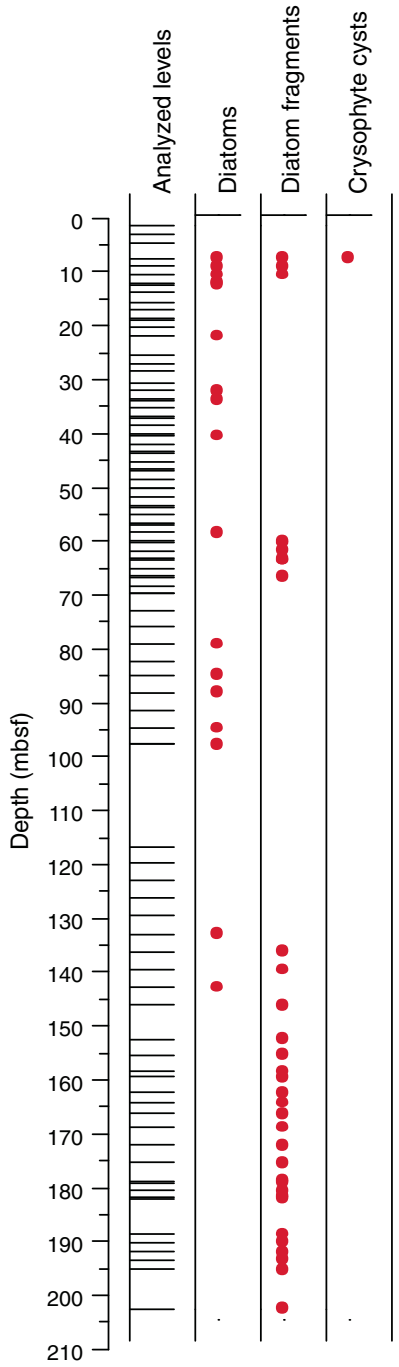

Figure F5. Foraminifers, Site M0060. **A.** Number of foraminifers per cubic centimeter sample (samples of very large volume were not always picked in their entirety). Number of foraminifers for samples with counts exceeding 125 individuals are shown on the right. **B.** Percent of assemblage composed of *Elphidium excavatum clavatum*. Only OSP samples are shown. **C.** Number of foraminiferal species/20 cm^3 sample (samples of very large volume were not always picked in their entirety).

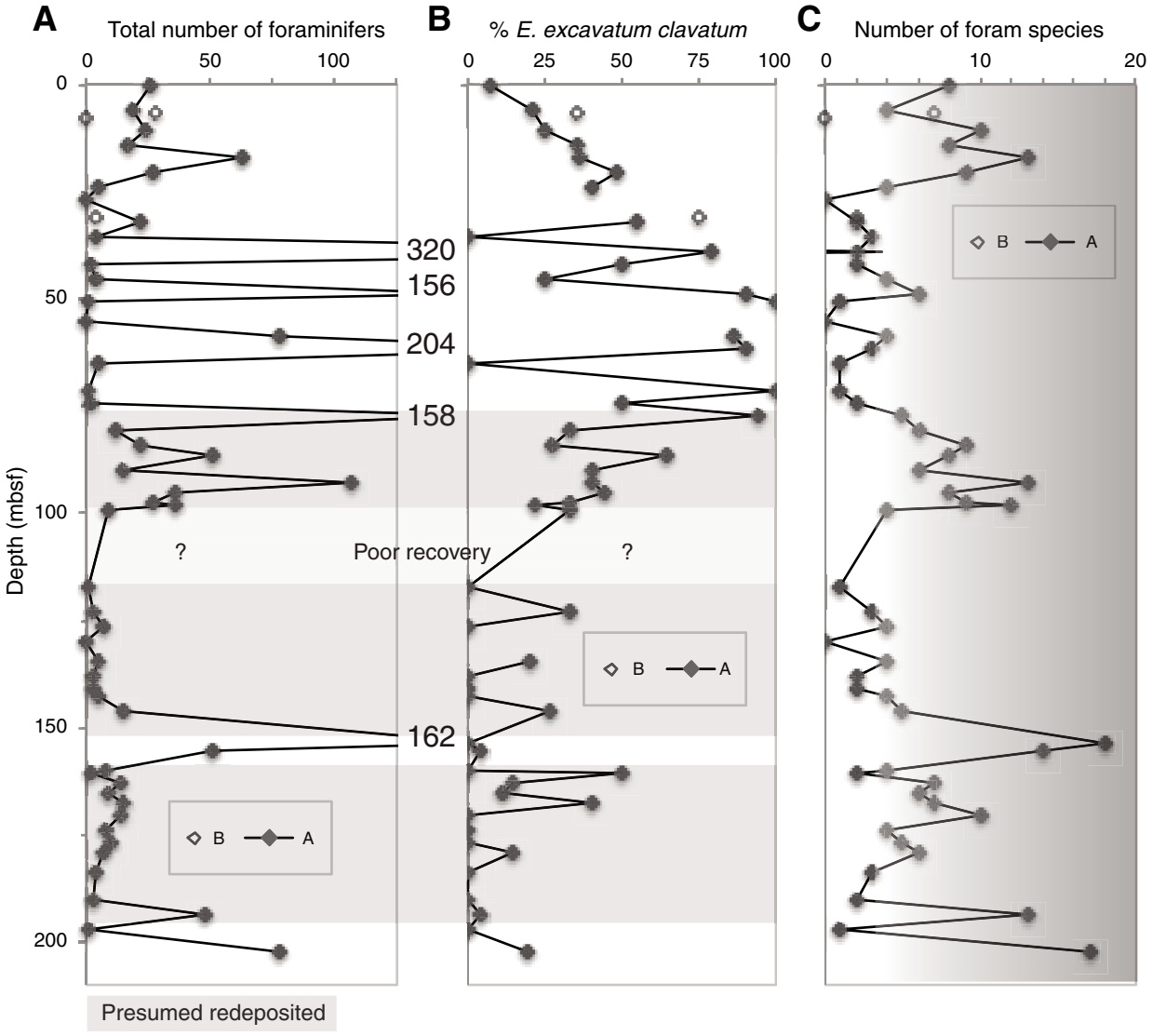

Figure F6. Distribution of ostracod ecological groups and their abundance, Site M0060. Abundance is shown per sediment volume.

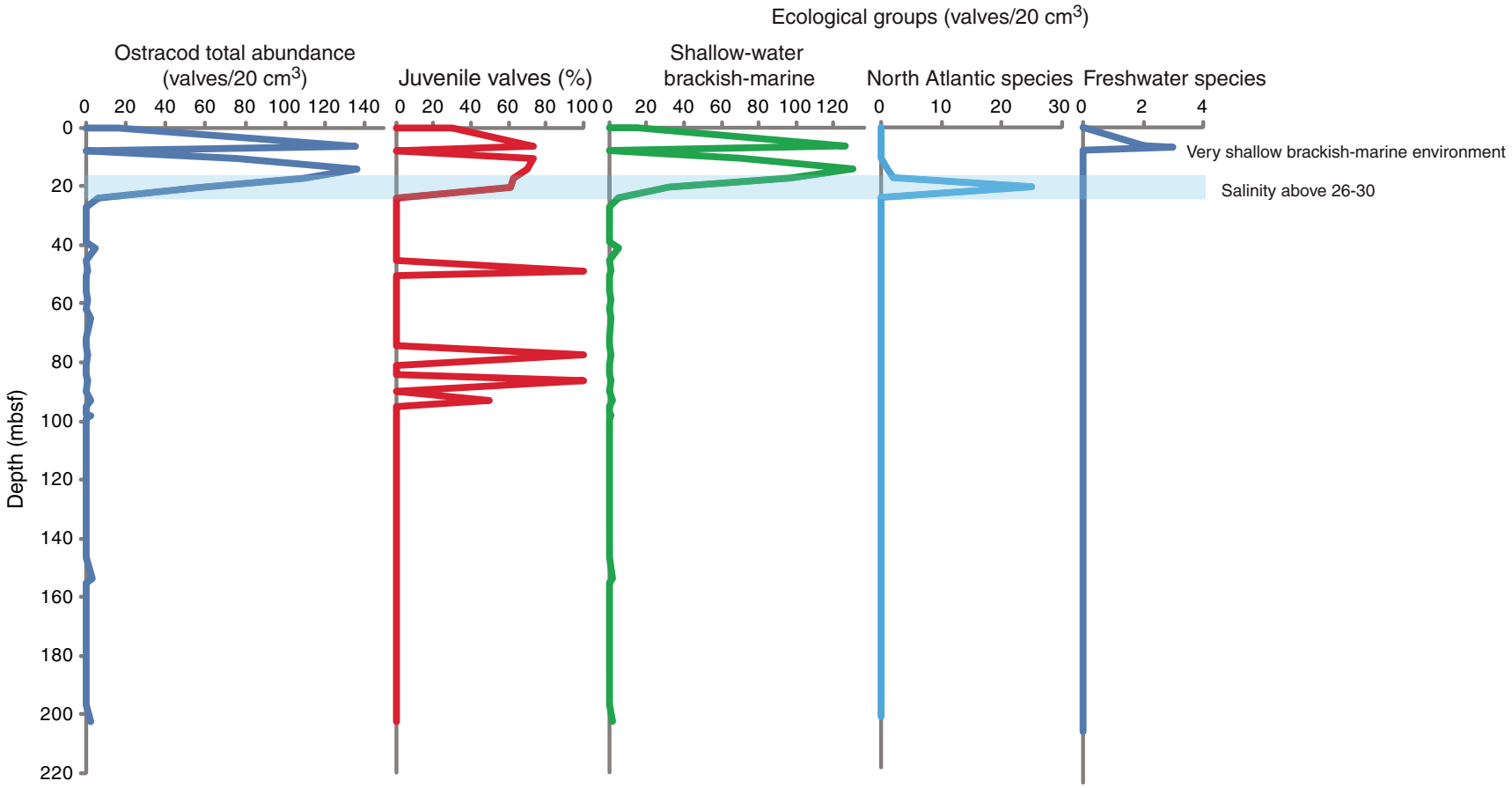

Figure F7. Simplified pollen diagram, dinocyst, and palynomorph data, Site M0060. Pollen and algae percentage calculations are based on the terrestrial pollen sum. Because of generally poor palynomorph preservation, counting sums were too low in some samples to get statistically relevant data (orange bars). The organic-walled-dinoflagellate-cyst/terrestrial-pollen ratio (*) could not be calculated in samples where in situ dinocysts were absent.

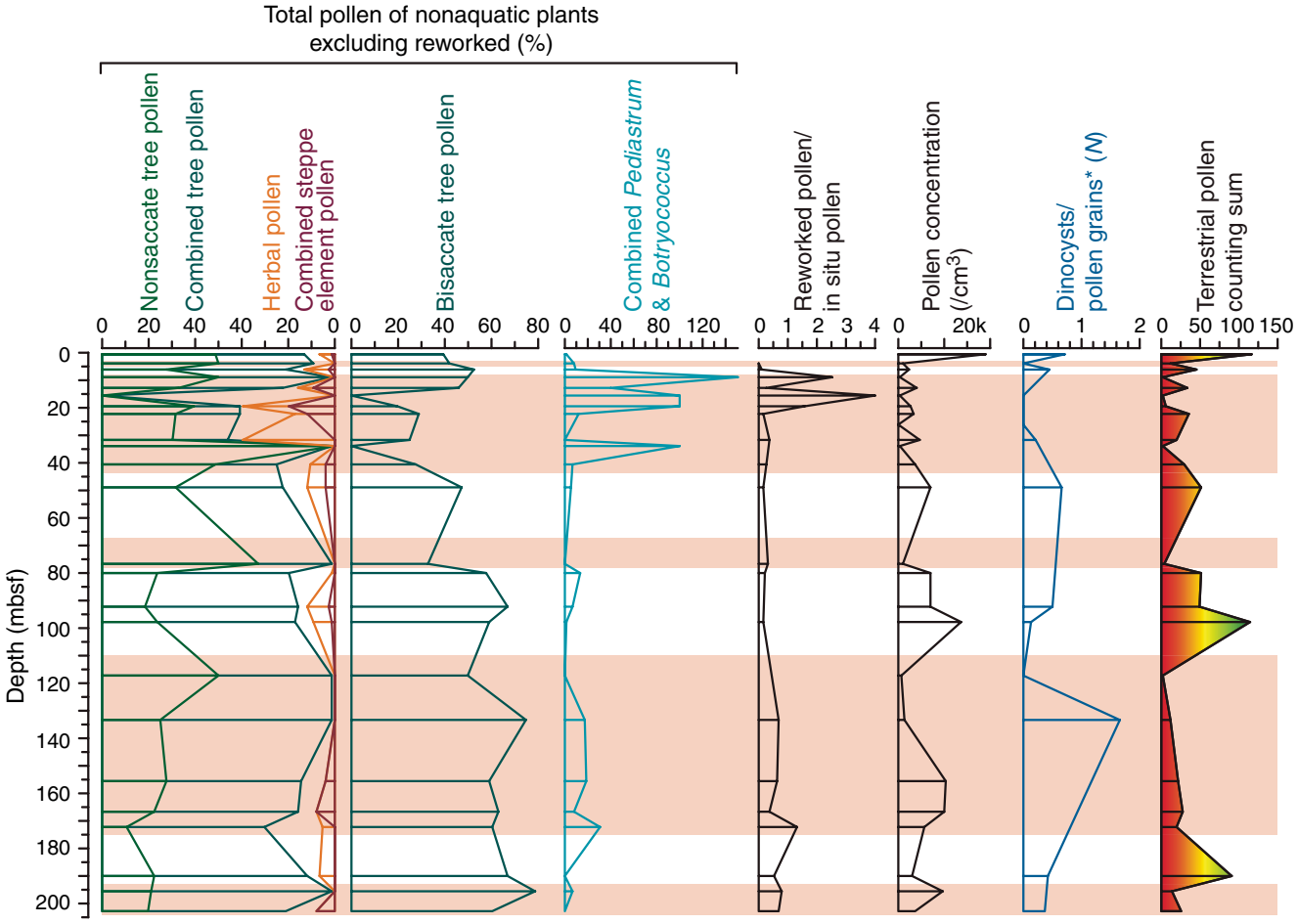

Figure F8. Concentrations of (**A**) shipboard salinity calculated from refractive index, (**B**) chloride, (**C**) chloride-based salinity, and (**D**) alkalinity in interstitial water samples, Site M0060.

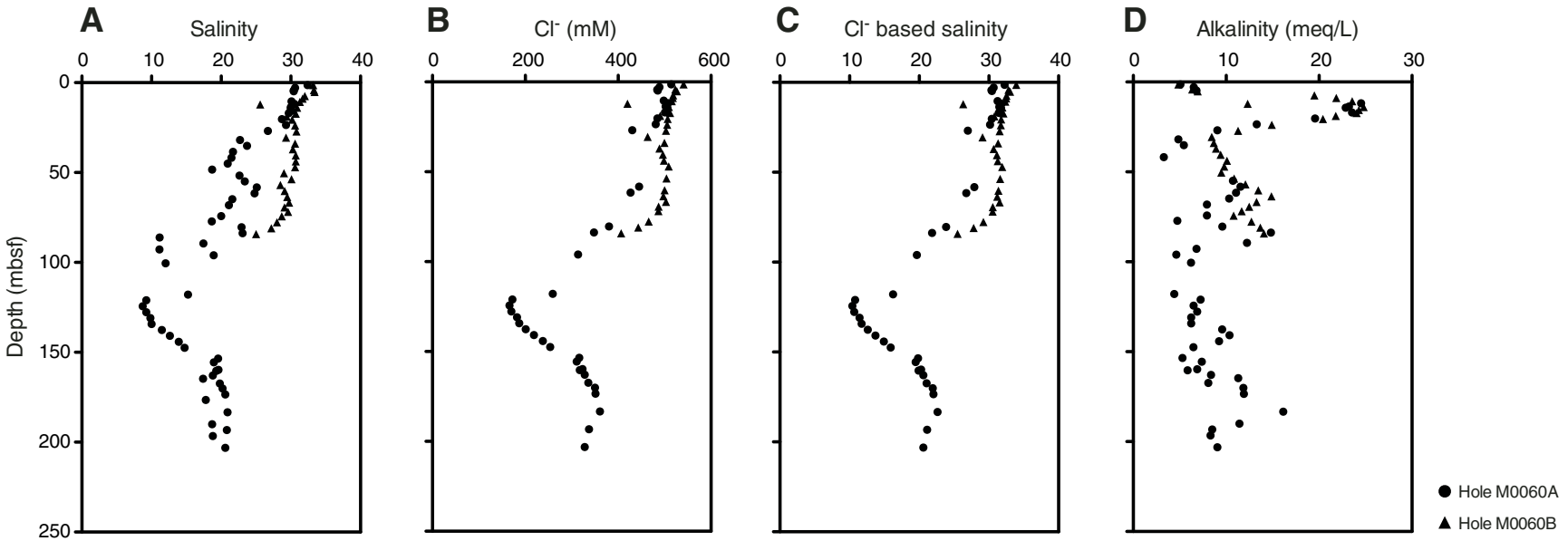

Figure F9. Concentrations of (**A**) methane, (**B**) sulfate, (**C**) hydrogen sulfide, (**D**) ammonium, (**E**) phosphate, (**F**) iron, (**G**) manganese, and (**H**) pH from interstitial water samples, Site M0060.

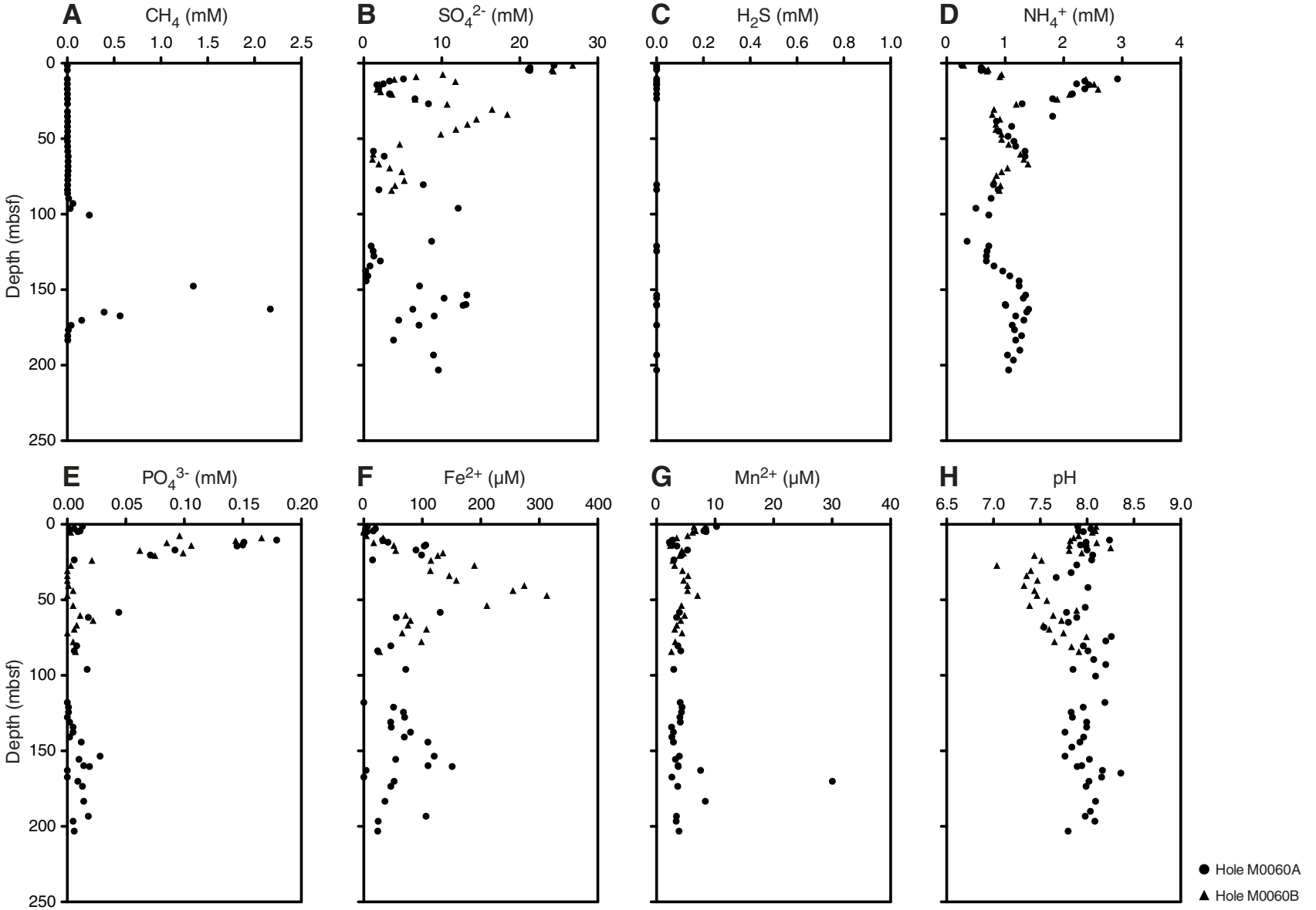

Figure F10. Concentrations of (**A**) bromide, (**B**) bromide/chloride, (**C**) boron, and (**D**) boron/chloride from interstitial water samples, Site M0060. Dashed lines = seawater ratio.

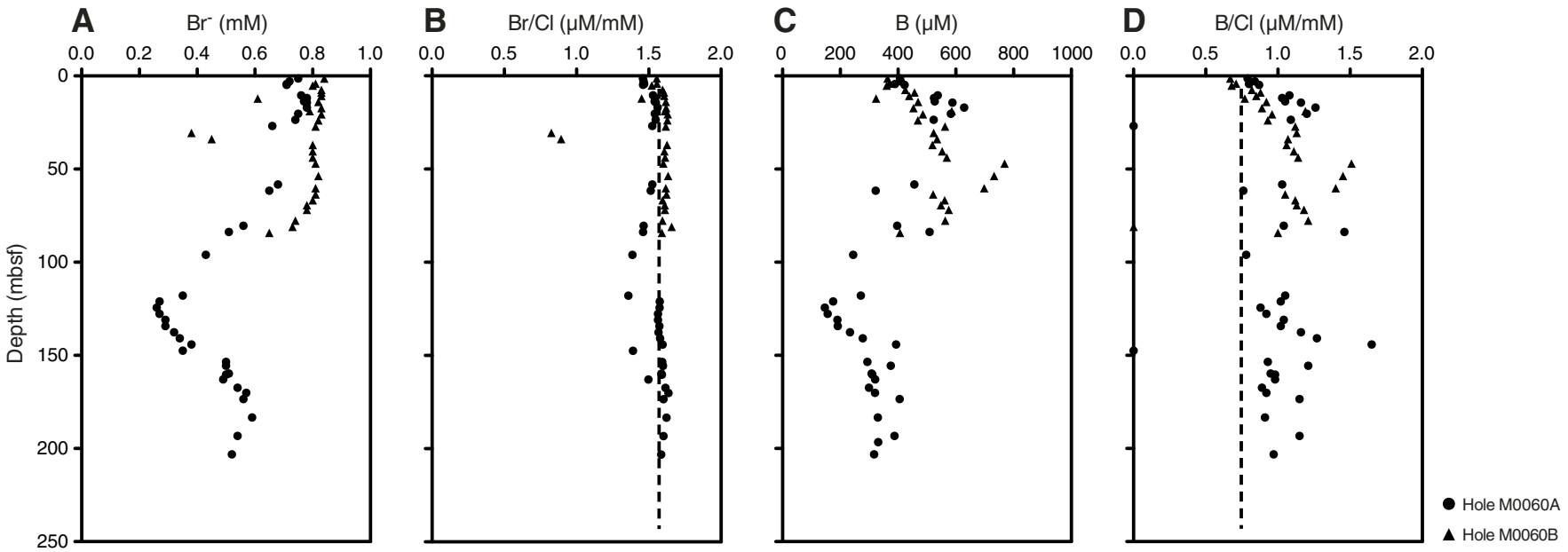

Figure F11. Concentrations of (**A**) sodium, (**B**) potassium, (**C**) magnesium, (**D**) calcium, (**E**) sodium/chloride, (**F**) potassium/chloride, (**G**) magnesium/chloride, and (**H**) calcium/chloride from interstitial water samples, Site M0060. Dashed lines = seawater ratio.

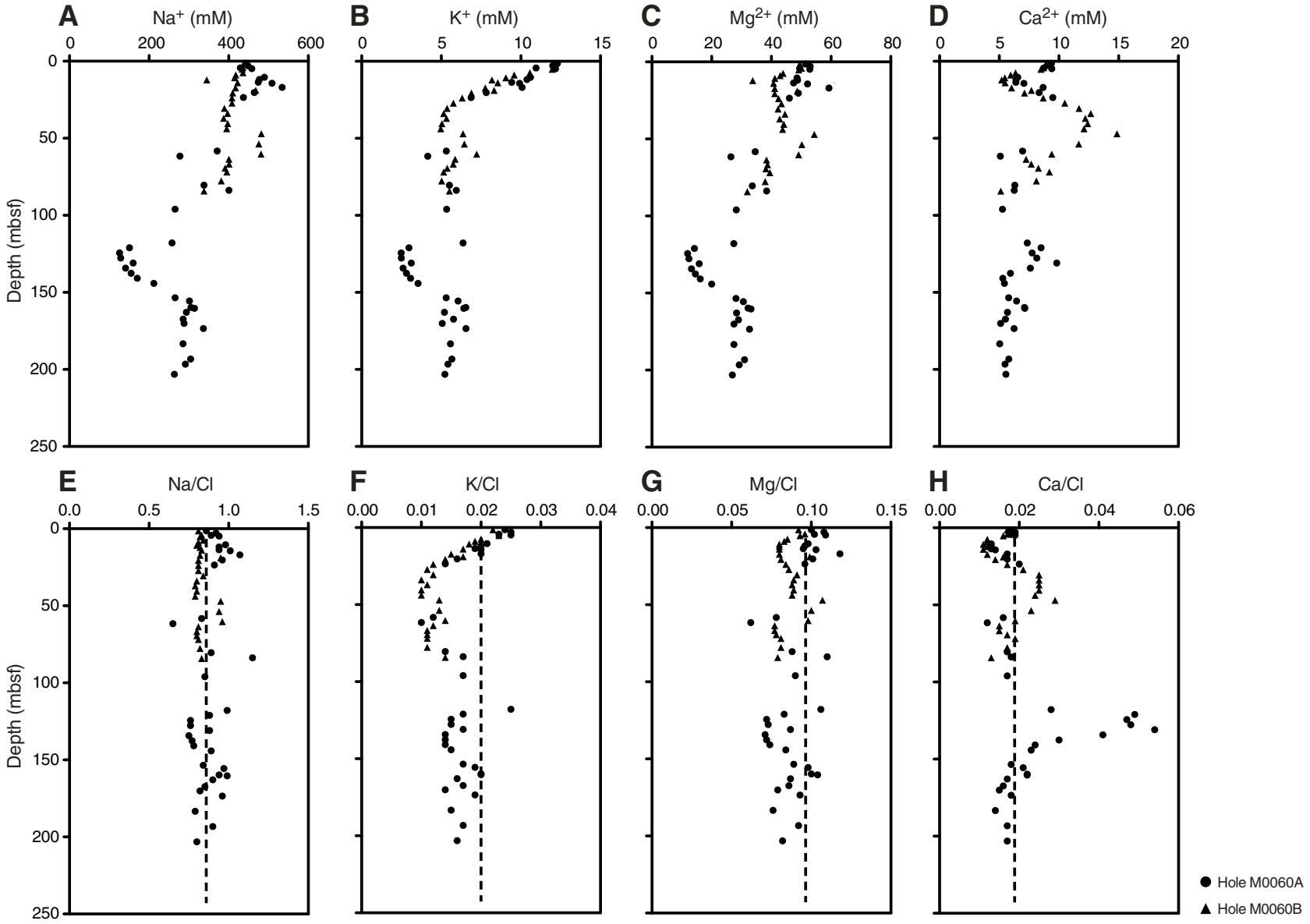

Figure F12. Concentrations of (**A**) strontium, (**B**) barium, (**C**) lithium, and (**D**) dissolved silica from interstitial water samples, Site M0060.

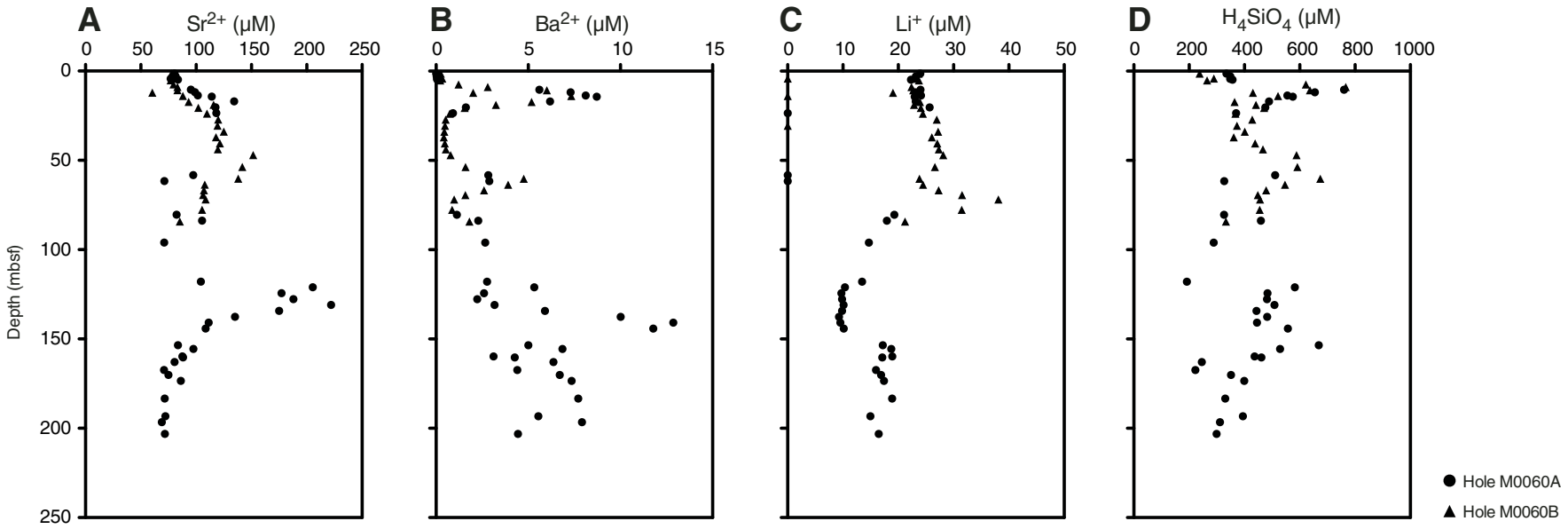

Figure F13. Sedimentary (**A**) total carbon (TC), (**B**) total organic carbon (TOC), (**C**) total inorganic carbon (TIC), and (**D**) total sulfur (TS), Site M0060.

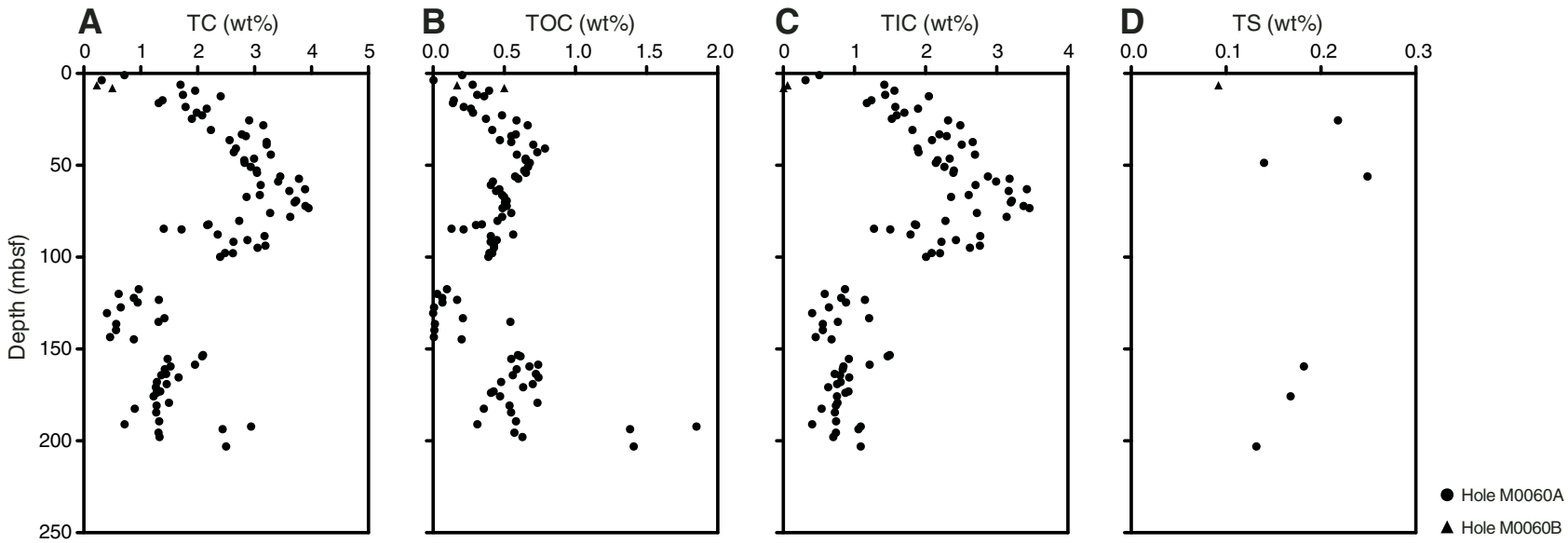

Figure F14. Natural gamma radiation (NGR) (cps), MSCL magnetic susceptibility (MS) (10^{-5} SI), and dry density (g/cm^3) with lithostratigraphic boundaries, Hole M0060A.

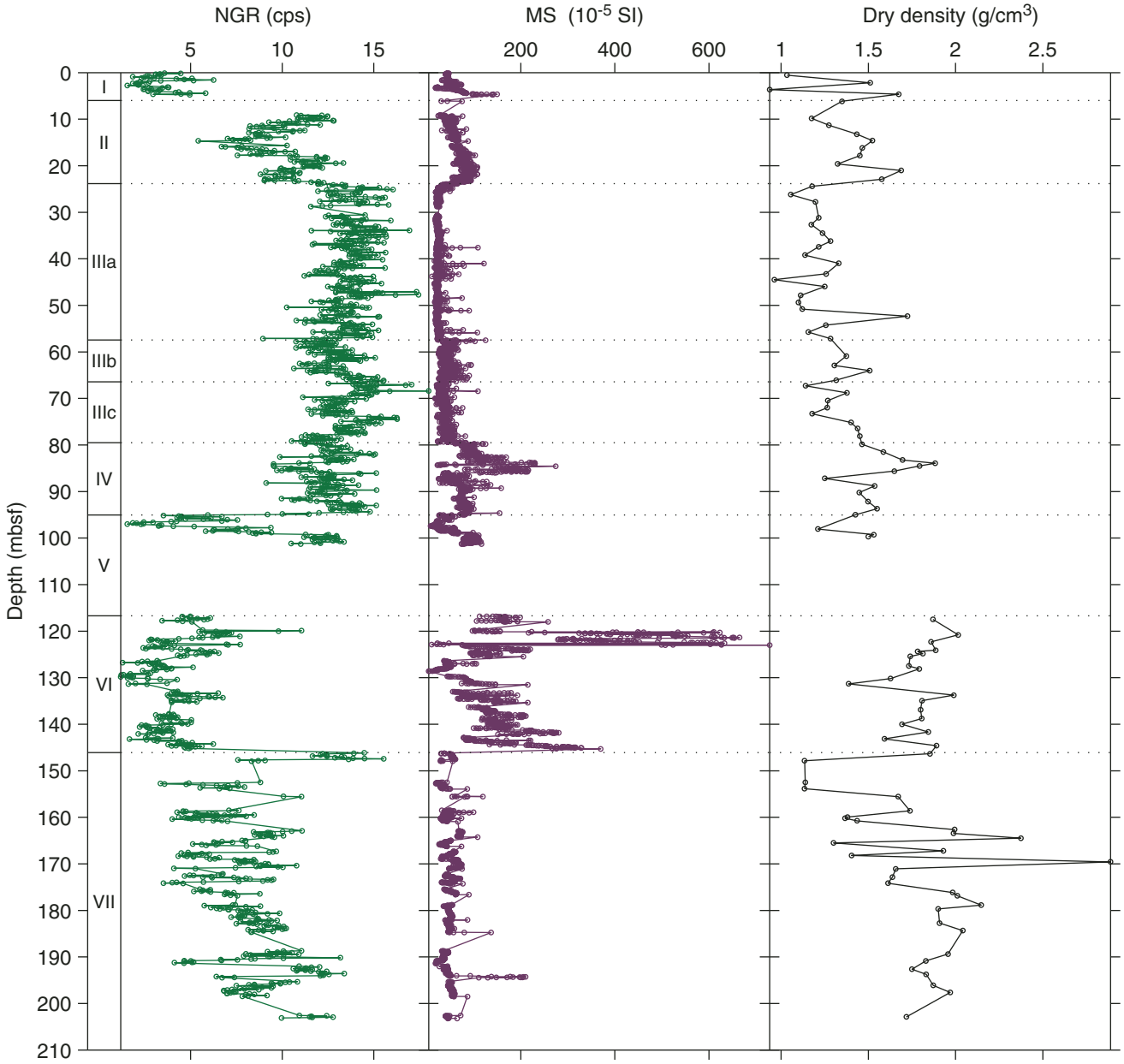

Figure F15. Gamma density (g/cm^3) and discrete bulk density (g/cm^3) measurements derived from pycnometer moisture and density analyses, Hole M0060A.

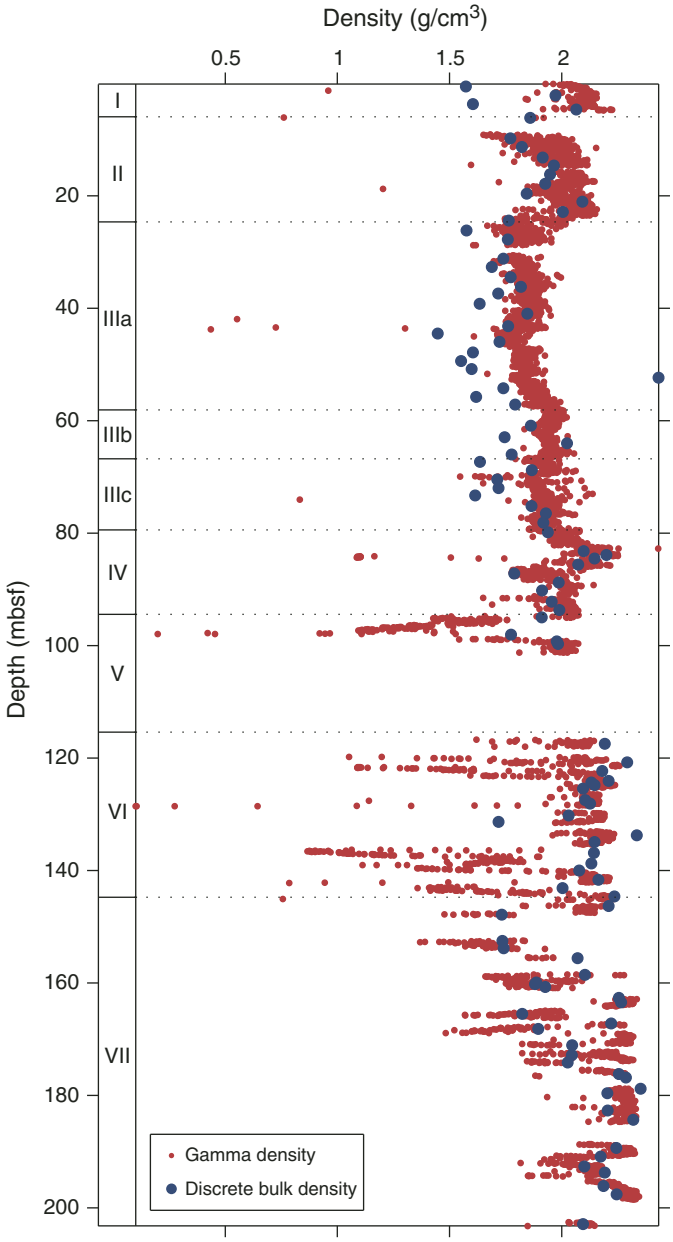

Figure F16. Plots and biplots of magnetic susceptibility (χ), natural remanent magnetization (NRM) intensity, and NRM inclination of discrete palaeomagnetic samples, Hole M0060A. Dashed line = geocentric axial dipole (GAD) prediction of inclination for the site latitude.

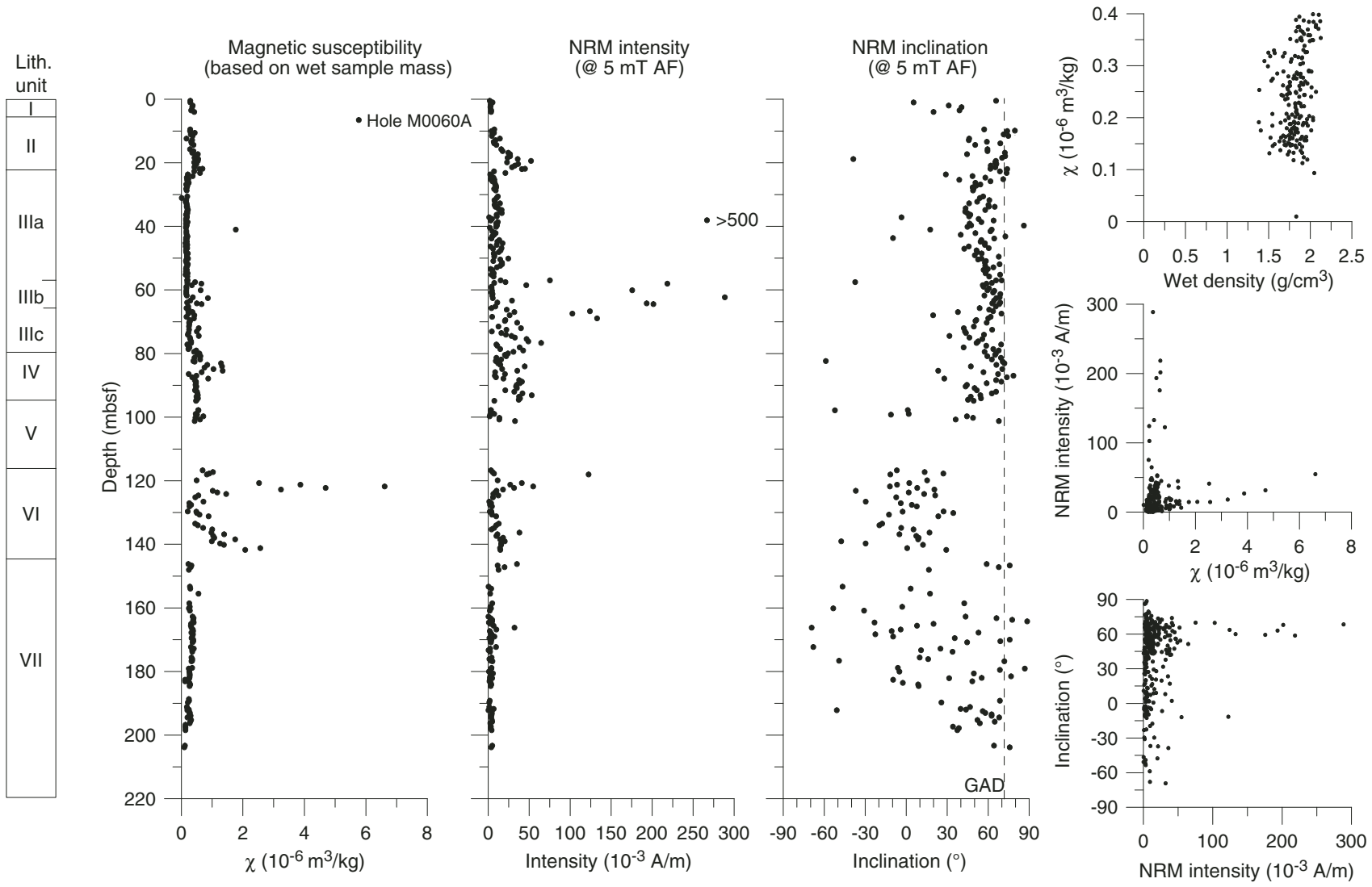

Figure F17. Plots of natural remanent magnetization (NRM) after AF demagnetization to 80 mT. **A.** Sample 347-M0060A-24H-2, 9 cm; 61.79 mcd. **B.** Sample 347-M0060A-15H-3, 26 cm; 33.77 mcd. **C.** Sample 347-M0060A-48H-1, 131 cm; 118.02 mcd. Category 1 and 2 vectors trend toward the origin, whereas Category 3 vectors veer into a plane perpendicular to the last demagnetization axis, which is a sign of gyroremanent magnetization acquisition. Open squares = vertical, solid squares = horizontal.

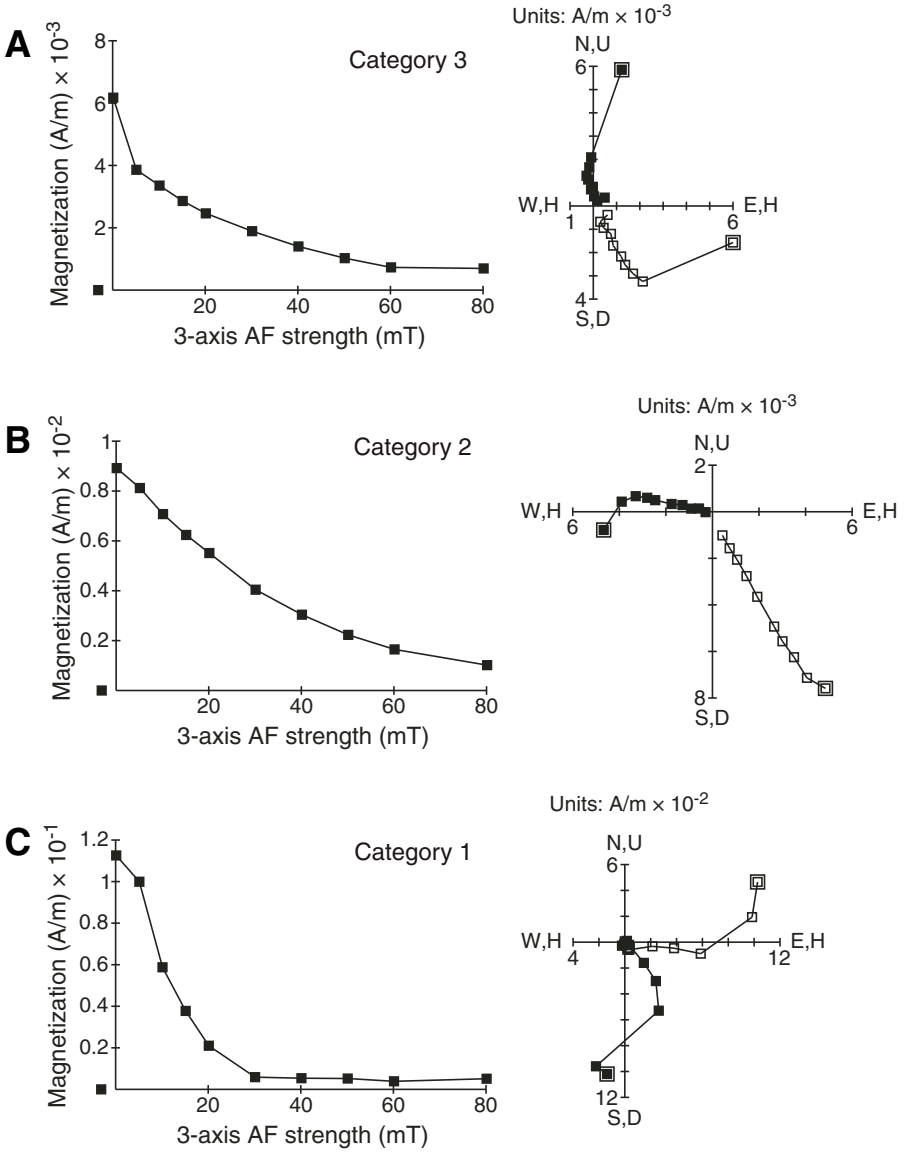

Figure F18. Plot of microbial cell abundances compared to chemical zonation and lithostratigraphy, Hole M0060B. **A.** Interstitial water alkalinity (blue dashed line) and salinity (red line). **B.** Cell numbers obtained by flow cytometry (blue circles) and acridine orange direct count (red diamonds). Solid black line = global regression line of prokaryote cell numbers with depth, dashed lines = upper and lower 95% prediction limits for regression line (Roussel et al., 2008). **C.** Lithology.

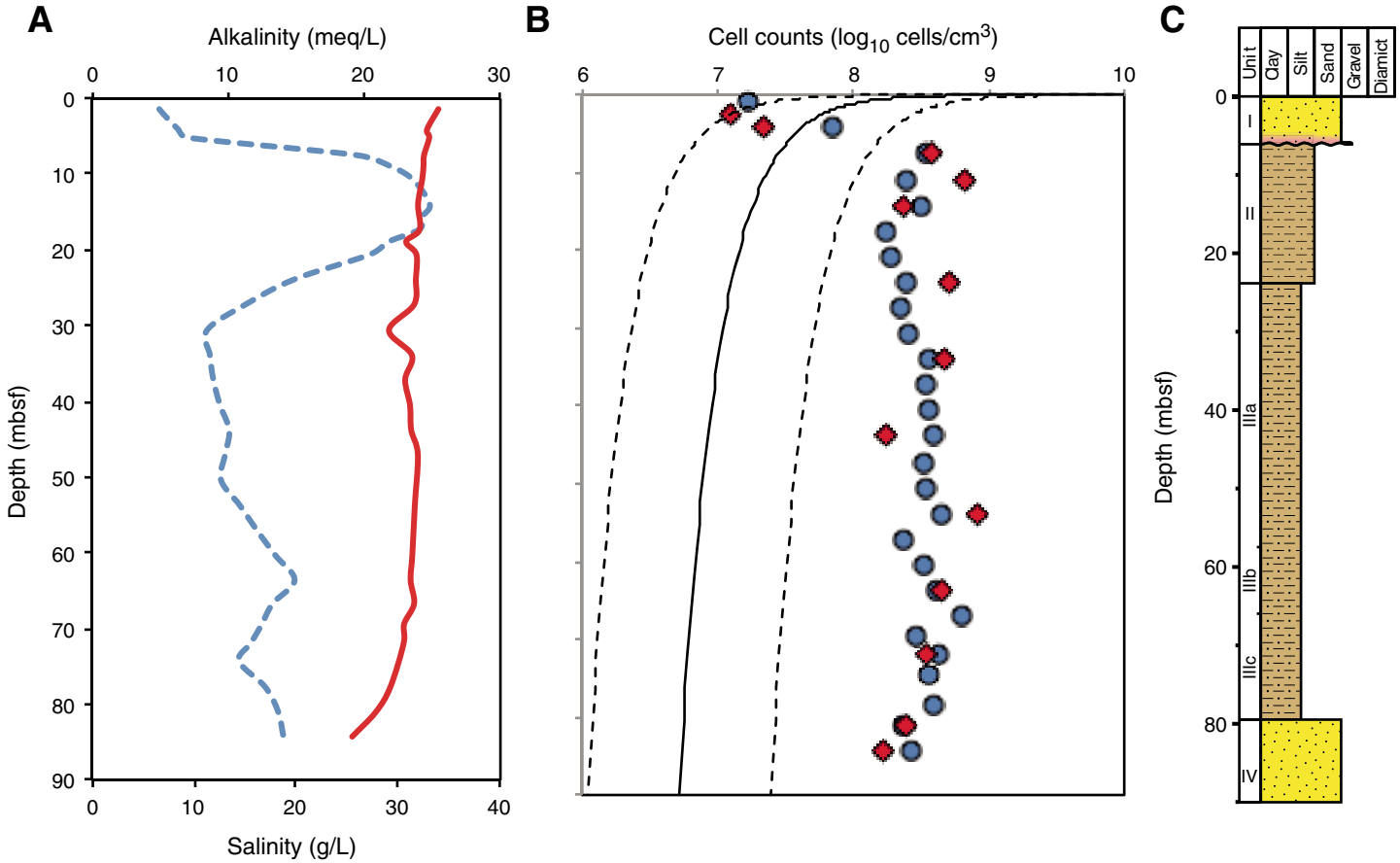

Figure F19. Comparison of paired counts between two methods of cell enumeration, Hole M0060B. Black dashed line = line of unity. FCM = flow cytometry, AODC = Acridine Orange Direct Count.

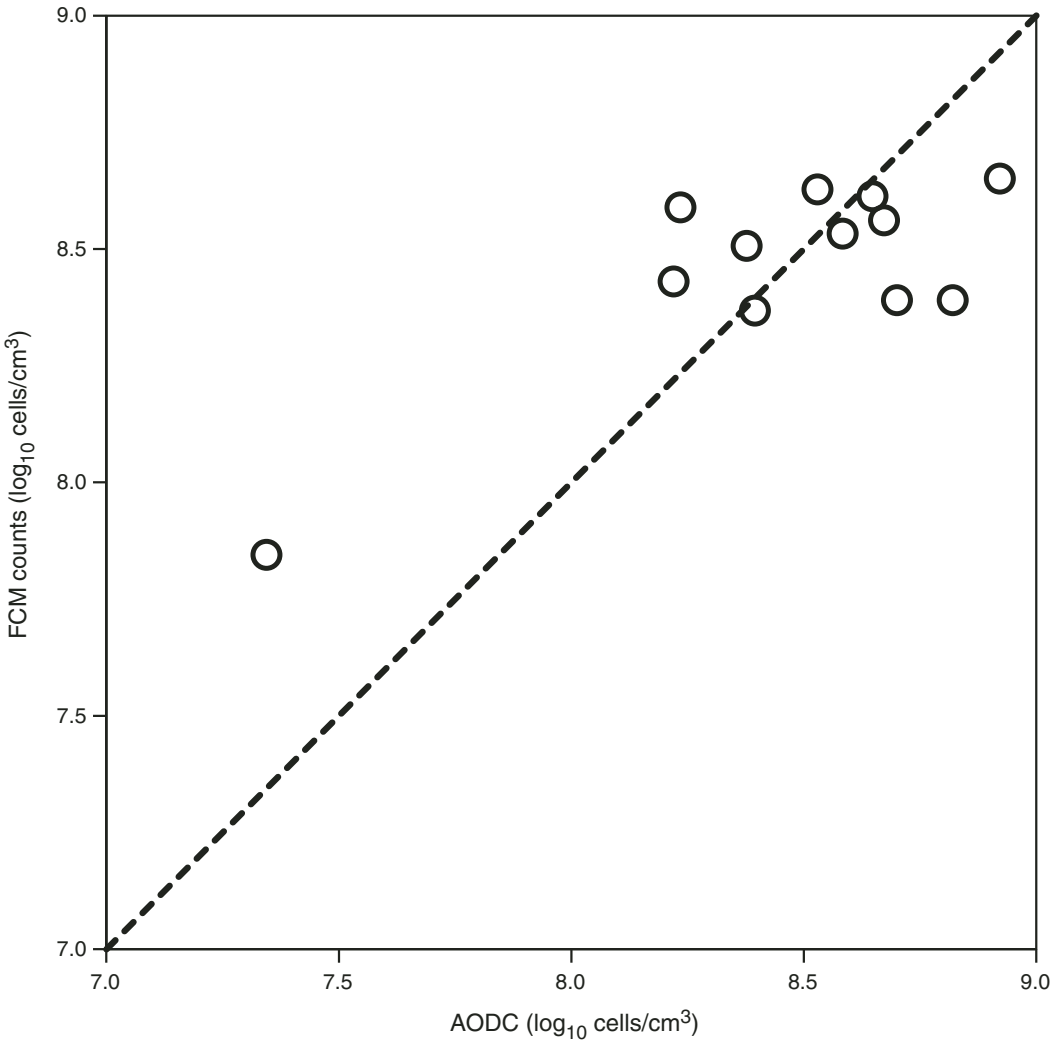

Figure F20. Plots of perfluorocarbon (PFC) tracer concentrations, Hole M0060B. **A.** Core liner fluid. **B.** Sediment core samples. (Continued on next page.)

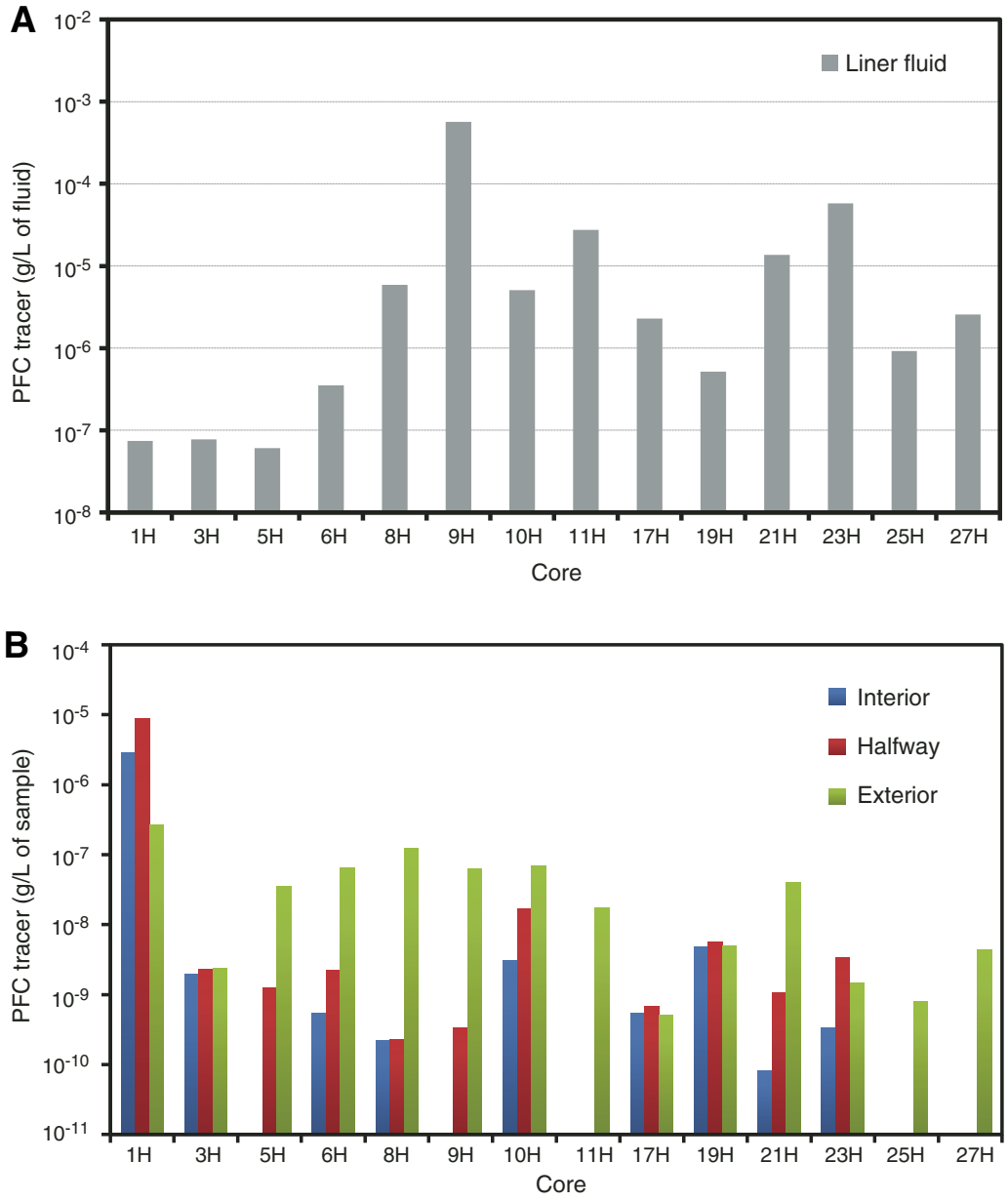

Figure F20 (continued). **C.** Estimated volume of liner fluid introduced into sediment cores shown as percentage of sediment core volume. **D.** Estimated potential number of contaminant cells per volume of sediment.

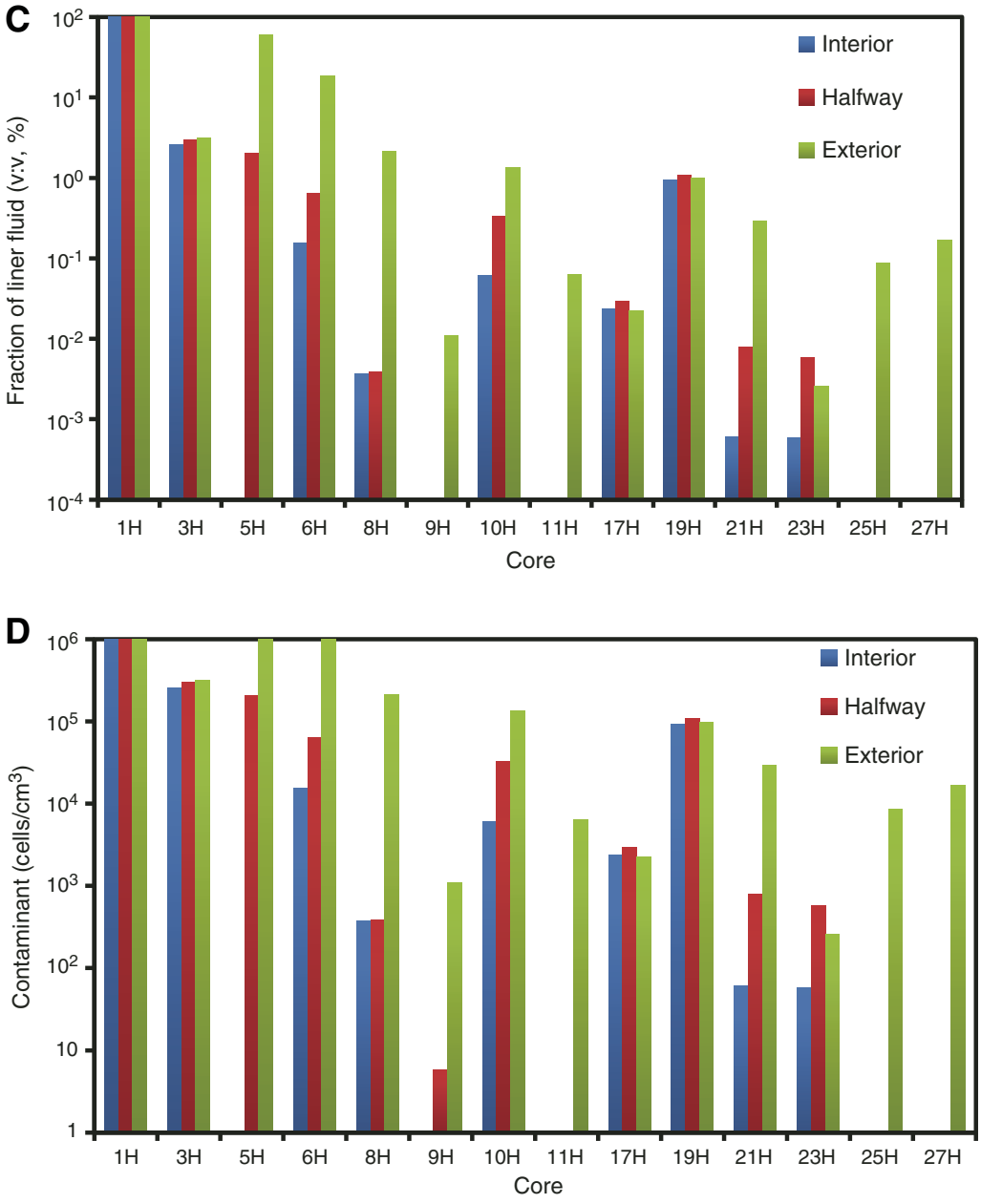

Figure F21. Plot of magnetic susceptibility (MS) data, Site M0060. MSCL = multisensor core logger, FT = Fast-track MSCL. Note that continuous MS data is only displayed for the uppermost 90 mbsf of Hole M0060A and 83 mbsf of Hole M0060B because of the poor recovery deeper than this depth.

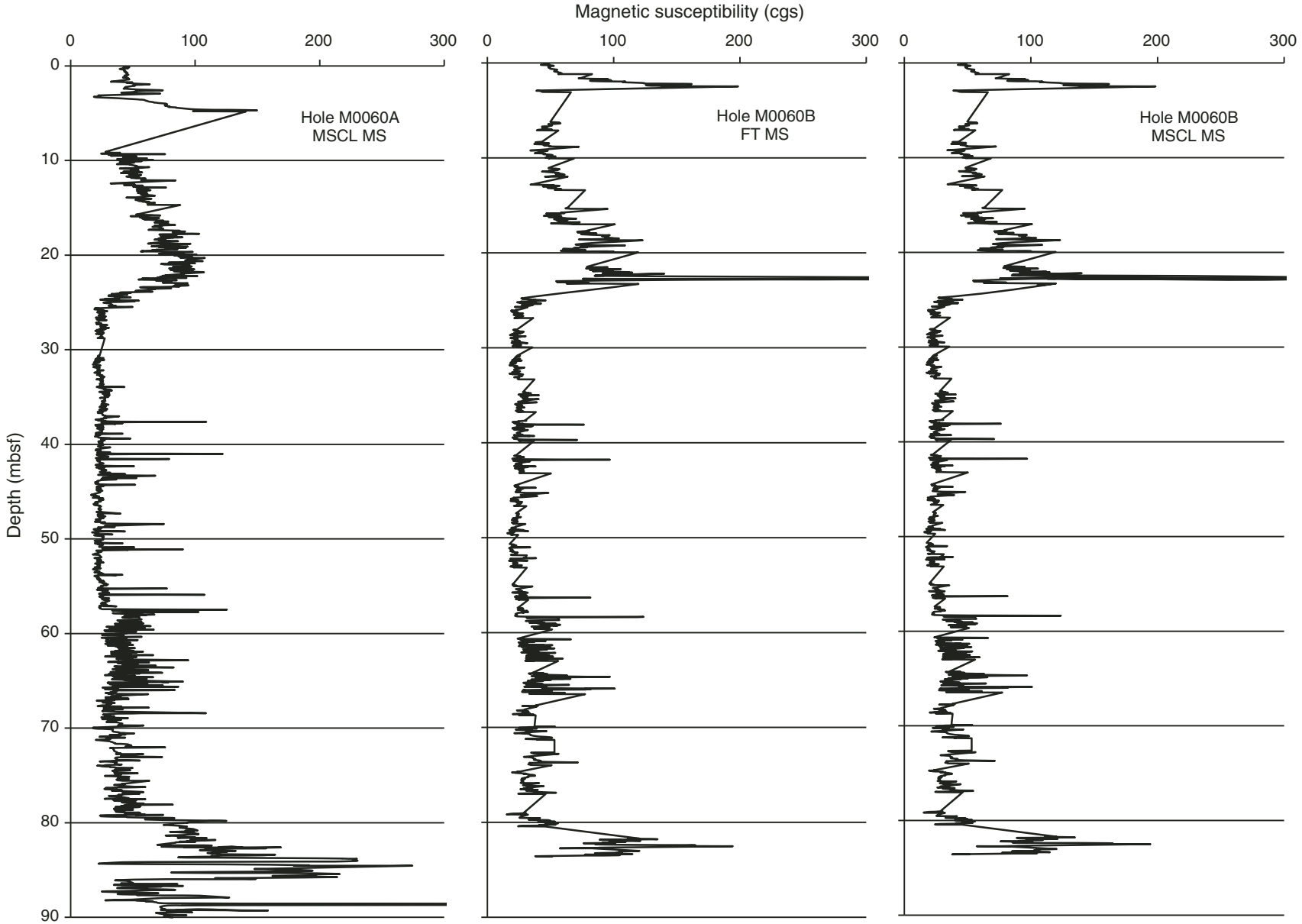

Figure F22. Correlation of the seismic profile with lithologic boundaries and multisensor core logger magnetic susceptibility data. Black arrows = unit boundaries. Precruise interpretation of seismic data is also shown: LG1 = bottom of late glacial Unit I, LG2 = lower boundary of late-glacial clays, BWT = bottom of Weichselian till, BR = bedrock. Seismic profile source: V. Spiess, 2013 (unpubl. data).

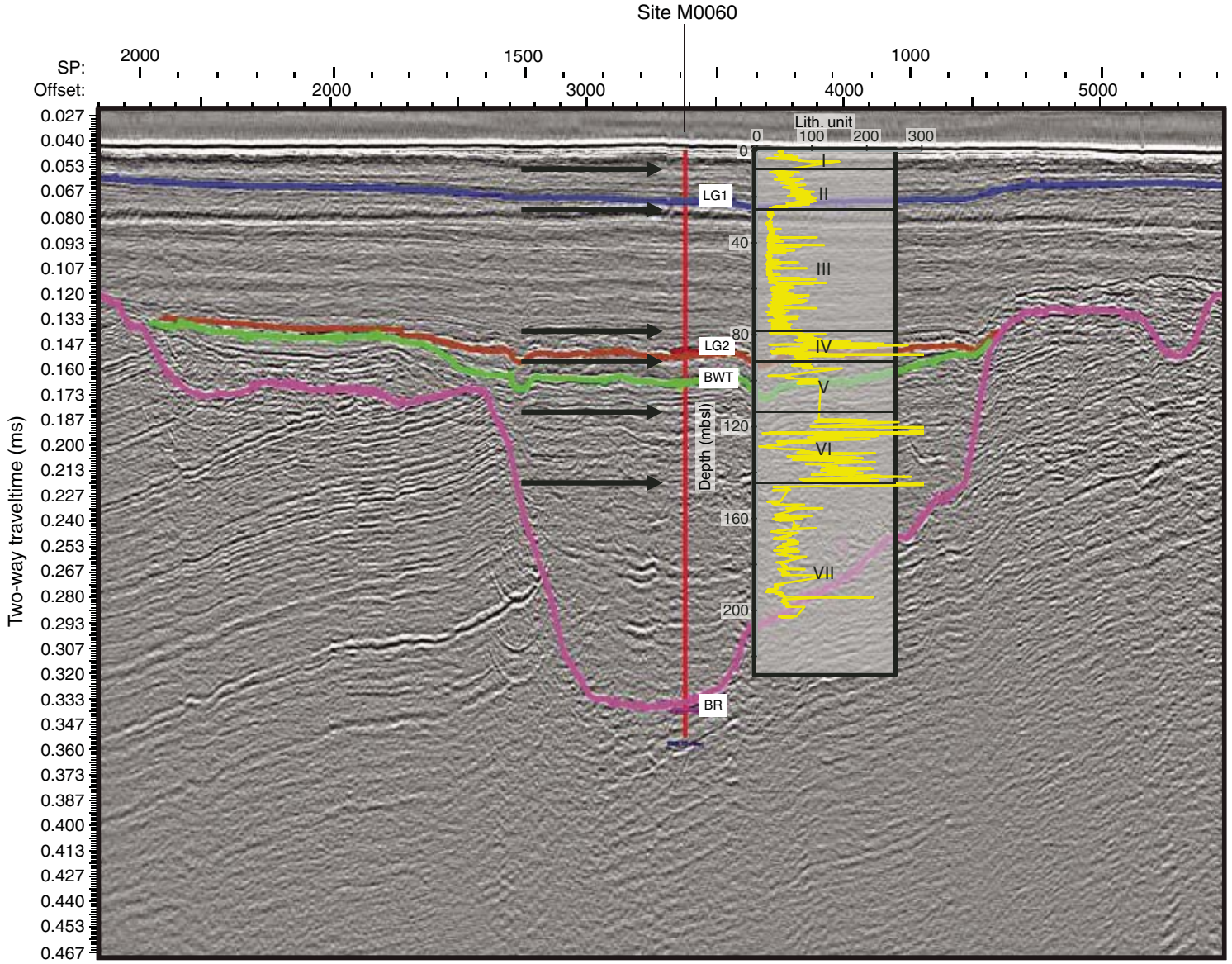

Figure F23. Caliper log, gamma ray log, spectral gamma ray log, resistivity log, and sonic log, Hole M0060B. The pipe set at 17.5 m WSF.

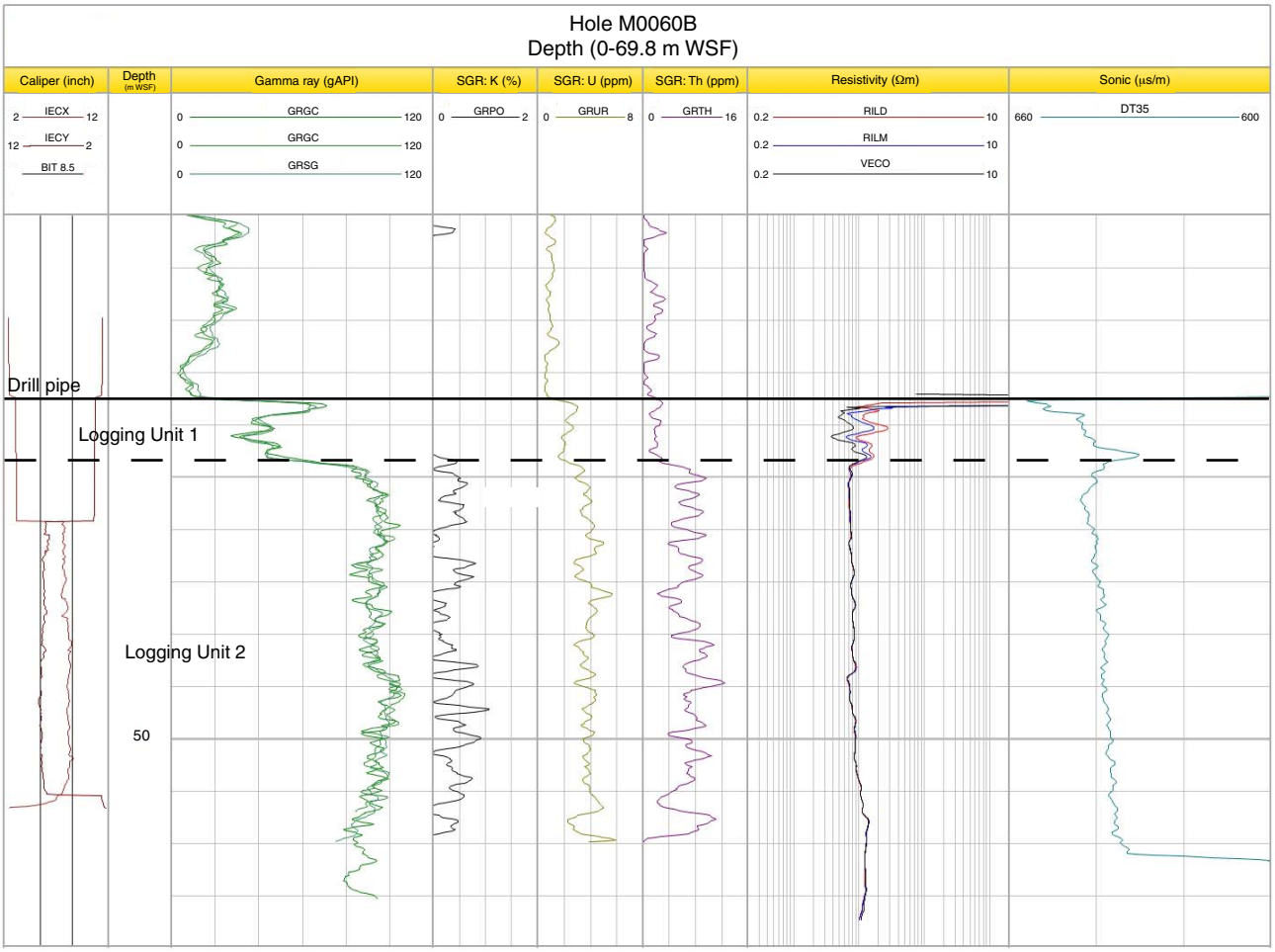

Table T1. Operations, Site M0060. (Continued on next four pages.)

Core	Coring method	Date (2013)	Time (UTC)	Depth (mbsf) Top	Depth (mbsf) Bottom	Recovered (m)	Recovery (%)	Mud type	Comments
347-M0060A-									
		23 Sep	0100						Rigged up and tested downhole camera system; system working but will not pass through the BHA
		23 Sep	0145						Ship on location in new position
		23 Sep	0445						Commenced operations; raised rooster box; checked new valve
		23 Sep	0506						Lowered template
		23 Sep	0600						Ran camera survey from in pipes only
		23 Sep	0745						Camera on deck, secured reel; set seabed template, still in the moonpool; retrieved drill pipe to drill floor; prepared drill floor with mouseholes, etc; made up BHA with core barrel + 2× collars and added pipe; did not use bit from Hole M0059C and fit new 6 cone rock roller
		23 Sep	0825						Reopened moonpool to fit bit into bit guide
		23 Sep	0845						Lowered seabed template to seabed; ready to run BHA and string
		23 Sep	0912						First drill pipe on
1H	PCS	23 Sep	0950	0.00	0.00	0.00	0	Seawater	No penetration, trace of sand on shoe
		23 Sep	1040						Second attempt; new valve (BOP) blew at 40 bar and pins did not shear; deck was sprayed with seawater
									New valve (BOP) broken beyond repair; continued operations with old procedure
2H	PCS	23 Sep	1113	0.00	0.00	0.00	0	Seawater	Pins sheared but string rose, reducing penetration; apparent failure of seabed template clamps; barrel on deck; ~20 cm of sand recovered
		23 Sep	1140						Recovered template to deck to investigate problem
		23 Sep	1155						Template in moonpool and rebuilding the drill floor
		23 Sep	1348						Mouseholes replaced
3H	PCS	23 Sep	1400	0.00	3.00	3.00	100	Seawater	100 bar, pressure did not release, left for 40 s before raising the rooster box
4H	PCS	23 Sep	1450	3.00	4.90	1.90	100	Seawater	65/70 bar then up to 100, again left for 30 s before releasing pressure; both seals missing
5O	NCA	23 Sep	1510	4.90	6.00	0.00	0	Seawater	Open hole by washing down, no insert bit
6H	PCS	23 Sep	1540	6.00	6.20	0.20	100	Seawater	60 bar, pressure released straight away
7O	NCA	23 Sep	1600	6.00	9.00	0.00	0	Seawater	
8H	PCS	23 Sep	1647	9.00	12.30	3.10	93.94	Seawater	Clay: basket catcher removed
9H	PCS	23 Sep	1730	12.30	15.60	2.46	74.55	Seawater	60 bar
10H	PCS	23 Sep	1810	15.60	18.90	3.27	99.09	Seawater	Double fire at 35 bar
11H	PCS	23 Sep	1845	18.90	22.20	3.19	96.67	Seawater	Replaced flapper catcher with a single basket and a spacer; double fire at 35 bar
12H	PCS	23 Sep	1945	22.20	25.50	3.33	100.91	Seawater	60 bar
13H	PCS	23 Sep	2020	25.50	28.80	3.37	102.12	Seawater	Sample winch rope parted; tripped pipe
		23 Sep	2045						Replacing snapped slip bowl
		23 Sep	2330						First collar in slips
14O	NCA	24 Sep	0000	28.80	30.53	0.00	0	Seawater	Open hole
15H	PCS	24 Sep	0045	30.53	33.83	3.53	106.97	Seawater	
16H	PCS	24 Sep	0120	33.83	37.13	3.32	100.61	Seawater	
17H	PCS	24 Sep	0200	37.13	40.43	3.31	100.3	Seawater	
18H	PCS	24 Sep	0240	40.43	43.73	3.39	102.73	Seawater	
19H	PCS	24 Sep	0315	43.73	47.03	3.68	111.52	Seawater	
	PCS	24 Sep	0355	47.03					First attempt failed to pressurize; pressure in hole, possibly did not drill out; flushed hole before reattempting
20H	PCS	24 Sep	0450	47.03	50.33	3.57	108.18	Seawater	
21H	PCS	24 Sep	0535	50.33	53.63	3.60	109.09	Seawater	Fired at 65 bar before dropping, then rising to 85 bar and then 100 bar
22H	PCS	24 Sep	0610	53.63	56.63	3.63	121	Seawater	Fired at 70 bar, then dropped to 50 bar before holding for a short time and then dropping to zero
23H	PCS	24 Sep	0645	56.63	60.23	3.49	96.94	Seawater	Small rounded stone in clay in the shoe
24H	PCS	24 Sep	0720	60.23	63.53	3.56	107.88	Seawater	High pressure: fired at 50 bar, rose to 100 bar, bled off, then pressurized again; on releasing the template clamps the pressure reduced as the rooster box rose
25H	PCS	24 Sep	0800	63.53	66.83	3.40	103.03	Seawater	Full with very hard clay in shoe; drilled ahead to ream hole and clean barrel; very hard then back to more "normal" drilling
26H	PCS	24 Sep	0845	66.83	69.83	3.01	100.33	Seawater	One each brass and steel pin; fired at 80 bar, dropped to 50 and then 40 bar; had to open clamps and let pipe rise to remove pressure fully; 3 m hard clay recovered

Table T1 (continued). (Continued on next page.)

Core	Coring method	Date (2013)	Time (UTC)	Depth (mbsf) Top	Depth (mbsf) Bottom	Recovered (m)	Recovery (%)	Mud type	Comments
27H	PCS	24 Sep	0930	69.83	72.83	3.01	100.33	Seawater	One each brass and steel pin; fired at just under 100 bar, dropped to 50 bar, back up to 60 bar until opened clamps, dropped to 25 bar almost straight away
		24 Sep	1037						2× steel pins; string pressurized to 100 bar before pump stalled; pressure dropped steadily to 60 bar before stopping until clamps opened and rooster box raised; tool recovered to deck for examination before running downhole again
28H	PCS	24 Sep	1105	72.83	75.80	2.83	95.29	Seawater	
		24 Sep	1125						Sample winch rope snapped attempting to recover piston core
		24 Sep	1135						Attempted to fish overshot; tool recovered to deck twice to evaluate progress; on third recovery pulled pipe
		24 Sep	1450						First collar in the slips
		24 Sep	1500						Overshot at deck level, assessing damage and possible cause of failing of rope
		24 Sep	1520						Carried out a pull test on the rope on the deck to determine if it had weakened with time
		24 Sep	1600						Running pipe; tongs tips cracked, so stopped to repair the IR
		24 Sep	1935						Realigned damaged IR frame
		24 Sep	1950						Running pipe
		24 Sep	2010						IR hydraulics not functioning correctly, working on the tongs
		24 Sep	2030						Collars on
		24 Sep	2200						Washed down to 75.8 mbsf
29H	PCS	24 Sep	2240	75.80	79.10	3.62	109.7	Seawater	
30H	PCS	24 Sep	2335	79.10	82.40	3.58	108.48	Seawater	
31H	PCS	25 Sep	0010	82.40	84.80	2.25	93.75	Seawater	Only a partial stroke after double high pressure firing
32H	PCS	25 Sep	0055	84.80	88.10	3.46	104.85	Seawater	
33H	PCS	25 Sep	0135	88.10	91.40	3.22	97.58	Seawater	Note some fingers of basket catcher ripped off and in core
34H	PCS	25 Sep	0245	91.40	94.70	3.30	100	Seawater	Strong backpressure when recovering sample, sand into tools; changed to Guar drill mud
		25 Sep	0350						Attempted piston core did not fire: returned to deck and flushed; lots of flowback so left out core barrel and flushed with mud; bottom 30 cm of hole seemed to be sand
35H	PCS	25 Sep	0450	94.70	97.70	3.00	100	Guar	Fired and then pressured to 100 bar; stayed at that pressure until released the string from the clamps and raised the rooster box; 3 m recovery but some may be reworked as very soft and not "core like"
		25 Sep	0530						Drilled and added pipe; very fast, no bit weight
36H	PCS	25 Sep	0550	97.70	97.70	0.00	0	Guar	Fired to 120 bar and only dropped when rooster box was lifted; attempted hammer sample at same depth
37S	HS	25 Sep	0615	97.70	98.01	0.31	100	Guar	Hard gray clay
38H	PCS	25 Sep	0630	98.70	101.20	2.66	106.4	Guar	2× steel pins; again pressurized to 100 then 120 bar, stayed until lifted rooster box
39H	PCS	25 Sep	0630	101.20	101.20	0.00	0	Guar	No penetration; 2× steel pins, blew pump pressure release valve at 120 bar; released pressure by lifting string
40X	ECS	25 Sep	0815	101.20	104.70	0.00	0	Guar	No recovery; sand on face of core bit
41S	HS	25 Sep	0905	104.70	104.70	0.10	100	Guar	20 blows
42X	ECS	25 Sep	0940	104.70	106.70	0.00	0	Guar	No recovery; shoe destroyed by stones
43O	NCA	25 Sep	1100	106.90	109.70	0.00	0	Guar	
44X	ECS	25 Sep	1120	109.70	112.70	0.00	0	Guar	
45P	PCA	25 Sep	1220	112.70	113.70	0.02	2	Guar	Only 0.5 metric ton required to push ahead
		25 Sep	1310	113.70					Attempted piston core with 2× brass pins; no penetration, no recovery
46H	PCS	25 Sep	1400	113.70	114.20	0.10	20	Guar	2× steel pins; fired at 110 bar, stalled pump, pressure only released by raising the rooster box; large granite stone in show with some slightly silty shelly sand with gravel
47O	NCA	25 Sep	1444	114.20	116.70	0.00	0	Guar	Easy drilling; no torque or pressure
48H	PCS	25 Sep	1535	116.70	118.20	1.50	100	Guar	115 bar; cracked pressure release to remove string pressure
		25 Sep	1545						Overshot unable to pick up sample tube; flushed string; pressure built before eventually going to zero
		25 Sep	1630						Flushed and rotated to ensure all sand(?) out of string
									Unable to pick up sample tube; flushed again; several attempts at picking up sample tube eventually paid off
		25 Sep	1915						Added pipe; breaking pipes at deck, high volume flowing water from string
49O	NCA	25 Sep	1950	118.20	119.70	0.00	0	Guar	Open hole to 3 m beyond last sample start
		25 Sep	2015						Stalled pump at 120 bar; not known if pins sheared; pressure dropped to 50 bar before rooster box was raised and took some time to bleed off completely; failed to fire: not a run
50H	PCS	25 Sep	2055	119.70	123.00	3.40	103.03	Guar	Stalled pump at 135 bar; not known if pins sheared; pressure dropped to zero when rooster box was raised

Table T1 (continued). (Continued on next page.)

Core	Coring method	Date (2013)	Time (UTC)	Depth (mbsf) Top	Depth (mbsf) Bottom	Recovered (m)	Recovery (%)	Mud type	Comments
51H	PCS	25 Sep	2235	123.00	126.30	2.57	77.88	Guar	
52H	PCS	25 Sep	2350	126.30	129.60	2.43	73.64	Guar	
53H	PCS	26 Sep	0045	129.60	132.90	2.00	60.61	Guar	
54H	PCS	26 Sep	0135	132.90	136.20	2.57	77.88	Guar	150 bar
		26 Sep	0220						Stopped drilling, cleared decks to lift seabed template after clamps on frame ceased working; lifted template, repaired, and tested; ready to be lowered to seabed again
		26 Sep	0530						Drill string rotated to bottom of borehole, less 1 m of infill
55H	PCS	26 Sep	0630	136.20	139.50	3.00	90.91	Guar	Fired and kept pressure to 150 bar and released only when pipe lifted
		26 Sep	0700						No obvious drilling change when drilling down to next sample point
56H	PCS	26 Sep	0710	139.50	142.80	2.83	85.76	Guar	Fired as before; same material
57H	PCS	26 Sep	0800	142.80	146.10	2.60	78.79	Guar	No change in conditions
		26 Sep	0850						Drilled to next sample point, started to get mud pressure and slower drilling for final meter or so; possibly clay
58H	PCS	26 Sep	0900	146.10	149.40	1.93	58.48	Guar	Fired at 80 bar; more of a pause before increasing to 125 bar and holding until pipe was released and lifted
59H	PCS	26 Sep	1025	149.40	152.40	0.15	5	Guar	
60H	PCS	26 Sep	1120	152.40	155.40	1.60	53.33	Guar	Pump stalled at 150 bar
61H	PCS	26 Sep	1220	155.40	155.70	0.30	100	Guar	Apparently reworked clay
62N	NRCB	26 Sep	1335	155.70	158.40	0.00	0	Guar	Because of near zero recovery and apparent reworked/cuttings recovered, cored 3 m using ECS; on recovery there was no sample in the barrel but the catchers were inverted
63H	PCS	26 Sep	1410	158.40	160.30	1.89	99.47	Guar	Piston again recovered 1.89 m of reworked material; possibly the slipped core from the previous run
64O	NCA	26 Sep	1525	158.40	159.40	0.00	0	Guar	Drilled down 1 m to clear dropped core and any possible disturbed ground from piston Core 63H
65H	PCS	26 Sep	1540	159.40	162.40	1.58	52.67	Guar	Apparent reworked material recovered; thought this is damage caused by the basket catchers and changed to flapper catcher and one basket
66H	PCS	26 Sep	1725	162.40	164.20	1.90	105.56	Guar	Liner deformed because of suction pressure
67H	PCS	26 Sep	1910	164.20	166.30	2.12	100.95	Guar	Liner deformed because of suction pressure
68H	PCS	26 Sep	2020	166.30	168.80	2.45	98	Guar	Liner deformed because of suction pressure
69H	PCS	26 Sep	2125	168.80	172.10	2.37	71.82	Guar	Sand jammed piston
70H	PCS	26 Sep	2300	172.10	175.40	2.30	69.7	Guar	Sand jammed piston
71H	PCS	27 Sep	0020	175.40	178.70	1.64	49.7	Guar	
72H	PCS	27 Sep	0115	178.70	182.00	3.48	105.45	Guar	
73H	PCS	27 Sep	0200	182.00	185.30	2.83	85.76	Guar	
74H	PCS	27 Sep	0313	185.30	188.60	0.05	1.52	Guar	PCS overshot wire snapped when trying to retrieve
		27 Sep	0315						Retrieved wireline to deck; ~15 m of rope on it
		27 Sep	0330						Prepared fishing tool with barbs; picked up but too sharp and shredded rope
		27 Sep	0430						Remade with smoother barbs; no success with two attempts
		27 Sep	0555						Prepared to trip pipe
		27 Sep	0615						Tripped pipe
		27 Sep	0710						Heated up pipe joints to free
		27 Sep	0845						Unable to free drill collar joint
		27 Sep	1000						Unable to free collars
		27 Sep	1100						Requested to use BGS Scorpion to free collars; successful on two joints
		27 Sep	1400						Ran pipe
		27 Sep	1530						Flowing water at joints between pipes 8 and 11 and again less so at various intervals down the hole
									Hole sticky from 105 mbsf
		27 Sep	1900						Mouseholes in place, piston corer ready with 2× steel pins
		27 Sep	1900						Worked on sample winch hydraulics; fit diverter/safety valve to avoid snapping rope again
		27 Sep	2010						Tested winch settings
		27 Sep	2045						Washed down to point before last piston sample attempt with NCA in place
		27 Sep	2100						Extracted NCA/deployed PCS
75H	PCS	27 Sep	2135	188.60	191.90	2.93	88.79	Guar	100 bar
									Hole caved in while washing down to 191.9 mbsf
76H	PCS	28 Sep	0000	191.90	195.20	2.66	80.61	Guar	

Table T1 (continued). (Continued on next page.)

Core	Coring method	Date (2013)	Time (UTC)	Depth (mbsf) Top	Depth (mbsf) Bottom	Recovered (m)	Recovery (%)	Mud type	Comments
77H	PCS	28 Sep	0115	195.20	198.50	3.42	103.64	Guar	
78S	HS	28 Sep	0335	198.50	198.80	0.25	100	Guar	Hammer sample used after two piston corer attempts failed to fire
79O	NCA	28 Sep	0355	198.80	199.50	0.00	0	Guar	
80S	HS	28 Sep	0415	199.50	199.54	0.00	0	Guar	Fired at 50 bar then stopped; started pump again and raised pressure to 150 bar, then lowered to almost zero; prepared insert bit and push sample tube
81O	NCA	28 Sep	0520	199.50	202.50	0.00	0	Guar	
82P	PCA	28 Sep	0600	202.50	203.55	1.05	100	Guar	
83O	NCA	28 Sep	0615	203.55	205.50	0.00	0	Guar	
84P	PCA	28 Sep	0715	205.50	205.60	0.10	100	Guar	
85O	NCA	28 Sep	0738	205.60	208.50	0.00	0	Guar	Insert bit stuck in mud valve
86P	PCA	28 Sep	0743	208.50	208.50	0.00	0	Guar	
87O	NCA	28 Sep	0830	208.80	211.50	0.00	0	Guar	
88S	HS	28 Sep	0900	211.50	211.70	0.20	100	Guar	20 blows with little penetration
89O	NCA	28 Sep	0920	211.70	214.50	0.00	0	Guar	Little pressure 2 m into run but then back into sand
		28 Sep	0955						Stopped operations to investigate mud leak from rotary valve stem when pipe is at lowest point
		28 Sep	1035						String broken in to allow the valve to be fully tightened by clamping it and turning swivel
90S	HS	28 Sep	1135	214.50	214.60	0.10	100		Hard, compacted fine gray sand
91O	NCA	28 Sep	1155	214.60	217.50	0.00	0	Guar	
92S	HS	28 Sep	1245	217.50	217.70	0.20	100		32 blows
93O	NCA	28 Sep	1310	217.70	220.50	0.00	0	Guar	
94S	HS	28 Sep	1355	220.50	220.55	0.05	100		30 blows
95O	NCA	28 Sep	1420	220.55	223.50	0.00	0	Guar	Back of water up pipe at tool change
96S	HS	28 Sep	1500	223.50	223.60	0.10	100		25 blows
97O	NCA	28 Sep	1555	223.55	226.50	0.00	0	Guar	String difficult to rotate following last sample; thought flowing water was bringing sand down with it; reamed entire pipe length to clear and stabbed ground to stop flow up string
98S	HS	28 Sep	1655	226.50	226.60	0.10	100		25 blows
99O	NCA	28 Sep	1715	226.60	229.50	0.00	0	Guar	
100S	HS	28 Sep	1807	229.50	229.60	0.10	100		30 blows
101O	NCA	28 Sep	1925	229.60	232.50	0.00	0	Guar	Water followed NCA through mud valve; mud valve closed with pumping; overshot could not be released from NCA (blocked with sand), so lowered to deck; string became stuck and work commenced to release it
		28 Sep	2015						Gained 5 m of string and small amount of mud flow but no more
		28 Sep	2050						Attempted to hammer sand from string; estimated 24 m of sand in string
		28 Sep	2250						Stopped to repair hydraulics leak
		28 Sep	2330						Recommenced hammer sampling in pipe; possibly making progress, but no circulation of mud possible
		29 Sep	0130						Rigged up Pilcon winch to remove need for manual hammering
		29 Sep	0310						Stopped hammering and tried rotation and pulling
		29 Sep	0650						Restarted HS, measured progress: apparently at start position, thought that sand was still flowing in to string
		29 Sep	0750						Investigated running high-pressure air intake to mudline, which might shift sand and allow mud flow
		29 Sep	0910						After discussions of options, investigated decision to look at backing of string
		29 Sep	0920						Raised seabed template to inside the moonpool but below the first tool joint
		29 Sep	1020						Rigged up downhole camera; backed off string using tongs: went well and accomplished on the first attempt
		29 Sep	1120						Weight suggested only 4 or 5 pipes recovered; had a stick up of ~14 m from seabed
		29 Sep	1115						Rigged up ROV to monitor stick up while pushing down with the template
		29 Sep	1515						Successful leveling of stick-up pipe; ROV showed pipe leveled to seafloor with no protrusion
									End of hole
347-M0060B-									
		29 Sep	1600						Prepared BHA including torquing subs and 6 cone rock roller bit
		29 Sep	1835						Template moved into moonpool and lowered to seafloor
		29 Sep	1925						Ran string with BHA, 2 collars, and drill pipe
1H	PCS	29 Sep	2050	0.00	2.80	2.71	96.79	Guar	First run fired ~0.5 m above mudline

Table T1 (continued).

Core	Coring method	Date (2013)	Time (UTC)	Depth (mbsf) Top	Depth (mbsf) Bottom	Recovered (m)	Recovery (%)	Mud type	Comments
2H	PCS	29 Sep	2140	2.80	2.80	0.00	0	Guar	Uncertain if any sample ever went up into the barrel; may have fired on the way down
3H	PCS	29 Sep	2225	2.80	6.10	2.70	81.82	Guar	
4H	PCS	29 Sep	2305	6.10	9.40	3.29	99.7	Guar	
5H	PCS	30 Sep	0010	9.40	12.70	2.87	86.97	Guar	Used drilling mud to help stabilize sand at top of hole
6H	PCS	30 Sep	0130	12.70	16.00	3.27	99.09	Guar	
7H	PCS	30 Sep	0240	16.00	19.30	3.46	104.85	Guar	Good, clean fire and pressure drop; good sample, catcher partially fell out; changed to flapper/basket catcher
8H	PCS	30 Sep	0325	19.30	22.60	3.41	103.33	Guar	Good fire/pressure drop, required more pressure to go to zero; microbiology mud sample taken at pipe break
9H	PCS	30 Sep	0530	22.60	25.90	3.30	100	Guar	Pressure only ~30 bar, but piston stroked out
10H	PCS	30 Sep	0615	25.90	29.20	3.66	110.91	Guar	Good fire and pressure but hole beginning to stick, so changed to water for drilling
11H	PCS	30 Sep	0715	29.20	32.50	3.66	110.91	Guar	Drilled down to next sample point and circulated for 20 min as hole still tightening; flushed, allowing seawater to fill the hole rather than mud, which may be causing the clay to swell Hole stable; circulated again after pipe addition and reaming down
12H	PCS	30 Sep	0835	32.50	35.80	3.29	99.7	Guar	Good firing sequence
13H	PCS	30 Sep	0910	35.80	39.10	3.55	107.58	Guar	50 bar then dropped before rising to 80 bar and dropping away
14H	PCS	30 Sep	0940	39.10	42.40	3.60	109.09	Guar	Good fire and dropped to zero right away
15H	PCS	30 Sep	1040	42.40	45.70	3.46	104.85	Guar	Could not recover the piston corer at first attempt; overshot brought back to the rooster box and pipe flushed, second attempt successful; very stiff clay
16H	PCS	30 Sep	1200	45.70	49.00	3.71	112.42	Guar	
17H	PCS	30 Sep	1200	49.00	52.30	3.62	109.7	Guar	75 bar straight down to zero
18H	PCS	30 Sep	1340	52.30	55.60	3.62	109.7	Guar	75 bar straight down to zero
19H	PCS	30 Sep	1430	55.60	58.90	3.57	108.18	Guar	
20H	PCS	30 Sep	1520	58.90	62.20	3.49	105.76	Guar	70 bar then down to 50 before up again
21H	PCS	30 Sep	1635	62.20	65.50	3.43	103.94	Guar	60 bar then down before up to 70 bar
22H	PCS	30 Sep	1705	65.50	68.00	2.50	100	Guar	
23H	PCS	30 Sep	1805	68.00	70.50	2.50	100	Guar	"Soft fire": low fire level with drop in pressure before rising, only dropped to zero with raising of the string
24H	PCS	30 Sep	1910	70.50	73.00	2.40	96	Guar	Liner collapsed top 75 cm; reverted to 2 brass pins
25H	PCS	30 Sep	2000	73.00	76.30	3.30	100	Guar	
26H	PCS	30 Sep	2100	76.30	79.60	3.33	100.91	Guar	
27H	PCS	30 Sep	2210	79.60	82.90	3.19	96.67	Guar	Strong artesian backflow when retrieving PC barrel
28H	PCS	30 Sep	2300	82.90	85.70	2.82	100.71	Guar	Overshot failed to pick up core barrel on two attempts; much pumping of mud required to free barrel End of hole; reamed out to 85.5 mbsf and filled with thick mud ready for logging
		1 Oct	0100					Guar	Lifted string to ~20 mbsf
		1 Oct	0240					Guar	Completed first downhole log, maximum depth 64 mbsf
		1 Oct	0340					Guar	Completed second downhole log, maximum depth 62 mbsf
		1 Oct	0554					Guar	Lifted logging wire; calipers not working properly on tool or in formation; on deck found clay behind them
		1 Oct	0635						Logging tools clear of deck
		1 Oct	0659						First collar in slips
		1 Oct	0735						Template on deck, doors closed, and BHA in template

ECS = extended coring system, HS = hammer sampler, NCA = noncoring assembly, NRCB = nonrotating core barrel, PCA = push coring assembly, PCS = piston coring system. BHA = bottom-hole assembly, BOP = blowout preventer, IR = iron roughneck, BGS = British Geological Survey, ROV = remotely operated vehicle, PC = piston core.

Table T2. Diatom taxa species and authorities with presence/absence data for selected depths, Site M0060.

Affinity	Life form	Diatoms	7.5 mbsf	9 mbsf	10.5 mbsf
F	Epipelic and epilithic	*Amphora copulata* (Kützing) Schoeman and Archibald		x	x
F	Pelagic	*Aulacoseira ambigua* (Grunow) Simonsen		x	
F	Pelagic	*Aulacoseira granulata* (Ehrenberg) Simonsen			
F	Pelagic	*Auloacoseira islandica* (O. Müller) Simonsen	x	c	x
F	Epipsammic	*Cocconeis disculus* (Schumann) Cleve	x		
BF	Epiphytic and epilithic	*Cocconeis placentula* Ehrenberg	x	x	
B	Pelagic	*Coscinodiscus granii* Gough			x
M		*Fragilaria capensis* Grunow		x	
BM	Epiphytic	*Gomphonemopsis exigua* (Kützing) L.K. Medlin		x	
F	Epipsammic	*Karayevia clevei* (Grunow) Bukhtiyarova			
M	Epiphitic	*Licmophora abbreviata* C. Agardh		x	
F	Epipsammic	*Martyana martyii* (Héribaud-Joseph) Round	x		x
B	Epipsammic	*Martyana schulzii* (Brockmann) Snoeijs	x	c	
B	Epipelic	*Navicula peregrina* (Ehrenberg) Kützing		x	
B	Epipsammic and epiphytic	*Opephora mutabilis* (Grunow) Sabbe and Wyverman			x
B	Tychoplanktonic	*Paralia sulcata* (Ehrenberg) Cleve			
M	Epipelic	*Pinnularia cruciformis* (Donkin) Cleve		x	
B	Epipelic	*Pinnularia halophila* Krammer		x	
M	Benthic	*Plagiogramma staurophorum* (W. Gregory) Heiberg			x
BF	Episammic and epilithic	*Planothidium delicatulum* (Kützing) Round and Bukhtiyarova			x
BM	Epiphytic and epilithic	*Rhabdonema arcuatum* (Lyngbye) Kützing			
BF	Epipelic and epilithic	*Rhopalodia gibba* (Ehrenberg) O. Müller		x	
F	Pelagic	*Stephanodiscus neoastraea* Håkansson and Hickel		x	
B	Pelagic	*Thalassiosira hyperborea* var. *lacunosa* Hasle			x
M?	Pelagic	*Thalassiosira oestrupii* (Ostenfeld) Hasle			

F = freshwater, BF = brackish-freshwater, B = brackish, BM = brackish-marine, M = marine. x = present, c = common.

Table T3. Diatoms, Hole M0060A. (Continued on next two pages.)

Affinity	Life form	Diatoms	Depth (mbsf):	1.5	3	4.5	7.5	9	10.5	12	12.3	13.8	15.6	17.1	18.6	18.9	20.4	21.9	25.5	27	28.5	30.5	32	33.5	33.8	35.3
			Core, section:	3H-2	4H-1	4H-2	6H-CC	8H-1	8H-2	8H-3	9H-1	9H-2	10H-1	10H-2	10H-3	11H-1	11H-2	11H-3	13H-1	13H-2	13H-3	15H-1	15H-2	15H-3	16H-1	16H-2
			Interval (cm):	0–1	0–1	0–1	0–1	0–1	0–1	0–1	0–1	0–1	0–1	0–1	0–1	0–1	0–1	0–1	0–1	0–1	0–1	0–1	0–1	0–1	0–1	0–1
F	Epipelic and epilithic	*Amphora copulata* (Kützing) Schoeman and Archibald						x	x																	
F		*Aulacoseira ambigua* (Grunow) Simonsen						x																		
F		*Aulacoseira granulata* (Ehrenberg) Simonsen																								
F	Pelagic	*Aulacoseira islandica* (O. Müller) Simonsen					x	c	x																	
F	Epipsammic	*Cocconeis disculus* (Schumann) Cleve					x											x								
BF	Epiphytic and epilithic	*Cocconeis placentula* Ehrenberg					x	x																		
B	Pelagic	*Coscinodiscus granii* Gough							x																	
M		*Fragilaria capensis* Grunow						x																		
BM	Epiphytic	*Gomphonemopsis exigua* (Kützing) L.K. Medlin						x																		
F	Epipsammic	*Karayevia clevei* (Grunow) Bukhtiyarova									x															
M	Epiphitic	*Licmophora abbreviata* C. Agardh						x																		
F	Epipsammic	*Martyana martyii* (Héribaud-Joseph) Round					x		x	x																
B	Epipsammic	*Martyana schulzii* Brockmann) Snoeijs					x	c		x																
B	Epipelic	*Navicula peregrina* (Ehrenberg) Kützing						x																		
B	Epipsammic and epiphytic	*Opephora mutabilis* (Grunow) Sabbe and Wyverman							x																	
B	Tychoplanktonic	*Paralia sulcata* (Ehrenberg) Cleve																x					x		x	
M	Epipelic	*Pinnularia cruciformis* (Donkin) Cleve						x																		
B	Epipelic	*Pinnularia halophila* Krammer						x																		
M	Benthic	*Plagiogramma staurophorum* (W. Gregory) Heiberg							x	x																
BF	Episammic and epilithic	*Planothidium delicatulum* (Kützing) Round and Bukhtiyarova							x	x																
BM	Epiphytic and epilithic	*Rhabdonema arcuatum* (Lyngbye) Kützing																x								
BF	Epipelic and epilithic	*Rhopalodia gibba* (Ehrenberg) O. Müller						x																		
F	Pelagic	*Stephanodiscus neoastraea* Håkansson and Hickel						x																		
B	Pelagic	*Thalassiosira hyperborea* var. *lacunosa* Hasle							x																	
M?	Pelagic	*Thalassiosira oestrupii* (Ostenfeld) Hasle																								
		Crysophyte cysts																								
		Dots					x																			

F = freshwater, BF = brackish-freshwater, B = brackish, BM = brackish-marine, M = marine. x = present, c = common. ? = uncertain.

Affinity	Life form	Diatoms	Depth (mbsf):	36.8	37.1	38.6	40.1	40.4	41.9	43.4	43.7	45.2	46.7	47	48.5	50	50.3	51.8	53.3	53.6	55.1	56.6	56.9	58.4	59.9
			Core, section:	16H-3	17H-1	17H-2	17H-3	18H-1	18H-2	18H-3	19H-1	19H-2	19H-3	20H-1	20H-2	20H-3	21H-1	21H-2	21H-3	22H-1	22H-2	22H-3	23H-1	23H-2	23H-3
			Interval (cm):	0–1	0–1	0–1	0–1	0–1	0–1	0–1	0–1	0–1	0–1	0–1	0–1	0–1	0–1	0–1	0–1	0–1	0–1	0–1	0–1	0–1	0–1
F	Epipelic and epilithic	*Amphora copulata* (Kützing) Schoeman and Archibald																							
F		*Aulacoseira ambigua* (Grunow) Simonsen																							
F		*Aulacoseira granulata* (Ehrenberg) Simonsen																							
F	Pelagic	*Aulacoseira islandica* (O. Müller) Simonsen																							
F	Epipsammic	*Cocconeis disculus* (Schumann) Cleve																							
BF	Epiphytic and epilithic	*Cocconeis placentula* Ehrenberg																							
B	Pelagic	*Coscinodiscus granii* Gough																						x	
M		*Fragilaria capensis* Grunow																							
BM	Epiphytic	*Gomphonemopsis exigua* (Kützing) L.K. Medlin																							
F	Epipsammic	*Karayevia clevei* (Grunow) Bukhtiyarova																							
M	Epiphitic	*Licmophora abbreviata* C. Agardh																							
F	Epipsammic	*Martyana martyii* (Héribaud-Joseph) Round																							
B	Epipsammic	*Martyana schulzii* Brockmann) Snoeijs																							
B	Epipelic	*Navicula peregrina* (Ehrenberg) Kützing																							
B	Epipsammic and epiphytic	*Opephora mutabilis* (Grunow) Sabbe and Wyverman																							
B	Tychoplanktonic	*Paralia sulcata* (Ehrenberg) Cleve																							
M	Epipelic	*Pinnularia cruciformis* (Donkin) Cleve																							
B	Epipelic	*Pinnularia halophila* Krammer																							
M	Benthic	*Plagiogramma staurophorum* (W. Gregory) Heiberg																							
BF	Episammic and epilithic	*Planothidium delicatulum* (Kützing) Round and Bukhtiyarova																							
BM	Epiphytic and epilithic	*Rhabdonema arcuatum* (Lyngbye) Kützing																							
BF	Epipelic and epilithic	*Rhopalodia gibba* (Ehrenberg) O. Müller																							
F	Pelagic	*Stephanodiscus neoastraea* Håkansson and Hickel																							
B	Pelagic	*Thalassiosira hyperborea* var. *lacunosa* Hasle																							
M?	Pelagic	*Thalassiosira oestrupii* (Ostenfeld) Hasle						x																	
		Crysophyte cysts																							
		Dots																							

Table T3 (continued). (Continued on next page.)

Affinity	Life form	Diatoms	Depth (mbsf):	60.2	61.7	63.2	63.5	65	66.5	66.8	68.3	69.6	69.8	72.8	75.8	79.1	82.4	84.8	88.1	91.4	94.7	97.7	97.7	116.7	119.7	123
			Core, section:	24H-1	24H-2	24H-3	25H-1	25H-2	25H-3	26H-1	26H-2	26H-3	27H-1	28H-1	29H-1	30H-1	31H-1	32H-1	33H-1	34H-1	35H-1	36H-1	37H-1	48H-1	50H-1	51H-1
			Interval (cm):	0–1	0–1	0–1	0–1	0–1	0–1	0–1	0–1	0–1	0–1	0–1	0–1	0–1	0–1	0–1	0–1	0–1	0–1	0–1	0–1	0–1	0–1	0–1
F	Epipelic and epilithic	*Amphora copulata* (Kützing) Schoeman and Archibald		Fragments	Fragments	Fragments	Fragments	Barren	Fragments	Barren	Barren	Barren	Barren	Barren	Barren	2 valves	Barren	1 valve	1 valve	Barren	1 valve	1 valve	Barren	Barren	Barren	Barren
F		*Aulacoseira ambigua* (Grunow) Simonsen																								
F		*Aulacoseira granulata* (Ehrenberg) Simonsen														x										
F	Pelagic	*Aulacoseira islandica* (O. Müller) Simonsen																								
F	Epipsammic	*Cocconeis disculus* (Schumann) Cleve																								
BF	Epiphytic and epilithic	*Cocconeis placentula* Ehrenberg																								
B	Pelagic	*Coscinodiscus granii* Gough																								
M		*Fragilaria capensis* Grunow																								
BM	Epiphytic	*Gomphonemopsis exigua* (Kützing) L.K. Medlin																								
F	Epipsammic	*Karayevia clevei* (Grunow) Bukhtiyarova																								
M	Epiphitic	*Licmophora abbreviata* C. Agardh																								
F	Epipsammic	*Martyana martyii* (Héribaud-Joseph) Round																								
B	Epipsammic	*Martyana schulzii* Brockmann) Snoeijs																								
B	Epipelic	*Navicula peregrina* (Ehrenberg) Kützing																								
B	Epipsammic and epiphytic	*Opephora mutabilis* (Grunow) Sabbe and Wyverman																								
B	Tychoplanktonic	*Paralia sulcata* (Ehrenberg) Cleve														x		x	x		x					
M	Epipelic	*Pinnularia cruciformis* (Donkin) Cleve																								
B	Epipelic	*Pinnularia halophila* Krammer																								
M	Benthic	*Plagiogramma staurophorum* (W. Gregory) Heiberg																								
BF	Episammic and epilithic	*Planothidium delicatulum* (Kützing) Round and Bukhtiyarova																								
BM	Epiphytic and epilithic	*Rhabdonema arcuatum* (Lyngbye) Kützing																								
BF	Epipelic and epilithic	*Rhopalodia gibba* (Ehrenberg) O. Müller																								
F	Pelagic	*Stephanodiscus neoastraea* Håkansson and Hickel																				x				
B	Pelagic	*Thalassiosira hyperborea* var. *lacunosa* Hasle																								
M?	Pelagic	*Thalassiosira oestrupii* (Ostenfeld) Hasle																								
		Crysophyte cysts																								
		Dots																								

Affinity	Life form	Diatoms	Depth (mbsf):	126.3	129.6	132.9	136.2	139.5	142.8	146.1	152.4	155.4	158.4	159.4	162.4	164.2	166.3	168.8	172.1	175.4	178.7	179.0	180.5	181.7
			Core, section:	52H-1	53H-1	54H-1	55H-1	56H-1	57H-1	58H-1	60H-1	61H-1	63H-1	65H-1	66H-1	67H-1	68H-1	69H-1	70H-1	71H-1	72H-1	72H-2	72H-3	72H-4
			Interval (cm):	0–1	0–1	0–1	0–1	0–1	0–1	0–1	0–1	0–1	0–1	0–1	0–1	0–1	0–1	0–1	0–1	0–1	0–1	0–1	0–1	0–1
F	Epipelic and epilithic	*Amphora copulata* (Kützing) Schoeman and Archibald		Barren	Barren	1 valve	Fragments	1 valve	1 valve	Fragments	Fragments	Fragments	Fragments	Fragments	Fragments	Fragments	Fragments	Fragments	Fragments	Fragments	Fragments	Fragments	Fragments	Fragments	Fragments
F		*Aulacoseira ambigua* (Grunow) Simonsen																						
F		*Aulacoseira granulata* (Ehrenberg) Simonsen																						
F	Pelagic	*Aulacoseira islandica* (O. Müller) Simonsen																						
F	Epipsammic	*Cocconeis disculus* (Schumann) Cleve																						
BF	Epiphytic and epilithic	*Cocconeis placentula* Ehrenberg																						
B	Pelagic	*Coscinodiscus granii* Gough																						
M		*Fragilaria capensis* Grunow																						
BM	Epiphytic	*Gomphonemopsis exigua* (Kützing) L.K. Medlin																						
F	Epipsammic	*Karayevia clevei* (Grunow) Bukhtiyarova																						
M	Epiphitic	*Licmophora abbreviata* C. Agardh																						
F	Epipsammic	*Martyana martyii* (Héribaud-Joseph) Round																						
B	Epipsammic	*Martyana schulzii* Brockmann) Snoeijs																						
B	Epipelic	*Navicula peregrina* (Ehrenberg) Kützing																						
B	Epipsammic and epiphytic	*Opephora mutabilis* (Grunow) Sabbe and Wyverman																						
B	Tychoplanktonic	*Paralia sulcata* (Ehrenberg) Cleve						x	x															
M	Epipelic	*Pinnularia cruciformis* (Donkin) Cleve																						
B	Epipelic	*Pinnularia halophila* Krammer																						
M	Benthic	*Plagiogramma staurophorum* (W. Gregory) Heiberg																						
BF	Episammic and epilithic	*Planothidium delicatulum* (Kützing) Round and Bukhtiyarova																						
BM	Epiphytic and epilithic	*Rhabdonema arcuatum* (Lyngbye) Kützing																						
BF	Epipelic and epilithic	*Rhopalodia gibba* (Ehrenberg) O. Müller																						
F	Pelagic	*Stephanodiscus neoastraea* Håkansson and Hickel																						
B	Pelagic	*Thalassiosira hyperborea* var. *lacunosa* Hasle																						
M?	Pelagic	*Thalassiosira oestrupii* (Ostenfeld) Hasle				x																		
		Crysophyte cysts																						
		Dots																						

Table T3 (continued).

			Depth (mbsf):	182	188.6	190.1	191.9	193.4	195.2	202.5
			Core, section:	73H-1	75H-1	75H-2	76H-1	76H-2	77H-1	82H-1
			Interval (cm):	0–1	0–1	0–1	0–1	0–1	0–1	0–1
Affinity	Life form	Diatoms		Fragments	Fragments	Fragments	Fragments	Fragments	Fragments	Fragments
F	Epipelic and epilithic	*Amphora copulata* (Kützing) Schoeman and Archibald								
F		*Aulacoseira ambigua* (Grunow) Simonsen								
F		*Aulacoseira granulata* (Ehrenberg) Simonsen								
F	Pelagic	*Aulacoseira islandica* (O. Müller) Simonsen								
F	Epipsammic	*Cocconeis disculus* (Schumann) Cleve								
BF	Epiphytic and epilithic	*Cocconeis placentula* Ehrenberg								
B	Pelagic	*Coscinodiscus granii* Gough								
M		*Fragilaria capensis* Grunow								
BM	Epiphytic	*Gomphonemopsis exigua* (Kützing) L.K. Medlin								
F	Epipsammic	*Karayevia clevei* (Grunow) Bukhtiyarova								
M	Epiphitic	*Licmophora abbreviata* C. Agardh								
F	Epipsammic	*Martyana martyii* (Héribaud-Joseph) Round								
B	Epipsammic	*Martyana schulzii* Brockmann) Snoeijs								
B	Epipelic	*Navicula peregrina* (Ehrenberg) Kützing								
B	Epipsammic and epiphytic	*Opephora mutabilis* (Grunow) Sabbe and Wyverman								
B	Tychoplanktonic	*Paralia sulcata* (Ehrenberg) Cleve								
M	Epipelic	*Pinnularia cruciformis* (Donkin) Cleve								
B	Epipelic	*Pinnularia halophila* Krammer								
M	Benthic	*Plagiogramma staurophorum* (W. Gregory) Heiberg								
BF	Episammic and epilithic	*Planothidium delicatulum* (Kützing) Round and Bukhtiyarova								
BM	Epiphytic and epilithic	*Rhabdonema arcuatum* (Lyngbye) Kützing								
BF	Epipelic and epilithic	*Rhopalodia gibba* (Ehrenberg) O. Müller								
F	Pelagic	*Stephanodiscus neoastraea* Håkansson and Hickel								
B	Pelagic	*Thalassiosira hyperborea* var. *lacunosa* Hasle								
M?	Pelagic	*Thalassiosira oestrupii* (Ostenfeld) Hasle								
		Crysophyte cysts								
		Dots								

Table T4. Distribution and abundance of benthic foraminifers, Site M0060. (Continued on next two pages.)

Core, section, interval (cm)	Depth (mbsf) Top	Depth (mbsf) Bottom	Abundance	Pre-Quaternary redeposited tests	Number of species	Total foraminifers	% *Elphidium excavatum clavatum*	*Ammonia beccarii*	*Bucella frigida*	*Bulimina marginata*	*Cassidulina reniforme* (formerly *crassa*)	*Cibicides lobatulus*	*Elphidium excavatum clavatum*	*Elphidium excavatum selseyensis*	*Elphidium albiumbilicatum*	*Elphidium williamsoni*	*Elphidium groenlandicum*	Other *Elphidium* and *Haynesina* spp.	*Hyalinea balthica*	*Islandiella helenae* (formerly *terretis*) *	*Melonis barleeanum*	*Nonionella labradorica*	*Planulina ariminensis*	*Pyrgo williamsoni*	*Quinqueloculina* sp.	*Stainforthia feylingia*	*Uvigerina mediterranea*	Agglutinated (all species)	Other species, total
347-M0060A-																													
3H-1, 11–13	0.11	0.13	F		8	28	7	R		V		R	V					V			V							V	V
6H-1, 7–9	6.07	6.09	F	x	4	19	21				V		V		V	F													
8H-2, 15–17	10.65	10.67	F		10	24	25			V	V		R	V	V	V		R							V	V			
9H-2, 15–17	13.95	13.97	R	x	8	17	35		V		V		R			V		V				V			V				
10H-2, 15–17	17.26	17.28	C		13	63	37		V	V	R		F	F	V	V		V		V					R	V			V
11H-2, 15–17	20.55	20.57	F	x	9	27	48			V	V		F	V				R		V		V				V			
12H-2, 15–17	23.85	23.87	V		4	5	40						V							V	V					V			
13H-2, 15–17	27.15	27.17	B		0	0																							
15H-2, 15–17	32.15	32.17	R		2	22	55				F		F													V			
16H-2, 16–18	35.46	35.48	V	x	3	4	0													V									V
17H-2, 22–24	38.82	38.84	A		2	320	79				F		A																
18H-2, 10–12	42.00	42.02	V		2	2	50						V													V			
19H-1, 100–102	45.35	45.37	V	x	4	4	25						V	V					V										V
20H-2, 15–17	48.65	48.67	C		6	156	90			V	R		C	R				V								V			
21H-1, 14–16	50.44	50.46	V		1	1	100						V																
22H-2, 27–29	55.37	55.39	B		0	0																							
23H-2, 15–17	58.55	58.57	C		4	78	86				R		F	V				V											
24H-2, 16–18	61.86	61.88	A		3	204	90				F		A	R															
25H-2, 17–19	65.17	65.19	V	x	1	5	0				R																		
27H-2, 15–17	71.45	71.47	V		1	1	100						V																
28H-2, 15–17	74.45	74.47	V		2	2	50			V			V																
29H-2, 15–17	77.45	77.47	C	x	5	158	94			V	R		C							V									V
30H-3, 14–16	80.86	80.88	R		6	12	33	V		V			V	V				V	V										
31H-2, 15–17	84.05	84.07	F	x	9	22	27			V	V		R	V			V		V	V		V				V			
32H-2, 15–17	86.45	86.47	F		8	51	65				V		F	R				R		V	V				V				
33H-2, 15–17	89.75	89.77	R		6	15	40						R	R				V	V			V							V
34H-2, 15–17	93.05	93.07	C	x	13	107	40		V	F			F	F		V	V	R	V	R			V		V		V		V
35H-1, 26–28	94.96	94.98	F		8	36	44		V				F	F				V	V	V	V	V							
36H-1, 4–6	97.74	97.76	F	x	9	27	33			V	V	V	R	R				V	V						V				V
37H-1, 21.5–23.5	97.92	97.94	F	x	12	36	22	V	V	V	V		R	R				V	V	V	V	V							V
38H-2, 15–17	99.28	99.30	F	x	4	9	33				V		V	V								V							
48H-1, 20–22	116.90	116.92	V	x	1	1	0							V															
51H-1, 15–17	123.15	123.17	V	x	3	3	33						V	V					V										
52H-1, 20–22	126.50	126.52	V	x	4	7	0			V									V	V					V				
53H-1, 12–14	129.72	129.74	B	1	0	0																							
54H-2, 15–17	134.55	134.57	V		4	5	20						V				V	V		V									
55H-2, 15–17	137.85	137.87	V		2	3	0											V		V									
56H-2, 12–14	141.12	141.14	V		2	3	0							V						V									
57H-1, 2–4	142.82	142.84	V	x	4	5	0			V							V	V		V									
58H-1, 27–29	146.37	146.39	V	x	5	15	27	V			V		V					V	V										
60H-2, 13–15	153.74	153.76	A		18	164	0	V		F	V						R	V	F	F	F	V	V	V	V		F	V	V
61H-1, 0–2	155.40	155.42	C		14	51	4			F	V		V	V			V	V	F	V	V		V		V	V	R		V
63H-2, 18–20	160.08	160.10	V		4	8	0										V						V		V				V
65H-2, 15–17	160.66	160.68	V		2	2	50						V				V												
66H-2, 15–17	162.95	162.97	V	x	7	14	14						V	V			V	V		V					V				
67H-2, 15–17	165.01	165.03	V	x	6	9	11			V			V				V			V					V		V		
68H-2, 15–17	167.39	167.41	R	x	7	15	40	V		V			R				V		V						V				V
69H-2, 15–17	170.45	170.47	R		10	14	0					V		V			V	V	V	V		V			V				V
70H-2, 15–17	173.75	173.77	R		4	8	0			V							V	V		V									
71H-2, 15–17	176.83	176.85	V	x	5	10	0			V							V	V		V							V		
72H-2, 15–17	179.19	179.21	V		6	8	13						V				V	V		V							V	V	
73H-2, 14–16	183.64	183.66	V	x	3	4	0			V								V			V								
75H-2, 12–14	190.22	190.24	V		2	3	0													V			V						
76H-2, 15–17	193.55	193.57	C		13	48	4		V	F	V		V	V			V	V	V	R		R		V	V		V		
77H-2, 15–17	196.85	196.87	V		1	1	0			V																			
82P-1, 7–9	202.57	202.59	A		17	78	19			V	V		F	V	V		V	V	R	R	V	R		V	V		V		

Table T4 (continued). (Continued on next page.)

Core, section, interval (cm)	Depth (mbsf) Top	Depth (mbsf) Bottom	Abundance	Pre-Quaternary redeposited tests	Number of species	Total foraminifers	% *Elphidium excavatum clavatum*	*Ammonia beccarii*	*Bucella frigida*	*Bulimina marginata*	*Cassidulina reniforme* (formerly *crassa*)	*Cibicides lobatulus*	*Elphidium excavatum clavatum*	*Elphidium excavatum selseyensis*	*Elphidium albiumbilicatum*	*Elphidium williamsoni*	*Elphidium groenlandicum*	Other *Elphidium* and *Haynesina* spp.	*Hyalinea balthica*	*Islandiella helenae* (formerly *terretis*) *	*Melonis barleeanum*	*Nonionella labradorica*	*Planulina ariminensis*	*Pyrgo williamsoni*	*Quinqueloculina* sp.	*Stainforthia feylingia*	*Uvigerina mediterranea*	Agglutinated (all species)	Other species, total
347-M0060B-																													
4H-1, 44–46	6.54	6.56	F	x	7	28	36				V		F		V	R		V							V	V			
4H-2, 15–17	7.75	7.75	B		0	0																							
11H-2, 15–17	30.85	30.87	V	x	2	4	75						R													V			
Occurrence data for offshore samples																													
347-																													
M0060A-3H2-bottom	2.88	2.98	B	x	0																								
M0060A-4H2-bottom	4.60	4.88	B		0																								
M0060B-3H2-bottom		5.50	B	x	0																								
M0060A-6HCC-bottom	6.00	6.20	R	x	1													x											
M0060B-4HCC-bottom	9.29	9.39	F	x	4						x							x											x
M0060A-8HCC-bottom		12.30	C	x	3						x							x							x				
M0060A-9H2-bottom		14.76	C	x	4								x		x			x											
M0060B-6HCC-bottom	15.92	15.97	C	x	7			x		x	x							x							x				x
M0060A-10H3-bottom		18.88	R		1													x											
M0060B-7HCC-bottom	19.26	19.46	F	x	3					x	x							x											
M0060A-11HCC-bottom		22.27	R	x	4					x								x						x					x
M0060B-8HCC-bottom	22.49	22.71	F		6					x	x							x	x	x									x
M0060A-12H3-bottom		25.53	R		1													x											
M0060B-9HCC-bottom	25.77	25.90	F	x	6					x	x							x	x	x									x
M0060A-13H3-bottom	28.85	28.87	C		2							x						x											
M0060A-15H3-bottom		34.03	V	x	1						x							x											
M0060B-12H3-bottom		35.79	R	x	1													x											
M0060A-16HCC-bottom	37.18	37.22	V	x	2						x	x																	
M0060B-13H3-bottom		39.35	R	x	2						x							x											
M0060A-17HCC-bottom	40.37	40.41	R	x	1						x																		
M0060B-14HCC-bottom	42.55	42.70	R		2						x							x											
M0060A-18HCC-bottom	43.77	43.79	C	x	2						x		x							x									
M0060B-15HCC-bottom	45.67	45.86	V	x	2													x											
M0060A-19HCC-bottom	47.36	47.38	R	x	3						x		x																
M0060B-16HCC-bottom	49.37	49.41	R	x	4						x							x											
M0060A-20H3-bottom	50.54	50.57	C	x	2						x		x																
M0060B-17HCC-bottom	52.48	52.53	F	x	2						x							x											
M0060A-21HCC-bottom	53.88	53.90	A		1								x																
M0060B-18HCC-bottom	55.85	55.92	F	x	3						x							x											
M0060A-22HCC-bottom	57.18	57.23	F	x	2						x							x											
M0060B-19HCC-bottom	59.02	59.17	V	x	3													x											x
M0060A-23HCC-bottom	60.37	60.39	F	x	2						x							x											
M0060B-20HCC-bottom	62.21	62.39	C	x	5				x		x							x							x				x
M0060A-24HCC-bottom	63.74	63.76	F	x	2						x							x											
M0060B-21HCC-bottom	65.57	65.61	C	x	2						x							x											
M0060A-25H3-bottom	66.87	66.90	C		1													x											
M0060A-26H3-bottom	69.79	69.81	B		0																								
M0060A-28H2-bottom	75.61	75.63	B		0																								
M0060B-25HCC-bottom	76.22	76.27	B		0																								
M0060A-29HCC-bottom	79.39	79.42	C	x	6					x	x							x	x	x									x
M0060B-26H3-bottom	79.60	79.63	V	x	1													x											
M0060A-30H4-bottom	82.66	82.68	F	x	7					x	x							x	x	x					x				
M0060A-31H2-bottom	84.62	84.65	C	x	6					x	x							x	x	x									x
M0060A-32HCC-bottom	88.24	88.26	V		1													x											
M0060A-33HCC-bottom	91.29	91.32	C	x	10				x	x	x							x	x	x		x							
M0060A-34H3-bottom	94.68	94.70	C	x	8					x	x							x	x	x				x	x				
M0060A-35HCC-bottom	97.66	97.71	F	x	7					x								x	x	x		x			x				
M0060A-37S1-bottom	97.70	98.01	C	x	9			x		x	x							x	x	x		x		x	x				
M0060A-39HCC-bottom	101.20	101.23	R	x	4													x	x	x									
M0060A-38HCC-bottom	101.34	101.54	F	x	5			x		x								x							x				
M0060A-41SCC-bottom	104.70	104.78	B		0																								
M0060A-45PCC-bottom	112.70	112.72	B		0																								

Table T4 (continued).

Core, section, interval (cm)	Depth (mbsf)		Abundance	Pre-Quaternary redeposited tests	Number of species	Total foraminifers	% *Elphidium excavatum clavatum*	*Ammonia beccarii*	*Bucella frigida*	*Bulimina marginata*	*Cassidulina reniforme* (formerly *crassa*)	*Cibicides lobatulus*	*Elphidium excavatum clavatum*	*Elphidium excavatum selseyensis*	*Elphidium albiumbilicatum*	*Elphidium williamsoni*	*Elphidium groenlandicum*	Other *Elphidium* and *Haynesina* spp.	*Hyalinea balthica*	*Islandiella helenae* (formerly *terretis*) *	*Melonis barleeanum*	*Nonionella labradorica*	*Planulina ariminensis*	*Pyrgo williamsoni*	*Quinqueloculina* sp.	*Stainforthia feylingia*	*Uvigerina mediterranea*	Agglutinated (all species)	Other species, total
	Top	Bottom																										
M0060A-46HCC-bottom	113.70	113.80	V		2													x							x			
M0060A-48HCC-bottom		118.20	V		1																							
M0060A-50HCC-bottom	123.09	123.19	V		1															x								
M0060A-51HCC-bottom	125.53	125.57	C	x	13			x		x	x							x	x	x	x				x		x	x
M0060A-52HCC-bottom	128.71	128.73	F	x	4														x	x					x			x
M0060A-53HCC-bottom	131.58	131.60	R	x	3			x				x								x								
M0060A-54HCC-bottom	135.43	135.48	F		5					x								x	x	x	x							
M0060A-55HCC-bottom	139.15	139.20	C	x	9					x	x							x	x	x	x				x		x	
M0060A-56HCC-bottom		142.33	V	x	1													x										
M0060A-57HCC-bottom	145.37	145.40	R	x	2			x										x										
M0060A-58H1-bottom	147.60	147.61	R		2													x										
M0060A-59HCC-bottom		149.55	R		5					x	x							x	x									x
M0060A-60H2-bottom		154	A		13			x		x	x							x	x	x	x	x			x		x	x
M0060A-61H1-bottom		155.7	F		5			x		x								x	x	x								
M0060A-63HCC-bottom	160.27	160.29	F		3													x	x			x						
M0060A-66H2-bottom		164.30	V	x	4					x								x		x								
M0060A-67H2-bottom		166.32	R		6						x							x	x	x					x			
M0060A-68H2-bottom		168.75	R		7				x	x								x	x	x					x			
M0060A-69HCC-bottom	171.13	171.17	V		3						x							x	x									
M0060A-70HCC-bottom	175.35	175.40	R	x	7					x	x							x	x	x					x			x
M0060A-71HCC-bottom	176.98	177.04	R		8													x	x	x					x		x	x
M0060A-72HCC-bottom	182.11	182.18	R		6					x								x	x			x			x			
M0060A-73HCC-bottom	184.81	184.83	R		5					x								x	x	x								x
M0060A-74HCC-bottom	185.30	185.35	V		2													x							x			
M0060A-75HCC-bottom	191.48	191.53	V		4													x		x					x			
M0060A-76HCC-bottom	194.51	194.56	C	x	9				x	x	x							x		x					x		x	x
M0060A-77HCC-bottom	198.55	198.62	R	x	8					x	x							x		x							x	x
M0060A-78S1-bottom		198.80	R	x	5													x		x					x		x	
M0060A-80HCC-bottom	199.50	199.54	F	x	8					x								x	x	x		x	x					
M0060A-82PCC-bottom	203.25	203.35	C	x	18			x	x	x	x							x	x	x		x		x	x		x	x
M0060A-84P1-bottom	205.50	205.56	C		10				x	x	x							x	x	x		x			x		x	x
M0060A-88SCC-bottom	211.60	211.66	V	x	2													x	x									
M0060A-90SCC-bottom		214.60	V		1																							x
M0060A-92SCC-bottom		217.72	B	x	0																							
M0060A-94SCC-bottom		220.55	R		6					x								x		x			x		x			
M0060A-96SCC-bottom		223.60	R	x	3													x										x
M0060A-98SCC-bottom		226.60	B		0																							
M0060A-100SCC-bottom		229.60	R		1													x										

* = possibly including *Cassidulina laevigata* in some intervals. Abundance: A = abundant, C = common, F = few, R = rare, V = very rare, B = barren.

Table T5. Distribution and abundance of ostracods, Site M0060. (Continued on next three pages.)

Core, section, interval (cm)	Depth (mbsf)	Abundance (offshore samples, 5–30 cm³)	Abundance (onshore samples, 20 cm³)	*Acanthocythereis dunelmensis*	*Baffinicythere* sp.	*Bythocythere constricta*	*Cluthia cluthae*	*Cythere lutea*	*Cytherois* spp.	*Cytheropteron arcuatum*	*Cytheropteron biconvexa*	*Cytheropteron latissimum*	*Cytheropteron nodosoalatum*	*Cytheropteron pseudomontrosiense*	*Cytheropteron* spp.	*Cytherura* spp.	*Elofsonella concinna*	*Finmarchinella* sp.	*Heterocyprideis sorbyana*	*Hirschmania viridis*	*Ilyocypris* sp.	*Jonesia acuminata*	*Krithe* sp.	*Leptocythere* spp.	*Normanicythere leioderma*	*Palmenella limicola*	*Polycope* sp.	*Pontocypris* sp.	*Rabilimis mirabilis*	*Robertsonites tuberculatus*	*Roundstonia globulifera*	*Sarsicytheridea bradii*	*Sarsicytheridea punctillata*	*Sclerochilus* sp.	*Semicytherura* sp.	Redeposited	Undetermined
347-M0060A-																																					
3H-1, 11–13	0.12		F	R				R																R							R	R	2				
3H-2, 138–148	2.88	B																																			
4H-2, 28–38	4.78	B																																			
6H-CC, 0–20	6.00	F		R													R		R					R							R					R
6H-1, 7–9	6.08		A	A				R								R	F		R		R			R							F		C				
8H-2, 15–17	10.66		A	R											R	F	F							F		R					R	R	F		R		R
8H-CC, 0–14	12.16	F														R	R							F								R					R
9H-CC, 0–96	13.80	F		R								R				R	R							R									R				R
9H-2, 15–17	13.96		A	R	R	R			R			R				R	C		R					A							R	R	C	R	R	R	
10H-2, 15–17	17.27		A	R	F			R							R	F	C	R	F				R	F			R					F	F				
10H-3, 0–27	18.61	R												R					R														R				
11H-2, 15–17	20.56		A	F					R	R	R	F	R	F			F		R												R		R	R			
11H-CC, 0–20	22.07	R		R										R			R																R				
12H-2, 15–17	23.86		F												R		R																				
12H-3, 0–33	25.20	B																																			
13H-2, 15–17	27.16		B																																		
13H-3, 35–37	28.85	B																																			
15H-2, 15–17	32.16		B																																		
15H-3, 51–53	34.01	B																																			
16H-2, 16–18	35.47		B																																		
16H-CC, 0–4	37.18	B																																			
17H-2, 22–24	38.83		B																																		
17H-CC, 0–4	40.37	B																																			
18H-2, 10–12	40.99		R												R																						
18H-CC, 0–2	43.77	R												R																							
19H-1, 100–102	45.36		B																																		
19H-CC, 19–21	47.36	R												R																							
20H-2, 15–17	48.66		R				R																														
21H-1, 14–16	50.43		B																																		
20H-3, 54–57	50.54	R												R																							
21H-CC, 18–20	53.88	B																																			
22H-2, 27–29	55.36		B																																		
22H-CC, 0–5	57.18	B																																			
23H-2, 15–17	58.54		R												R																						
23H-CC, 13–15	60.37	R												R																							
24H-2, 16–18	61.85		B																																		
24H-CC, 11–13	63.74	R		R										R																							

Table T5 (continued). (Continued on next page.)

Core, section, interval (cm)	Depth (mbsf)	Abundance (offshore samples, 5–30 cm³)	Abundance (onshore samples, 20 cm³)	*Acanthocythereideis dunelmensis*	*Baffinicythere* sp.	*Bythocythere constricta*	*Cluthia cluthae*	*Cythere lutea*	*Cytherois* spp.	*Cytheropteron arcuatum*	*Cytheropteron biconvexa*	*Cytheropteron latissimum*	*Cytheropteron nodosoalatum*	*Cytheropteron pseudomontrosiense*	*Cytheropteron* spp.	*Cytherura* spp.	*Elofsonella concinna*	*Finmarchinella* sp.	*Heterocyprideis sorbyana*	*Hirschmania viridis*	*Ilyocypris* sp.	*Jonesia acuminata*	*Krithe* sp.	*Leptocythere* spp.	*Normanicythere leioderma*	*Palmenella limicola*	*Polycope* sp.	*Pontocypris* sp.	*Rabilimis mirabilis*	*Robertsonites tuberculatus*	*Roundstonia globulifera*	*Sarsicytheridea bradii*	*Sarsicytheridea punctillata*	*Sclerochilus* sp.	*Semicytherura* sp.	Redeposited	Undetermined
25H-2, 17–19	65.16		R																								R								
25H-3, 37–40	66.87	B																																		
26H-3, 19–21	69.79	B																																		
27H-2, 15–17	71.44		B																																	
28H-2, 15–17	74.44		B																																	
28H-2, 131–133	75.61	B																																		
29H-2, 15–17	77.46		R												R																					
29H-CC, 15–18	79.39	B																																		
30H-3, 14–16	80.87		B																																	
30H-4, 44–46	82.66	B																																		
31H-2, 15–17	84.06		B																																	
31H-2, 72–75	84.62	R																					R													
32H-2, 15–17	86.46		R												R																					
32H-CC, 20–22	88.24	R		R																																
33H-2, 15–17	89.76		B																																	
33H-CC, 21–24	91.29	B																																		
34H-2, 15–17	93.06		R												R					R																
34H-3, 28–30	94.68	R																											R							
35H-1, 26–28	94.97		B																																	
35H-CC, 0–5	97.66	R																								R										
36H-1, 4–6	97.75		B																																	
37H-1, 21.5–23.5	97.925		R									R																								
37S-1	98.01	B																																		
38H-2, 15–17	99.29		B																																	
39H-CC, 0–3	101.20	B																																		
38H-CC, 0–20	101.34	B																																		
41S-CC, 0–8	104.70	B																																		
45P-CC, 0–2	112.70	B																																		
46H-CC, 0–10	113.70	B																																		
48H-1, 20–22	116.91		B																																	
48H-CC, 13–15	118.18	B																																		
50H-CC, 0–10	123.09	B																																		
51H-1, 15–17	123.16		B																																	
51H-CC, 0–4	125.53	R																																	R	
52H-1, 20–22	126.51		B																																R	
52H-CC, 6–8	128.71	B																																		
53H-1, 12–14	129.73		B																																	
53H-CC, 0–2	131.58	B																																		
54H-2, 15–17	134.56		B																																	

Table T5 (continued). (Continued on next page.)

Core, section, interval (cm)	Depth (mbsf)	Abundance (offshore samples, 5–30 cm³)	Abundance (onshore samples, 20 cm³)	*Acanthocythereideis dunelmensis*	*Baffinicythere* sp.	*Bythocythere constricta*	*Cluthia cluthae*	*Cythere lutea*	*Cytherois* spp.	*Cytheropteron arcuatum*	*Cytheropteron biconvexa*	*Cytheropteron latissimum*	*Cytheropteron nodosoalatum*	*Cytheropteron pseudomontrosiense*	*Cytheropteron* spp.	*Cytherura* spp.	*Elofsonella concinna*	*Finmarchinella* sp.	*Heterocyprideis sorbyana*	*Hirschmania viridis*	*Ilyocypris* sp.	*Jonesia acuminata*	*Krithe* sp.	*Leptocythere* spp.	*Normanicythere leioderma*	*Palmenella limicola*	*Polycope* sp.	*Pontocypris* sp.	*Rabilimis mirabilis*	*Robertsonites tuberculatus*	*Roundstonia globulifera*	*Sarsicytheridea bradii*	*Sarsicytheridea punctillata*	*Sclerochilus* sp.	*Semicytherura* sp.	Redeposited	Undetermined
54H-CC, 0–5	135.43	B																																		
55H-2, 15–17	137.86		B																																	
55H-CC, 0–5	139.15	B																																	R	
56H-2, 12–14	141.13		B																																	
56H-CC, 3–5	142.31	B																																		
57H-1, 2–4	142.83		B																																	
57H-CC, 5–8	145.37	B																																		
58H-1, 27–29	146.38		B																																	
58H-1, 150–151	147.60	B																																		
59H-CC, 13–15	149.53	B																																		
60H-2, 13–15	153.75		R																					R					R							
60H-2, 37–39	153.98	B																																		
61H-1, 0–2	155.41		B																																	
61H-2, 28–30	155.68	B																																		
63H-2, 18–20	160.09		B																																	
63H-CC, 0–2	160.27	B																																		
66H-2, 148–150	164.28	B																																		
67H-2, 15–17	165.02		B																																	
67H-2, 144–146	166.30	B																																		
68H-2, 15–17	167.40		B																																	
68H-2, 149–151	168.73	B																																		
69H-2, 15–17	170.46		B																																	
69H-CC, 0–4	171.13	B																																		
70H-2, 15–17	173.75		B																																	
70H-CC, 0–5	174.35	B																																		
71H-2, 15–17	176.84		B																																	
71H-CC, 0–6	176.98	B																																		
72H-2, 15–17	179.20		B																																	
72H-CC, 0–7	182.11	B																																		
73H-2, 14–16	183.65		B																																	
73H-CC, 0–2	184.81	B																																		
74H-CC, 0–5	185.30	B																																		
75H-2, 12–14	190.23		B																																	
75H-CC, –	191.53	B																																		
76H-2, 15–17	193.56		B																																	
76H-CC, 0–5	194.51	B																																		
77H-2, 15–17	196.86		B																																	
77H-CC, 0–7	198.55	B																																		
78S-1	198.80	B																																		

Table T5 (continued).

Core, section, interval (cm)	Depth (mbsf)	Abundance (offshore samples, 5–30 cm³)	Abundance (onshore samples, 20 cm³)	*Acanthocythereideis dunelmensis*	*Baffinicythere* sp.	*Bythocythere constricta*	*Cluthia cluthae*	*Cythere lutea*	*Cytherois* spp.	*Cytheropteron arcuatum*	*Cytheropteron biconvexa*	*Cytheropteron latissimum*	*Cytheropteron nodosoalatum*	*Cytheropteron pseudomontrosiense*	*Cytheropteron* spp.	*Cytherura* spp.	*Elofsonella concinna*	*Finmarchinella* sp.	*Heterocyprideis sorbyana*	*Hirschmania viridis*	*Ilyocypris* sp.	*Jonesia acuminata*	*Krithe* sp.	*Leptocythere* spp.	*Normanicythere leioderma*	*Palmenella limicola*	*Polycope* sp.	*Pontocypris* sp.	*Rabilimis mirabilis*	*Robertsonites tuberculatus*	*Roundstonia globulifera*	*Sarsicytheridea bradii*	*Sarsicytheridea punctillata*	*Sclerochilus* sp.	*Semicytherura* sp.	Redeposited	Undetermined
80H-CC, 0–4	199.50	B																																		
82P-1, 7–9	202.58		R														R																			R
82P-CC, 0–10	203.25	B																																		
84P-1, 5–6	205.55	B																																		
88S-CC, 0–6	211.60	B																																		
90S-CC, 8–10	214.58	B																																		
92S-CC, 20–22	217.70	B																																		
94S-CC, 3–5	220.53	R																											1							
96S-CC, 8–10	223.58	B																																		
98S-CC, 8–10	226.58	B																																		
100S-CC, 8–10	229.58	B																																		
347-M0060B-																																				
3H-2, 118–120	5.48	B																																		
4H-1, 44–46	6.55			A				R								F	F		R		R			F						R	R		C			
4H-2, 15–17	7.75		B																																	
4H-CC, 0–10	9.29	F		R				R									R														R		R			
6H-CC, 0–5	15.92	A		R	F	R		R	R			R	F			R	F		R					F			R	R			R	R	C		R		R
7H-CC, 0–20	19.26	F		R									R	R			R		R												R		R			
8H-CC, 0–22	22.49	F										R		R			R		R												R		R			
9H-CC, 0–13	25.77	R												R																			R			
11H-2, 15–17	30.86		B																																	
12H-3, bottom	35.79	B																																		
13H-3, 53–55	39.33	B																																		
14H-CC, 0–15	42.55	B																																		
15H-CC, 0–19	45.67	B																																		
16H-CC, 67–71	49.37	B																																		
17H-CC, 0–5	52.48	B																																		
18H-CC, 63–70	55.93	B																																		
19H-CC, 0–15	59.02	B																																		
20H-CC, 0–18	62.21	B																																		
21H-CC, 0–4	65.57	B																																		
25H-CC, 0–5	76.22	B																																		
26H-3, 30–33	79.60	B																																		

Abundance: A = abundant, C = common, F = few, R = rare, V = very rare, B = barren.

Table T6. Occurrences of tertiary pollen types in samples, Site M0060A.

Tertiary pollen type	Core	Depth (mbsf)
Tertiary pollen taxa		
Pinus (mostly haploxylon type)	8H	9.15
	9H	12.65
	10H	15.69
	11H	19.38
	12H	22.35
	15H	31.40
	18H	40.60
	20H	48.68
	29H	76.48
	30H	80.10
	37H-CC	
	54H	133.54
	61H	155.42
	68H	166.92
	70H	172.34
	76H-CC	
	77H	194.40
	82P	202.67
Picea	9H	12.65
	11H	19.38
	20H	48.68
	30H	80.10
	37H-CC	
	61H	155.42
	70H	172.34
	76H-CC	
	77H	194.40
	82P	202.67
Taxodiaceae/*Cuppressaceae*	9H	12.65
	10H	15.69
	11H	19.38
	12H	22.35
	15H	31.40
	18H	40.60
	20H	48.68
	30H	80.10
	37H-CC	
	61H	155.42
	68H	166.92
	70H	172.34
	76H-CC	
	77H	194.40
	82P	202.67
Sequoia	61H	155.42
Sciadopitys	9H	12.65
	54H	133.54
Tsuga	9H	12.65
	11H	19.38
Ginkgo	82P	202.67
Tilia	6H	6.10
Carya	37H-CC	
	54H	133.54
	76H-CC	
	82P	202.67
Nyssa	37H-CC	
	76H	194.40
Quercus/*Quercoidites*	15H	31.40
Tricolporopollenites	11H	19.38
Loranthus type	37H-CC	
Tertiary Triletae spores	9H	12.65
	12H	22.35
	29H	76.48
	30H	80.10
	54H	133.54
	61H	155.42
	68H	166.92
	70H	172.34
	77H	194.40
	82P	202.67

Table T7. Interstitial water geochemistry, Site M0060. This table is available in **oversized format.**

Table T8. Calculated Cl^- based salinity and elemental ratios of interstitial waters, Site M0060. (Continued on next page.)

Core, section, interval (cm)	Type	Depth (mbsf)	Cl^- based salinity	Na/Cl (mM/mM)	Ca/Cl (mM/mM)	Mg/Cl (mM/mM)	K/Cl (mM/mM)	Br/Cl (µM/mM)	B/Cl (µM/mM)
347-M0060A-									
3H-1, 135–140	Rh	1.38	32.26	0.86	0.02	0.10	0.02	1.46	0.79
3H-2, 133–138	Rh	2.86	30.68	0.92	0.02	0.11	0.02	1.46	0.84
4H-1, 135–140	Rh	4.38	30.37	0.89	0.02	0.10	0.02	1.47	0.80
4H-2, 28–28	Rh	4.78	30.43	0.94	0.02	0.11	0.03	1.46	0.87
8H-1, 135–140	Rh	10.38	31.25	0.98	0.01	0.10	0.02	1.53	1.08
8H-2, 135–140	Rh	11.88	31.82	0.94	0.01	0.10	0.02	1.54	1.03
9H-1, 135–140	Rh	13.68	31.50	0.94	0.01	0.09	0.02	1.54	1.05
9H-2, 50–60	Rh	14.35	31.74	1.01	0.01	0.10	0.02	1.55	1.16
10H-1, 135–140	Rh	16.98	31.41	1.07	0.02	0.12	0.02	1.56	1.26
11H-1, 135–140	Rh	20.28	30.40	0.96	0.02	0.10	0.02	1.54	1.20
12H-1, 135–140	Rh	23.58	30.16	0.91	0.02	0.10	0.01	1.55	1.09
13H-1, 135–140	Rh	26.88	26.98	—	—	—	—	—	—
23H-1, 135–140	Rh	58.28	27.91	0.83	0.02	0.08	0.01	1.52	1.03
24H-1, 135–140	Rh	61.58	26.76	0.65	0.01	0.06	0.01	1.51	0.76
30H-1, 133–138	Rh	80.46	23.86	0.89	0.02	0.09	0.01	1.46	1.04
31H-1, 135–140	Rh	83.78	21.83	1.15	0.02	0.11	0.02	1.46	1.46
35H-1, 135–140	Rh	96.08	19.66	0.85	0.02	0.09	0.02	1.39	0.78
48H-1, 120–125	Rh	117.93	16.24	0.99	0.03	0.11	0.02	1.36	1.05
50H-1, 135–140	Rh	121.08	10.80	0.88	0.05	0.08	0.02	1.58	1.02
51H-1, 135–140	Rh	124.38	10.40	0.76	0.05	0.07	0.01	1.57	0.88
52H-1, 135–140	Rh	127.68	10.66	0.76	0.05	0.07	0.01	1.56	0.92
53H-1, 135–140	Rh	130.98	11.43	0.88	0.05	0.09	0.02	1.56	1.04
54H-1, 135–140	Rh	134.28	11.73	0.75	0.04	0.07	0.01	1.57	1.02
55H-1, 135–140	Rh	137.58	12.61	0.77	0.03	0.07	0.01	1.57	1.16
56H-1, 135–140	Rh	140.88	13.71	0.78	0.02	0.07	0.01	1.58	1.27
57H-1, 135–140	Rh	144.18	14.92	0.89	0.02	0.08	0.01	1.60	1.65
58H-1, 135–140	Rh	147.48	15.91	—	—	—	—	—	—
60H-1, 105–110	Rh	153.48	19.84	0.84	0.02	0.09	0.02	1.59	0.93
61H-1, 15–20	Rh	155.58	19.49	0.97	0.02	0.10	0.02	1.60	1.21
63H-1, 135–140	Rh	159.78	20.27	0.94	0.02	0.10	0.02	1.59	0.95
65H-1, 95–100	Rh	160.38	19.91	0.99	0.02	0.10	0.02	1.59	0.98
66H-2, 10–15	Rh	162.93	20.55	0.90	0.02	0.09	0.02	1.50	0.98
68H-2, 10–15	Rh	167.37	21.06	0.85	0.02	0.09	0.02	1.61	0.89
69H-1, 135–140	Rh	170.18	21.95	0.82	0.01	0.08	0.01	1.64	0.92
70H-1, 135–140	Rh	173.48	22.03	0.96	0.02	0.09	0.02	1.60	1.15
73H-1, 135–140	Rh	183.38	22.63	0.79	0.01	0.08	0.02	1.62	0.91
76H-1, 135–140	Rh	193.28	21.14	0.90	0.02	0.09	0.02	1.60	1.15
82P–1, 60–65	Rh	203.13	20.58	0.80	0.02	0.08	0.02	1.59	0.97
347-M0060B-									
1H-1, 135–145	Sq	1.40	33.92	0.81	0.02	0.09	0.02	1.55	0.67
3H-1, 125–135	Sq	4.10	32.82	0.83	0.02	0.10	0.02	1.56	0.71
3H-2, 80–90	Sq	5.15	33.03	0.82	0.02	0.09	0.02	1.52	0.68
4H-1, 135–145	Sq	7.50	32.52	0.84	0.01	0.08	0.02	1.60	0.82
4H-2, 125–135	Sq	8.90	32.47	0.81	0.01	0.08	0.02	1.60	0.88
5H-1, 125–135	Sq	10.70	32.34	0.80	0.01	0.08	0.02	1.61	0.85
5H-2, 122–132	Sq	12.17	26.33	0.82	0.01	0.08	0.02	1.45	0.77
6H-1, 120–130	Sq	13.95	31.93	0.83	0.01	0.08	0.02	1.62	0.92
7H-1, 125–135	Sq	17.30	32.09	0.82	0.01	0.08	0.02	1.62	0.89
7H-2, 135–145	Sq	18.90	30.77	0.95	0.02	0.10	0.02	1.61	1.19
8H-1, 125–135	Sq	20.60	31.77	0.81	0.01	0.08	0.01	1.63	0.96
9H-2, 120–130	Sq	23.85	31.72	0.81	0.02	0.08	0.01	1.63	0.93
10H-1, 125–135	Sq	27.20	31.55	0.81	0.02	0.09	0.01	1.62	1.12
11H-1, 135–145	Sq	30.60	29.09	0.84	0.03	0.09	0.01	0.83	1.13
12H-1, 135–145	Sq	33.90	31.33	0.80	0.03	0.09	0.01	0.89	1.07
13H-1, 125–135	Sq	37.10	30.67	0.79	0.02	0.09	0.01	1.63	1.06
14H-1, 135–140	Sq	40.48	31.14	0.80	0.02	0.09	0.01	1.61	1.11
15H-1, 135–145	Sq	43.80	31.27	0.79	0.02	0.09	0.01	1.61	1.14
16H-1, 125–135	Sq	47.00	31.91	0.95	0.03	0.11	0.01	1.60	1.51
18H-1, 135–145	Sq	53.70	31.62	0.94	0.02	0.10	0.01	1.63	1.45
20H-1, 135–145	Sq	60.30	31.37	0.96	0.02	0.10	0.01	1.62	1.40
21H-1, 135–145	Sq	63.60	31.20	0.81	0.01	0.08	0.01	1.62	1.05
22H-1, 115–125	Sq	66.70	31.54	0.80	0.02	0.08	0.01	1.60	1.12
23H-1, 135–145	Sq	69.40	30.56	0.80	0.02	0.08	0.01	1.61	1.13
24H-1, 135–145	Sq	71.90	30.53	0.81	0.02	0.08	0.01	1.61	1.18
26H-1, 135–145	Sq	77.70	29.22	0.82	0.02	0.08	0.01	1.59	1.21
27H-1, 135–145	Sq	81.00	27.80	—	—	—	—	—	—

Table T8 (continued).

Core, section, interval (cm)	Type	Depth (mbsf)	Cl^- based salinity	Na/Cl (mM/mM)	Ca/Cl (mM/mM)	Mg/Cl (mM/mM)	K/Cl (mM/mM)	Br/Cl (μM/mM)	B/Cl (μM/mM)
28H-1, 130–140	Sq	84.25	25.49	0.83	0.01	0.08	0.01	1.59	1.00
347-M0060B-									
1H-1, 108–113	Rh	1.11	—	—	—	—	—	—	—
1H-2, 86–91	Rh	2.39	—	—	—	—	—	—	—
3H-1, 18–23	Rh	3.01	—	—	—	—	—	—	—
4H-1, 90–95	Rh	7.03	—	—	—	—	—	—	—
4H-2, 55–60	Rh	8.18	—	—	—	—	—	—	—
5H-1, 56–61	Rh	9.99	—	—	—	—	—	—	—
6H-1, 59–64	Rh	13.32	—	—	—	—	—	—	—
7H-1, 90–95	Rh	16.93	—	—	—	—	—	—	—
8H-1, 54–59	Rh	19.87	—	—	—	—	—	—	—
9H-1, 60–65	Rh	23.23	—	—	—	—	—	—	—
10H-1, 89–94	Rh	26.82	—	—	—	—	—	—	—
11H-1, 65–70	Rh	29.88	—	—	—	—	—	—	—
12H-1, 76–81	Rh	33.29	—	—	—	—	—	—	—
13H-1, 89–94	Rh	36.72	—	—	—	—	—	—	—
14H-1, 65–70	Rh	39.78	—	—	—	—	—	—	—
15H-1, 75–80	Rh	43.18	—	—	—	—	—	—	—
16H-1, 88–93	Rh	46.61	—	—	—	—	—	—	—
17H-1, 63–68	Rh	49.66	—	—	—	—	—	—	—
18H-1, 76–81	Rh	53.09	—	—	—	—	—	—	—
19H-1, 87–92	Rh	56.50	—	—	—	—	—	—	—
20H-1, 65–70	Rh	59.58	—	—	—	—	—	—	—
21H-1, 71–76	Rh	62.94	—	—	—	—	—	—	—
22H-1, 88–93	Rh	66.41	—	—	—	—	—	—	—
23H-1, 63–68	Rh	68.66	—	—	—	—	—	—	—
24H-1, 70–75	Rh	71.23	—	—	—	—	—	—	—
25H-1, 87–92	Rh	73.90	—	—	—	—	—	—	—
26H-1, 63–68	Rh	76.96	—	—	—	—	—	—	—
27H-1, 75–80	Rh	80.38	—	—	—	—	—	—	—
28H-1, 59–64	Rh	83.52	—	—	—	—	—	—	—

Rh = Rhizon sample, Sq = squeezed sample. — = no data are reported for samples with insufficient pore water volumes.

Table T9. Concentration of methane in interstitial water, Site M0060.

Core, section, interval (cm)	Depth (mbsf)	CH_4 (mM)
347-M0060A-		
3H-1, 145–150	1.48	0.00
4H-1, 145–150	4.48	0.00
8H-1, 145–150	10.48	0.00
9H-1, 145–150	13.78	0.00
10H-1, 146–151	17.09	0.00
11H-1, 145–150	20.38	0.00
12H-1, 145–150	23.68	0.00
13H-1, 145–150	26.98	0.00
15H-1, 145–150	31.98	0.00
16H-1, 145–150	35.28	0.00
17H-1, 145–150	38.58	0.00
18H-1, 145–150	41.88	0.00
19H-1, 145–150	45.18	0.00
20H-1, 145–150	48.48	0.00
21H-1, 145–150	51.78	0.00
22H-1, 145–150	55.08	0.00
23H-1, 145–150	58.38	0.01
24H-1, 145–150	61.68	0.01
25H-1, 145–150	64.98	0.01
26H-1, 145–150	68.28	0.01
27H-1, 145–150	71.28	0.01
28H-1, 145–150	74.28	0.01
29H-1, 145–150	77.28	0.01
30H-2, 9–14	80.70	0.00
31H-1, 145–150	83.88	0.00
32H-1, 145–150	86.28	0.00
33H-1, 145–150	89.58	0.01
34H-1, 145–150	92.88	0.06
35H-1, 145–150	96.18	0.03
38H-2, 145–150	100.61	0.24
58H-1, 145–150	147.58	1.35
66H-2, 0–5	162.83	2.17
67H-1, 61–66	164.84	0.39
68H-2, 0–5	167.27	0.56
69H-1, 145–150	170.28	0.15
70H-1, 145–150	173.58	0.04
71H-1, 123–128	176.66	0.01
72H-2, 145–150	180.52	0.01
73H-1, 145–150	183.48	0.01

Table T10. Total carbon (TC), total organic carbon (TOC), total inorganic carbon (TIC), and total sulfur (TS) in sediment, Site M0060. (Continued on next page.)

Core, section, interval (cm)	Depth (mbsf)	TC (wt%)	TOC (wt%)	TIC (wt%)	TS (wt%)
347-M0060A-					
3H-1, 90–91	0.90	0.71	0.20	0.51	—
4H-1, 70–71.5	3.70	0.32	0.00	0.31	—
6H-1, 11–12	6.11	1.70	0.28	1.42	—
8H-1, 40–41	9.40	1.96	0.39	1.56	—
8H-2, 111–112	11.61	1.74	0.31	1.43	—
9H-1, 10–11	12.40	2.41	0.36	2.05	—
9H-2, 78–79	14.58	1.38	0.15	1.24	—
10H-1, 51–52	16.11	1.31	0.14	1.17	—
10H-2, 115–117	18.26	1.79	0.21	1.57	—
11H-1, 23.5–24.5	19.14	2.16	0.27	1.89	—
11H-2, 96.5–97.5	21.37	1.98	0.28	1.70	—
12H-2, 96–97.5	22.79	1.90	0.37	1.53	—
12H-1, 58.5–60	24.66	2.08	0.48	1.60	—
13H-1, 8–9	25.58	2.23	0.41	1.82	—
13H-2, 124–125	28.24	2.77	0.58	2.19	—
15H-1, 25–26	30.75	2.90	0.59	2.32	—
15H-2, 115–116	33.15	3.15	0.67	2.49	0.22
16H-1, 30–31	34.10	2.85	0.55	2.30	—
16H-2, 100–111	36.30	2.56	0.47	2.09	—
17H-1, 20–21	37.30	3.21	0.55	2.66	—
17H-2, 20–21	38.80	3.21	0.70	2.51	—
18H-1, 46–47	40.86	3.29	0.59	2.70	—
18H-2, 96–97	42.86	2.99	0.65	2.34	—
19H-1, 52–53	44.22	2.67	0.79	1.89	—
19H-2, 116–117	46.36	2.63	0.73	1.90	—
20H-1, 20–21	47.20	2.82	0.65	2.17	—
20H-2, 20–21	48.70	2.82	0.68	2.14	—
21H-1, 50–51	50.80	2.93	0.67	2.27	0.14
21H-2, 100–101	52.80	3.04	0.64	2.40	—
22H-1, 46–47	54.06	3.04	0.65	2.39	—
22H-2, 102–103	56.12	3.45	0.58	2.88	—
23H-1, 42–43	57.32	3.78	0.60	3.18	0.25
23H-2, 42–43	58.82	3.41	0.42	2.99	—
24H-1, 54–55	60.74	3.11	0.41	2.70	—
24H-2, 132–133	63.02	3.89	0.47	3.42	—
25H-1, 48–49	63.98	3.61	0.44	3.17	—
25H-2, 119–120	66.19	3.09	0.49	2.61	—
26H-1, 42–43	67.22	2.86	0.50	2.36	—
26H-2, 100–101	69.30	3.73	0.52	3.21	—
27H-1, 35–36	70.15	3.70	0.50	3.20	—
27H-2, 90–91	72.20	3.89	0.52	3.38	—
28H-1, 54–55.5	73.34	3.95	0.49	3.46	—
29H-1, 20–21	76.00	3.27	0.55	2.72	—
29H-2, 80–81	78.10	3.63	0.49	3.14	—
30H-1, 110.5–112	80.21	2.73	0.45	2.28	—
30H-3, 138.5–140	82.11	2.19	0.34	1.85	—
31H-1, 10–11	82.50	2.17	0.30	1.87	—
31H-2, 65–66	84.55	1.40	0.13	1.27	—
32H-1, 11–12.5	84.91	1.72	0.21	1.50	—
32H-2, 135–136.5	87.65	2.35	0.56	1.79	—
33H-1, 45–47	88.55	3.18	0.41	2.77	—
33H-2, 112–113.5	90.72	3.19	0.43	2.76	—
34H-1, 30–31	91.70	2.87	0.45	2.43	—
34H-2, 84–85	93.74	2.63	0.40	2.22	—
35H-1, 23–24	94.93	3.05	0.43	2.62	—
36H-1, 18–20	97.88	2.62	0.42	2.20	—
38H-2, 73–74	97.79	2.40	0.39	2.01	—
37S-1, 9–10	99.86	2.48	0.40	2.09	—
48H-1, 69–70	117.39	0.96	0.10	0.87	—
50H-1, 30–31	120.00	1.32	0.17	1.15	—
50H-2, 100–101	122.19	0.95	0.07	0.88	—
51H-1, 21–22	123.21	0.61	0.03	0.58	—
51H-2, 21–22	124.71	0.88	0.06	0.81	—
52H-1, 100–101	127.30	0.65	0.01	0.64	—
53H-1, 90–91	130.50	0.41	0.00	0.41	—
54H-1, 37–38	133.27	1.31	0.54	0.77	—

Table T10 (continued).

Core, section, interval (cm)	Depth (mbsf)	TC (wt%)	TOC (wt%)	TIC (wt%)	TS (wt%)
54H-2, 78–79	135.18	0.57	0.01	0.56	—
55H-1, 21–22	136.41	1.42	0.21	1.21	—
56H-1, 17–18	139.67	0.57	0.01	0.56	—
57H-2, 45–46	143.47	0.88	0.20	0.68	—
57H-1, 67–68	144.75	0.46	0.01	0.46	—
60H-1, 88–89	153.28	2.09	0.60	1.50	—
60H-2, 35–36	153.96	2.08	0.61	1.47	—
61H-1, 2–3	155.42	1.95	0.74	1.21	—
63H-1, 14–15	158.54	1.47	0.55	0.92	—
65H-1, 7–8	159.47	1.52	0.68	0.85	—
65H-2, 44.5–45.5	160.96	1.42	0.59	0.84	0.18
66H-2, 73.5–75	163.54	1.45	0.72	0.72	—
67H-1, 8–9	164.28	1.36	0.56	0.80	—
67H-2, 60–61	165.46	1.67	0.74	0.93	—
68H-2, 70–72	167.94	1.28	0.48	0.81	—
69H-1, 25–26	169.05	1.46	0.70	0.76	—
69H-2, 50–51	170.80	1.27	0.63	0.63	—
70H-1, 99–100	173.09	1.28	0.41	0.87	—
70H-2, 23–24	173.83	1.22	0.47	0.75	—
71H-1, 35–36.5	175.75	1.34	0.42	0.92	—
72H-2, 26–27	179.30	0.90	0.36	0.54	—
72H-3, 24.5–25.5	180.79	1.27	0.55	0.73	—
73H-1, 55–56	182.55	1.50	0.73	0.76	0.17
73H-2, 99–100	184.49	1.28	0.54	0.74	—
75H-1, 80–81	189.40	1.33	0.58	0.74	—
75H-2, 87–88	190.97	0.72	0.31	0.41	—
76H-1, 28–29	192.18	2.94	1.85	1.09	—
76H-2, 28–29	193.68	2.44	1.38	1.06	—
77H-1, 38–39	195.58	1.31	0.57	0.74	—
77H-2, 122–123	197.92	1.33	0.63	0.70	—
82P-1, 53–54	203.03	2.50	1.41	1.09	—
347-M0060B-					
4H-1, 31–32	6.41	0.23	0.17	0.06	0.13
4H-2, 31–32	7.91	0.50	0.50	0.00	0.09

Table T11. Samples taken for cell counts by flow cytometry and acridine orange direct count (AODC), Hole M0060B.

Core, section	Top depth (mbsf)	Cytometer counts (log cells/cm^3)	AODC (log cells/cm^3)
347-M0060B-			
1H-1, 100	1.00	7.22	
1H-2, 108	2.58		7.10
3H-2, 2	4.33	7.84	7.35
4H-2, 2	7.63	8.53	8.58
5H-2, 2	10.93	8.39	8.82
6H-2, 2	14.23	8.51	8.38
7H-2, 2	17.53	8.25	
8H-2, 2	20.83	8.28	
9H-2, 2	24.13	8.39	8.70
10H-2, 2	27.43	8.36	
11H-2, 2	30.73	8.40	
12H-2, 2	34.03	8.56	8.67
13H-2, 2	37.33	8.54	
14H-1, 2	40.63	8.55	
15H-2, 2	43.93	8.59	8.24
16H-2, 2	47.23	8.52	
17H-2, 2	50.53	8.54	
18H-2, 2	53.83	8.65	8.92
19H-2, 2	57.13	8.36	
20H-2, 2	60.43	8.53	
21H-2, 2	63.73	8.61	8.65
22H-2, 2	67.03	8.81	
23H-2, 2	69.53	8.47	
24H-2, 2	72.03	8.63	8.53
25H-2, 2	74.52	8.56	
26H-2, 55	78.36	8.60	
27H-2, 2	81.13	8.37	8.40
28H-2, 2	84.43	8.43	8.22

Respective count data are presented in the last two columns in logarithmic format.

Table T12. Drilling fluid contamination, Hole M0060B. (Continued on next page.)

Core	Depth (mbsf)	PFC (g/L)	LF fraction in sample	Contaminant (cells/cm^3)
347-M0060B-				
Core interior				
1H	1.45	2.91E–06	3.94E+01	3.94E+08
3H	4.20	1.99E–09	2.58E–02	2.58E+05
5H	10.85	BD	BD	BD
6H	14.15	5.41E–10	1.54E–03	1.54E+04
8H	20.75	2.19E–10	3.71E–05	3.71E+02
9H	24.05	BD	BD	BD
10H	27.35	3.10E–09	6.11E–04	6.11E+03
11H	30.65	BD	BD	BD
17H	50.45	5.39E–10	2.36E–04	2.36E+03
19H	57.05	4.80E–09	9.31E–03	9.31E+04
21H	63.65	8.28E–11	6.05E–06	6.05E+01
23H	69.45	3.37E–10	5.84E–06	5.84E+01
25H	74.44	BD	BD	BD
27H	81.05	BD	BD	BD
Core halfway				
1H	1.45	8.85E–06	1.20E+02	1.20E–09
3H	4.20	2.31E–09	3.00E–02	3.00E+05
5H	10.85	1.24E–09	2.04E–02	2.04E+05
6H	14.15	2.25E–09	6.40E–03	6.40E+04
8H	20.75	2.26E–10	3.84E–05	3.84E+02
9H	24.05	3.32E–10	5.83E–07	5.83E+00
10H	27.35	1.67E–08	3.29E–03	3.29E+04
11H	30.65	BD	BD	BD
17H	50.45	6.72E–10	2.94E–04	2.94E+03
19H	57.05	5.59E–09	1.08E–02	1.08E+05
21H	63.65	1.08E–09	7.90E–05	7.90E+02
23H	69.45	3.35E–09	5.80E–05	5.80E+02
25H	74.44	BD	BD	BD
27H	81.05	BD	BD	BD
Core exterior				
1H	1.45	2.72E–07	3.68E–00	3.68E+07
3H	4.20	2.40E–09	3.12E–02	3.12E+05
5H	10.85	3.59E–08	5.92E–01	5.92E+06
6H	14.15	6.57E–08	1.87E–01	1.87E+06
8H	20.75	1.25E–07	2.12E–02	2.12E+05
9H	24.05	6.25E–08	1.10E–04	1.10E+03
10H	27.35	6.86E–08	1.35E–02	1.35E+05
11H	30.65	1.75E–08	6.34E–04	6.34E+03
17H	50.45	5.09E–10	2.23E–04	2.23E+03
19H	57.05	5.05E–09	9.80E–03	9.80E+04
21H	63.65	3.99E–08	2.91E–03	2.91E+04
23H	69.45	1.49E–09	2.58E–05	2.58E+02
25H	74.44	7.94E–10	8.61E–04	8.61E+03
27H	81.05	4.34E–09	1.69E–03	1.69E+04
Liner fluid				
1H	1.45	7.39E–08	NA	NA
3H	4.20	7.69E–08	NA	NA
5H	10.85	6.07E–08	NA	NA
6H	14.15	3.51E–07	NA	NA
8H	20.75	5.89E–06	NA	NA
9H	24.05	5.69E–04	NA	NA
10H	27.35	5.07E–06	NA	NA
11H	30.65	2.76E–05	NA	NA
17H	50.45	2.28E–06	NA	NA
19H	57.05	5.16E–07	NA	NA
21H	63.65	1.37E–05	NA	NA
23H	69.45	5.78E–05	NA	NA
25H	74.44	9.22E–07	NA	NA
27H	81.05	2.56E–06	NA	NA
Drilling fluid				
1H	1.45	1.30E–04	NA	NA
2H	2.80	8.00E–04	NA	NA
3H	4.20	1.01E–04	NA	NA
4H	6.10	1.75E–03	NA	NA
6H	14.15	5.77E–08	NA	NA

Table T12 (continued).

Core	Depth (mbsf)	PFC (g/L)	LF fraction in sample	Contaminant (cells/cm^3)
7H	16.00	4.61E–07	NA	NA
8H	20.75	8.80E–07	NA	NA
10H	27.35	8.17E–07	NA	NA
11H	30.65	1.83E–06	NA	NA
22H	65.50	2.46E–06	NA	NA

The contaminant cell numbers in samples represent an estimated potential maximum. PFC = perfluorocarbon tracer, LF = liner fluid, BD = below detection, NA = not applicable.

Table T13. Composite depth scale, Site M0060.

Core	Offset (m)	Top depth (mbsf)	Top depth (mcd)
347-M0060A-			
3H	0.00	0	0
4H	0.00	3	3
6H	0.00	6	6
8H	0.00	9	9
9H	0.00	13.8	13.8
10H	0.00	15.6	15.6
11H	0.00	18.9	18.9
12H	0.00	22.2	22.2
13H	0.00	25.5	25.5
15H	0.00	30.5	30.5
16H	0.00	33.8	33.8
17H	0.00	37.1	37.1
18H	0.00	40.4	40.4
19H	0.00	43.7	43.7
20H	0.00	47	47
21H	0.00	50.3	50.3
22H	0.00	53.6	53.6
23H	0.00	56.9	56.9
24H	0.00	60.2	60.2
25H	0.00	63.5	63.5
26H	0.00	66.8	66.8
27H	0.00	69.8	69.8
28H	0.00	72.8	72.8
29H	0.00	75.8	75.8
30H	0.00	79.1	79.1
31H	0.00	82.4	82.4
32H	0.00	84.8	84.8
33H	0.00	88.1	88.1
34H	0.00	91.4	91.4
35H	0.00	94.7	94.7
36X	0.00	97.7	97.7
37S	0.00	97.7	97.7
38H	0.00	98.7	98.7
39H	0.00	101.2	101.2
41S	0.00	104.7	104.7
45P	0.00	112.7	112.7
46H	0.00	113.7	113.7
48H	0.00	116.7	116.7
50H	0.00	119.7	119.7
51H	0.00	123	123
52H	0.00	126.3	126.3
53H	0.00	129.6	129.6
54H	0.00	132.9	132.9
55H	0.00	136.2	136.2
56H	0.00	139.5	139.5
57H	0.00	142.8	142.8
58H	0.00	146.1	146.1
59H	0.00	149.4	149.4
60H	0.00	152.4	152.4
61H	0.00	155.4	155.4
63H	0.00	158.4	158.4
65H	0.00	159.4	159.4
66H	0.00	162.4	162.4
67H	0.00	164.2	164.2
68H	0.00	166.3	166.3
69H	0.00	168.8	168.8
70H	0.00	172.1	172.1
71H	0.00	175.4	175.4
72H	0.00	178.7	178.7
73H	0.00	182	182
74H	0.00	185.3	185.3
75H	0.00	188.6	188.6
76H	0.00	191.9	191.9
77H	0.00	195.2	195.2
78S	0.00	198.5	198.5
80S	0.00	199.5	199.5
82P	0.00	203.25	203.25
347-M0060B-			
1H	0.35	0	0.35
2H	0.35	0	0.35
3H	0.84	2.8	3.64
4H	1.09	6.1	7.19
5H	0.87	9.4	10.27
6H	0.31	12.7	13.01
7H	0.70	16	16.70
8H	–0.18	19.3	19.12
9H	–0.52	22.6	22.08
10H	–0.55	25.9	25.35
11H	–0.33	29.2	28.87
12H	–0.42	32.5	32.08
13H	–0.42	35.8	35.38
14H	–0.21	39.1	38.89
15H	–0.45	42.4	41.95
16H	–0.51	45.7	45.19
17H	–0.40	49	48.60
18H	–0.49	52.3	51.81
19H	–1.04	55.6	54.56
20H	–0.84	58.9	58.06
21H	–0.72	62.2	61.48
22H	–0.84	65.5	64.66
23H	–1.02	68	66.98
24H	–0.50	70.5	70.00
25H	–0.74	73	72.26
26H	–0.63	76.3	75.67
27H	–0.82	79.6	78.78
28H	–0.35	82.9	82.55

Table T14. Sound velocity data for lithostratigraphic units, Site M0060.

Unit	Thickness of unit (m)	Sound velocity (m/s)*	TWT (ms)	Depth (m)	Depth (mbsf)
Seafloor	34	1450	0.0468	34.00	0.00
I	6	1663	0.0541	40.00	6.00
II	17.84	1569	0.0768	57.84	23.84
III	55.68	1532	0.1495	113.52	79.52
IV	15.52	1654	0.1683	129.04	95.04
V	21.66	1643	0.1946	150.70	116.70
VI	29.4	1752	0.2282	180.10	146.10
VII	83.4	1789	0.3214	263.50	229.50

* = sound velocities are based on values measured during the OSP. TWT = two-way traveltime.

13. Appendix B Cruise report DAN-IODP-SEIS KAT2013 High Resolution 2D seismic survey i

Cruise report

DAN-IODP-SEIS KAT2013 High Resolution 2D seismic survey

1.1 Introduction

A formalised Geocenter Denmark cooperation has been established between the Geological Suvey of Denmark and Greenland (GEUS), Institut of Geoscience (IG) at the University of Aarhus and Department of Geosciences and Natural Resource Management (IGN).

GEUS, IGN and IG has initiated a 3 years study of the Kattegat region called DAN-IODP-SEIS. It is the aim of the project besides investigating all available archive data to collect new high resolution 2D seismic, sparker and chirp data in a general grid and in detail around the Baltic Sea IODP drill sites planed for the IODP Baltic Sea Expedition 347 - History of the Baltic Sea Basin during the last 130000 years

SGU carries out a long term mapping program of the Swedish waters and planned to carry out survey in the Kattegat Region in 2013.

The planed investigations of the Quaternary sediments of the Kattegat region by both partners have leaded to the interest of joining forces and resulted in the DAN-IODP-SEIS KAT13 High Resolution 2D seismic survey, reported in this cruise report.

The cruise was carried out in the summer 2013 (12. Juni – 14. July) on board the SGU survey ship Ocean Surveyor. The expenses of the ship time was covered partly by the funding that is provided by the Danish Centre for Marine Research (DCH) and partly by the SGU mapping program.

The Ocean Surveyor standard equipment includes 10 inch sleevegun and SIG 6-channel streamer, Edo Western sediment echosounder, Benthos 1624 and Klein 3000 side scan sonars and Kongsberg EM2040 multibeam echosounder. In addition GEUS, IGN and IG provided high resolution 2D airgun and sparker energy sources and a multichannel streamer. The purpose was to collect airgun seismic data down to maximum 1.5 sec., sparker seismics down to 0.5 sec. as well as an Innomar medium parametric sediment echo sounder, in order to collect very high resolution data down to maximum 100 ms.

The survey was at all times manned by the Ocean Surveyor crew and SGU personnel as well as scientists from GEUS, IGN and IG.

Planning of the seismic grid was done in full cooperation between the partners, starting with a general regional grid, followed by detailed studies distributed evenly between Danish and Swedish waters.

Preliminary processing was performed on-board Ocean Surveyor while the final processing will be performed in Aarhus with IG as the responsible partner, but in cooperation with SGU and the other partners.

The data collected under the umbrella of this cooperation will be available for all partners and joint mapping publications will be carried out as example.

- Prequaternary surface map
- Lateglacial basin thickness and distribution
- Glacial tectonic zones and stratigraphy
- Distribution of Eemian and interstadial basins

1.2 Objectives and scope

It is the aim of this Kattegat cooperation to exploit the unique Baltic Sea IODP drilling campaign in 2013 to gain detailed spatial knowledge of the deeper Kattegat Quaternary basins through the last interglacial – glacial cycle (late Saalian to present) by combining new regional 2D seismic mapping with borehole studies.
The distribution of Eemian Sea deposits and optimisation of the finding of complete Quaternary time series are vital geological questions that needs to be investigated in the Danish and Swedish waters. Complex glacial advances - with highly oscillating ice margins-, marine and glacial lake deposits and not least the drainage of the Baltic Ice Lake and the impact onto the local and regional environment is poorly understood. A number of research questions still need to be answered: Was the Eemian climate really more unstable than that of the Holocene? Was the drainage of the Baltic Ice Lake catastrophic or gradual and did the flow change in time and space,? Is it possible to correlate the major changes in sedimentation regionally? In order to describe the Quaternary geological and climatic development in general and to answer the above questions it is required to obtain an understanding of the 3 dimensional evolution of the Quaternary deposits, which were deposited in the Kattegat area and to relate it to the palaeo-climatic and sedimentological information, which will be obtained by means of the IODP borehole scheduled for 2013.
Therefore it is objective to gather all available existing seismic data (conventional 2D, high resolution 2D Sparker and Boomer data) and map the evolution of the deposits in time and space. It is furthermore our intention to perform an infill data collection survey including high resolution 2D seismic, sparker and chirp data in a general grid and around the drill sites in Kattegat. The infill data will give an unprecedented dataset with all scales of resolution which will optimize both the 3 dimensional analyses and the scientific outcome of the IODP boreholes. The data from this seismic study will be compared with the sedimentary and climatic/environmental record from the IODP boreholes as well as other existing cores in the region. In addition linkage to large-scale climatic and oceanographic changes in the North Atlantic region will be tested.
The joint transnational cooperation will give the possibilities to make a seamless mapping of the Kattegat region covering the last interglacial – glacial cycle and to optimise the marine mapping resources of Denmark and Sweden. Besides the mapping results the project is a unique chance to exchange scientific knowledge on high resolution

multichannel seismic acquisition and processing as well as seismic interpretation and geological development history of the quaternary sediments in the Kattegat region..

1.3 Scientific context

Deep-sea records, ice-cores, and numerical modelling are the traditional tools to show that the North Atlantic Ocean circulation plays an important role in the global climate system that affects North America and Europe in particular.
The Baltic Sea is a scarce example of long high-resolution marine records that are possible alternatives to show continental response to the oceanic forcing.
It is the largest European intercontinental basin, and contains a possible sediment archive for past and present climate. High sedimentation rates (1-5 m/1000 years) provides an excellent opportunity to reconstruct climatic variability of global importance, controlled by e.g. changes in the NADW formation, the North Atlantic Oscillation (NAO) and the Arctic Oscillation (AO) in great detail (up to interannual time-scale). This is unique, and comparable sequences cannot be retrieved anywhere in the surrounding onshore regions.
The Baltic Sea Basin development history during the last glacial cycle is very complex and must be regarded as most complete in the westernmost Danish basins, located in the marginal zone of the Scandinavian Ice sheet.
A complete series of the last interglacial Eemian Sea has not been recovered in situ in any part of the Baltic Sea, where only thin and incomplete marine Eemian sediment sequences has been found, such as a dislocated coast cliff in the western Baltic (e.g. Kristensen & Knudsen, 2006; Gibbard & Glaister, 2006), but Kattegat and Lillebælt are good candidates for better time series.
Glacial advances are numerous and the preservation potential must be highest in the basin areas such as the first Weichselian Baltic ice lobe advance into Denmark dated to 50-55 kyr BP (Houmark-Nielsen, 2007). The glacial period was also characterised by glacial lakes as covered large parts of the Baltic Sea filled in with sediments during > 50 kyrs, and any accumulated sediments most likely registered climate-related changes with a very high resolution. The complex Danish glacial stratigraphy indicates a highly oscillating ice margin, partly free of ice at several occasions prior to Last Glacial Maximum (LGM) at c. 20 kyr BP, when the Weichselian ice sheet covered the entire Baltic Sea (Houmark-Nielsen & Kjær, 2003).
The deglaciation of the southern Baltic Sea between 22-16 kyr BP was very complex, with major deglacial phases interrupted by some intriguing still-stands and even re-advances (Houmark-Nielsen & Kjær, 2003). The Baltic Ice Lake dammed in front of the retreating ice front, released huge amounts of freshwater into the North Atlantic during the early stage of the deglaciation between c. 16 and 11.5 kyr BP. Previous investigations indicate that the drainage occurred both through the Öresund straight and via south central Sweden (Gyldenholm et al., 1993; Björck, 1995; Majoram & Nordberg, 1997; Jiang et al., 1998), but physical identification of the Öresund drainage is still to be proven.
Late Weichselian reactivation of faulting in the south central Kattegat was caused by fast isostatic rebound (Jensen et al., 2002), which may imply that drainage of the Baltic Ice Lake have been triggered by neo-tectonic activity in the region.
During the final drainage of the Baltic Ice Lake at c. 11.6 kyr BP, almost 8,000 km^3 of freshwater was released rapidly into the North Atlantic (Jakobsson et al., 2007), but the

effects on the North Atlantic thermohaline circulation may only have been minor (Andrén et al., 2002), but it has also been suggested that it may have triggered the Preboreal oscillation (Björck et al., 1996) and ice advances in N Norway (Hald & Hagen, 1998).
In the Kattegat region a late Weichselian sea-level highstand, was followed by forced regression until the Younger Dryas–Preboreal transition, when the relative sea level began to rise because the eustatic sea level rise surpassed the isostatic rise of the crust (e.g. Mörner 1969, Bennike et al. 2000). In the Kattegat IODP site area, a continuous Holocene transgression indicates the possibility of a complete sediment record with a maximum thickness of several tens of meters, dependent of local basin movements and changes in the current system.

In the light of the described complexity of the IODP sites in the Danish region it is even more appropriate to state that boreholes and associated local site surveys are one-dimensional data points.
Detailed seismic interpretation of existing scientific and commercial data will optimise the final site selection and will offer a general 3 dimensional understanding of the last interglacial – glacial cycle in the Danish IODP site regions.

1.4 Primary goals of the cruise

The seismic support will secure the optimal information on the distribution of Eemian Sea deposits and the possibilities of finding a complete time series.
The complexity of glacial advances with highly oscillating ice margins as well as marine and glacial lake deposits makes it a speculative task to establish a trustful glacial stratigraphy and to make detailed climate-related conclusions on the lake deposits. It is the aim of the seismic cruise to produce data that will be able to show the architecture of the glacial deposits and any possible glacial or structural disturbances as well as detailed information on the depositional sedimentation composition.
The final drainage of The Baltic Sea is an important part of the Baltic IODP project with the aim in details to describe the timing, location and volumes of the event in order to link it to the changes in the North Atlantic circulation system. Again seismic information is crucial to be able to evaluate the timing of the episodic event and its possible drainage pathways as well as the sedimentological evolution of possible channel, deltaic or basin infill. Special focus on glacio isostatic rebound reactivation of the Fennoscandian Border Zone fault system is a possible key to the understanding of the drainage.
In the Kattegat IODP site area a continuous Holocene transgression indicates the possibility of a complete sediment record with a maximum thickness of several tens of meters, dependent of local basin movements and changes in the current system. Recent high resolution seismic studies in the Bornholm Basin shows that it is possible acoustically to divide the Holocene marine deposits in subunits related to climate-related changes in sedimentation rates and local bottom current systems. The combination of detailed sediment startigraphy and seismic facies interpretation will optimise the evaluation of possible links to the North Atlantic circulation system.
Detailed high resolution 2D surveys are necessary infill in areas with no existing data as well as for focussing on details in seismic facies analyses on basin depositional sedimentation composition and syn-sedimentary neo-tectonic basin movements. This is needed for detailed- local architecture, drainage patterns and linkage in time, volume and effect.

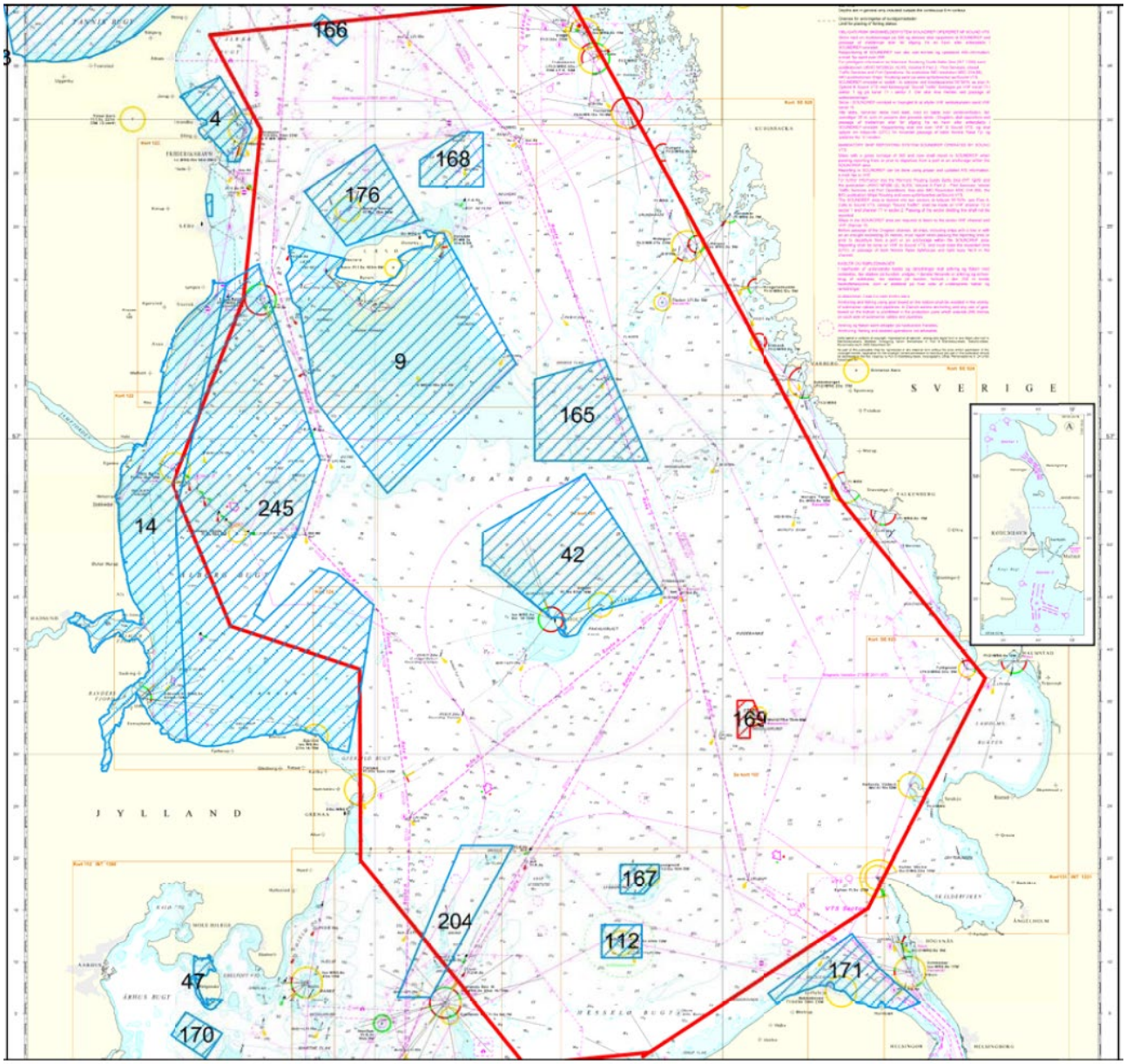

Planed survey area inside the heavy red frame and blue numbered areas are Natura 2000 protection areas. Area 169 St. Middelgrund Natura 2000 area is marked as red.

1.5 Agenda

Date	Approx. board Time (UTC)	Programme and event	Weather

11-06-2013	11:30	Ocean surveyor arrival Århus Harbour	
12-06-2013	08:00 – 22:00	Start MOB airgun equipment, Innomar and sparker. Innomar transducer mounted.	
13-06-2013	08:00 – 15:00 15:00 : 22:00	MOB continued. Sparker problems tricker computers and software testet. Minisymposium at University of Århus all partners GEUS, IG, IGN, SGU represented and continued MOB.	
14-06-2013	08:00 – 22:00	Continued instalation of equipment with focus on airgun birds and tricking problems. First possible transit next morning, due to weather.	Much wind
15-06-2013	08:00 – 17:00 17:00 -	Departure from Århus Harbour 08:00. Deployment of streamer with test of birds and start of of test survey, with airgun and sparker acquisition as well as Innomar sedimentechosounder and multibeam. Powerfull wind and rain shelter in Grenå Havn.	5 – 8m/s 12 – 13m/s
16-06-2013	08:00 – 22:00	Heavy wind improvements of setup of equipment and collection of new tricker box.	12 – 14m/s
17_06-2013	08:00 14:30 16:30 20:00	Departure Grenå ajustment of airgun position in water, tricker problems. SOL KAT 13_0009 reduced setup without sparker. Sparker included. SOL Kat13_0008 south	5 – 8m/s
18-06-2013	03:32 18:30	SOL Kat13_0007 Worked on line 7 all dai through the IODP coring area SOL kat13_0008 north	3 – 5m/s
19-06-2013	01:00	Eol Kat_0008 and transit to Århus	3 – 5m/s

20_06-2013 24-06-2013		Ocean Surveyor in Århus Harbour Sweedish mid summer holliday. Streamer winch enlarged diameter.	
25-06-2013	11:00 16:00 21:30 23:30	Crew arrival Ocean Surveyor Sparkerv tricker problems possibly solved Departure transit to line Kat13_0006 Streamer in the water shows leachage. Streamer repair. Sparker and airgun in the water but weather getting very windy. Transit to Hundested Harbour	5 – 8m/s 12 – 13m/s
26-06-2013	04:30 09:30	Arrival Issefjorden ancoring. Arrival Hundested Harbour	10 – 13m/s NW
27-06-2013	07:00 10:00	Departure SOL Kat13_0001. Survey vith only minor problems with generator oil filter the rest of the day. SOL Kat13_0002	5 – 8m/s
28_06_2013	12:30	Generator problems cleaning of oil filter. Survey Kat13_0003 and SOL Kat13_0004	8 -10m/s 10 - 12m/s
29-06-2013	05:50 07:00 17:00	EOL kat13_0004 SOL Kat13_0005 Wind increasing stop survey and transit to Halmstad. Arrival Halmstad	12m/s 10m/s 12m/s
30-06-2013	08:00 – 22:00 23:00	In Halmstad Harbour due to rough weather Repair of compressor data backup. Departure for survey	> 12m/s
01-07-2013	02:30 03:00 05:00 12:00	Arrival survey area St. Middelgrund still some old swells SOL Kat13_5008, 5007, 5006, 5005, 5003, 5002. Generator problems during the night. New oil filter	5m/s

	12:30 -15:00 15:00 17:30 17:45 18:20 22:00	installed. St. Middelgrund finished. SOL Anholt detailed line Kat13_8006 EOL SOL Kat13_0005a Stop survey. Streamer was cut during retrieave and rescue was performed. We succeded to save the streamer. Arrival Varberg Harbour	8m/s
02-07-2013	08:00 12:00 13:00 - 17:00 18:00	Streamer unroaled on the kay and checked Found ok and put back on the winch. Crue schift. Error check and atempt to repair on compressor. Kongsberg Multibeam specialists arrived for repair of multibeam. Divers must be involved to solv the multibeam problem so we continue with one multibeam channel. The weather had imprioved and we left harbour 23:00 against line kat 13_0006.	
03-07-2013	01:00 15:00 21:00	Start survey on line kat13_0006 and arrived at the end close to Sjællands Odde. Less wind than expectet so we continued transit to line kat13_0014 SOL 21:00. Continued survey	10-12m/s 5m/s
04-07-2013	07:00 07:00 21:30 22:00	EOL kat13_0014 SOL kat13_0012 and change of oilfilter on airgun generator EOL kat13_0012 SOL kat13_0011	 0-5m/s
05-07-2013	 07:00 16:30 16:30 19:30	Continue on line kat13_0011 SOL kat13_0016 EOL kat13_0016 SOL kat13_0010 Havd to stop survey due to	5m/s

	21:30	1,5m swells At Varberg Harbour	
06-07_2013	09:00 13:00 16:00	Left Varberg harbour Continued survey on line kat13_0016 Airgun cable broken stop for repair and ships generator had problems. We agreed to continue and go to harbour the day after. Restart of survey on line kat13_8002 and kat13_8003.	
07-07-2013	01:30 06:00 13:00 17:00 19:00 19:30 23:00 -	SOL kat13_8005 nice weather Stop of survey and transit to Varberg for ships generator repair. Repair finished and takeoff from Varberg SOL kat13_8004 EOL kat13_8004 Airgun cable broken again and repaire necessary. During repair of airgun streamer came to close to the sparker source and the streamer was damaged by the sparker pulse. Search for streamer failor and repair was very extensive. Line kat13_8007 was surveyed only with Innomar sedimente chosounder.	2-5m/s
08-07-2012	- 02:00 03:00 06:00 09:30 11:00	Streamer temporary repaired (one section not responding) SOL kat13_8008 EOL kat13_8008 SOL kat13_2005 Survey stoppet in the middle of the line Because Ocean Surveyor had to be in Varberg at noon. Crusing back to Varberg Ocean Surveyor had an	5m/s

	13:30	engin damage and we had to go with reduced speed. Arrived at Varberg Harbour Streamer fully repaired during the afternoon. Seismic equipment ready again. The weather has been calm and sunny all day	0 – 5m/s
09-07-2012		A day in Varberg harbour Ships crue was exchanged and repair of engin started from the morning, but a lot had to be done. Nice weater all day	5m/s
10-07-2012			

Map with survey lines

1.6 Participants

1.7 Survey ship

Ocean surveyor

Ocean Surveyor

1.8 Scientific Equipment

1.8.1 Institute for Geoscience Aarhus University

Streamer and Airgun system:

I. **Instrumentation on deck**

- Hydraulic streamer winch
  Dimensions : 244 x 299 x 170 cm
  Weight : 5000 Kg.
  Power consumption : 3 x 380 V, 15 kW (32 Amp. plugs)

- Description of Multi-channel streamer:
  Type: Geomerics GeoEel
  Length of tow section (m): 60,5
  Length of live section (m): 525
  No. of live section: 13
  No. of channels: 104
  No. of AD modules : 12
  No. of channels/live section: 8
  Channel interval (m): 3,125 and 6,25
  No. of hydrophones/channel: 4 and 8
  Hydrophone type Benthos Geopoint
  Planned depth (m): 1,5
  Vib/Stretch section: S1070

5 Digicourse depth controllers ("birds"): type 5010, S/N 14610, 14514, 14510,14497 and 26567. At ch 1, 24, 40, 80 and 104

Seismic compressor container

Dimensions : Standard 20 ft container with two compressors
Weight : 12000 Kg.
Power consumption : 3 x 380 V 50 Hz, 100 kW.
Air delivery : 5000 l/min @ 200 bar
Only one compressor used, the other is a spare.

Power generator

Dimensions : 390 x 120 x 190 cm
Weight : 3000 kg
Power unit for the compressors. Total capacity of generator is 200 Kwatt
.

- Air guns

GI gun

GI-Gun, with Generator chamber of 75 cubic inch and Injector of 75 cubic inch
Dimensions : 80 x 35 x 35 cm
Weight : 100 kg
Injector delay: 47mS
Discharge port: 603_120. Medium
Delay: 500ms
Pressure (bar): 120
Planned depth (m): 4
Air consumption : 5000 L/min

- Umbilical winch

Dimensions : 110 x 120 x 100 cm
Weight : 300 kg
Hand driven

Description :
80 m bundles of hoses for compressed air, trigger cables, timing cables

II. **Instrumentation in recording room**

- Recording units

Geometrics GeoEel system, SPSU with 4 AUX ch,
Dimensions: 40 x 30 x 30 cm
Weight : 5 kg.
Power consumption : 60 VDC, 1.4 A (Powered from an external power supply)

- Acquisition control unit (PC)

Geometrics software program CNT-2
Dimensions: 20 x 25 x 8 cm
Weight : 2 kg

Power consumption : 12 V Dc, 5 amp
With two external HD of 1 Tbyte each (eSATA)

- GI gun triggering unit

Macha TGS-8
Dimensions : 49 x 60 x 52 cm
Weight : 20kg
Power consumption : 220 VAC, 200 Watt

- Digicourse Birds Control and Interface

Dimensions : 49 x 60 x 52 cm
Weight : 20 kg
Power consumption : 220 V 500 W

1.8.2 Geological survey of Denmark and Greenland (GEUS):

Sparker system:

Geo-source 800 deep water multi-tip sparker system

Marine Multi-Tip Sparker System
- VHR marine seismic source
- Water depths from 2 to 2500 m
- Penetration to 400 ms below seabed
- Vertical resolution up to 30 cm

Equipment description Geo-source 800

Geo-Spark 6 kJ Power Supply

Solid State Pulsed Power Supplies

- Up to 6000 Joules real power
- No electrical oscillations
- Selectable capacitance
- Online variable voltage

Equipment description Geo-Spark 6 kJ .

SES-2000 medium Parametric Sub-bottom Profiler:

Main Technical Parameters

Primary frequency (PHF) about 100 kHz (range 90 – 115 kHz)

PHF source level >246 dB//µPa re 1m

Secondary low frequencies (SLF) 4, 5, 6, 8,10,12, 15 kHz (centre frequency, user selectable)

SLF pulse width 0.07 – 2 ms (user selectable)

SLF pulse type Ricker, CW, LFM (chirp)

SLF bandwidth 2 – 22 kHz

Beam width (-3dB) about ±1° for all frequencies (footprint <3.5% of water depth)

Water depth range 2 – 2,000 m

Sediment penetration up to 70 m (depending on sediment type and noise)

Layer resolution up to 5 cm

Pulse rate up to 30 pings/s (multi ping, burst ping available)

Heave / Roll / Pitch compensation yes / yes (30°) / option (25°)

Data acquisition 24 bit / 96kHz full waveform data

External sensor interfaces HRP sensor, GPS, Depth

Bottom detection internal (HF and LF data) or external depth

Power supply 100-240 V AC / 50-60 Hz

Power consumption <900 W (fuse 16A/slow)

Hardware

Transceiver Units (mobile installation)

For mobile installations the transceiver unit can be delivered split

into two units:

Dimensions (L×W×H) 52 cm × 42 cm × 57 cm

Housing 19 inch / 12U

Weight about 57 kg

Dimensions (L×W×H) 52 cm × 53 cm × 21 cm

Housing 19 inch / 4U

Weight about 29 kg

Transducer (pole-mounted)

Dimensions (L×W×H) 55 cm × 50 cm × 12 cm

Weight in air about 80 kg (incl. 30m cable)

1.8.3 Block diagram of the airgun/sparker set-up, see next page

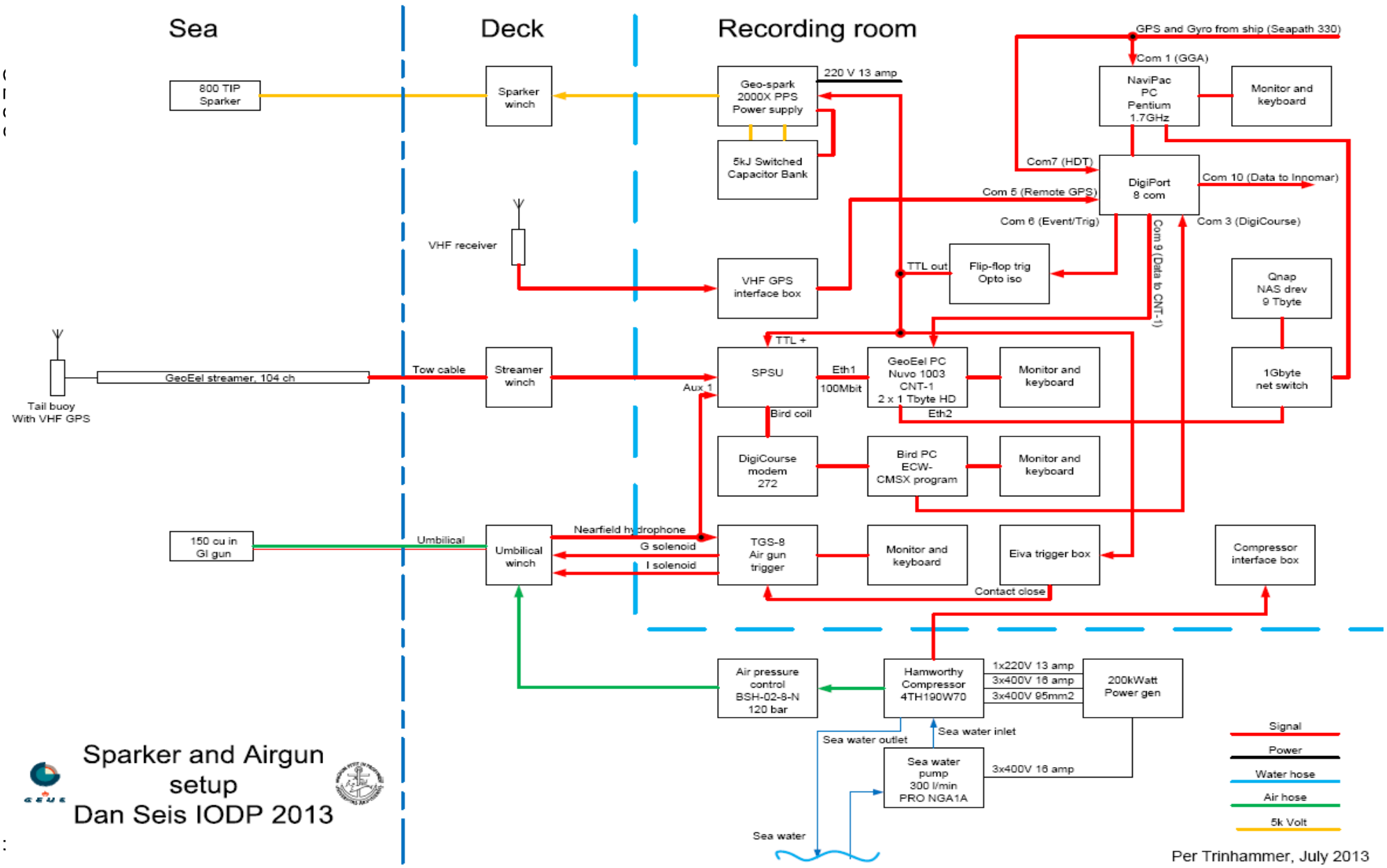
Sea
Deck
Recording room
800 TIP Sparker
Sparker winch
Geo-spark 2000X PPS Power supply
220 V 13 amp
5kJ Switched Capacitor Bank
GPS and Gyro from ship (Seapath 330)
Com 1 (GGA)
NaviPac PC Pentium 1.7GHz
Monitor and keyboard
Com7 (HDT)
DigiPort 8 com
Com 10 (Data to Inpomar)
Com 5 (Remote GPS)
Com 6 (Event/Trig)
Com 3 (DigiCourse)
Com 9 (Data to CNT-1)
VHF receiver
VHF GPS interface box
TTL out
Flip-flop trig Opto iso
Qnap NAS drev 9 Tbyte
TTL +
Tail buoy With VHF GPS
GeoEel streamer, 104 ch
Tow cable
Streamer winch
SPSU
Eth1
100Mbit
GeoEel PC Nuvo 1003 CNT-1 2 x 1 Tbyte HD
Monitor and keyboard
1Gbyte net switch
Aux 1
Bird coil
Eth2
DigiCourse modem 272
Bird PC ECW-CMSX program
Monitor and keyboard
150 cu in GI gun
Umbilical
Umbilical winch
Nearfield hydrophone
G solenoid
I solenoid
TGS-8 Air gun trigger
Monitor and keyboard
Eiva trigger box
Contact close
Compressor interface box
Air pressure control BSH-02-8-N 120 bar
Hamworthy Compressor 4TH190W70
1x220V 13 amp
3x400V 16 amp
3x400V 95mm2
200kWatt Power gen
Sea water outlet
Sea water inlet
Sea water pump 300 l/min PRO NGA1A
3x400V 16 amp
Sea water
Signal
Power
Water hose
Air hose
5k Volt
Sparker and Airgun setup
Dan Seis IODP 2013
Per Trinhammer, July 2013

1.8.4 Geological survey of Sweden (SGU)

Multibeam Kongsberg EM2040D:

Sediment echosounder Edo Western

Navigational system Sepath 330 RTK GPS-receiver

Navipac survey software on PC

1.9 Preliminary results

Survey grid, seismic examples airgun, sparker, innomar

1.10 Marine mammal observations

2. Appendix I Ocean Surveyor

2.1 Undersökningsfartyg av katamarantyp

S/V Ocean Surveyor är en katamaran byggd i glasfiber och kevlar-armerad plast. Hon är konstruerad för bottenundersökning i kustområden.

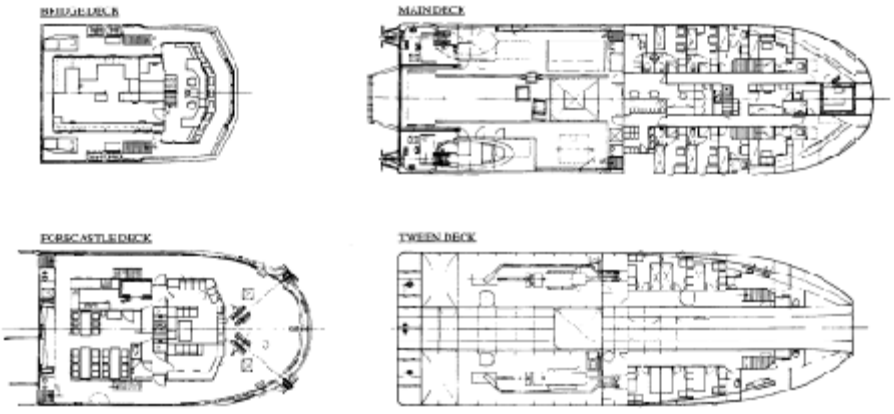

2.2 Specifikationer:

- Klass enligt Det Norske Veritas A1-E0 och svenska Sjöfartsverkets normer.
- Byggd av Båtservice Verft A/S Norge 1984 och modifierad av Egeröy Slipp 1991
- Svenskflaggad

2.3 Huvuddimensioner:

- Längd 38,0 m

- Största bredd 12,0 m
- Djupgående 3,4 m
- Bruttotonage 514 brt

2.4 Tankkapacitet:

- Diesel 95 m^3
- Färskvatten 19 m^3

2.5 Förbrukning:

- 250 l/h vid 10,5 knop
- 185 l/h vid 9 knop

2.6 Maskin och framdrivning:

- Två GM Detroit 12V-149 N 750AHK
- Två reverserbara propellrar Schaffran för tyst gång
- Två förliga tvärpropellrar Brunwoll 250 hkr
- Två aktra tvärpropellrar Brunwoll 150 hkr.
- Dubbla roder

2.7 Hjälpmaskineri:

- 2 GM Detriot 6-71 N med Stamford MC 334 C-generatorer, totalt 340 kVA-256 kW-60 hz-3 faser
- 1 Cummins hamngenerator 42 kVA-35,2 kW
- Omformare 440 V-220 V, 220 VAC-24 VDC
- UPS-stabilicerad strömförsörjning 220 V-50 hz-10 kVA

2.8 Däcksutrustning

- Moonpool 3,4 x 3,6 m
- A-ram 5 t. Räckvidd 5,5 m förut 3,5 m akterut
- Däckskran Tico 20 t/m. Räckvidd 7 m utanför bb sida.
- Sonarvinch med 12-kanalig slipring 1 t, max 150 m/min med fjärrkontroll från instrumentrum
- 8 t vinch med 12-kanals slipring
- 5 t geoteknisk frifallsvinch
- Bom över moonpool med 2 t vinchar, en med 12-kanals slipring
- 4-punkts ankring med 400 m wire

2.9 Inredning:

- Luftkonditionerad inredning enligt följande:
- 4 enkel- och 10 dubbel-hytter, varav 8 med egen toalett och dusch. 1 sjukhytt.
- Våtlabb. (20 m^2), torrlabb. (7 m2), tvättstuga, frysrum, torrförråd och omklädningsrum på huvuddäck
- Mäss, pentry, kylrum, kontor och dagrum på backdäck
- Instrumentrum (50 m^2)och radiohytt i anslutning till kommandobrygga

2.10 Räddningsutrustning:

- 4 st 16-mans livflottar
- 25 överlevnadsdräkter
- 1 pickupbåt i aluminium och 1 arbets/transportbåt med 225 hkr dieselmotor

2.11 Kommunikationsutrustning:

- Enligt SOLAS GMDSS area A 2 samt mobiltelefoner NMT och fax

2.12 Navigationsutrustning:

- 2 Sperry Rascar radar med ARPA 3 cm och 10 cm
- 1 SKR-82 gyrokompass
- 1 2-axlig dopplerlogg
- 2 DGPS satellit-navigatorer
- 1 HPR 309

2.13 Dynamisk positionering:

1 Albatross dynamisk positionering ADP-100 som står i direktkontakt med Qubit Trac V survey-dator

3. Appendix II Konsekvensvurdering af seismisk støj på havpattedyr

I forbindelse med ansøgning om sejlads i Kattegat området i perioden 11. Juni til 15. juli 2013 vil vi gerne præsentere følgende konsekvensvurdering:

• I overensstemmelse med Marine Strategy Framework Directive (MSFD) krav til "god miljøtilstand" Hvorved forstås at: ... menneskeskabte tilførsler af stoffer og energi, herunder støj, i havmiljøet ikke må skabe forurenende virkninger ", Har vi udført et litteratur-studie for at finde en standard for brug af seismiske udstyr i kortlægning og kunne ikke finde noget, der refererer til en dansk standard for mindskelse af seismisk genereret støj for pattedyr.

• Derfor kontaktede vi eksperter i pattedyrs adfærd og vi fik forklaret, at der ikke er nogen retningslinjer for støj grænseværdier for marine pattedyr i Danmark Der er ligeledes ikke danske standarder for brug af marint seismiske udstyr til opmåling, selv om der er afleveret et baggrunds dokument til EU-MSFD, baseret på den seneste rapport fra ICES (M.L. Tasker et al. 2010).

• Den bedste tilgængelige publikation om virkningen af støj på marine pattedyr er skrevet af Southall et al. 2007 " Marine Mammal Noise Exposure Criteria ", hvor målinger af skadepåvirknings kriterier for marine pattedyr er præsenteret. Men der er ingen direkte målinger af seismiske udstyr og deres virkning på forskellige typer af marine pattedyr.

• En anden artikel er offentliggjort i 2010 af Di Lorio og Clark, som drøfter virkningen af et sparker system på blåhvaler, og det afslører en stigning i antallet af hvalopkald når sparkeren skyder.

• En grundig undersøgelse blev foretaget af en forsker fra TNO for at vurdere arten af menneskeskabt støj i Nordsøen i 2009, men igen er der ingen direkte målinger præsenteret, der viser effekten af forskellige seismiske udstyr på pattedyr.

• Den Britiske Joint National Conservation Committee JNCC har i april 2004 offentliggjort en "Vejledning om minimering af akustik forstyrrelse af Havpattedyr fra seismi-ske Surveys. Deres retningslinje, (JNCC procedure) gælder for brug af Air Gun-systemer, medens der ikke er nogen specifik omtale af sparker udstyr, som ligeledes anvendes i vores undersøgelse.

• I Danmark Har DMU igennem længere tid foretaget satellitsporing af marsvin, hvilket har vist sig at være et godt redskab til at studere hvilke områder dyrene benytter, deres migrationsruter og deres adfærd.

Af DMU's hjemmeside

http://www2.dmu.dk/1_om_dmu/2_afdelinger/3_am/4_expertise/5_research/6_Marine_Mammals/Harbourporpoise.asp

fremgår det at:
Det har vist sig at fire ud af fem voksne mærkede hunner, alle foretrak de kystnære områder langs Sjællands kyster fra Helsingør til Korsør. Fælles for de fire mor/unge par var at de alle blev mærket i Storebælt. Vi ved ikke hvorfor vi for det meste har haft voksne hunner fra dette område. Selvom der bliver set hunner med unger i andre områder, kunne det tænkes at området fra Helsingør til Korsør er særlig vigtigt for hunner med unger.
De fire voksne hanner vi har mærket har opholdt sig i flere forskellige områder men et fælles træk er at de ikke har lavet særlig lange vandringer.
Vi har mærket flest af de unge dyr som endnu ikke er kønsmodne. Derfor ved vi nu at disse dyr kan strejfe langt omkring men at de ofte vender tilbage til det område de blev mærket i.
Ingen af de marsvin vi har mærket ved Skagen er svømmet syd for Anholt. Man kunne derfor forestille sig at disse dyr tilhører en bestand der ikke synes om det ferskere vand i de indre farvande. Denne foreløbige hypotese kan have stor betydning når man skal lave optællinger for at få et overblik over hvor godt de enkelte bestande har det.

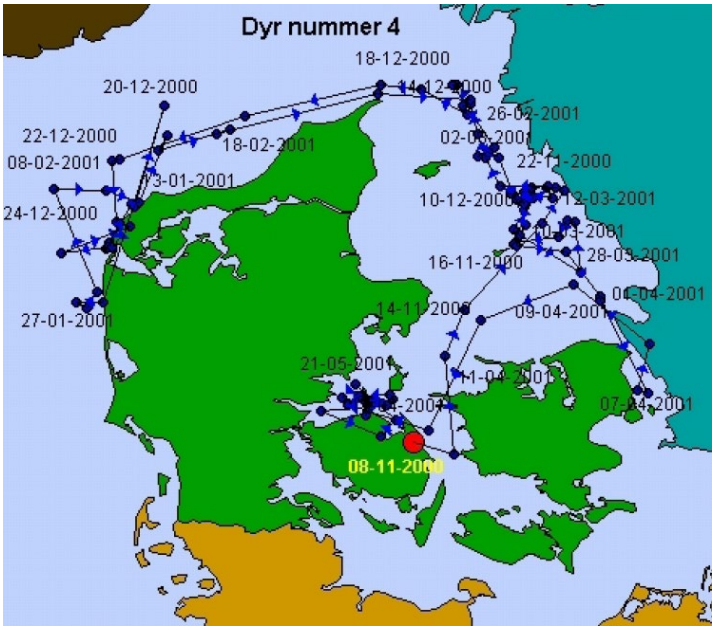

Kortet viser marsvin nummer 4's vandringer. Marsvinet blev mærket ved Kerteminde den 8. november 2000. De små pile på stregerne mellem prikkerne vi-ser den retning marsvinet er vandret

• Signe Sveegaard har på Århus Universitet netop afsluttet Phd med kortlægning af Marsvin i de danske farvande og publiceret (Signe Sveegaard et al. 2011) resultaterne i Marine Mammal science.
Nedenstående kort viser fordelingen af marsvin dels i skagerrak og i de indre farvande årstidsopdelt.

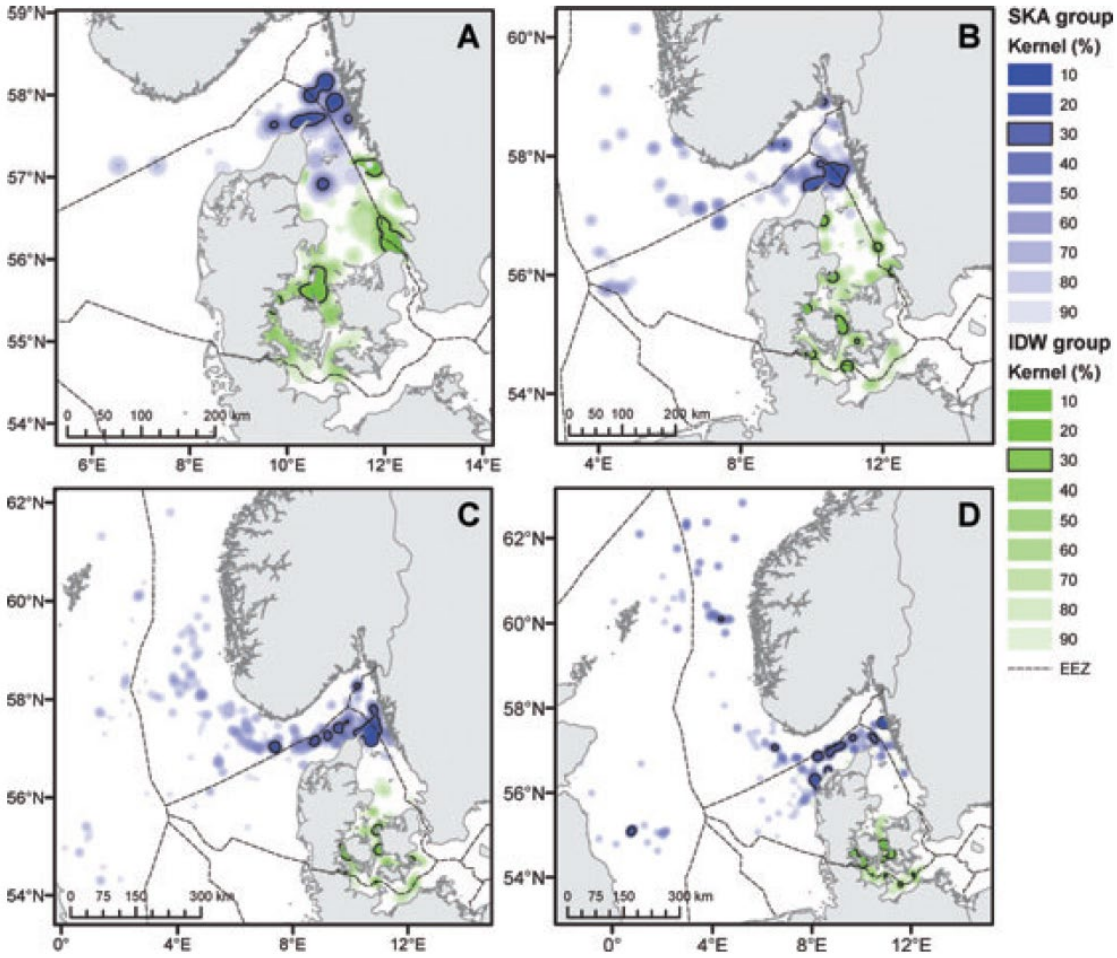

Figure 5. Seasonal distribution for harbor porpoises *Phocoena phocoena* tagged in the Inner Danish Waters (IDW) population (green) and in Skagerrak (blue) displayed by fixed kernel density estimations based on one location every four days from each other. Black line indicates high-density areas defined as the 30% kernel contour. (A) spring (IDW: $N = 29$, $n = 268$; Skagerrak: $N = 12$, $n = 103$), (B) summer (IDW: $N = 27$, $n = 353$; Skagerrak: $N = 18$, $n = 155$), (C) autumn (IDW: $N = 17$, $n = 210$; Skagerrak: $N = 19$, $n = 250$) and (D) winter (IDW: $N = 8$, $n = 119$; Skagerrak: $N = 12$, $n = 157$). Projections as in Figure 2. Dashed line indicates international Exclusive Economic Zones (EEZ). Kernel layers are placed below the land layer.

Figur B viser fordelingen i sommerperioden med klare maksimum ved Skagens Rev, Store Middelgrund, i Storebælt regionen, Femer Bælt samt ved Flensborg Fjord.

Habitatområdernes udpegningsgrundlag I undersøgelsesområdet 31/12 2012

Med hensyn til marine pattedyr

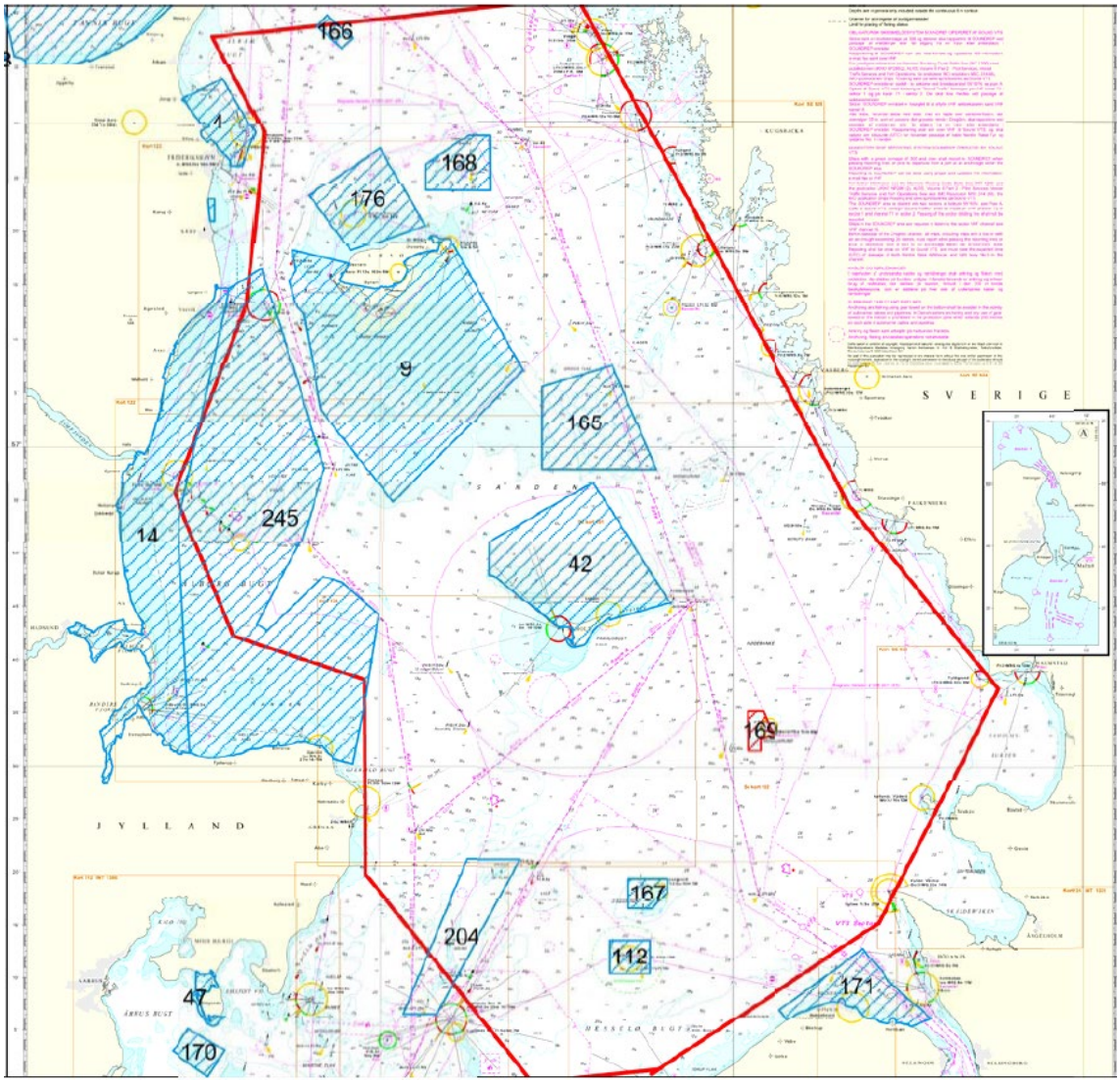

Kortet viser undersøgelsesområdet omkranset af røde polygon. Natura 2000 områder angivet med blå skråskravering undtagen St. Middelgrund som er rød skråskraveret.

9 Strandenge på Læsø og havet syd
1364 Gråsæl (Halichoerus grypus)
1365 Spættet sæl (Phoca vitulina)

42 Anholt og havet nord for
1364 Gråsæl (Halichoerus grypus)

1365 Spættet sæl (Phoca vitulina)

112 Hesselø med omliggende stenrev
1364 Gråsæl (Halichoerus grypus)
1365 Spættet sæl (Phoca vitulina)

165 Kims Top og den Kinesiske Mur

166 Herthas Flak

167 Lysegrund

168 Læsø Trindel og Tønneberg banke

169 Store Middelgrund
1351 Marsvin (Phocoena phocoena)

176 Havet omkring Nordre Rønner
1364 Gråsæl (Halichoerus grypus)
1365 Spættet sæl (Phoca vitulina)

204 Schultz og Hastens Grund samt Brise

245 Kyndby Kyst

Gennemgangen af habitatområderne viser at man generelt skal passe på Gråsæl og Spættet sæl, medens der kun er Marsvin udpegningsgrundlag på Store Middelgrund.

konklusion:

Undersøgelserne i danske farvande viser at marsvin kan findes over alt i det planlagte undersøgelsesområde. Hvilket betyder at man er nødt til generelt at tage hensyn ved udførelsen af de seismiske undersøgelser. Dog bør der udvises ekstra forsigtighed ved Skagens Rev, Store Middelgrund og nordlige Storebælt region.

I mangel af en certificeret national standard og protokol for hvad støj forårsaget af seismiske undersøgelser kan betyde for havpattedyr i nærheden af undersøgelses fartøjet, har GEUS besluttede at følge JNCC protokol og gøre følgende:

1. Før starten af undersøgelsen vil der vil blive udført en visuel look-out efter pattedyr.

2. Det vil blive registreret i undersøgelses logbog, hvis der observeres pattedyr i nærheden af undersøgelsesskibet, før påbegyndelsen af undersøgelsen.

3. En langsom start procedure (Slow start) vil blive fulgt inden begyndelsen af undersøgelsen. Dvs. at den leverede energi til de seismiske systemer gradvist i løbet af 15minutter vil blive øget til normalt niveau.

4. Hvis der observeres marsvin, vil der blive forsøgt survey med reduceret effekt og om nødvendigt begrænses dataindsamlingen til kun at omfatte sedimentekkolod og side scan ind til der ikke længere er marsvin inden for en 500m sikkerhedszone.

5. Der vil blive lavet en sikkerhedszone på 500m omkring Natura 2000 området Store Middelgrund

Litteratur:

1. Southall et al. (2007). Marine Mammals Noise Exposure Criteria. Jour. Aquat. Mamm. 33, 411-521.

2. Ainslie M.A, de Jong C., Dol H., Blacqui'ere G. And Marasini C. (2009). Assessment of Natural and anthropologenic sound sources and acoustic propagation in the North Sea. TINO Report, TNO-DV 2009 C085.

3. Di Iorio L. and Clarck Ch. (2010). Exposure to seismic survey alters blue whale acoustic communication. Bio. Lett. 2010 (6), 51-54.

4. Joint National Conservation Committee. (2004). Guidelines For Minimising Acoustic Disturbance to Marine Mammals From Seismic Surveys. JNCC Publication, April 2004.

5. M.L. Tasker, M. Amundin, M. Andre, A. Hawkins, W. Lang, T. Merck, A. Scholik-Schlomer, J.Teilmann, F. Thomsen, S. Werner & M. Zakharia. Marine Strategy Framework Directive Task Group 11 Report "Underwater noise and other forms of energy". April 2010. EUR 24341 EN-2010. pp.64.

6. Signe Sveegaard et al. 2011: High-density areas for harbor porpoises (Phocoena phocoena) identified by satellite tracking. Marine Mammal Science Volume 27, 230 – 246.